



City Research Online

City, University of London Institutional Repository

Citation: Sun, T. (1999). Fluorescence-based fibre optic sensor systems for temperature and strain measurement. (Unpublished Doctoral thesis, City, University of London)

This is the accepted version of the paper.

This version of the publication may differ from the final published version.

Permanent repository link: <https://openaccess.city.ac.uk/id/eprint/30666/>

Link to published version:

Copyright: City Research Online aims to make research outputs of City, University of London available to a wider audience. Copyright and Moral Rights remain with the author(s) and/or copyright holders. URLs from City Research Online may be freely distributed and linked to.

Reuse: Copies of full items can be used for personal research or study, educational, or not-for-profit purposes without prior permission or charge. Provided that the authors, title and full bibliographic details are credited, a hyperlink and/or URL is given for the original metadata page and the content is not changed in any way.

Fluorescence-based fibre optic sensor systems for temperature and strain measurement

Tong Sun

Thesis submitted for examination for the degree of

Doctor of Philosophy

at

City University

Department of Electrical, Electronic and Information
Engineering

January 1999

Table of Contents

1.4.2.	Rayleigh backscatter systems.....	41
1.4.3.	Raman scattering.....	43
1.4.4.	Brillouin scattering.....	45
1.4.5.	Single-shot distributed optical-fibre temperature sensing...47	
1.5.	Fibre Bragg grating sensors.....	47
1.5.1.	Bragg grating point sensors.....	48
1.5.1.1.	Quasi-static strain monitoring.....	50
1.5.1.2.	Time and wavelength-division multiplexing.....	51
1.5.1.3.	Dynamic strain sensing.....	53
1.5.1.4.	Temperature/Strain discrimination.....	54
1.5.2.	Chirped grating sensors.....	55
1.5.3.	Long period grating sensors.....	56
1.5.4.	Bragg grating laser sensors.....	57
1.5.5.	Interferometric sensors.....	59
1.6.	Luminescent optical fibre sensors.....	60
1.6.1.	Luminescent plastic optical fibre (POF) sensors.....	61
1.6.1.1.	Fluorescent POF sensors.....	61
1.6.1.2.	Scintillating POF sensors.....	62
1.6.2.	Luminescent silica-based optical fibre sensors.....	62
1.6.2.1.	Neodymium-doped fluorescence-based sensors.....	63
1.6.2.2.	Erbium-doped fluorescence-based sensors.....	63
1.6.2.3.	Thulium-doped fluorescence-based sensors.....	64
1.6.2.4.	Other rare-earth doped sensors.....	65

Table of Contents

1.6.2.5.	Quasi-distributed and average temperature sensors ..	65
1.6.3.	Other material based luminescent sensors	66
1.7.	Summary of recent work – influence on the direction of this thesis..	67
1.8.	Aims and objectives of the work	68
1.9.	Structure and design of the thesis.....	69
1.10.	Summary	70
1.11.	References	70
2.	Fibre Optic Luminescence Thermometry: Background and Previous work..	95
2.1.	Abstract.....	95
2.2.	Introduction.....	95
2.3.	Background	97
2.3.1.	The nature of luminescent materials.....	97
2.3.2.	Physical principles of fluorescence thermometry	98
2.4.	Instrumentation and experimental techniques	103
2.4.1.	The generic thermometry system	103
2.4.2.	Fluorescence thermometer schemes.....	105
2.4.2.1.	Fluorescence intensity-based schemes	105
2.4.2.2.	Fluorescence lifetime-based schemes.....	106
2.4.2.3.	Fluorescence line shift scheme.....	109

Table of Contents

2.4.2.4.	Absorption band and excitation spectra temperature dependence	110
2.4.3.	Calibration methodology	111
2.4.3.1.	General approach and thermal considerations.....	111
2.4.3.2.	Signal processing considerations	113
2.4.3.3.	Low temperature arrangements.....	115
2.4.4.	Thermometry of moving surfaces	117
2.4.5.	Surface and volumetric thermography.....	118
2.5.	Discussion	120
2.5.1.	Performance characteristics	120
2.5.2.	Comparison with other techniques.....	121
2.5.3.	Opportunities for further research.....	123
2.6.	References.....	124
3.	Point Optical Temperature Sensors using Different Fluorescent Materials...	133
3.1.	Abstract.....	133
3.2.	Introduction.....	134
3.2.1.	Sensor specification.....	135
3.3.	Bulk active material-based thermometry.....	136
3.3.1.	Alexandrite-based thermometry	136
3.3.1.1.	Previous work	136
3.3.1.2.	Experimental configuration	138
3.3.1.3.	Experimental results.....	139

Table of Contents

3.3.1.4.	Theoretical explanation of the system configuration .	142
3.3.1.5.	Intensity-based measurements for temperature sensing	144
3.3.1.6.	Comparison of the methods	145
3.3.1.7.	Discussion	147
3.3.2.	Praseodymium-based thermometry	148
3.3.2.1.	Previous work	148
3.3.2.2.	Experimental configuration	150
3.3.2.3.	Theoretical background and system model	152
3.3.2.4.	Results of the experimental investigation	155
3.3.2.5.	Discussion of praseodymium results	158
3.3.3.	General discussion of alexandrite and praseodymium systems	159
3.4.	Intrinsic doped fibre based thermometry	160
3.4.1.	Previous work	160
3.4.2.	Erbium-doped fibre for cryogenic temperature measurement	166
3.4.2.1.	Introduction	166
3.4.2.2.	Experimental arrangement	168
3.4.2.3.	Experimental results obtained	170
3.4.2.4.	Discussion of the Er-doped cryogenic fibre sensor ...	171

Table of Contents

3.4.3.	Yb doped fibre temperature sensors.....	173
3.4.3.1.	Introduction.....	173
3.4.3.2.	Ytterbium doped fibre characteristics.....	173
3.4.3.3.	Spectroscopic properties.....	175
3.4.3.4.	Experimental arrangement and initial tests.....	178
3.4.3.5.	Fluorescence decay characteristics	180
3.4.3.6.	Heat treatment and annealing	181
3.4.3.7.	Probe calibration.....	184
3.4.3.8.	Model of thermal behaviour of Yb-doped fibres ..	185
3.4.3.9.	Discussion of Yb ³⁺ thermometer schemes.....	189
3.5.	Summary	191
3.6.	References.....	192
4.	Multiple Exponential Decay Deconvolution and Fluorescence-based Quasi-distributed Temperature Sensing System	198
4.1.	Abstract.....	198
4.2.	Introduction.....	199
4.3.	Use of Prony's and Marquardt's algorithm.....	203
4.3.1.	Signal processing consideration	203
4.3.2.	Prony's method.....	205
4.3.3.	Prony's estimation of fluorescence lifetimes	206
4.3.3.1.	Two-parameter model.....	206
4.3.3.2.	Three-parameter model.....	208
4.4.	Double exponential temperature sensing system	210

Table of Contents

4.4.1.	Prony's estimation of double exponential decay lifetimes.....	210
4.4.1.1.	Four-parameter model	210
4.4.1.2.	Five-parameter model	212
4.4.2.	Simulation results	213
4.4.3.	Comparison with the Marquardt method.....	217
4.4.4.	Application of the technique in multi-exponential decay time sensor system	218
4.4.4.1.	Sensor systems	218
4.4.4.2.	Experimental results from these systems.....	220
4.5.	Triple exponential temperature sensing system	223
4.5.1.	Theoretical background.....	223
4.5.2.	Simulation results	225
4.5.3.	Experimental arrangement for quasi-distributed fibre optic sensor scheme	227
4.5.3.1.	System characteristics.....	228
4.5.3.2.	System calibration.....	230
4.5.3.3.	System test and evaluation.....	231
4.6.	Summary	235
4.7.	References	236
5.	Average and Local Temperature Rare Earth Fibre-based Sensing Systems..	239
5.1.	Abstract.....	239

Table of Contents

5.2.	Average temperature sensing system.....	240
5.2.1.	Introduction.....	240
5.2.2.	Fluorescence-based measurement approach.....	242
5.2.3.	Theoretical background and simulation.....	243
5.2.3.1.	One lifetime, one probe system.....	245
5.2.3.2.	Two lifetimes, two probe system.....	250
5.2.3.3.	Three lifetimes, three probe system.....	253
5.2.4.	Experimental verification and results.....	256
5.2.4.1.	Experimental setup.....	256
5.2.4.2.	Use of two probes.....	258
5.2.4.3.	Use of three probes.....	259
5.2.5.	Discussion of the SV scheme in average temperature measurement.....	261
5.3.	Local temperature excursion detection.....	263
5.3.1.	Introduction.....	263
5.3.2.	Theoretical background.....	264
5.3.2.1.	Correlation ratio scheme.....	266
5.3.3.	Experimental arrangement.....	267
5.3.4.	Results obtained from the sensor systems.....	270
5.3.4.1.	Temperature excursion effect.....	270
5.3.4.2.	Location effect.....	275
5.3.5.	Discussion of local temperature measurement.....	276
5.4.	Summary.....	277

Table of Contents

5.5.	References.....	277
6.	Temperature and Strain Sensitivities of Rare-earth Doped Fibres.....	280
6.1.	Abstract.....	280
6.2.	Introduction.....	281
6.2.1.	Simultaneous strain and temperature monitoring.....	281
6.2.2.	Cr ³⁺ and rare earth doped fluorescence-based sensor systems	283
6.3.	Theoretical background	285
6.4.	Temperature and strain effects on Nd-doped fibres.....	287
6.4.1.	Experimental arrangement	287
6.4.2.	Experimental results	288
6.4.2.1.	Multi-mode fibre.....	288
6.4.2.2.	Single-mode fibre.....	293
6.4.3.	Discussion of the results for Nd-doped fibre	294
6.5.	Temperature and strain effect on Yb-doped fibres	295
6.5.1.	Experimental arrangement	295
6.5.2.	Experimental results	297
6.5.3.	Discussion of Yb-doped fibre results	300
6.6.	Summary	301
6.7.	References.....	302
7.	Comparison of Two Fluorescence-based Schemes using Intensity and Decay Time Approaches.....	306
7.1.	Abstract.....	306

Table of Contents

7.2.	Introduction.....	307
7.3.	Background theory	309
7.3.1.	FL scheme.....	309
7.3.2.	FIR scheme	310
7.4.	Theoretical temperature dependence and sensitivity.....	311
7.5.	Comparison of theory with data	315
7.6.	Temperature responses and sensitivities	317
7.7.	Discussion	321
7.8.	References.....	323
8.	Conclusions and Future Work	325
8.1.	Summary of achievements.....	325
8.2.	Future work.....	328
8.3.	References.....	330
	List of Publications	331

List of Tables

Table 2.1 Summary of characteristics of representative arrangements

Table 3.1 Values of parameters of the appropriate model fitted to the lifetime data and comparison with the previous work

Table 3.2 The comparative sensitivities of the three possible measurement methods (long lifetime, short lifetime and intensity ratio), at selected temperatures over a wide temperature region

Table 3.3 Doped fibre samples test by Zhang et al

Table 3.4 Slopes m_1 and m_2 for different temperature regions

Table 3.5 List of parameters estimated from the two level model for the three samples, before and after annealing and compared with the work of Maurice et al

List of Figures

- Fig.1.1 (a) Point, (b) intrinsic distributed, and (c) quasi-distributed sensing
- Fig.1.2 Experimental system used to determine intrinsic thermal phase noise in optical fibres
- Fig.1.3 Frequency division multiplexed interferometric sensor array (3×3)
- Fig.1.4 Basic time division multiplexed interferometric sensor array
- Fig.1.5 Low-coherence reflectometry technique
- Fig.1.6 Interferometric fibre Fabry-Perot implementations: (a) intrinsic fibre Fabry-Perot, (b) extrinsic fibre Fabry-Perot, and (c) in-line fibre etalon
- Fig.1.7 Principle of Rayleigh backscatter-based optical time domain reflectometry (OTDR) sensing
- Fig.1.8 Experimental setup for high spatial resolution distributed optical fibre sensor
- Fig.1.9 Experimental arrangement for Brillouin scattering based measurements
- Fig.1.10 Basic Bragg grating-based sensor system with transmissive or reflective detection options
- Fig.1.11 WDM/TDM addressing topologies for FBG arrays. (a) Serial system with low reflectivity gratings, (b) parallel network, and (c) branching network
- Fig.1.12 Basic fibre Bragg grating laser sensor systems: (a) short cavity FBG-pair lasers and (b) extended cavity FBG lasers
- Fig.1.13 Schematic diagram of the probe arrangement. LD, laser diode; PD, photodiode; WDM, wavelength division multiplexer
- Fig.2.1 Electron energy levels for rare-earth glasses in fibres, including laser transitions (wavelengths in microns)
- Fig.2.2 The fundamental elements of a remote fluorescence thermometry system

List of Figures

- Fig.2.3 Schematic representation of Luxtron model 1000
- Fig.2.4 The temperature-dependent excitation spectra of $\text{Y}_2\text{O}_3:\text{Eu}$, as measured with a Perkin-Elmer model 650-10S spectrometer with a resolution of approximately 1nm
- Fig.2.5 The characteristic experimental arrangement used to calibrate the temperature dependence of fluorescence
- Fig.2.6 The experimental arrangement used to measure the armature temperature of an operating, high speed, permanent-magnet motor
- Fig.2.7 Illustration of the effect of motion on the fluorescence signal in the sensor system
- Fig.3.1 Experimental arrangement used in the temperature sensing tests
- Fig.3.2 Fluorescence decay signal following the termination of pulse excitation at a temperature of 100°C
- Fig.3.3 Experimental data on the two lifetimes observed, as a function of temperature, and the fitting curves obtained from the use of the configurational coordinate model
- Fig.3.4 Schematic of the configurational coordinate model for Cr^{3+} fluorescence in alexandrite. r : the configurational coordinate (Zhang et al)
- Fig.3.5 Intensity ratio (A_2/A_1) associated with the two intensities in alexandrite as a function of temperature
- Fig.3.6 (a) Partial energy level diagram of praseodymium showing absorption to the ^3P levels and emission $^3\text{P}_0 \rightarrow ^3\text{F}_2$. (b) Three-level model configuration, showing the parameters involved in the model

List of Figures

- Fig.3.7 Experimental arrangement for the temperature sensor
- Fig.3.8 Fluorescence decay signal of Pr^{3+} : ZBLAN with different doping levels, at a temperature of 320K, showing single exponential behaviour
- Fig.3.9 Fluorescence lifetime of Pr^{3+} : ZBLAN, as a function of temperature, with different concentrations of 500 and 4000ppm. Points represent measured data with the solid line the prediction of the three level model
- Fig.3.10 Fluorescence lifetime of Pr^{3+} : ZBLAN, as a function of temperature, with different concentrations of 1000 and 4000ppm. Points represent measured data with the solid line the prediction of the three level model
- Fig.3.11 Experimental arrangement used for Er and Nd doped fibre intrinsic fluorescence-based sensors
- Fig.3.12 Experimental results of the thermal characteristics of Nd^{3+} doped fibre
- Fig.3.13 Fluorescence lifetimes of Er-doped fibres as a function of temperature
- Fig.3.14 Comparison of different rare-earth doped fibre based thermometry
- Fig.3.15 System arrangement used in the temperature sensing tests
- Fig.3.16 Results of the different Er-doped silica fibres over the wide temperature range ($77\text{K} \leq T \leq 1200\text{K}$)
- Fig.3.17 (a) Cross sections for absorption and emission of Yb^{3+} in a germanosilicate glass. (b) Schematic of energy levels of ytterbium ions
- Fig.3.18 Experimental arrangement for the Yb^{3+} doped fibre thermometry. LD-laser diode; PD-photodiode; PLD module – phase locked detection module
- Fig.3.19 Fluorescence signals as a function of time from samples of YbH and YbL, shown separately at the same temperature of 1000°C

List of Figures

- Fig.3.20 Temporal response of YbH at 700°C for more than 100 hours, showing the decay-time plateau
- Fig.3.21 Temporal response of YbH at 700°C over a period of 15 hours taken after a temperature excursion, following initial annealing
- Fig.3.22 Fluorescence lifetime variation of YbH as a function of temperature before and after annealing recorded during several temperature cycles from 60°C to 700°C and back to 60°C
- Fig.3.23 Fluorescence lifetime variation of YbM as a function of temperature after annealing, recorded during several similar temperature cycles to that of Fig.3.22
- Fig.3.24 Fluorescence lifetime variation of YbL as a function of temperature after annealing, recorded during several similar temperature cycles to that of Fig.3.22
- Fig.3.25 Comparison of fluorescence lifetimes from YbH, YbM and YbL as a function of temperature
- Fig.3.26 Sensitivity comparison of the three samples, YbH, YbM and YbL over the temperature region from 60°C to 700°C
- Fig.4.1 Cross comparison between various two-parameter, model based, lifetime-estimation algorithms
- Fig.4.2 Cross comparison between the three-parameter Marquardt algorithm and its Prony's counterparts
- Fig.4.3 Noise-to-error transfer factor, m_1 , as a function of ΔN and β

List of Figures

- Fig.4.4 Noise-to-error transfer factor, m_1 , as function of the ratio of the two lifetime constants, r_{12} ($= \tau_1/\tau_2$)
- Fig.4.5 Relationship between the optimized observation window, β_{opt} and the time-constant ratio, r_{12} ($= \tau_1/\tau_2$)
- Fig.4.6 The optimum values of ΔN as a function of r_{12} ($= \tau_1/\tau_2$)
- Fig.4.7 Comparison of accuracies of Marquardt and Prony's methods
- Fig.4.8 Schematic of the dual sensor arrangement, where two different sensor combinations for the probe are tested, system A: alexandrite-ruby; system B: alexandrite-YAG:Cr³⁺
- Fig.4.9 Experimental comparison of lifetimes of ruby and alexandrite with the use of the double and single Prony's method (-10-60°C)
- Fig.4.10 Experimental comparison of lifetimes of YAG:Cr³⁺ and alexandrite with the use of the double and single Prony's methods (-10-50°C)
- Fig.4.11 Experimental comparison of lifetimes of YAG:Cr³⁺ and alexandrite with double and single Prony's analysis in the subroom temperature region
- Fig.4.12 Noise-to-error transfer factor, m_1 , as a function of ΔN and β
- Fig.4.13 The optimized observation window, β_{opt} , and the time-constant ratios
- Fig.4.14 The optimal values of ΔN as a function of time-constant ratio
- Fig.4.15 Schematic of the experimental arrangement used in this work. LD-laser diode; PD-photodiode
- Fig.4.16 The superposed fluorescence decay signal when the temperature of elements 2 and 3 is 25°C and that of element 1 is 100°C (with the residue results coming from the double and triple exponential fitting separately)

List of Figures

- Fig.4.17 Deconvolved constants for the three elements using Marquardt's as well as Prony's approach when the temperature for elements 2 and 3 is 25°C and that of element 1 varies from 100 to 900°C
- Fig.4.18 Deconvolved lifetime constants for the three elements using Marquardt's as well as Prony's approach when the temperature for element 2 is 20°C and that of elements 1 and 3 varies from 100 to 900°C
- Fig.4.19 The superposed fluorescence decay signals when the temperature of elements 2 is 20°C and that of element 1 and 3 is 800 and 900°C, respectively, for the upper and lower graphs
- Fig.5.1 Behaviour of the singular value, SV, as a function of normalized noise deviation in a one-probe sensing system, showing its comparative insensitivity as the noise-to-signal ratio varies from 0.1% to 1% (signal-to-noise ratio varies from 30 to 20dB)
- Fig.5.2 Behaviour of the singular value, SV, as a function of fluorescence lifetime in a one-probe sensing system, showing sensitivity to fluorescent lifetime
- Fig.5.3 Noise-to-error transfer factor, m_e , as a function of the normalized observation window width β in a one-probe system
- Fig.5.4 Variation of SV as a function of average lifetime τ , $2/\tau=1/\tau_1+1/\tau_2$, and the amplitude ratio in a two-probe sensing system ($\tau_1/\tau_2=1.1$)
- Fig.5.5 Noise-to-error transfer factor, m_e , as a function of the amplitude ratio and the normalized observation window width β in a two-probe sensing system ($\tau_1/\tau_2=1.1$)

List of Figures

- Fig.5.6 Variation of SV as a function of average lifetime τ , $3/\tau=1/\tau_1+1/\tau_2+1/\tau_3$, and the amplitude ratio in a three-probe sensing system ($\tau_1/\tau_2=1.1$, $\tau_1/\tau_3=1.21$)
- Fig.5.7 Noise-to-error transfer factor, m_e , as a function of the amplitude ratio and the normalized observation window width β in a three-probe sensing system ($\tau_1/\tau_2=1.1$, $\tau_1/\tau_3=1.21$)
- Fig.5.8 Variation of noise-to-error transfer factor m_e , as a function of average lifetime showing consistent behaviour under different sensing systems of two and three probes
- Fig.5.9 Behaviour of SV as a function of average lifetime, showing consistent performance under different sensing systems of two and three probes
- Fig.5.10 Schematic of the experiment setup used illustrated with three doped fibre sensor elements. The separation of the Nd^{3+} fibre elements can vary widely in practical situations. LD–laser diode source; PD–photodetector
- Fig.5.11 Experimental data showing the SV variation with the average temperature from 20-100°C with two sensing elements located in the measuring area, under different temperature conditions
- Fig.5.12 Experimental data showing the SV variation with the average temperature from 20-100°C with three sensing elements located in the measuring area, under different temperature conditions
- Fig.5.13 Schematic of the two configurations demonstrated. (a) sensing system based on short, single lengths of Nd doped fibres, fused into a network (b) sensing area formed by using a long length of Er doped fibre, one short piece of which is exposed to the temperature excursion

List of Figures

- Fig.5.14 The fluorescence decay time signals detected using the configuration shown in Fig.5.13(a), for sensors (1) both at 20°C and (2) one at 20°C and the other at 100°C
- Fig.5.15 The results of the correlation ratio scheme employed using the system shown in Fig.5.13(a), showing the variation of the ratio with temperature, with a two and a three probe system
- Fig.5.16 The fluorescence decay time signals detected from the configuration shown in Fig.5.13(b) for a range of temperatures (24°C, 111°C, 204°C and 290°C) and the apparent lifetime variation with temperature due to a simple analysis assuming a single exponential decay
- Fig.5.17 The results of the correlation coefficient ratio scheme employed in the system shown in Fig.5.13(b), for a range of temperatures up to 300°C
- Fig.5.18 The correlation coefficient as a function of temperature, showing no effect of the location of the temperature excursion applied to the sensing fibre, with three different positions of the heater with respect to the fibre listed as shown
- Fig.6.1 Simplified schematic of the experimental arrangement for the strain test of Nd doped fibre
- Fig.6.2 The lifetime variation of multimode Nd doped fibre as a function of strain over a range of temperatures before and after “stress annealing”, (graphs marked (*)) showing the strain sensitivity of the fluorescence lifetime keeps almost constant regardless of the variation of temperature and strain. (a)-(d) Temperatures are room temperature, 60°C, 100°C, 150°C respectively ($\pm 2^\circ\text{C}$ in each case)

List of Figures

- Fig.6.3 The normalized strain sensitivity of the fluorescence lifetime for multimode Nd doped fibre, as a function of temperature
- Fig.6.4 Lifetime variation of multimode Nd doped fibre as a function of temperature as well as strain: solid line 180 $\mu\epsilon$ applied, dashed line 1210 $\mu\epsilon$ applied
- Fig.6.5 Lifetime variation of single-mode Nd doped fibre as a function of strain, at 150°C, for both strain applied (strain up) and removed (strain down)
- Fig.6.6 The lifetime variation of the single mode Yb doped fibre as a function of strain over a range of temperatures showing the strain sensitivity of the fluorescence lifetime. (a)-(d) Temperatures are 30°C, 60°C, 100°C, 150°C respectively ($\pm 5^\circ\text{C}$ in each case)
- Fig.6.7 The normalized strain sensitivity of the fluorescence lifetime for single mode Yb doped fibre, as a function of temperature over the region 30-150°C
- Fig.6.8 Lifetime variation of single mode Yb doped fibre as a function of temperature as well as strain: solid line 200 $\mu\epsilon$ applied, dashed line 800 $\mu\epsilon$ applied
- Fig.7.1 Schematic energy level diagram of the three level model of a typical fluorescent ion
- Fig.7.2 Comparison of the performance of the FIR and FL methods with scaled temperature variation, for various parameter values
- Fig.7.3 Sensitivity-energy gap products of the FIR and FL methods as a function of the scaled temperature, for various parameter values
- Fig.7.4 The lifetime ratio data as a function of the scaled temperature for crystals of ruby, alexandrite, Cr³⁺:YAG and bulk Pr³⁺:ZBLAN, where fitting curves are plotted based on Eqs.(7.3) and (7.2)

List of Figures

Fig.7.5 Normalized FIR data as a function of the scaled temperature for Er^{3+} -doped fibre, Yb^{3+} -doped fibre and bulk Pr^{3+} :ZBLAN, where fitting curves are plotted based on Eq.(7.5)

Fig.7.6 The temperature responses for the FL scheme for crystals of ruby, alexandrite, Cr^{3+} :YAG and bulk Pr^{3+} :ZBLAN, where fitting curves are plotted based on Eq.(7.2) and Eq.(7.3)

Fig.7.7 The temperature responses for the FIR scheme using Er^{3+} -doped fibre, Yb^{3+} -doped fibre and bulk Pr^{3+} :ZBLAN, where fitting curves are plotted based on Eq.(7.5)

Fig.7.8 A global comparison of the sensitivities of both methods, comparing experimental and theoretical data

Acknowledgements

Acknowledgements

The work reported here was carried out under the supervision of Prof. K T V Grattan and Dr Z Y Zhang. I would like to take the chance to express my tremendous gratitude to their excellent supervision and encouragement in the course of study.

I am grateful to the financial support provided by City University and the Engineering and Physical Science Research Council (EPSRC). The travel grants coming from the Worshipful Scientific Instrument Makers and the Institute of Physics are also greatly appreciated.

Thanks are due to Prof. A W Palmer and to my colleagues in Optical Instrumentation Group, who contributed practically to the measurements.

I am grateful to my former colleagues in China who provided so much steady encouragement.

Most of all I thank my dearest parents, sister and husband, Xiaonan Fan for their precious support and understanding, especially my dearest mother, who dreamed so much of her daughter's success but never had the chance to see it.

Copyright Declaration

Copyright Declaration

The author hereby grant powers of discretion to the City University Librarian to allow the thesis to be copied in whole or in part without further reference to the author. This permission covers only single copies made for study process, subject to normal conditions of acknowledgement.

Abstract

Commencing with a review of the development of fibre optic sensor technology and especially previous work in the phosphor thermometry area, this thesis covers research on fibre optic fluorescence thermometry. Several luminescent materials, e.g. crystalline materials, doped bulk glasses and rare-earth ion doped fibres, are evaluated. Theoretical models have been developed and are considered to provide underpinning support for the experimental results obtained, and applied to the optimization of the selection of particular suitable fluorescent materials for thermometric use, which lays an appropriate theoretical basis for the fluorescence thermometry discussed herein.

The fluorescence based point temperature sensing system developed has been expanded to multi-point or quasi-distributed temperature sensing application by using Prony's method, which enables the exponential decays from either single material, two-material or even several element quasi-distributed sensors to be analyzed and thus data and associated measurand information encoded in each individual signal to be recovered.

As a further development, the fluorescence based system has been modified to measure average and local temperatures, which are important in a number of industrial situations. Corresponding signal processing schemes, the singular value (SV) scheme and the correlation coefficient ratio scheme, are introduced and tested to meet the requirement of high speed and consistency.

Abstract

Whilst recognizing their strong dependence on temperature variation, the fluorescence lifetimes of rare earth doped fibres are investigated for the first time in terms of their sensitivity to another physical quantity, strain. Their characteristics and sensitivity are explored in detail in the work

Finally, two most promising fluorescence-based temperature sensing techniques, namely the fluorescence intensity ratio (FIR) and fluorescence lifetime (FL) schemes, are compared and contrasted.

The significance of the work is considered and suggestions for future work made.

Chapter 1

Fibre Optic Sensor Technology

1.1 Abstract

This work in this chapter reports some of the significant developments in fibre optic sensor technology which have occurred over the past 5 to 10 years and aims to set the scene for the work described in this thesis. Particular emphasis is given to advances in interferometric sensors, intrinsic distributed sensors, Bragg grating based systems and their comparison with luminescent optical fibre sensing system. The aims and objectives of the work are put forward and the structure of the thesis to achieve these aims is outlined in this Chapter.

1.2 Introduction

It has now been more than two decades since the first experiments on the use of optical fibres as sensing elements were conducted. Interest in this early work quickly generated a thriving research community which has sustained a strong focus on this technology through the 1980s to the present time[1][2]. The motivation behind this work continues to be the same: fibre optic-based techniques provide the basis for a

sensor technology which can produce sensors that are, in general, lightweight, small, easily multiplexable, non-invasive[3] and immune to electromagnetic interference (EMI), requiring no electrical power at the sensing point, and in most cases having the potential to be produced at low cost. Recent investigations conducted by a team from the Belgian Nuclear Research Centre, Faculté Polytechnique de Mons and the National Optics Institute in Canada has confirmed that fibre sensors survive stringent radiation tests[4], especially the rapidly developing field of Bragg-grating based sensors, in which the width, amplitude and temperature sensitivity of the Bragg resonance remains unaltered up to a dose of at least 1MGy and the Bragg wavelength changes by no more than 0.025nm.

1.2.1 Sensor types and configurations

For many sensing applications, the parameter of interest is measured at a specific location. This “point” measurement capability is the standard, or conventional, measurement mode of many widely used sensors, e.g., as with the use of a pressure probe, thermistor, accelerometer. In general, they tend to operate in the same basic way, as depicted in Fig.1.1(a)[5], with for example, a sensor tip sensitized via a luminescent active material to respond to temperature. Another option is the ability to spatially discriminate the measurand at different locations along a fibre length, as depicted in Fig.1.1(b)[5], leading to the capability to perform distributed sensing. If the fibre is not sensitive along its entire length, but is locally sensitized at various points, the system becomes a “quasi-distributed” sensor system, as depicted in Fig.1.1(c)[5].

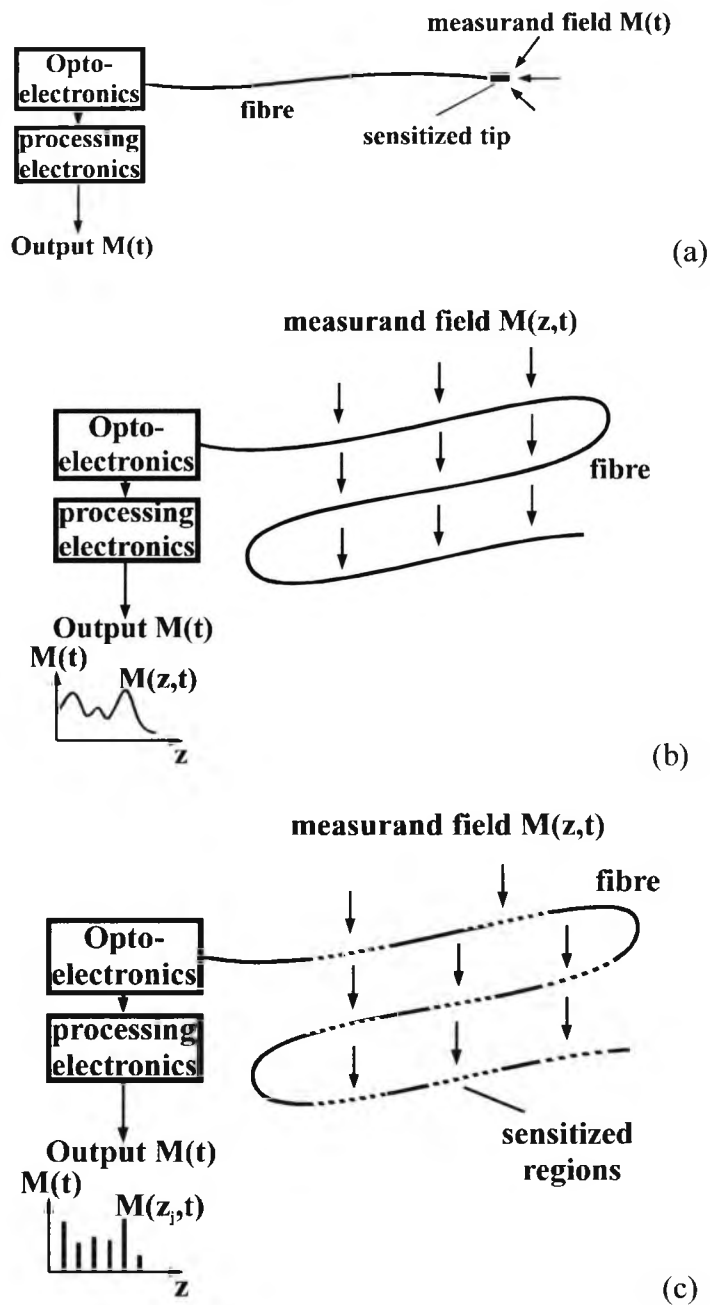


Fig.1.1 (a) Point, (b) intrinsic distributed, and (c) quasi-distributed sensing

There is a wide variety of optical fibre sensors which are difficult to discuss in full in a single chapter, but the focus will be on developments in the area of optical fibre sensing techniques for physical measurands, that is, interferometric sensors, distributed fibre

optic sensors, Bragg grating based systems, luminescent fibre sensors and their industrial applications as representative of the major types of system involved.

1.3 Interferometric sensing

Interferometric sensors have become widely accepted as the configuration which can provide the ultimate in sensitivity to a range of weak physical fields. The earliest work in this area examined the sensitivity of fibres to weak acoustic perturbations[6][7], and this work has continued to date, with several significant advances in the technology since the mid- to late- 1980s. Much of the “generic” work in the areas of interferometric demodulation, noise sources, polarization control, multiplexing and the progress in low-coherence interferometry which has occurred over the past decade has been motivated by the need to enhance the capabilities of this technology for a range of applications.

1.3.1 Demodulation

Much of the early work on interferometric sensors addressed this issue[5]. The measurand induces a phase shift proportional to the measurand strength, but this phase is then encoded by the interferometer transfer function nonlinearly into an intensity change at the detector. Early work on active homodyne phase tracking schemes[8] showed that these were useful in providing a means to stabilize the interferometer signal for laboratory-based experimentation and transducer development and characterization, but proved unsuitable for most practical applications due to the need to incorporate an electrically active element in the interferometer. A series of developments using laser frequency modulation-based techniques[9][10][11] to induce

“carrier” phase shifts in an unbalanced interferometer were developed over the period from 1982 to 1985. The most successful of these approaches is the “phase-generated carrier” (PGC) technique[12]. The self-noise of this approach has been reported to be in the $\sim 1\mu\text{rad}/\sqrt{\text{Hz}}$, and the bandwidth can be tailored to frequencies from as low as a few Hz to $>10\text{kHz}$. Recently, Lu et al[13] have analyzed the effects of phase modulator characteristics on performance of a two-beam interferometer with active homodyne processing techniques.

1.3.2 Phase noise

A number of laser sources have become available which, due to their narrow linewidth and low-frequency jitter, have allowed for improvements in the phase detection sensitivity of interferometric systems[5]. One particular type of device of note is the diode-pumped nonplanar ring cavity Nd:YAG laser[14]. It was reported that the noise at frequencies $>10\text{kHz}$ is low enough to begin to approach the fundamental noise limit of interferometric sensors arising due to intrinsic thermal phase noise. This noise limitation was investigated by Wanser et al[15] and subsequently by Krakenes and Blotekjær[16]. Fig.1.2 shows an experimental system used to determine this noise level. A fibre Mach-Zehnder interferometer with arms each of 1000m was constructed and carefully packaged to shield it from environmental perturbations due to mechanical (vibration) and acoustic noise sources. The arms were balanced to within 1cm, which effectively completely eliminated phase noise due to the laser frequency jitter. With this system, the system phase noise was measured over the 0- to 100-kHz range. The fibre arms were then cut back first to 100m and then to 10m, and the noise spectrum

was recorded for each case. For the 100m interferometer arms, the noise in the $\sim 1\text{kHz}$ range was $\sim 0.3\mu\text{rad}/\sqrt{\text{Hz}}$. Even level of noise could be significant in sensor systems designed for very high sensitivity applications, where sub $\mu\text{rad}/\sqrt{\text{Hz}}$ phase resolutions would be required.

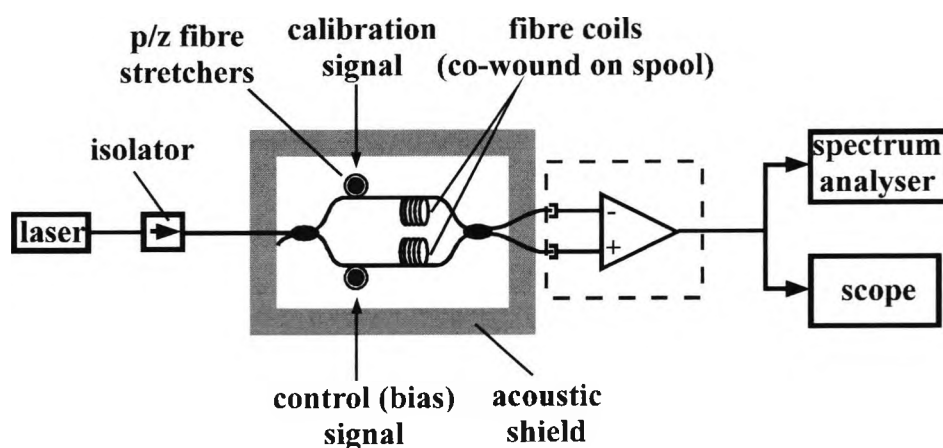


Fig.1.2 Experimental system used to determine intrinsic thermal phase noise in optical fibres

Fibre lasers have also become more widely available and show promise as suitable sources for various interferometric sensor applications[17]. Short cavity Bragg grating-based erbium lasers[18][19] have been shown to exhibit narrow linewidth and low-frequency jitter. Intensity noise due to relaxation oscillations may introduce noise in some application: however, pump feedback techniques to suppress this noise have been demonstrated[5].

1.3.3 Polarization effects

A serious issue with the practical implementation of fibre interferometric sensors has been the problem of polarization-induced fading (PIF) in low-birefringence fibre interferometers. This problem is rooted in the fact that as the light is split into two

separate paths in the Michelson and Mach-Zehnder configurations, the evolution of the state of polarization (SOP) of light guided in these fibres varies independently in a random and unpredictable manner. Consequently, the SOP of the recombined optical components from the two interferometer arms vary independently, and this leads to a reduction of the interferometric optical mixing efficiency and a loss (“fading”) of the interference signal[5]. This polarization-induced fading problem was identified as early as 1980 by Stowe et al[20], and a number of techniques have been proposed to overcome this limitation using a variety of polarization-state selection techniques[21][22][23]. Work in the late-1980s led to the development of a clearer understanding of the polarization behaviour of interferometric systems[24][25][26] and showed for the first time the dependence of the interferometric output visibility on the system input SOP. In particular, this work showed that the visibility of an interferometer can always be optimized by control of the input SOP, thus allowing control of the visibility of a remotely located interferometer.

A significant advance in this area, however, came in 1990, when it was shown by Pistoni and Martinelli[27] that the evolution of the SOP along a low birefringence fibre was retraced by light propagating back along the fibre if the light was reflected from a combination of a 45° Faraday rotator and mirror combination. This led to the development of a polarization-independent Michelson configuration[28][29], in which the use of Faraday rotator mirror at the distal ends of each arm provided passive compensation for random polarization drifts in the fibre arms.

1.3.4 Multiplexing

One advantage of fibre sensors is the relative ease with which elements can be multiplexed into arrays using common input and output fibres. Three important multiplexing topologies have been developed are briefly introduced below.

1.3.4.1 Frequency division-based scheme (FDM)

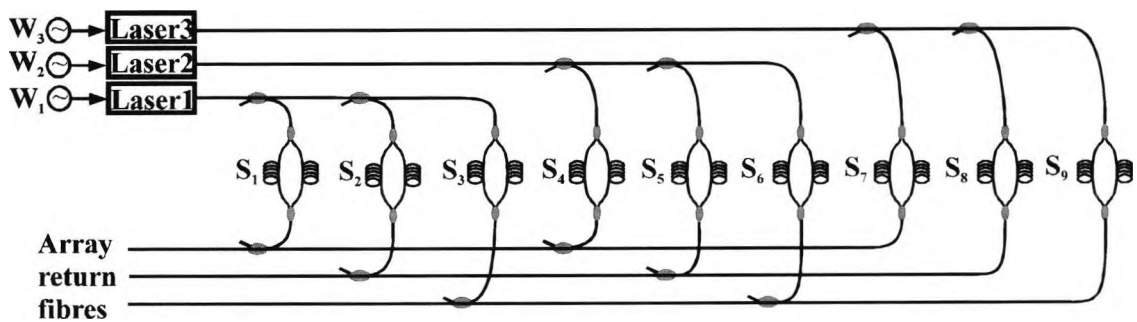


Fig.1.3 Frequency division multiplexed interferometric sensor array (3×3)

The frequency division-based scheme[30] is shown in Fig.1.3 for a simple 3×3 sensor array. Here, the three lasers each power three slightly unbalanced sensor interferometers, and the nine sensor outputs are combined onto three output fibres in such a way that each output fibre carries only one signal from each laser. Thus, if the lasers are modulated at different frequencies, the outputs carried by each output fibre will consist of signals at each modulation frequency, and the sensor outputs can be separated by frequency selection using appropriate band filtering or synchronous detection.

Using this technique, the multiplexing of 48 interferometric acoustic sensors has been demonstrated as part of the US Navy's all-optical towed array (AOTA) programme[31].

1.3.4.2 Time division multiplexing scheme (TDM)

The most straightforward version of this scheme involves the interrogation of a number of discrete Mach-Zehnder (or Michelson) interferometers using a pulsed (or gated CW) source in conjunction with appropriate optical delays between the sensors[32], an example of which is shown in Fig.1.4. The input pulse width is set $\leq \Delta T$ (delay in the fibre delay coils), such that at the output of the N sensor array a series of N distinct output pulses is generated for each input pulse. As the path imbalance in the sensors is small, the pulses from the signal and reference arms overlap and interfere at the output of each interferometer, and the output pulse train simply represents samples of the interferometer outputs interleaved in time sequence. However, the number of sensors is rather limited because the power lost in coupling into the return bus increases as the number of sensors increases. The power budget also suffers from a reduction of the duty cycle when the number of sensors is increased. A practical limit seems to be of the order of ten sensors[5][33]. It has been suggested recently that incorporation of fibre-optic amplifiers in the network will improve the performance and raise the maximum number of sensors that may be used[34][35][36][37].

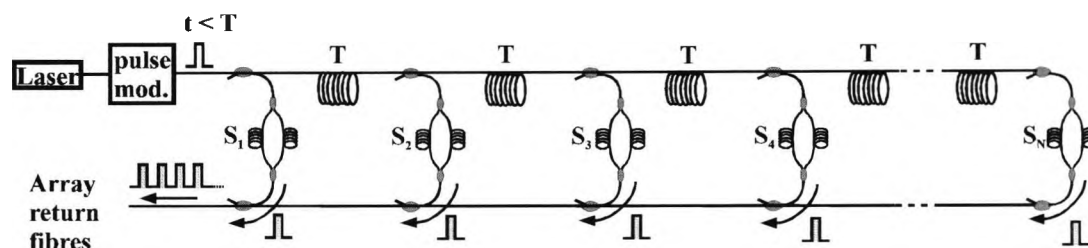


Fig.1.4 Basic time division multiplexed interferometric sensor array

1.3.4.3 Wavelength division multiplexing scheme (WDM)

The use of wavelength division multiplexing to augment the number of sensors that can be multiplexed has received only limited attention, probably due to the limited availability of WDM components required to implement this type of scheme. Such schemes are being extended, for example, a WDM/TDM (W-T/DM) system allowing 14 sensors to be addressed has been demonstrated[38] based on the use of simple 2×2 WDM couplers designed for operation at 780 and 830nm.

1.3.5 Low-coherence interferometry

This low-coherence concept has been applied to single mode interferometric sensors for absolute interferometric OPD sensing[5]. Applications include temperature[39][40], displacement[41], strain[42], and disturbance location sensing[43]. Also, the detection of backscatter in fibres and from fibre components has been monitored using low-coherence interferometric techniques[44][45][46]. Fig.1.5 illustrates this type of system. Light from a low-coherence source is coupled into a fibre through a coupler, and the backscattered light (Rayleigh) and light directly reflected from fibre-fibre interfaces, fibre-waveguide interfaces, or fibre ends is directed via the coupler to a detector. A second portion of the light from the source is fed via the coupler to a reference leg which contains a variable path length formed by a

collimating lens and movable mirror. Light in this arm is then also reflected back toward the detector and serves as a strong “local oscillator” mixing with the weak light from the sensing arm. Interference between the two optical components on the detector occurs only for optical components which have traversed optical paths within the short coherence length of the source (typically, $10\mu\text{m}$).

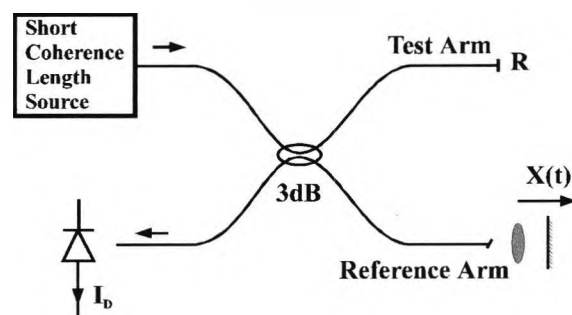


Fig.1.5 Low-coherence reflectometry technique

With high-power fibre amplified spontaneous emission (ASE) sources becoming available, the sensitivity of this technique can be sufficiently high to allow the intrinsic backscatter of fibres to be measured with spatial resolutions of $<100\mu\text{m}$ [5].

The concept of “low-coherence” or “white light” interferometry has also been applied to a variety of other sensing configurations, one typical setup of which is a Fabry-Perot interferometer[5], where by scanning the Optical Path Difference (OPD) of the receiver interferometer, the interferogram detected during this process yields the sensor OPD by measurement of the receiver OPD at the “central” fringe of the interferogram[47].

One important development in this area is the discrimination between strain- (or pressure) and temperature- induced effects. A number of approaches have been demonstrated, such as multi-wavelength interferometric sensing[48], dispersive Fourier transform spectroscopy[49], polarimetric and two-mode differential sensing[50], a combination of in-line fibre etalon (ILFE) and intrinsic Fabry-Perot (IFP) device[51] and others using dual modes, two polarizations, dual wavelengths and two material interrogation schemes[52][53][54][55]. These approaches in general produce output responses which exhibit normalized responsivity factors that are different and thus perform well at separating strain and temperature perturbations.

1.3.6 Other interferometric sensors

Other developments in the area of interferometric sensing included considerable work on Fabry-Perot configurations. Lee and Taylor[56] developed techniques to introduce “internal” mirrors in a fibre by fusion splicing end-coated fibres, forming Intrinsic Fabry-Perot interferometers (IFPI), shown in Fig.1.6(a). One of the most widely reported Fabry-Perot configurations has been the extrinsic Fabry-Perot interferometer (EFPI)[57], shown in Fig.1.6(b). This system has been extensively used for structural monitoring application of strain. In the most basic configuration, the two fibres are held with epoxy adhesive into the alignment tube, and changes in the internal gap due to the strain applied to the tube are sensed by shifts in the interferometric signal. The “directionality” limitations of this type of sensor arising due to the ambiguous cosine interference fringe output of the device have been addressed in part by a quadrature-phase-shifted EFPI[58]. The other limitation of this sensor (and other FP sensors) is

that it is not an absolute sensor, relying as it does on relative fringe counts and the Virginia Institute of Technology group has focused on the investigation of an absolute EFPI configuration[59]. A variation on this type of compact interferometric sensor element, developed by Sirkis et al[60] is the in-line fibre etalon (ILFE)[60], shown in Fig.1.6(c). The two fibres are fusion spliced to a section of hollow core fibre (micro tube) of the same outside diameter. This creates a sensor without the mechanical discontinuities of the EFPI.

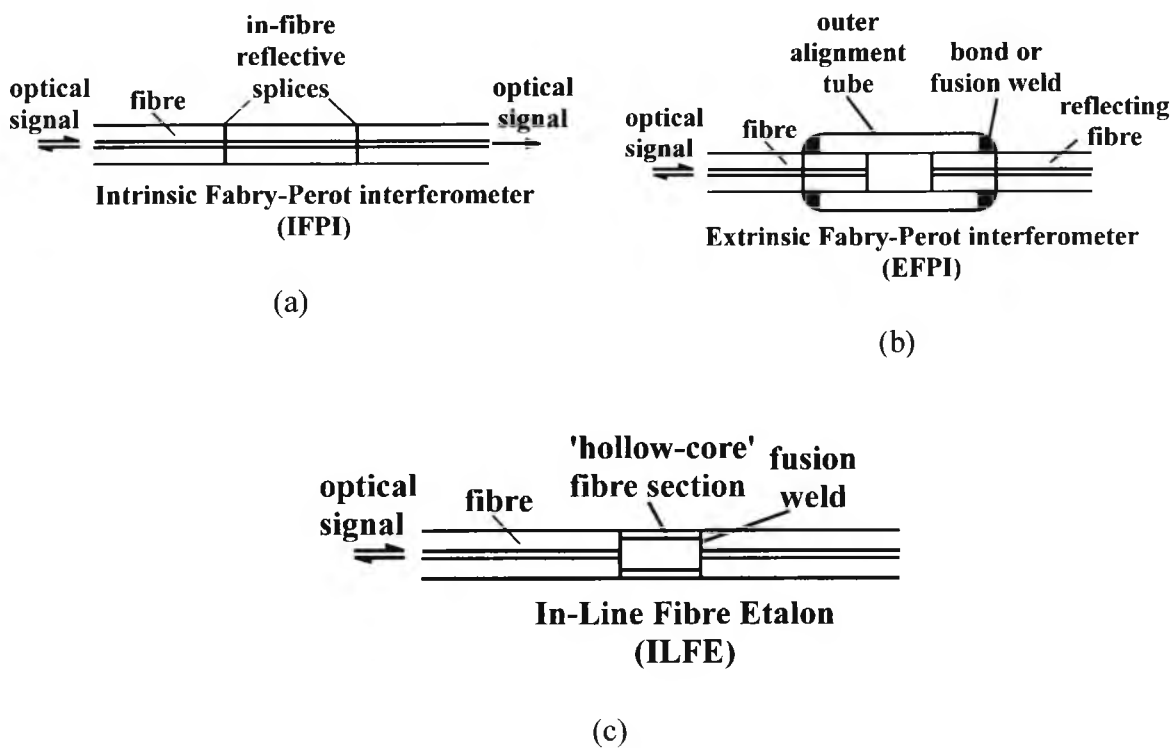


Fig.1.6 Interferometric fibre Fabry-Perot implementations: (a) intrinsic fibre Fabry-Perot, (b) extrinsic fibre Fabry-Perot, and (c) in-line fibre etalon

1.4 Distributed fibre optic sensing

The ability to make distributed measurements on extended structures is of increasing importance. For example, the measurement of strain distributions on aircraft operating

close to their performance limits, the distribution of temperature in boilers, pressure vessels, high voltage transformers etc., are all examples of application areas where the distributed measurement of critical performance parameters offers an additional dimension for the purposes of monitoring, control or improved understanding which can lead to significant enhancements in design.

Optical fibres, via the linear and non-linear effects which they sustain, offer unique advantages for distributed sensing. However, in order to achieve optimum performance appropriate to a given measurand and measurement environment, careful matching of system to environment, and detailed system design are necessary.

This section highlights some of the optimization methods which were studied, with a view to providing improved system performance and thus greater application flexibility.

1.4.1 Backscatter and forward-scatter methods

Most distributed optical fibre methods employ non-linear optical effects. The fundamental reason for this is that these effects exhibit varied and distinctive responses to external measurands, thus providing for a range of applications-specific sensors[61].

Backscatter methods, employing Optical Time Domain Reflectometry (OTDR)[62] to achieve a useful spatial resolution[63], have the advantages of high sensitivity and

single-ended operation. Their disadvantage is that of a low-level signal and thus a long response time, resulting from the necessity to integrate over many pulses.

The forward-scatter techniques[61], usually employing counter-propagating pulse-wave interactions, generally are of lower sensitivity and (normally) need access to both ends of the fibre, but they often provide sufficiently powerful signals to operate in a single-shot mode, thus leading to a response time not greater than that of the “go-and - return” light passage along the fibre.

Clearly, the choice of system must depend on the required system performance and the details of these systems are shown below in the following sections.

1.4.2 Rayleigh backscatter systems

The principle of operation is shown in Fig.1.7. In the case of measurand-dependent loss, a region of localized high loss due to the perturbation of the fibre by the measurand field (stress, temperature, external refractive index, etc.) causes a change in the slope of the detected backscatter signal versus time delay curve (OTDR curve) at a time delay corresponding to the spatial position of the perturbation.

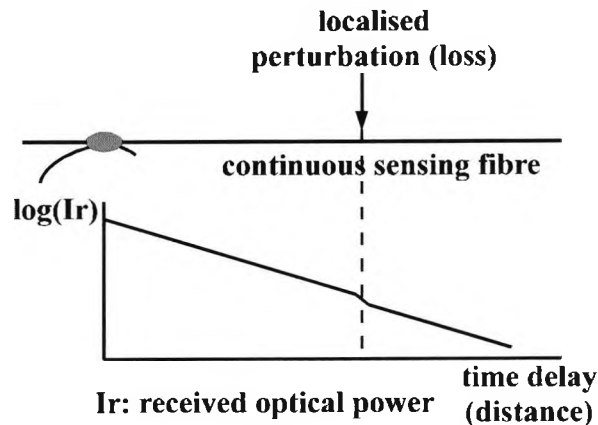


Fig.1.7 Principle of Rayleigh backscatter-based optical time domain reflectometry (OTDR) sensing

The first reported intrinsic distributed sensor concept was based on a variant-OTDR approach, polarization-optical time domain reflectometry (POTDR)[64][65], in which the state of polarization of Rayleigh-backscattered light in a monomode fibre was detected as a function of time. Although little follow-up work was conducted on this approach during the 1980s, it is interesting to note that it has recently been the subject of renewed study by several researchers[66]-[70].

The first demonstration of the use of measurand-dependent scattering as a means of distributed sensing was reported by Hartog in 1983[71], who utilized the change in the Rayleigh scattering coefficient with temperature to perform distributed temperature sensing. In general, this dependence is extremely weak in solid core fibres, and liquid core fibres were used to provide a higher sensitivity with a spatial resolution of ~few metres and temperature of $\sim\pm 1^\circ\text{C}$.

The utilization of temperature-dependent absorption in appropriately doped fibres has been proposed and demonstrated as a means of distributed sensing. A number of rare-earth elements have been used as dopants, such as neodymium and holmium, in a variety of host fibres in such research[72][73] with a temperature resolution of $\sim 1^\circ\text{C}$ and a spatial resolution of $\sim 3.5\text{m}$.

Various loss mechanisms can be utilized in distributed sensing, such as the temperature dependence of the bending loss in plastic clad (PCS) fibres[74], the evanescent field radiative loss due to continuous microbending loss in fibre[75] and more recently the introduction of interferometric optical time-domain reflectometry for distributed optical fibre sensing[76].

1.4.3 Raman scattering

Probably the most successful distributed fibre optic sensor developed to date is the Raman-distributed temperature sensor system. Distributed sensing using the temperature dependence of Raman scattering was proposed and first demonstrated in the mid-1980s[77]-[79], and has since been developed into a commercial instrument by several companies. In the standard Distributed anti-Stokes Raman Thermometer (DART)[79], an intense laser pulse is launched into the sensing fibre. As a result of spontaneous Raman scattering, some anti-Stokes and Stokes photons are generated along the fibre. A fraction of these scattered photons is captured in the guided modes of the fibre and then propagated back towards the launching end where they are

detected by a fast photodetector. Standard DART sensors are capable of operation over fibre lengths of up to 10km with $\sim 1^\circ\text{C}$ temperature and 1m spatial resolution.

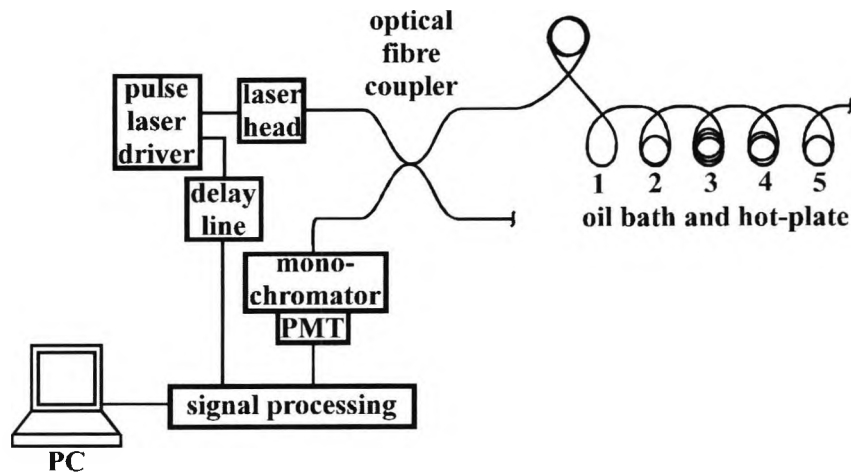


Fig.1.8 Experimental setup for high spatial resolution distributed optical fibre sensor

A digital time-correlated single-photon counting technique[61][80][81][82] permits the achievement of a high spatial resolution of 0.1m and a temperature resolution of $\sim 2^\circ\text{C}$. The experimental arrangement is shown in Fig.1.8. Laser pulses from a semiconductor gain-switched laser are launched into a multimode graded-index fibre through a fibre coupler. The laser pulse width was adjusted to be 200ps. Anti-Stokes and Stokes backscattered photon distributions were measured for different temperatures of the hot regions and the measurement time for each temperature was 1 minute. This represents the best performance achieved for a DART system to date.

Improvements to a Raman-scattering based temperature system in terms of its special application have been reported very recently, such as high temperature sensing[82], temperature sensing in the nuclear environment[83] and a low cost distributed sensing system[84]etc.

1.4.4 Brillouin scattering

Several systems based on Brillouin scattering in optical fibres have been demonstrated since the Brillouin frequency shift depends linearly on the fibre strain[85][86]. However as the Brillouin shift also depends on the fibre temperature[87], this approach has suffered from temperature cross-sensitivity problems. The spontaneous Brillouin scattering efficiency is approximately 20dB weaker than that of Rayleigh scattering, but can be enhanced by using the stimulated scattering process[88].

Several developments have occurred in this area over the past years which have led to dramatic advances in the capabilities of the Brillouin approach. The University of Kent has demonstrated an arrangement where the sensing fibre follows a double path in the structure to be monitored, attached to the structure one way, and thus subjected to both temperature and strain, and loose on the return path, measuring the temperature only[89]. A temperature resolutions of 1°C and a strain sensitivity of 25µε with a spatial resolution of ~1m have been achieved[90]. However, further efforts are necessary to realize a cost effective and viable system in field applications.

An attractive alternative is to determine simultaneously the temperature and strain by measuring both the Brillouin frequency shift and the spontaneous Brillouin power level[91], the system arrangement for which is shown in Fig.1.9. Any variation in the Brillouin power due to fluctuations in the input power, or to fibre attenuation, can be corrected for by ratioing the Brillouin signal to the Rayleigh signal (Landau-Placzek ratio)[92][93][94], but this process is only accurate in the linear regime and hence

limits the obtainable signal level. A further development has shown[91][95] that it is feasible to work with increased laser power, in the non-linear backscatter regime, by using a linearized Brillouin power which is defined in terms of the measured Stokes and anti-Stokes powers. Preliminary results show a strain resolution of $100\mu\text{m}$ strain, a temperature resolution of 4°C , and a spatial resolution of 40m, over a sensing length of 1200m.

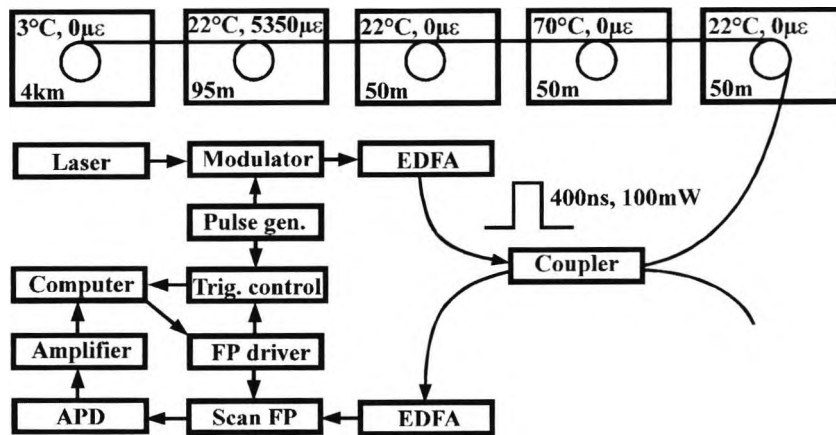


Fig.1.9 Experimental arrangement for Brillouin scattering based measurements

Spontaneous Brillouin scattering is temperature-dependent and provides a signal which is an order of magnitude greater than that from spontaneous Raman scattering. Advances in narrow bandwidth pulsed laser technology and low loss all-fibre filters allow the Brillouin signal to be separated from the Rayleigh signal. Theoretical analysis has demonstrated that distributed temperature sensing based on Brillouin scattering offers a considerably increased range, beyond the theoretical limit of the spontaneous Raman based sensor[96].

1.4.5 Single-shot distributed optical-fibre temperature sensing

A forward scattering-based system, providing “single-shot” distributed optical-fibre temperature sensing using the frequency-derived technique, would be useful in industrial environments that require rapid hot-spot detection, for example. In this technique[97] a high power, circularly polarized pulse of light launched into a high-birefringence fibre induces a transient birefringence grating by means of the optical Kerr effect; the grating spacing will be equal to the birefringence beat length. The local fluctuation of power at any point occurs at a rate (the derived frequency) that depends on the value of the local birefringence at each location which is effectively scanned by the pump pulse as it propagates along the length of the fibre. Hence the technique permits making a distributed measurement of any physical parameter, such as temperature, that is capable of modifying the fibre birefringence.

This technique could be a valuable asset for measurement of either temperature or strain when the allowable measurement time is very limited. The temperature accuracy was $\pm 1.2^{\circ}\text{C}$ and spatial resolution, although temperature dependent, was 0.56m at 150°C [61].

1.5 Fibre Bragg grating sensors

Gratings are simple, intrinsic sensing elements which can be photo-inscribed into a silica fibre[98-104] and have all the advantages normally attributed to fibre sensors. In addition, the devices have an inherent self referencing capability and are easily multiplexed in a series fashion along a single fibre[105][106]. Grating-based sensors

appear to be useful for a variety of applications, in particular the area of distributed embedded sensing in materials for creating “smart structures” is of primary interest[107]. Gratings may also prove to be useful as the optical sensing element in a range of other fibre sensor configurations; grating-based chemical sensors, pressure sensors, and accelerometers are examples.

This Chapter will give particular emphasis to the area of grating based sensors, including basic quasi-distributed sensors based on Bragg gratings, chirped grating sensing, fibre Bragg grating laser sensors, long period grating sensors and interferometric configurations based on gratings.

1.5.1 Bragg grating point sensors

The basic principle of operation commonly used in a FBG-based sensor system is to monitor the shift in wavelength of the returned “Bragg” signal with the changes in the measurand (e.g. strain, temperature). The Bragg wavelength, or resonance condition of a grating, is given by the expression (1.1)[105]

$$\lambda_B = 2n\Lambda \quad (1.1)$$

where Λ is the grating pitch and n is the effective index of the core. With such a device, injecting light from a spectrally broadband source into the fibre, a narrowband spectral component at the Bragg wavelength is reflected by the grating. In the transmitted light, this spectral component is missing, as depicted schematically in Fig.1.10.

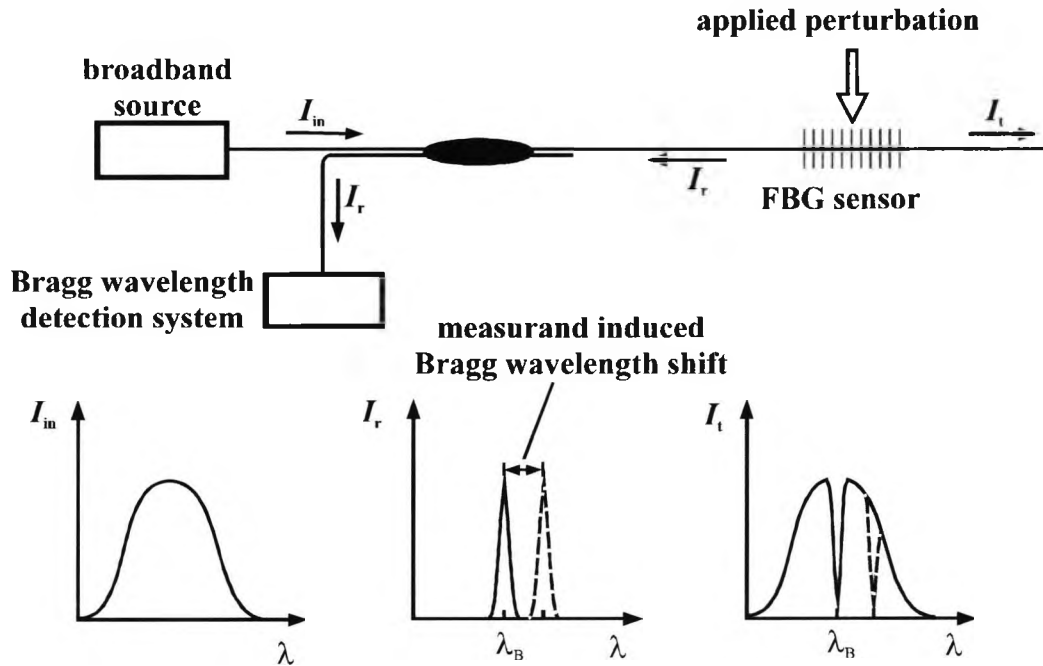


Fig.1.10 Basic Bragg grating-based sensor system with transmissive or reflective detection options

Most of the recent work on fibre Bragg grating sensors has focused on the use of these devices for providing quasi-distributed point sensing of strain or temperature. The strain response arises due to both the physical elongation of the sensor (and corresponding fractional change in grating pitch), and the change in fibre index due to photoelastic effects, whereas the thermal response arises due to the inherent thermal expansion of the fibre material and the temperature dependence of the refractive index.

The nature of the output of Bragg gratings provide these sensors with a built-in self-referencing capability. As the sensed information is encoded directly into wavelength, which is an absolute parameter, the output does not depend directly on the total light levels, losses in the connecting fibres and couplers, or source power[107]. This is widely acknowledged as one of the most important advantages of these sensors. The

wavelength encoded nature of the output, however, also facilitates wavelength division multiplexing by allowing each sensor to be assigned to a different “slice” of the available source spectrum. This enables quasi-distributed sensing of strain, temperature, or potentially other measurands by associating each spectral slice with a particular spatial location. The upper limit to the number of gratings which can be addressed in this way is a function of the source profile width and the operational wavelength bandwidth required for each grating element.

1.5.1.1 Quasi-static strain monitoring

Several techniques have been demonstrated and shown to be quite reliable for performing this wavelength analysis. A ratiometric approach based on the use of broadband filters was the first approach to be demonstrated[108]. This method allows the shift in the FBG wavelength of the sensor element to be assessed by comparing the transmittance of the FBG-reflected light through a filter to that passed through a direct reference path. In order to enhance its sensitivity, an improved method using fibre-wavelength-division multiplexing coupler has been demonstrated [109][110] and other types of filters, such as biconical fibre filters have also been used for this purpose[111].

One of the most successful techniques for interrogating FBG sensors is based on the use of a tunable passband filter for tracking the FBG signal. The most commonly used technique is based on the use of Fabry-Perot (FP) filters[112], acousto-optic filters[113][114] and FBG-based filters[115][116]. Resolutions on the order of $\pm 1 \mu\epsilon$ (microstrain) have been achieved with the FP approach, and up to 16 gratings have

been multiplexed on a single fibre[107]. The use of an optical switch allows such an instrumentation system to address several “arrays” of gratings and a system for tracking up to 60 grating sensors has been developed[117].

Other forms of direct spectroscopic tools for analyzing the return signals are analysis via use of a CCD spectrometer[107] and Fourier transform spectroscopy (FTS)[107]. An all-fibre scanning interferometer[118] has been demonstrated with a 30-cm optical path difference (OPD) scan capability for FTS analysis with a wavelength resolution of 0.015nm. An alternative is to obtain higher wavelength resolution (0.005nm) for a far shorter OPD scan (1.2mm)[119][120]

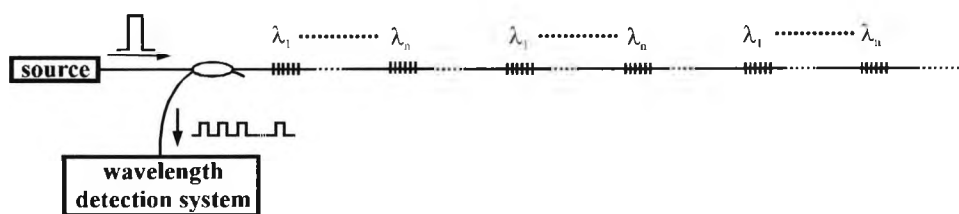
Another recently developed demodulation scheme has utilized the broadband, ultra-short pulses generated by a passively mode locked fibre laser[121] and it is believed that 1 $\mu\epsilon$ sensitivities could be obtained by this method.

1.5.1.2 Time- and wavelength-division multiplexing

A primary advantage of using FBGs for distributed sensing is that large numbers of sensors may be interrogated along a single fibre. WDM provides for tens of sensors per fibre, but time-division multiplexing (TDM) can multiply this number several times by re-using of the spectrum of the source[107]. With mixed WDM/TDM in the serial configuration of Fig.1.11(a), several wavelength-stepped arrays are concatenated, each as a greater distance along the fibre. By launching a short pulse of light from the source, the reflections from FBGs at successively more distant positions along the

fibre, will return to the detector at successively later times. The detection instrumentation is configured to respond to the reflected signals only during a selected window of time after the pulse is launched, so that a single WDM set of sensors is selected for detection. This approach has been demonstrated using a 3×3 grating array with a time-gating at the detector combined with a scanning FP filter wavelength detection[122]. This approach has the potential to be expanded to much larger arrays, e.g., 10×10 for example for a 100-element system would be feasible with current components: however, two deleterious effects can arise with strong reflectors. FBGs whose reflected light signals are separated in time, but which overlap in wavelength can experience cross-talk through what can be termed “multiple-reflection” and “spectral shadowing”[107]. The TDM/WDM parallel and branching optical fibre network topologies of Fig.1.11(b) and (c) eliminate these deleterious effects, but at the price of reduced overall optical efficiency and the need for additional couplers and stronger FBGs.

A new multiplexing scheme was developed and experimentally realized very recently by Dakin et al[123]. It uses pairs of gratings with different spacings along a fibre line and with interrogation of their reflections using a scanning Michelson interferometer to separate their returns in the coherence domain.



(a)

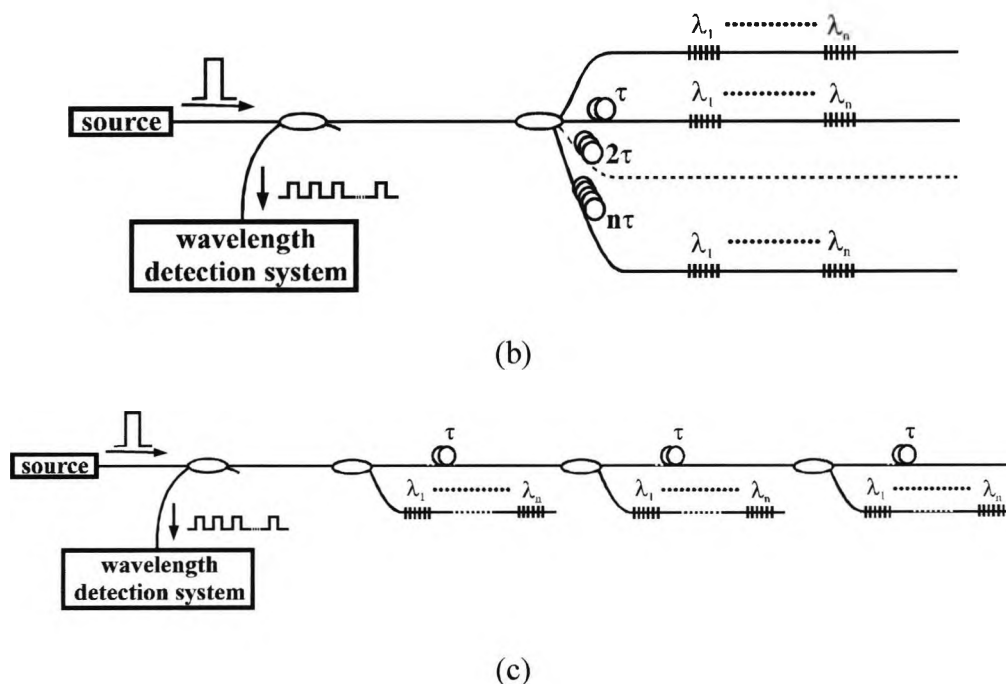


Fig.1.11 WDM/TDM addressing topologies for FBG arrays. (a) Serial system with low reflectivity gratings, (b) parallel network, and (c) branching network

Another important alternative is the combination of wavelength and spatial division multiplexing which has been developed by Yu et al[124][125].

1.5.1.3 Dynamic strain sensing

The interferometric configurations, due to the inherent wavelength dependence of the phase of an unbalanced interferometer on the input wavelength, have been shown to be very sensitive to dynamic strains[126][127]. Very recently, a method to improve the sensing resolution by locking a diode laser wavelength to the mid-reflection wavelength of a fibre-Bragg grating has been discussed[128].

1.5.1.4 Temperature/Strain discrimination

One approach to this problem is to locate two sensor elements which have very different responses to strain (K_{ϵ_1} , K_{ϵ_2}) and temperature (K_{T_1} , K_{T_2}) at the same point on the structure (collocated sensors). Then a matrix equation

$$\begin{pmatrix} \Delta\lambda_1 \\ \Delta\lambda_2 \end{pmatrix} = \begin{pmatrix} K_{\epsilon_1} & K_{T_1} \\ K_{\epsilon_2} & K_{T_2} \end{pmatrix} \begin{pmatrix} \epsilon \\ T \end{pmatrix} \quad (1.2)$$

can be written and inverted to yield strain and temperature from measurements of the two wavelength shifts. The success of this technique depends on the ratio of the strain responses of the two sensors being different from the ratio of their temperature responses, so that the determinant of the matrix is non-zero[107]. Sensitivities of $1\text{pm}(\mu\epsilon)^{-1}$ and $10\text{pm}(\text{°C})^{-1}$ have been reported[129][130] for a wavelength of $1.3\mu\text{m}$. Several techniques have been discussed and demonstrated for parameter discrimination, including incorporating reference gratings, using two gratings in series with one isolated from strain[131]; or two gratings on opposite sides of a thin test-object, so each has experienced the same temperature[132]; or the use of a grating and an extrinsic FP in series, so that the extrinsic sensor depends mainly to strain variations and the grating is used to determine temperature[133][134]. Alternatively, in a dual wavelength approach, Xu et al[135] measured the responses of a co-located 850 and 1300nm pair of FBGs, and found that the responses were 6.5% higher for strain and 9.8% less for temperature at 1300nm compared to 850nm. Using different gratings, a composite sensor formed from two gratings with different cladding diameters[136], spliced together, so that when subjected to strain, they experience different individual strains, greater in the one with the smaller cladding. The temperature sensitivity,

however, is similar in the two gratings. In another version, a single grating is used with a tapering cladding diameter[137]. Further, using an FBG and a long period rocking filter, Kanellopoulos et al[138] reported simultaneous strain and temperature measurement using an FBG and a long period rocking filter in the 800nm band, and obtained errors of $\pm 165 \mu\epsilon$ and $\pm 1.5^\circ\text{C}$. A Long period grating (LPG) combined with FBG[139] has been used, for in the long period grating, the wavelength shifts for strain and temperature were $0.5\text{pm}(\mu\epsilon)^{-1}$ and $60\text{pm}(\text{C})^{-1}$, and for the Bragg grating were $1.0\text{pm}(\mu\epsilon)^{-1}$ and $9\text{pm}(\text{C})^{-1}$, giving a well-conditioned transformation. Resolutions of $10\mu\epsilon$ and 1°C were inferred. Using only long-period gratings[140], the two wavelengths relate to two different cladding modes, and with a fibre Bragg grating rosette[141], satisfactory results were obtained that allowed the use of this rosette on plane structures under different loading conditions.

1.5.2 Chirped grating sensors

Byron et al. first demonstrated a method for making chirped gratings by tapering a fibre in the region of the grating[142]. An alternative method, demonstrated by Hill et al[143], involves bonding an unchirped grating to a substrate with a “soft glue” that allows a strain gradient to be formed along the grating length through the differential shear strength of the glue.

The response of a tapered grating to strain results in a broadening and a shift in the Bragg condition, while temperature affects only the location of the centroid through the temperature-dependent index of refraction (dn/dT). By carefully calibration and

simultaneously measuring the spectral shift and its broadening, in principle such devices can be used to measure simultaneously strain and temperature[144].

Another example of the use of chirped fibre Bragg grating sensing elements is to utilize a grating with an asymmetric broadband spectral response as a strain sensitive reflective filter[145]. The concept is particularly suitable for use with simple optical time domain reflectometry addressing a large number of such weakly reflecting gratings.

The changes in the reflection spectrum caused by a nonuniform measurand field along the length of a grating forms the basis of a relatively recent and potentially powerful technique called intra-grating sensing. This approach involves detailed analysis of the reflection spectrum in order to obtain a continuous profile of the measurand over the length of the grating. Profiles of grating lengths ranging from 5mm to 10cm have been reported[146]-[150], with a spatial resolution as low as 0.4mm[146].

1.5.3 Long period grating sensors

In 1995, Vengsarkar et al[151] introduced a new type of fibre grating device, the long period grating (LPG), to the optics community. LPGs have presented unique opportunities as fibre optic sensors. The centre wavelengths of the LPG resonances depend critically on the index difference between the core and the cladding, and hence any variation caused by strain or temperature, or changes in the external refractive index can cause large wavelength shifts in the resonances. The strain and temperature

response of a long period grating resonance can be either positive or negative, depending on the differential responses of the core and cladding[152-155]. The long period grating is particularly useful for multi-parameter sensors such as the strain and temperature sensors discussed earlier in this Chapter. Another important application of the long period grating is the area of environmental monitoring by using the sensitivity of the LPG to the surrounding refractive index[156] as a means to determine the measurand.

1.5.4 Bragg grating laser sensors

The basic form of a fibre Bragg grating laser sensor (FBGLS) utilizes either two gratings of matched Bragg wavelength to create an in-fibre cavity, or one grating combined with a broadband reflector. The use of a doped fibre section (e.g. using erbium) between the gratings or a grating and a reflector allows the system to be optically pumped to provide cavity gain and thus allow lasing to occur. The device can be implemented in various ways and operated in either a single frequency or multimode fashion[157]-[159]. When configured as a sensor element, changes in the environmental conditions experienced by the laser cavity and the gratings can be detected by monitoring the change in some specific characteristic of the output. For strain or temperature variations of the gratings themselves, the shift in the wavelength of the laser output is identical to that obtained with the passive approach for monitoring FBGs. With FBG laser sensor configurations, however, it is also possible to detect some effects as the beating between different longitudinal cavity or polarization modes in the system[160]. As with basic FBG sensing, the inherent

wavelength division-addressing capabilities of the gratings also allows distributed laser-sensors to be implemented[161][162].

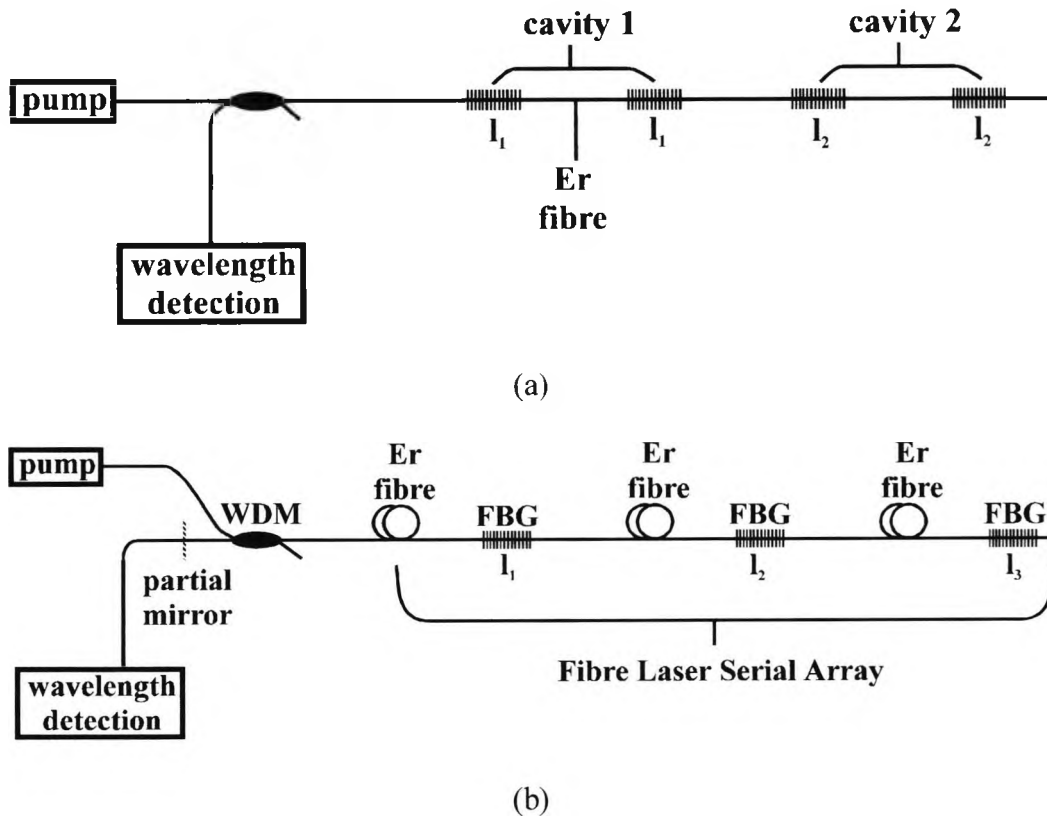


Fig.1.12 Basic fibre Bragg grating laser sensor systems: (a) short cavity FBG-pair lasers and (b) extended cavity FBG lasers

Fig.1.12 illustrates two examples of the types of fibre laser sensors which have been demonstrated[107]. In Fig.1.12(a), short cavity fibre lasers created by gratings of matched wavelength are remotely pumped. The grating lasers, which can be as short as ~3cm in length, behave as sensors with a gauge length equal to the length of the cavity, with the same spectral responsivity as a normal FBG element. The advantage of the laser configuration is, however, the fact that the bandwidth of the output light from the laser sensor can be much narrower than that from a passive FBG sensor system. In Fig.1.12(b), a system which incorporates a series of FBG reflectors in a

composite cavity configuration is shown[162]. In this system, each laser (defined by the partial broadband reflector and each of the FBG elements) can lase simultaneously. Providing each laser is preset (by the FBG wavelengths) to operate at a nominally different wavelength, the outputs can be analyzed simultaneously using a wavelength detection system of the type described in Section 1.5.1. A system capable of resolving very small shifts in the wavelength of the output, such as the unbalanced Mach-Zehnder interferometric technique, can produce a very high sensitivity to weak dynamic strains[163]. Fibre lasers can be used for the detection of various measurands, such as in fibre laser gyroscopes[164], current sensors[165][166] etc.

1.5.5 Interferometric sensors

An additional use of Bragg gratings is to form interferometric sensor elements[167-169]. In this case, the gratings serve merely as reflectors which define the interferometric paths. In addition to acting simply as full or partial reflectors, the wavelength selective nature of the gratings provides unique capabilities and configurations to be implemented. The most obvious extension of this is to the implementation of WDM/TDM interferometric arrays[170]. It has also demonstrated that the use of gratings can allow selective interrogation of overlapping “nested” interferometers implemented in common fibre paths[171]. Other interesting possibilities also exist for implementing novel interferometric sensors such as operating Michelson and FP elements using chirped grating reflectors[172].

1.6 Luminescent optical fibre sensors

The development of fibres doped with materials through which luminescence is generated has a long history, which follows upon the original proposal by Snitzer[173] in the early 1960s of the use of an optical fibre geometry for lasers and optical amplification, employing 300 μm core diameter neodymium doped fibre[174]. Subsequent development of this concept has been the major reason for the production of a range of different types of optical fibre, doped with appropriate materials to show fluorescence. The discussion of the use of luminescent fibres in sensing in this section excludes the considerable use of optical fibre in lasers and amplifiers, which has been discussed in detail formerly by Langford[175] and latterly by Kim[176]. Further, the use of other luminescent phenomena such as are produced by nonlinear effects, typically Raman and Brillouin scattering, has been discussed in section 1.4 and elsewhere, for example in the work of Grattan and Zhang[177][178] and Rogers[179].

The use of luminescent phenomena, concentrating particularly on fluorescence for optical sensing, has been observed with a range of different fibre hosts. Clearly those rare earths which have been doped into silica-based fibres particularly, or alternatively into fluoride glass or more exotic fibre materials, can equally be applied to the creation of laser action as to the generation of simple fluorescence. However, there is a wide range of other fluorescent materials which have been doped into plastic fibres, offering an alternative medium, particularly for sensing applications, where the loss mechanisms in plastic hosts, usually responsible for quenching laser action, are largely unimportant when the fluorescent output only is used. A major difference between silica and plastic

fibre is the extreme flexibility of the latter, which allows it to be bent, often to a greater extent and with a smaller radius than silica fibre.

1.6.1 Luminescent plastic optical fibre (POF) sensors

There are two main types of POFs (as categorized by Laguesse and Rebourgeard[180]). These are: (1) fluorescent fibres which are sensitive to visible radiation containing dopants which produce longer wavelength (usually visible) emission; (2) scintillating fibres which are excited by either ultraviolet or deep ultraviolet radiation, or are excited by alpha, beta and gamma emission, or X-rays (ionizing radiation). These are discussed separately in the following.

1.6.1.1 Fluorescent POF sensors

Fibres in this category are typically doped with organic dyes, of the type used extensively in the printing industry and for display. They are frequently used for decorative purposes, but clad and coated fibres with a fluorescent core are often exploited in sensing and measurement as a result of their ability to capture light, which excites them over their whole length. They can be used to measure mean ambient lighting[174], monitor faults in electrical circuits and switches[174] and for level detection[181], intruder detection and hole detection in moving tapes, etc.[174]. Other important applications involve environmental sensing with plastic fibres, such as the humidity sensor developed by Muto et al[182] and the sensor developed by Sawada et al for detecting gaseous pollutants[183].

1.6.1.2 Scintillating POF sensors

Scintillating optical fibres are similar to those discussed previously, except that the dopant used has an absorption at a shorter wavelength and in particular responds to ionizing radiation, yielding a luminescent (fluorescence) emission. They can be used as track detectors, high-resolution spatial detectors and for particle and energy measurement. Recent work has allowed their application in molecular biology[174].

1.6.2 Luminescent silica-based optical fibre sensors

Fluorescent techniques in optical sensing using crystalline materials coupled to optical fibres have been applied regularly to the measurement of pressure and temperature, and such work has been discussed in detail by Grattan and Zhang[177][178]. However, with the rise in the use of rare earth doped fibres for communications, a number of valuable devices have been produced for sensing as well.

Silica-based fibres have the advantage of both lower attenuation and higher durability over plastic fibres for some specific sensing applications. The variety of such fibres available has increased dramatically over the years, from the early use of the most successful of the laser solid-state media, neodymium-doped glass, to sensors containing erbium, thulium, praseodymium, holmium and ytterbium, for example. Their potential for high-temperature use is particularly important, and has strongly influenced the development of a range of devices, especially temperature sensors for use in extreme environment.

1.6.2.1 Neodymium-doped fluorescence-based sensors

A detailed investigation of the characteristics of an Nd^{3+} doped fibre, based on alumino-silicate glass and in particular under extreme temperature conditions, has been reported by Zhang et al[184], in which the annealing behaviour of the fibre has been exploited and discussed in detail so as to achieve a stable and reproducible response. The relationship between the fluorescence intensity and the length of the doped fibre has also been investigated[174].

An unusual exotic neodymium fibre reported by Satoh and Imai[185], comprising a multilayered concentric structure consisting of a neodymium-doped optical fibre, an inner electrode, a piezoelectric copolymer and an outer aluminum electrode, may have wider non-laser uses in interferometric sensing.

1.6.2.2 Erbium-doped fluorescence-based sensors

The effects of high temperature on sensors based on commercial erbium-doped fibres, at temperatures up to 1100°C , have been discussed in a comprehensive paper by Zhang et al[186]. The underpinning science of the luminescent effects in such fibres, for example the upper levels of Er-doped silica fibres, was explored by authors such as Mazzali et al[187] and Maurice et al[188], who developed a spectroscopic study of the fluorescence resulting from the pumping of Er-doped fibre, excited in the 800nm region. In further work, Maurice et al[189] reported results on an intensity-based sensor, dependent on the thermal behaviour of the relative emission at 530nm and 555nm, obtaining a calibration curve in the temperature region from 100 to 1000K.

Research by Imai et al[190] reported pumping at $1.48\mu\text{m}$, observing the more familiar broad $1.54\mu\text{m}$ fluorescence spectrum, using the intensity ratio of the fluorescence emission at $1.530\mu\text{m}$ and $1.552\mu\text{m}$ as a means of temperature sensing. In addition, Ko et al[191] have reported a distributed temperature sensor, the characteristics of which were an operational range of 77-425K, a spatial resolution of 10m and a measurement length of 100m, with a sensitivity of $-0.23\%K^{-1}$.

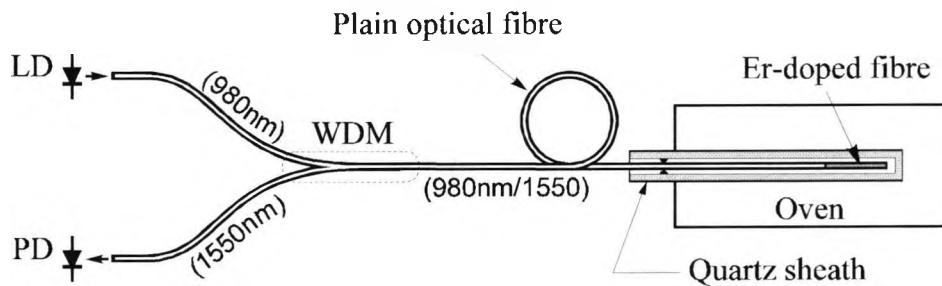


Fig.1.13 Schematic diagram of the probe arrangement. LD, laser diode; PD, photodiode; WDM, wavelength division multiplexer

An investigation of the fluorescence characteristics of Er^{3+} -doped fibres in high temperature sensing has been given by Zhang et al[192]. The experimental arrangement used in the study is depicted in Fig.1.13. Their temperature sensitivities increase significantly at temperatures above $\sim 500^\circ\text{C}$, from $\sim 2.5\mu\text{sK}^{-1}$ to $\sim 12\mu\text{sK}^{-1}$ over $0\text{-}400^\circ\text{C}$ and $700\text{-}900^\circ\text{C}$ regions, respectively.

1.6.2.3 Thulium-doped fluorescence-based sensors

The fluorescence lifetime of the Tm-doped fibre was measured, along with the intensity, against temperatures from 50°C to 1250°C as has been reported recently by Zhang et al[193], where it was seen that the lifetime decreases monotonically from $\sim 63\mu\text{s}$ at 100°C to $\sim 15\mu\text{s}$ at 1250°C .

1.6.2.4 Other rare-earth doped sensors

In the work of Oh and Pack[194], detection of CO₂ as low as 1 weight% was made with an amplified spontaneous emission (ASE) light source of high spectral density in the 2µm region from a Tm³⁺/Ho³⁺ co-doped silica fibre pumped at 800nm. Such a scheme could have wider applications to the sensing of other gases, especially due to the higher absorption of many gases in the spectral region with wavelengths greater than 2.0µm, using a wide variety of doped and codoped fibres, exploiting the far infrared emission available in a wide spectral bandwidth. Sm³⁺ doped fibre, pumped by light from an Ar ion laser, has been used by Wang et al[195] to generate the synthetic wavelength from two individual wavelengths which are closely matched spatially for the extension of the range of an interferometer[196]. The use of Yb doped fibre for temperature sensing has been investigated by the author and the others and will be discussed in detail in Chapter 3. The Yb co-doped Er laser has been used for the detection of neptunium using the 980nm emission line[197].

1.6.2.5 Quasi-distributed and average temperature sensors

There is a rising interest in developing both multipoint sensor systems, which are cheaper than the fully distributed plain silica fibre devices available which exploit nonlinear effects in fibres[198] and average temperature sensing systems, for which a number of industrial applications exist. Doped fibre fluorescence-based sensors, each best suited to a particular temperature range, yet pumped by the same light source and emitting over the same spectral region, make for a very simple, convenient and promising optical arrangement, well suited to real-time, temperature sensor systems,

which has been investigated by the author and the others and will be discussed in detail in Chapter 4.

1.6.3 Other material based luminescent sensors

The work of Digonnet[199] lists the wide range of transitions over a significant wavelength range from the blue, through to the mid-infrared region, in both oxide (silica) and fluoride materials. Except for the applications discussed above, the potential for new uses can also be seen, such as those for gas sensing[200] and chemical sensing[201]. As discussed, the bulk of fibre sensor and laser applications have been using silica or plastic fibres. Alternatives include the heavy metal fluoride glass fibres, which possess characteristics different from those of silica. They show superior optical and mechanical properties in fibre form to the bulk material, which dated from the work of Poulain et al[202] in the mid-1970s. Typically the most stable heavy-metal fluoride glass is the so-called ZBLAN (made up from fluorides of zirconium, barium, lanthanum, aluminum and sodium)[174]. A significant breakthrough has been seen for the important 3-5 μ m wavelength region through the use of new glasses based on gallium lanthium sulfide(GLS), where the first lasing results with neodymium-doped multimode GLS fibre have been reported[203][204]. The convenience of fibre optic methods for remote radiation monitoring in hazardous or difficult to access sites, such as nuclear waste dumps, or in sampling methods for *in situ* ground water monitoring, has made them the subject of considerable research[174].

1.7 Summary of recent work – influence on the direction of this thesis

Some of the significant developments in fibre optic sensing which have occurred over the past 5 to 10 years have been reviewed, particularly in the areas of interferometric sensing, distributed sensors, Bragg grating based systems and luminescent optical fibre sensing system. Interferometric continue to attract strong interest, with steady, incremental improvements in the performance of the technology.

In the area of distributed fibre sensors, very significant advances have been realized, particularly in the area of Brillouin scattering-based systems.

Fibre Bragg grating sensors currently represent one of the most exciting and strongest growth areas in fibre sensing. Much of this work is driven by the need to develop distributed strain sensor systems for the smart structures community. Bragg gratings can , however, be used as the fibre sensing element in a host of other applications, and some interesting possibilities exist for the development of multiparameter sensor suites based on FBGs. Gratings are also currently being investigated for use in fibre laser sensors configurations, which can be configured for ultrahigh strain sensitivity applications.

Compared with other techniques discussed above, the structure of the luminescent sensing system is relatively simple, cheap and because most of the systems are lifetime based, they are robust as well. The sensing system is quite popular and promising in

temperature sensing due to the fact that most of the active luminescent materials are strong temperature-dependent. Chapter 2 will focus on the development of luminescence-based thermometry and the rest of the Chapters in this thesis will discuss further improvements based on the previous work.

1.8 Aims and objectives of the work

This work is aimed to further research on luminescence-based sensors, mainly for temperature sensing, taking as a basis the previous work done by the City University group and others as discussed earlier and in more detail in subsequent Chapters. The major objectives of the work are to:

- Develop several different temperature sensor systems to cover a wide range from the cryogenic to up to several hundred degrees celsius
- Meet the specification given in Chapter 3 for competitive temperature sensor systems using optical techniques
- Explore new active fluorescent materials, especially those cheap, available “spin-off’s from telecommunications research, for their sensing range, sensitivity and accuracy for each specific application.
- Explore the underpinning science of the luminescent effects to support the system design activity
- Extend the point luminescence-based temperature sensing approach to multipoint and average or local temperature sensing, where a number of industrial applications exist and develop corresponding mathematical approaches suited for real time processing

- Explore the potential strain sensitivity of rare earth doped fibres for their possible application for the discrimination of temperature and strain.
- Intercompare different luminescence-based temperature sensing techniques and their corresponding applications range
- Publication in the international literature

1.9 Structure and design of the thesis

The structure of the thesis is such as to illustrate a range of developments in optical fibre sensor technology to meet the objectives given.

Following upon an Introduction (Chapter 1) which sets the scene and reviews in some detail the background to various fibre optic sensing techniques, the aims and objectives and structure of the thesis are laid out at the end of the Chapter. Chapter 2 presents a more detailed background discussion and review of fibre optic luminescent thermometry, discussing a major effect in the field of phosphor thermometry over the past few decades from cryogenic temperatures to those approaching 2000°C. Chapter 3 discusses a large variety of luminescent materials for wide-range fluorescence-lifetime based point temperature measurement, with corresponding underpinning science. Chapter 4 introduces a new signal processing technique in multiple exponential decay deconvolution and its application in fluorescence based quasi-distributed temperature sensing system. Chapter 5 extends luminescent sensing system for specific application, such as average temperature sensing and local temperature detection, accompanied by relevant signal processing schemes. Chapter 6 presents for

the first time the fact that rare earth doped fibres are sensitive to strain as well as to temperature. Sensitivity comparison has been made and discussed for possible simultaneous strain and temperature discrimination. Finally in Chapter 7, the performance of the two most promising fluorescence-based temperature sensing techniques, namely the fluorescence intensity ratio (FIR) and fluorescence lifetime (FL) schemes, have been compared. Chapter 8 presents an overall summary and suggestions for future work.

1.10 Summary

This chapter has contained a brief review of some recent developments in the area of fibre optic sensor technology, focusing on four of the most important techniques, that is, the interferometric sensing technique, intrinsic distributed sensing, Bragg grating based sensing and luminescent sensing. Practical achievements have also been influencing various industrial sectors, like the petroleum industry, water resources management, energy production or aerospace and aeronautics. The aim of this thesis is to further the research on one of the techniques, luminescence based temperature sensing building on the previous work done by the researchers all over the world and the detail will be expanded on in the following Chapters.

1.11 References

- [1] H.C.Lefèvre, Optical fibre sensors: has their time come? *European Workshop on Optical Fibre Sensors*, 8-10 July 1998, Peebles, Scotland, 3483, 2(1998)

Chapter 1 Fibre Optic Sensor Technology

- [2] Eds. K.T.V.Grattan and B.T.Meggitt, *Optical Fibre Sensor Technology*, Chapman & Hall, London, 1995
- [3] D.N.Payne and J.P.Dakin, Communicating with fibres, *EUROSENSORS XII*, Southampton, 13-16 September 1998, Plenary Papers, 1(1998)
- [4] Fibre sensors survive radiation tests, *Opto & Laser Europe*, Issue 57, December 1998, 15(1998)
- [5] A.D.Kersey, A review of recent developments in fiber optic sensor technology, *Optical Fiber Technology*, 2, 291(1996)
- [6] J.A.Bucaro et al, Fiber optic hydrophone, *J. Acoust. Soc. Am.*, 62, 1302(1977)
- [7] C.D.Butter and G.E.Hocker, Fiber optics strain gauge, *Appl. Opt.*, 17, 2867(1978)
- [8] D.A.Jackson et al, Elimination of drift in a single-mode optical fiber interferometer using a piezoelectrically stretched coiled fiber, *Appl. Opt.*, 19, 2926(1980)
- [9] A.Dandridge and A.B.Tveten, Phase compensation in interferometric fiber optic sensors, *Opt. Lett.*, 7, 279(1982)
- [10] J.H.Cole, B.A.Danver and J.A.Bucaro, Synthetic heterodyne interferometric demodulation, *J. Quant. Electron.*, 18, 694(1982)
- [11] A.D.Kersey, D.A.Jackson and M.Corke, Passive compensation scheme suitable for use in single mode fiber interferometer, *Electron. Lett.*, 18, 392(1982)
- [12] A.Dandridge, A.B.Tveten and T.G.Giallorenzi, Homodyne demodulation scheme for fiber-optic sensors using phase generated carrier., *J. Quant. Electron.*, 18, 1647(1982)

Chapter 1 Fibre Optic Sensor Technology

- [13] Y.Lu and R.Pechstedt, A study of effects of phase modulator characteristics on interferometer system performance, *European Workshop on Optical Fibre Sensors*, 8-10 July 1998, Peebles, Scotland, 3483, 146(1998)
- [14] K.J.Williams, A.Dandridge, A.D.Kersey, J.F.Weller, A.M.Yurek and A.B.Tveten, Interferometric measurement of low frequency phase noise characteristics of a diode pumped Nd:YAG ring laser, *Electron. Lett.*, 25, 774(1989)
- [15] K.H.Wanser et al, Measurement of fundamental thermal phase fluctuations in optical fiber, *Proc. OFS-9*, Florence, 255(1993)
- [16] K.Krakenes and K.Blotekjær, Thermal noise in optical fibers – Mach-Zehnder vs. Sagnac interferometers, *Proc. OFS-10*, Glasgow, 572(1994)
- [17] B.Y.Kim, Fiber lasers for sensing, *European Workshop on Optical Fibre Sensors*, 8-10 July 1998, Peebles, Scotland, 3483, 12(1998)
- [18] G.A.Ball and W.W.Morey, Continuously tunable single mode erbium fiber laser, *Opt. Lett.*, 17, 420(1992)
- [19] G.A.Ball and W.W.Morey, Narrow linewidth fiber laser with integrated master oscillator-power amplifier, *Proc. OFC'92*, 97(1992)
- [20] D.W.Stowe, D.R.Moore and R.G.Priest, Polarization fading in fibre interferometric sensors, *J. Quant. Electron.*, 18, 1644(1982)
- [21] N.J.Frigo, A.Dandridge and A.B.Tveten, Technique for the elimination of polarization fading in fiber interferometers, *Electron. Lett.*, 20, 319(1984)
- [22] A.D.Kersey and M.J.Marrone, Input-polarization scanning technique for overcoming polarization-induced signal fading in interferometric fiber sensors, *Electron. Lett.*, 24, 931(1988)

Chapter 1 Fibre Optic Sensor Technology

- [23] K.H.Wanser and N.H.Safar, Remote polarization control for fiber optic interferometers, *Opt. Lett.*, 12, 217(1987)
- [24] A.D.Kersey, A.Dandridge and A.B.Tveten, Dependence of visibility on input polarization in interferometric fiber-optic sensors, *Opt. Lett.*, 13, 288(1988)
- [25] A.D.Kersey, M.J.Marrone, A.Dandridge and A.B.Tveten, Optimization and stabilization of visibility in interferometric fiber optic sensors using input polarization control, *J. Lightwave Technol.*, 6, 1599(1988)
- [26] A.D.Kersey, M.J.Marrone and A.Dandridge, Observation of input polarization induced phase noise in interferometric fiber optic sensors, *Opt. Lett.*, 13, 847(1988)
- [27] N.C.Pistoni and M.Martinelli, Birefringence effects suppression in optical fiber sensor circuits, *Proc. 7th Int. Conf. on Optical Fiber Sensors*, 125(1990)
- [28] A.D.Kersey, M.J.Marrone and M.A.Davis, Polarization-insensitive fiber optic Michelson interferometer, *Electron. Lett.*, 26, 518(1991)
- [29] M.J.Marrone and A.D.Kersey, Visibility limits in fiber optic Michelson interferometer with birefringence compensation, *Electron. Lett.*, 27, 1422(1991)
- [30] A.Dandridge, A.B.Tveten, A.D.Kersey and A.M.Yurek, Multiplexing of interferometric sensors using phase carrier techniques, *J. Lightwave Technol.*, 5, 947(1987)
- [31] A.Dandridge et al, AOTA tow test results, *Proc. AFCEA/DoD Conf. on Fiber Optics '90*, McLean, 104(1990)
- [32] A.D.Kersey, A.Dandridge and A.B.Tveten, Time-division multiplexing of interferometric fiber sensors using passive phase-generated carrier interrogation, *Opt. Lett.*, 12, 775(1987)

- [33] J.L.Brooks, B.Moslehi, B.Y.Kim and H.J.Shaw, Time-domain addressing of remote fiber-optic interferometric arrays, *J. Lightwave Technology*, 5, 1014(1987)
- [34] J.Sæther and K.Bløtekjær, Optical amplifiers in multiplexed sensor systems-theoretical predictions of noise performance, *Proc. 11th Optical Fiber Sensors Conference*, Sapporo, May 21-24, 1996, 518(1996)
- [35] J.Sæther and K.Bløtekjær, Noise performance of multiplexed fiber-optic sensor systems with optical amplifiers, *Optical Review*, 4, 138(1997)
- [36] J.L.Wagener, C.W.Hodgson, M.J.F.Digonnet and H.J.Shaw, Noise figure characteristics of amplified fiber sensor arrays, *J. Lightwave Technology*, 1999
- [37] J.Sæther and K.Bløtekjær, Optical amplifiers in time domain multiplexed sensor systems, *Proc. 12th International Conference on Optical Fiber Sensors*, Williamsburg, Virginia, October 28-31, 1997, 586(1997)
- [38] A.D.Kersey et al, Demonstration of a 64 channel TDM fiber sensor array, *Proc. OFC96*, San Jose, 1996
- [39] L.Yuan, Optical path automatic compensation low-coherence interferometric fibre-optic temperature sensor, *Optics & Laser Technology*, 30, 33(1998)
- [40] H.S.Choi, H.F.Taylor and C.E.Lee, High performance fiber optic temperature sensor using low-coherence interferometry, *Proc. 12th International Conference on Optical Fiber Sensors*, Williamsburg, Virginia, October 28-31, 1997, 570(1997)
- [41] G.M.Nau, B.A.Danver, A.B.Tveten, A.Dandridge and S.T.Vohra, Fiber optic interferometric displacement sensors for vibration measurements, *Proc. 12th International Conference on Optical Fiber Sensors*, Williamsburg, Virginia, October 28-31, 1997, 582(1997)

- [42] R.Posey, Jr., A.D.Kersey, M.LeBlanc and M.Davis, Low-coherence, wavelength-encoded addressing for integrated long-gauge length fiber optic strain sensing, *Proc. 12th International Conference on Optical Fiber Sensors*, Williamsburg, Virginia, October 28-31, 1997, 574(1997)
- [43] H.C.Lefevre, White light interferometry in optical fiber sensors, *Proc. OFS-7*, Sydney, Australia, 345(1990)
- [44] W.V.Sorin, High resolution optical fiber reflectometry techniques, *Distributed and Multiplexed Fiber Optic Sensors, II*, Proc. SPIE, 1797, 108(1992)
- [45] K.Takada, K.Vukimatsu, M.Kobayashi and J.Noda, Rayleigh backscattering measurements of single mode fibers by low coherence optical time-domain reflectometer with 14 μ m spatial resolution, *Appl. Phys. Lett.*, 59, 143(1991)
- [46] M.V.Sorin and D.M.Baney, Measurement of Rayleigh backscattering at 1.55 μ m with a 32 μ m spatial resolution, *IEEE Photon. Technol. Lett.*, 4, 374(1992)
- [47] D.Romare, D Sabry-Rizk and K T V Grattan, Digital signal processing techniques for central fringe identification in white-light interferometry, *Applied Optics and Optoelectronics*, 16-19 March 1998, Brighton (Ed. K T V Grattan), 205(1998)
- [48] V.Gusmeroli et al, Absolute and simultaneous strain and temperature measurements by a coherent optical fiber sensor, *Proc. OFS-10*, Glasgow, 199(1994)
- [49] D.A.Flavin, R.Mcbride and J.D.C.Jones, Interferometric fiber optic sensing based on the modulation of group delay and first order dispersion: Application to strain-temperature measurand, *IEEE J. Lightwave Technol.*, 13, 1314(1995)

Chapter 1 Fibre Optic Sensor Technology

- [50] A.M.Vengsarkar, W.C.Michie, L.Jankovic, B.Culshaw and R.O.Claus, Fiber-Optic dual-technique sensor for simultaneous measurement of strain and temperature, *J. Lightwave Technol.*, 12, 170(1994)
- [51] H.Singh and J.S.Sirkis, Simultaneous measuring temperature and strain using optical fiber microcavities, *J. Lightwave Technol.*, 15, 647(1997)
- [52] F.Farahi, D.J.Webb, J.D.C.Jones and D.A.Jackson, Simultaneous measurement of temperature and strain: cross sensitivity considerations, *J.Lightwave Technol.*, 8, 138(1990)
- [53] A.M.Vengsarker, W.C.Michie, L.Jancovic, B.Culshaw and R.O.Claus, Fiber optic sensor for simultaneous measurement of strain and temperature, *Fiber Optic and Laser Sensors, VIII*, Proc. SPIE, 1367, 249(1990)
- [54] W.C.Michie, B.Culshaw, S.S.J.Roberts and R.Davidson, Fiber optic technique for simultaneous measurement of strain and temperature – variations in composite-materials, *Active Materials and Adaptive Structures*, Chap163, 809(1992)
- [55] E.J.Friebele, M.A.Putnam, H.J.Patrick, A.D.Kersey, A.S.greenblatt, G.P.Ruthven, M.H.Krim and K.S.Gottschalck, Ultrahigh-sensitivity fiber-optic strain and temperature sensor, *Optics Letters*, 23, 222(1998)
- [56] C.E.Lee and H.F.Taylor, Interferometric optical fiber sensors using internal mirrors, *Electron. Lett.*, 24, 193(1988)
- [57] K.A.Murphy, Extrinsic Fabry Perot optical fiber sensor, *Proc. OFS-8*, Monterey, CA, 193(1992)
- [58] K.Murphy et al, Quadrature phase shifted, extrinsic Fabry-Perot optical fiber sensors, *Opt. Lett.*, 16, 273(1991)

Chapter 1 Fibre Optic Sensor Technology

- [59] Bhatia et al, Applications of 'absolute fiber optic sensors to smart materials and structures, *Proc. OFS-10*, Glasgow, 171(1994)
- [60] J.Sirkis, T.A.Berkoff, R.T.Jones, H.Singh, A.D.Kersey, E.J.Friebele and M.A.Putnam, In-line fiber etalon (ILFE) fiber optic strain sensors, *IEEE J. Lightwave Technol.*, 13, 1256(1995)
- [61] A.J.Rogers, V.A.Handerek, M.Farhadiroushan, R.Feced, T.R.Parker and F.Parvaneh, Advances in distributed optical-fibre sensing, *European Workshop on Optical Fibre Sensors*, 8-10 July 1998, Peebles, Scotland, 3483, 5(1998)
- [62] M.K.Barnoski and S.M.Jensen, Fiber waveguides: A novel technique for investigating attenuation characteristics, *Appl. Opt.*, 15, 2112(1976)
- [63] J.P.Dakin, Distributed optical fiber sensors, *Distributed and Multiplexed Fiber Optic Sensors, II*, Proc. SPIE, 1797, 76(1992)
- [64] A.J.Rogers, Polarization optical time domain reflectometry, *Electron. Lett.*, 16, 489(1980)
- [65] J.N.Ross, Birefringence measurement in optical fibers by polarization optical time domain reflectometry, *Appl. Opt.*, 21, 3489(1982)
- [66] A.J.Rogers, High resolution frequency-derived distributed optical fiber sensing, *Distributed and Multiplexed Fiber Optic Sensors, IV*, Proc. SPIE, 2294, 2(1994)
- [67] R.E.Schuh et al, Theoretical analysis and measurement of the effect of fibre twist on the polarisation OTDR of optical fibres, *Conference on Optical Fibre Communications, OFC'96*, San Jose, California, FA5(1996)

- [68] R.E.Schuh, J.G.Ellison, A.S.Siddiqui and D.H.O.Bebbington., Polarisation OTDR measurements and theoretical analysis on fibres with twist and their implications for estimation of PMD, *Electron. Lett.*, 32, 387(1996)
- [69] D.H.O.Bebbington et al., Fully polarimetric optical time domain reflectometer with one metre spatial resolution, *Conference on Optical Fibre Communications, OFS'97*, Dallas, Texas, WL24(1997)
- [70] J.J.Ellison and A.S.Siddiqui, A fully polarimetric optical time domain reflectometer, *IEE Photonic Technol. Lett.*, 10, 246(1998)
- [71] A.H.Hartog, A distributed temperature sensor based on a liquid-core optical fiber, *IEEE J. Lightwave Technol.*, 1, 498(1983)
- [72] M.C.Farries, M.E.Fermann, R.I.Laming, S.B.Poole and D.N.Payne, Distributed temperature sensor using Nd³⁺-doped fiber, *Electron. Lett.*, 22, 418(1986)
- [73] M.C.Farries et al, Distributed temperature sensor using Ho³⁺ doped fiber, *Proc. OFS'87*, Reno, NV, 170(1987)
- [74] P.Heinzmann and R.Hofstetter, Temperature dependence of PCS Fiber Characteristics, *Proc. SPIE*, 584, 1985
- [75] G.Oscroft, Intrinsic fiber optic sensors, *J. Opt. Sensors*, 2, 269(1987)
- [76] S.V.Shatalin, V.N.Treschikov and A.J.Rogers, Interferometric optical time-domain reflectometry for distributed optical-fiber sensing, *Applied Optics*, 37, 5600(1998)
- [77] J.P.Dakin et al, Distributed anti-Stokes ratio thermometry, *Proc. OFS-3, San Diego*, postdeadline presentation, 1985

Chapter 1 Fibre Optic Sensor Technology

- [78] J.P.Dakin and D.J.Pratt, Temperature distribution measurement using Raman ratio thermometry, *Fiber Optic and Laser Sensors, III*, Proc. SPIE, 566, 249(1985)
- [79] J.P.Dakin, D.J.Pratt, G.W.Bibby and J.N.Ross, Distributed optical fiber Raman temperature sensor using a semiconductor light source and detector, *Electron. Lett.*, 21, 569(1985)
- [80] R.Stierlin, J.Ricka, B.Zysset, R.Battig, H.P.Weber, T.Binkert and W.J.Borer, Distributed fiber optic temperature sensor using single photon detection, *Appl. Opt.*, 26, 1368(1987)
- [81] D.A.Thorncraft et al. An ultra high resolution distributed temperature sensor, *Proc. OFS-8*, Monterey, 258(1992)
- [82] R.feced, M.Farhadiroushan, V.A.Handerek and A.J.Rogers, A high spatial resolution distributed optical fiber sensor for high-temperature measurements, *Rev. Sci. Instrum.*, 68, 3772(1997)
- [83] F.B.H.Jensen, E.Takada, M.Nakazawa, T.Kakuta and S.Yamamoto, Consequences of radiation effects on pure-silica-core optical fibers used for Raman-scattering-based temperature measurements, *IEEE Transactions on Nuclear Science*, 45, 50(1998)
- [84] Z.Bo, The distributed temperature sensor (DTS) based on correlation technology, *European Workshop on Optical Fibre Sensors*, 8-10 July 1998, Peebles, Scotland, 3483, 142(1998)
- [85] T.Horiguchi, T.Kurashima and M Tateda, Tensile strain dependence of Brillouin frequency shift in silica optical fibres, *IEEE Photon. Technol. Lett.*, 1, 107(1989)

- [86] T.Horiguchi, K.Shimizu, T.Kurashima, M.Tateda and Y.Koyamada, Development of a distributed sensing technique using Brillouin scattering, *J. Lightwave Technol.*, 13, 1296(1995)
- [87] D.Culverhouse, F.Farahi, C.N.Pannel and D.A.Jackson, Potential of stimulated Brillouin scattering as sensing mechanism for distributed temperature sensors, *Electron. Lett.*, 25, 913(1989)
- [88] A.Fellay, L.Thévenaz, M.Facchini, M.Niklès and P.Robert, Distributed sensing using stimulated Brillouin scattering: towards ultimate resolution, *Proc. 12th International Conference on Optical Fiber Sensors*, Williamsburg, Virginia, October 28-31, 1997, 324(1997)
- [89] X.Bao, D.J.Webb and D.A.Jackson, Combined distributed temperature and strain sensor based on Brillouin loss in an optical fibre, *Opt. Lett.*, 16, 141(1994)
- [90] Y.J.Rao, N.Fisher, P.Henderson, V.Lecouche, C.N.Pannell, D.J.Webb and D.A.Jackson, Recent developments in fibre optic sensors for point and distributed sensing in large structures, *European Workshop on Optical Fibre Sensors*, 8-10 July 1998, Peebles, Scotland, 3483, 138(1998)
- [91] T.R.Parker, M.Farhadiroushan, R.Faced, V.A.handerek and A.J.Rogers, Simultaneous distributed measurement of strain and temperature from noise-initiated Brillouin scattering in optical fibers, *IEEE Journal of Quantum Electronics*, 34, 645(1998)
- [92] P.C.Wait and T.P.Newson, Laudau-Placzek ratio applied to distributed fiber sensing, *Opt. Commun.*, 122, 141(1996)

- [93] G.P.Lees, P.C.Wait, M.J.Cole and T.P.Newson, Advances in optical fiber distributed temperature sensing using the Landau-Placzek ratio, *IEEE Photonics Technology Letters*, 10, 126(1998)
- [94] NTT Access Network Systems Laboratories, Distributed sensing techniques using Brillouin scattering, *Proc. 12th International Conference on Optical Fiber Sensors*, Williamsburg, Virginia, October 28-31, 1997, 316(1997)
- [95] R.Faced, T.R.Parker, M.M.Farhadiroushan, V.A.Handerek and A.J.Rogers, Power measurement of noise initiated Brillouin scattering in optical fibres for sensing applications, *Opt. Lett.*, 23, 79(1998)
- [96] P.C.Wait, K.D.Souza and T.P.Newson, A theoretical comparison of spontaneous Raman and Brillouin based fibre optic distributed temperature sensors, *Optics Communications*, 144, 17(1997)
- [97] F.Parvaneh, V.A.Handerek and A.J.Rogers, Frequency-derived remote measurement of birefringence in polarization maintaining fibre by using the optical Kerr effect, *Opt. Lett.*, 17, 1346(1992)
- [98] K.O.Hill, Y.Fujii, D.C.Johnson and B.S.kawasaki, Photosensitivity in optical fiber waveguides: Application to reflection filter fabrication, *Appl. Phys. Lett.*, 32, 647(1978)
- [99] J.Stone, Photorefractivity in GeO₂-doped silica fibers, *J. Appl. Phys.*, 62, 4371(1987)
- [100] F.P.Payne, Photorefractive gratings in single-mode optical fibers, *Electron. Lett.*, 25, 498(1989)

- [101] D.P.Hand and R.St.J.Russell, Photoinduced refractive-index changes in germanosilicate fibers, *Opt. Lett.*, 15, 102(1990)
- [102] G.Meltz, W.W.Morey and W.H.Glenn, Formation of Bragg gratings in optical fibers by a transverse holographic method, *Opt. Lett.*, 14, 823(1989)
- [103] R.Kashyap, Photosensitive optical fibers: Devices and applications, *Optic. Fiber Technol.*, 1, 17(1994)
- [104] A.Othonos, Fiber Bragg gratings, *Rev. Sci. Instrum.*, 68, 4309(1997)
- [105] W.W.Morey, G.Meltz and W.H.Glenn, Fiber Bragg grating sensors, *Proc. SPIE Fiber Optic & Laser Sensors VII*, 1169, 98(1989)
- [106] W.W.Morey, J.R.Dunphy and G.Meltz, Multiplexing fiber Bragg grating sensors, *Proc. SPIE Distributed and Multiplexed Fiber Optic Sensors*, Boston, MA, 1991, 1586, 216(1991)
- [107] A.D.Kersey, M.A.Davis, H.J. Patrick, M.LeBlanc, K.P.Koo, C.G.Askins, M.A.Putnam and E.J.Friebele, Fiber grating sensors, *J. Lightwave Technol.*, 15, 1442(1997)
- [108] S.M.Melle, K.Liu and R.M.Measures, A passive wavelength demodulation system for guided-wave Bragg grating sensors, *IEEE Photon. Technol. Lett.*, 4, 516(1992)
- [109] M.A.Davis and A.D.Kersey, All fiber Bragg grating strain sensor demodulation technique using a wavelength division coupler, *Electron. Lett.*, 30, 75(1994)
- [110] Q.Zhang, D.A.Brown, H.Kung, J.E.Townsend, M.Chen, L.J.Reinhart and T.F.Morse, Use of highly overcoupled couplers to detect shifts in Bragg wavelength, *Electron. Lett.*, 31, 480(1995)

- [111] A.B.Lobo Riberio, L.A.Ferreira, M.Tsvetkov and J.L.Santos, All fiber interrogation technique for fiber Bragg grating sensors using a biconical fiber filter, *Electron. Lett.*, 32, 382(1996)
- [112] M.A.Davis, D.G.Bellemore and A.D.Kersey, Design and performance of a fiber Bragg grating distributed strain sensor system, *Proc. SPIE, North American Conf. Smart Structures Materials*, San Diego, CA, 1995, 2446, 227(1995)
- [113] M.G.Xu, H.Geiger, J.L.Archambault, L.Reekie and J.P.Dakin, Novel interrogation system for fiber Bragg grating sensors using an acousto-optic tunable filter, *Electron. Lett.*, 29, 1510(1993)
- [114] J.R.Dunphy et al, Instrumentation development in support of fiber grating sensor arrays, *Proc. SPIE, Distributed and Multiplexed Fiber Optic Sensors*, Boston, MA, 1993, 2071,2(1993)
- [115] D.A.Jackson, A.B.L.Ribeiro, L.Reekie and J.L.Archambault, Simple multiplexing scheme for a fiber optic grating sensor network, *Opt. Lett.*, 18, 1192(1993)
- [116] M.A.Davis and A.D.Kersey, Matched-filter interrogation technique for fiber Bragg grating arrays, *Electron. Lett.*, 31, 822(1995)
- [117] M.A.Davis, D.G.Bellemore, M.A.Putnam and A.D.Kersey, Interrogation of 60 fiber Bragg grating sensors with μ strain resolution capability, *Electon. Lett.*, 32, 1393(1996)
- [118] M.A.Davis and A.D.Kersey, A fiber Fourier transform spectrometer for decoding fiber Bragg grating sensors, *J. Lightwave Technol.*, 13, 1289(1995)

- [119] D.A.Flavin, Short optical path scan interferometric interrogation of a fibre Bragg grating embedded in a composite, *Electron. Lett.*, 33, 319(1997)
- [120] D.A.Flavin, Absolute measurement of wavelengths from a multiplexed in-fibre Bragg grating array by short-scan interferometry, *Proc. 12th International Conference on Optical Fiber Sensors*, Williamsburg, Virginia, October 28-31, 1997, 24(1997)
- [121] M.A.Putnam, M.L.Dennis, J.U.Kang, T.T.Tsai, I.N.Duling III and E.J.friebele, Sensor grating array demodulation using a passively mode locked fiber laser, 1997 *Tech. Dig. Optic. Fiber Commun. Conf.* (Ed. J.Onstott), OSA, 6, 156(1997)
- [122] T.A.Berkoff, M.A.Davis, D.G.Bellemore, A.D.Kersey, G.M.Williams and M.A.Putnam, Hybrid time and wavelength division multiplexed fiber grating array, *Proc. SPIE*, 2444, 288(1995)
- [123] J.P.Dakin, W.Ecke, M.Rothardt, J.Schauer, K.Usbeck and R.Willsch, New multiplexing scheme for monitoring fiber optic Bragg grating sensors in the coherence domain, *Proc. 12th International Conference on Optical Fiber Sensors*, Williamsburg, Virginia, October 28-31, 1997, 31(1997)
- [124] Y.Hu and S.Chen, Multiplexing Bragg gratings using combined wavelength and spatial division techniques with digital resolution enhancement, *Electron. Lett.*, 33, 1973(1997)
- [125] Y.Hu, B.Bridge, L.Zhang, I.Bennion and S.Chen, Improvements on the multiplexing system using a 2D spectrograph for FBG based sensor arrays, *European Workshop on Optical Fibre Sensors*, 8-10 July 1998, Peebles, Scotland, 3483, 288(1998)

- [126] A.D.Kersey, T.A.Berkoff and W.W.Morey, High resolution fiber Bragg grating based strain sensor with interferometric wavelength shift detection, *Electron. Lett.*, 28, 236(1992)
- [127] A.D.Kersey and T.A.Berkoff, Fiber optic Bragg grating differential temperature sensor, *IEEE Photon. Technol. Lett.*, 4, 1183(1993)
- [128] B.Lissak, A.Arie and M.Tur, High resolution strain sensing by locking lasers to fiber-Bragg gratings, *European Workshop on Optical Fibre Sensors*, 8-10 July 1998, Peebles, Scotland, 3483, 250(1998)
- [129] J.D.C.Jones, Review of fibre sensor techniques for temperature-strain discrimination, *Proc. 12th International Conference on Optical Fiber Sensors*, Williamsburg, Virginia, October 28-31, 1997, 36(1997)
- [130] Y.J.Rao, In-fibre Bragg grating sensors, *Meas. Sci. Technol.*, 8, 355(1997)
- [131] F.M.Haran, J.K.Rew and P.D.Foote, A strain-isolated fibre Bragg grating sensor for temperature compensation of fibre Bragg grating strain sensors, *Meas. Sci. Technol.*, 9, 1163(1998)
- [132] M.G.Xu, H.Geiger, J.L.Archambault, L.Reekie and J.P.Dakin, Thermally-compensated bending gauge using surface-mounted fiber gratings, *Int J Optoelectron*, 9, 281(1994)
- [133] T.Liu, G.Fernando, Y.Rao, D.A.Jackson, L.Zhang and I.Bennion, Simultaneous strain and temperature – measurements in composites using a multiplexed fiber Bragg grating sensor and an extrinsic Fabry-Perot sensor, *Proc.SPIE*, 3042, 203(1997)

- [134] L.A.Ferreira, A.B.L.Ribeiro, J.L.Santos and F.Farahi, Simultaneous measurement of displacement and temperature using a low finesse cavity and a fiber Bragg grating, *IEEE Photon. Tech. Letts.* 8, 1519(1996)
- [135] M.G.Xu, J.L.Archambault, L.Reekie and J.P.Dakin, Discrimination between strain and temperature effects using dual-wavelength fiber grating sensors, *Electron. Lett.*, 30, 1085(1994)
- [136] S.W.James, M.L.Dockney and R.P.Tatam, Simultaneous independent temperature and strain measurement using in-fibre Bragg grating sensors, *Electron. Lett.*, 32,1133(1996)
- [137] M.G.Xu, L.Dong, L.Reekie, J.A.Tucknott and J.L.Cruz, Temperature-independent strain sensor using a chirped Bragg grating in a tapered optical-fiber, *Electron. Letts.*, 31, 823(1995)
- [138] S.E.Kanellopoulos, V.A.Handerek and A.J.Rogers, Simultaneous stain and temperature sensing with photogenerated in-fiber gratings, *Opt. Lett.*, 20, 333(1995)
- [139] H.J.Patrick, G.M.Williams, A.D.Kersey, J.R.Pedrazzani and A.M.Vengsarkar, Hybrid fiber Bragg grating/long period fiber grating sensor for strain/temperature discrimination, *IEEE Phot. Tech. Letts.*, 8, 1223(1996)
- [140] V.Bhatia, D.Campbell, R.O.Claus and A.M.Vengsarkar, Simultaneous strain and temperature measurement with long period gratings, *Opt. Lett.*, 22, 648(1997)
- [141] V.Magne, S.Rougeault, M.Vilela and P.Ferdinand, State-of-strain evaluation with fiber Bragg grating rosettes: application to discrimination between strain and temperature effects in fiber sensors, *Applied Optics*, 36, 9437(1997)

- [142] K.C.Byron, K.Sugden, T.Bricheno and I Bennion, Fabrication of chirped Bragg gratings in photosensitive fiber, *Electron. Lett.*, 29, 1659(1993)
- [143] P.C.Hill and B.J.Eggleton, Strain gradient chirp of fiber Bragg gratings, *Electron. Lett.*, 30, 1172(1994)
- [144] M.A.Putnam, G.M.Williams and E.J.Friebele, Fabrication of tapered, strain-gradient chirped fiber Bragg gratings, *Electron. Lett.*, 31, 309(1995)
- [145] A.D.Kersey, M.A.Davis and T.Tsai, Fiber optic Bragg grating strain sensor with direct reflectometric interrogation, *Proc. 11th Int. Conf. Optical Fiber Sensors, OFS'96*, Sapporo, Japan, may 1996, 634(1996)
- [146] M.LeBlanc, S.Huang, M.Ohn, R.M.Measures, A.Guemes and A.Othonos, Distributed strain measurement based on a fiber Bragg grating and its reflection spectrum analysis, *Opt Lett.*, 21, 1405(1996)
- [147] M.LeBlanc, S.Y.Huang, M.Ohn, R.M.Measures, A.Guemes and A.Othonos, Distributed strain measurement based on a chirped fiber Bragg grating and reflection spectrum analysis, *Opt. Lett.*, 21, 1405(1996)
- [148] S.Huang, M.M.Ohn and R.M.Measures, A novel Bragg grating distributed-strain sensor based on phase measurements, *Proc. SPIE Smart Sensing, Processing and Instrumentation*, 1995, Vol. SPIE 2444, 158(1995)
- [149] S.Huang, M.M.Ohn, M.LeBlanc and R.M.Measures, Continuous arbitrary strain profile measurements with fiber Bragg gratings, *Smart Materials and Structures*, 1997
- [150] S.Huang, M.M.Ohn, and R.M.Measures, Phase-based Bragg intra-grating distributed strain sensor, *Appl. Opt.*, 35, 1135(1996)

Chapter 1 Fibre Optic Sensor Technology

- [151] A.M.Vengsarkar, P.J.Lemaire, J.B.Judkins, v.Bhatia, T.Erdogan and J.E.Sipe, Long period fiber gratings as band-rejection filters, *Tech. Dig. Conf. Opt. Fiber Commun.*, San Diego, CA, 1995, postdeadline paper PD4-2(1995)
- [152] V.Bhatia and A.M.Vengsarkar, Optical fiber long period grating sensors, *Opt. Lett.*, 21, 692(1996)
- [153] H.J.Patric and S.T.Vohra, Fiber Bragg grating with long period fiber grating superstructure for simultaneous strain and temperature measurement, *European Workshop on Optical Fibre Sensors*, 8-10 July 1998, Peebles, Scotland, 3483, 264(1998)
- [154] J.B.Judkins, J.R.Pedrazzani, D.J.DiGiovanni and A.M.Vengsarkar, Temperature-insensitive long-period fiber gratings, *Tech. Dig. Conf. Opt. Fiber Commun.*, San Jose, CA, 1996, postdeadline paper PD1-1(1996)
- [155] H.P.Patric et al, Fiber Bragg grating demodulation system using in-fiber long period grating filters, *Proc. SPIE* 2838, 60(1996)
- [156] V.Bhatia, D.K.Campbell, T.D'Alberto, G.A.Ten Eyck, D.Sherr, K.A.Murphy and R.O.Claus, Standard optical fiber long-period gratings with reduced temperature sensitivity for strain and refractive-index sensing, *Tech. Dig. Conf. Opt. Fiber Commun.*, Dallas, TX, 346(1997)
- [157] G.A.Ball, W.W.Morey and P.K.Cheo, Singlepoint and multipoint fiber laser sensors, *IEEE Photon. Technol. Lett.*, 5, 267(1993)
- [158] S.M.Melle, A.T.Alavie, S.Karr, T.Coroy, K.X.Liu and R.M.Measures, A Bragg grating tuned fiber laser strain sensor system, *IEEE Photon. Technol. Lett.*, 5, 263(1993)

- [159] A.D.Kersey and W.W.Morey, Multiplexed Bragg grating fiber laser strain sensor system with mode-locked interrogation, *Electron. Lett.*, 29, 112(1993)
- [160] G.A.Ball, G.Meltz and W.W.Morey, Polarimetric heterodyning Bragg grating fiber laser sensor, *Opt. Lett.*, 18, 1976(1993)
- [161] A.D.Kersey and W.W.Morey, Multi-element Bragg grating based fiber laser strain sensor, *Electron. Lett.*, 29, 964(1993)
- [162] A.T.Alavie, S.E.Karr, A.Othonos and R.M.Measures, A multiplexed Bragg grating fiber laser system, *IEEE Photon. Technol. Lett.*, 5, 1112(1993)
- [163] K.P.Koo and A.D.Kersey, Bragg grating based laser sensor systems with interferometric interrogation and wavelength division multiplexing, *J. Lightwave Technol.*, 13, 1243(1995)
- [164] B.W.Lee, H.J.Jeong and B.Y.Kim, High-sensitivity mode-locked fiber laser gyroscope, *Opt. Lett.*, 22, 129(1997)
- [165] M.L.Lee, J.S.Park, W.J.Lee, S.H.Yun, Y.H.Lee and B.Y.Kim, A polarimetric current sensor using orthogonally-polarized dual-frequency fiber laser, *Meas. Sci. and Technol.*, 9, 952(1998)
- [166] B.Y.Kim, Fiber lasers for sensing, *European Workshop on Optical Fibre Sensors*, 8-10 July 1998, Peebles, Scotland, 3483, 12(1998)
- [167] J.P.Dakin, C.A.Wade and M.Henning, Novel optical fiber hydrophone array using a single laser source and detector, *Electron. Lett.*, 20, 53(1984)
- [168] A.D.Kersey et al, Analysis of intrinsic crosstalk in tapped serial and Fabry-Perot interferometric fiber sensor arrays, *Proc. SPIE Fiber Optic Laser Sensors*, 985, 113(1988)

- [169] W.W.Morey, Distributed fiber grating sensors, *Proc. OFS'90*, Sydney, Australia, 285(1990)
- [170] S.Vohra, A.Dandridge, B.Danver and A.Tveten, An hybrid WDM/TDM reflectometric array, *Proc. 11th Int. Conf. Optic. Fiber Sensors, OFS'96*, Sapporo, Japan, 534(1996)
- [171] A.D.Kersey and M.J.Marrone, Nested interferometric sensors utilizing fiber Bragg grating reflectors, *Proc. 11th Int. Conf. Optic. Fiber Sensors, OFS'96*, Sapporo, Japan, 618(1996)
- [172] A.D.Kersey and M.A.Davis, Interferometric fiber sensor with a chirped Bragg grating sensing element, *Proc. OFS'10*, Glasgow, Scotland, 319(1994)
- [173] E.Snitzer, Optical laser action of Nd^{3+} in a barium crown glass, *Phys. Rev. Lett.*, 72, 36(1961)
- [174] K.T.V.Grattan, Z.Y.Zhang and T.Sun, Luminescent optical fibers in sensing, in *Optical Fiber Sensor Technology, 4. Environmental and Chemical Sensing* (eds. K.T.V.Grattan and B.T.Meggitt). Chapman & Hall, London, 205(1998)
- [175] N.Langford, Optical fibre lasers, in *Optical Fiber Sensor Technology, 2. Devices and Technology* (eds. K.T.V.Grattan and B.T.Meggitt). Chapman & Hall, London, 37(1998)
- [176] B.Y.Kim, Fiber lasers in optical sensors, in *Optical Fiber Sensor Technology, 2. Devices and Technology* (eds. K.T.V.Grattan and B.T.Meggitt). Chapman & Hall, London, 99(1998)

Chapter 1 Fibre Optic Sensor Technology

- [177] K.T.V.Grattan and Z.Y.Zhang, Fiber optic luminescent thermometry, in *Optical Fiber Sensor Technology 4. Environmental and Chemical Sensing* (eds. K.T.V.Grattan and B.T.Meggitt). Chapman & Hall, London, 133(1998)
- [178] K.T.V.Grattan and Z.Y.Zhang, *Fiber Optic Fluorescence Thermometry*, Chapman & Hall, London, 1995
- [179] A.J.Rogers, *Essentials of Optoelectronics*, Chapman & Hall, London, 329(1998)
- [180] M.Languesse and P.Rebourgeard, Luminescent optical fibres, in *Plastic Optical Fibres-Practical Applications* (ed. Club des Fibres Optiques). Wiley, Chichester, 127(1997)
- [181] A.T.Augousti, J.Mason and K.T.V.Grattan, A simple fiber optic level sensor using fluorescent fiber, *Rev. Sci. Instrum.*, 61, 3854(1990)
- [182] S.Muto, A.Fukasawa, M.Kamimura, F.Shinmura and H.Ito, Fiber humidity sensor using fluorescent dye-doped plastics, *Jpn. J. Appl. Phys.*, 28, 1065(1989)
- [183] H.Sawada, A.Tanaka and N.Wakatsuki, Plastic optical fiber doped with organic fluorescent materials, *Fujitsu Sci. Technol. J.*, 25, 163(1989)
- [184] Z.Y.Zhang, K.T.V.Grattan, A.W.Palmer and B.T.Meggitt, Spectral characteristics and effects of heat treatment on intrinsic Nd-doped fiber thermometer probes, *Rev. Sci. Instrum.*, 69, 139(1998)
- [185] S.Satoh and M.Imai, Mode-locked all-fiber laser with a piezoelectric copolymer jacketed fiber for phase modulation, in *Proc. 11th Int. Optical Fiber Sensors Conf.*, 506(1996)
- [186] Z.Y.Zhang, K.T.V.Grattan, A.W.Palmer, T.Sun and B.T.Meggitt, Rare earth doped intrinsic fiber optic sensors for high temperature measurement up to 1100°C,

Proc. 12th International Conference on Optical Fiber Sensors, Williamsburg, Virginia, October 28-31, 1997, 556(1997)

[187] C.Mazzali, H.L.Fraguto, E.Palange and D.C.Dini, Fast method for obtaining erbium-doped fiber intrinsic parameters, *Electron. Lett.*, 32, 921(1996)

[188] E.Maurice, G.Monnom, B.Dussardier, A.Saissy, D.B.Ostrowsky and G.Baxter, Thermalization effects between upper levels of green fluorescence in Er-doped silica fibers, *Opt. Lett.*, 19, 990(1994)

[189]] E.Maurice, G.Monnom, B.Dussardier, A.Saissy, D.B.Ostrowsky and G.Baxter, High dynamic range temperature point sensor using green fluorescence intensity ratio in Er-doped silica fiber, *IEEE J. Lightwave Technol.*, 13, 1349(1995)

[190] Y.Imai, T.Hokazono and T.Yoshida, Fluorescence-based temperature sensing using erbium-doped optical fibers with 1.48 μ m pumping, *Opt. Rev.*, 4, 117(1997)

[191] P.K.Y.Ko, M.S.Demokan and H.Tam, Distributed temperature sensing with erbium-doped fiber amplifiers, *IEEE J. Lightwave Technol.*, 14, 2236(1996)

[192] Z.Y.Zhang, K.T.V.Grattan, A.W.Palmer, T.Sun and B.T.Meggitt, Fluorescence decay time characteristics of erbium-doped optical fiber at elevated temperatures, *Rev. Sci. Instrum.*, 68, 2764(1997)

[193] Z.Y.Zhang, K.T.V.Grattan, A.W.Palmer and B.T.Meggitt, Thulium-doped intrinsic fibre optic sensor for high temperature measurements (>1100°C), *Rev. Sci. Instrum.*, 69, (1998)

[194] K.Oh and Un-C.Pack, Fiber optic absorption spectroscopic gas sensor using an amplified spontaneous emission light source from Tm³⁺/Ho³⁺ co-doped silica fiber,

Chapter 1 Fibre Optic Sensor Technology

Proc. 12th International Conference on Optical Fiber Sensors, Williamsburg, Virginia, October 28-31, 1997, 432(1997)

[195] D.N.Wang, B.T.Meggitt, A.W.Palmer, K.T.V.Grattan and Y.N.Ning, Use of a Sm^{3+} -doped fiber as a low coherence light-source, *IEEE Photonics Technol. Lett.*, 7, 620(1995)

[196] Y.N.Ning and K.T.V.Grattan, White light interferometric optical fiber sensing techniques, in *Optical Fiber Sensor Technology, 4. Environmental and Chemical Sensing* (eds. K.T.V.Grattan and B.T.Meggitt). Chapman & Hall, London, 1998

[197] S.Magne, Etude d'un laser a fiber dopee Ytterbium-spectroscopie laser de fibers dopees, Thesis, University of St-Etienne, 1993

[198] A.H.Hartog, Distributed fiber optic sensors, in *Optical Fiber Sensor Technology* (eds. K.T.V.Grattan and B.T.Meggitt). Chapman & Hall, London, 347(1995)

[199] M.J.F.Digonnet, *Rare Earth Doped Fiber Lasers and Amplifiers*, Marcel Dekker, New York, 1993

[200] G.Boisde and A.Harmer, *Chemical and Biochemical Sensing with Optical Fibers and Waveguides*. Artec House, Norwood, USA, 1996

[201] D.Flannery, S.W.James, R.P.Tatam and G.J.Ashwell, Single mode fiber optic chemical sensor using Langmuir-Blodgett waveguide overlays, *Proc. 12th International Conference on Optical Fiber Sensors*, Williamsburg, Virginia, October 28-31, 1997, 382(1997)

[202] M.Poulain, M.Poulain and J.Lucas, Verres fluores au tetrafluorure de zirconum: Proprietes optiques d'un verre dope au Nd^{3+} , *Mater. Res. Bull.*, 10, 243(1975)

Chapter 1 Fibre Optic Sensor Technology

[203] D.Richardson, J.Minelly and D.Hanna. Fiber laser systems shine brightly, *Laser Focus World*, September, 87(1997)

[204] T.Schweitzer, New fiber laser glasses using gallium lanthium sulfide, *Proc. CLEO'97*, Paper CWQ4, Baltimore, MD, 1997

Chapter 2

Fibre Optic Luminescence Thermometry: Background and Previous Work

2.1 Abstract

The temperature dependent characteristics of luminescence effects in certain materials, coupled with the use of fibre optics, has made it the focus of a major aspect of research in the field of thermometry over the past few decades. This Chapter reviews the background to such work and in so doing summarizes the physical mechanisms that form the basis for the technique, and catalogues and discusses the instrumentation-related aspects of several different luminescence based thermometry systems from cryogenic temperatures to those approaching 2000°C, "setting the scene" for the work discussed in subsequent Chapters.

2.2 Introduction

The measurement of temperature is a virtually ubiquitous requirement in all of the experimental and/or applied fields of science, engineering and medicine. Moreover, the accelerating proliferation of technology in these areas has led to an ever-

Chapter 2 Fibre Optic Luminescence Thermometry: Background and Previous Work

increasing variety of situations that requires knowledge of the temperature of some specimen, component, system or process. As a result, new approaches to the measurement of temperature are often called for, and this has led to the development of novel instrumentation systems aimed at meeting these needs.

The most common temperature transducers are: the thermocouple, the RTD (Resistance Temperature Detector), the thermistor and the integrated circuit sensor[1]. Very recently, the Au/Pt thermocouple has received considerable attention for its potential in high temperature measurement, due to its little thermoelectric inhomogeneity and good stability[2][3]. There are several methods reported to measure temperature, such as the scheme based on the thermo-optic effect in titanium dioxide[4], pyrometry, use of a wavelength-encoded fibre optic sensor[5] and an infrared fibre optic probe[6].

Among them, one of the most important thermometric techniques that is adaptable to the needs of a wide variety of situations is based on fluorescing materials, many of them phosphors, rare earth doped materials or active ion-doped glasses, crystals or garnets. The thermal dependence of fluorescence may be exploited to provide for a non-contact, emissivity-independent, optical alternative to the above mentioned more familiar techniques. As discussed below, there are certain situations in which the advantages that fluorescence-based thermometry has over other methods make it the most viable approach. The region to be measured may be extremely hostile to the sensor, have restricted access, or there may even be a limit on the physical contacting of the sensing probe, where the presence of interference from the electromagnetic

noise excludes the use of electronic thermometers. A wide range of examples of such interactions exists, including their use in turbine-engines, the monitoring of winding temperatures in electrical transformers, and temperature monitoring during clinical radio-frequency (RF) heat treatment, and so on.

There is considerable diversity in the technical apparatus used in fibre optic temperature sensors. Extensive reviews have been given earlier by Grattan et al[7][8] and Wickersheim[9], and most recently by Grattan and Zhang[10][11] and Allison et al[12], on a range of sensing schemes. This Chapter aims to review the progress on luminescence based thermometry and set a solid background for the further work discussed in this thesis.

2.3 Background

2.3.1 The nature of luminescent materials

Luminescence refers to the absorption of energy by a material, with the subsequent emission of light. This is a phenomenon distinct from blackbody radiation, incandescence, or other such effects that cause materials to glow at high temperature. Fluorescence refers to the same process as luminescence, but with the qualification that the emission is usually in the visible band and has a duration of typically 10^{-9} – 10^{-3} s. Phosphorescence is a type of luminescence of greater duration, $\approx 10^{-3}$ - 10^3 s. Emission, luminescence, phosphorescence, and fluorescence are closely related terms[13], and with different definitions of the above durations of the emission.

There is an increasingly wide range of potentially useful luminescent materials for use in optical sensors. A valuable source of such materials is in phosphors used in television tubes, which are semiconductors such as ZnS, CdS or CdZnS, the emission from which corresponds approximately to the wavelengths associated with the semiconductor band edges observed in absorption. There is also a wide range of organic materials, both liquid and solid, that exhibit 'molecular' fluorescence, and such materials, familiar as the active medium of the 'dye' laser, are widely used in commercial printing, packaging and as 'brightening agents' in commercial detergents. Finally, there are self-activated materials and materials with charged defects (colour centres) that also exhibit fluorescence, but are less easy to use reliably at room temperature, and have fallen out of favour as laser media[10].

The choice of sensor material determines the range, sensitivity and stability of any associated sensor and inorganic insulating compounds, such as most lamp phosphors and many solid-state laser materials. These are most suitable for thermometric applications as these factors are optimized in such materials, being most commonly used in several existing, and previously reported fluorescence thermometer schemes.

2.3.2 Physical principles of fluorescence thermometry

The fundamental aspects of the fluorescence of solid materials are well understood. Prior to excitation, the electronic levels in the material are populated in the ground state. A means to deposit energy in the material is required in order to excite a higher electronic state. This may be accomplished by exposure to electromagnetic radiation (visible or ultraviolet light, or X or gamma-rays), particle beams (electrons, neutrons,

or ions), or, as is the case for semiconductors, electrical current. Conservation principles dictate that the amount of energy absorbed must also be released. This may be manifested by emission of a photon with energy equal to that of the energy-level difference, by transfer of energy via quantized vibrational (phonon) exchange in the material, or by other more complicated energy exchange mechanisms.

Fluorescence, as referred to here, is the emission occurring from electronic transitions and is usually in the visible region of the spectrum, but may also be in the near infrared (IR), as from Nd, or in the UV, as is typical for Gd. Fig.2.1 presents the energy-level diagram for various well-known states of some rare earths that are commonly used as the luminescent centre in a typical thermometry application[14].

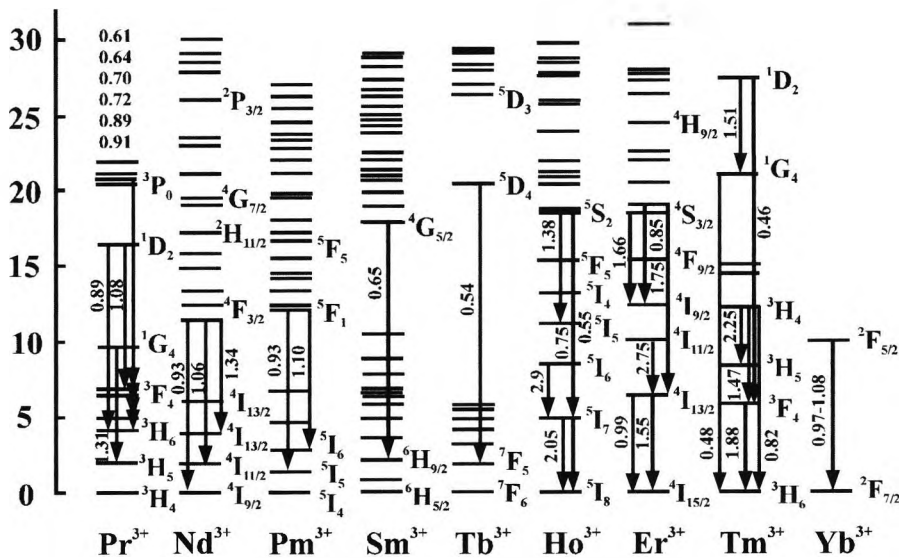


Fig.2.1 Electron energy levels for rare-earth glasses in fibres, including laser transactions (wavelengths in microns)

Chapter 2 Fibre Optic Luminescence Thermometry: Background and Previous Work

It is generally true that the fluorescent spectral properties of any material will change with temperature. This is so in part because the Boltzmann distribution governs the partitioning of the populations in the various participating vibrational levels of the ground, excited, and emitting states. The rate of change of the population of an emitting state, 2, to a ground state, 1, is the sum of a constant, purely radiative spontaneous emission, $A_{1,2}$, and a nonradiative component, $W_{1,2}$, which is temperature dependent, i.e.

$$k = 1/\tau = A_{1,2} + W_{1,2} \quad (2.1)$$

where the measured lifetime, τ , is the reciprocal of the decay rate, k . One model for temperature dependence for some fluorescence materials used for thermometry is based on thermal promotion to a non-emitting electronic state followed by non-radiative relaxation, called thermal quenching, described in some detail by Fonger and Struck[15][16] and later by Zhang et al[17] and used to explain Cr^{3+} fluorescence, as will be expanded upon in Chapter 3, to explain the fluorescence in other rare earth doped systems.

For some materials, a temperature-dependent de-excitation pathway based on multiphonon emission[18] exists. If the energy difference between the ground and emitting states is four to five times the highest vibrational frequency of the surrounding lattice, then at sufficiently high temperatures a multi-phonon transition is allowed and the transition probability is temperature dependent. This explanation has been applied to emission from dopants in YAG hosts[19][20].

Chapter 2 Fibre Optic Luminescence Thermometry: Background and Previous Work

There are several factors influencing the fluorescence process, which are shown below.

(1) *Dopant concentration.* Overall intensity, relative spectral distribution, decay time, rise time, and response to temperature are all affected to some degree by dopant concentration. However, when the concentration levels reach a certain point, another non-radiative de-excitation pathway becomes important. As the activator density is increased, the probability that an excited activator will transfer energy non-radiatively to a neighboring dopant ion increases. The arrival at a cut-off in this process is usually referred to as concentration quenching[12].

In thermometry applications, there are other considerations that may warrant the use of different strategies. For instance, at high concentrations the fluorescence decay profile may not be that of simple single-exponential decay. This is important for decay-time based approaches since multi-exponential and non-exponential decay profiles are more difficult to model. The more complex waveforms resulting in the output signals from such systems can make calibration and data analysis difficult but not intractable, an example of which is the introduction of the Förster model[21][22]. The role and implications of the Förster model model with respect to fluorescence thermometry were discussed by Dowell[22][23]. Further discussion on the relevant model will form part of Chapter 3.

(2) *Saturation effects.* High incident fluxes, whether from a laser, particle beam, or any other excitation source, can lead to luminescence saturation effects. When this occurs, the phosphor efficiency changes as a function of the incident flux. Saturation

effects in YAG:Tb and $Y_2O_3S:Eu$ have been discussed by de Leeuw et al[24] and Imanaga et al[25] separately and it was found that the effect was more pronounced at higher concentrations. Above a certain threshold value, the overall intensity decreases, but for a the lower concentration, this threshold value itself is lower and the rate of decrease is faster than at higher concentrations. Generally, for all concentrations, the saturation thresholds are lower at higher temperatures.

(3) *Impurities.* At concentrations greater than 1ppm, transition metal impurities will decrease phosphor brightness[12]. This occurs because they absorb at wavelengths similar to those of the typical activators, thus effectively "stealing" excitation energy and decreasing the number of excited fluorescence centres. Moreover, non-radiative energy transfer from an excited activator to such impurities is efficient, thus increasing the decay rate and quenching the emission.

(4) *Sensitizers.* A sensitizer is a material that, when added to a phosphor, increases the fluorescence output. The sensitizing dopant will absorb energy and, rather than emitting fluorescence, it will transfer its energy to the main dopant from which an optical transition occurs. For example, Weber[26] noted that erbium has found to be a sensitizer for dysprosium, while gadolinium is a sensitizer for terbium. A prospective sensitizer must exhibit no absorption at the emission wavelength of interest. It must also have absorption bands that do not remove excitation energy from the activator. Finally, it must have energy levels that are above the fluorescing line which feed the activator but which do not quench it[27].

2.4 Instrumentation and experimental techniques

2.4.1 The generic thermometry system

A luminescence-based optical thermometry system will generally consist, at least, of the following components: (1) a source of excitation energy, (2) a means to deliver the energy to the target (typically beam-steering elements or a fibreoptic bundle if the energy is in the transmission optical spectrum of the fibres), (3) a fluorescing medium that is bonded to the target and illuminated by the incident flux, (4) an optical system to collect and transport the fluorescence that is subsequently generated, (5) a detector or an array of detectors to monitor the fluorescence signal, and (6) a data acquisition and analysis system that ultimately yields the target temperature. Fig.2.2 shows an elementary yet interesting illustrative example of this general arrangement[12]. In this, the energy source is a pulsed N₂ laser of 3ns pulse length, emitting in the ultraviolet at 337nm. The laser light is guided to the fluorescent target by two mirrors. The first is front surface coated for beam steering, and the second is dichroic and hence able to reflect ultraviolet light while transmitting visible light. The excitation beam strikes a band of phosphor that is bonded onto a heated cylindrical brass target mounted on the shaft of a motor so that either static or dynamic measurements can be made. The fluorescence emanates from each illuminated point on the surface of the target into a solid angle of 2π steradians. A significant fraction of this light thus falls within the acceptance angle of the collection optics, in this case shown as a single plastic Fresnel lens of 15cm diameter. The La₂O₂S:Eu phosphor used here produces simultaneous, bright emissions at several wavelengths across the visible spectrum. Because the temperature dependence of the lines varies, a narrow

Chapter 2 Fibre Optic Luminescence Thermometry: Background and Previous Work

band pass filter is used to allow the desired wavelength to reach the detector, which transduces the fluorescence decay signal into an electrical wave form, which is then digitized, acquired and analyzed. Such a system suffers from the need for the use of an expensive and usually relatively large N_2 laser, but is more useful in non-contact thermometry e.g. to examine rotating machinery. The development of temperature probes for specific applications have been discussed in detail by Grattan and Zhang[10], such a ruby-based thermometer with a range from 20 to 600°C, an alexandrite-based thermometer with a range from -100°C to 700°C, a Cr:LiSAF-based thermometer for biomedical applications (primarily 30-50°C), a Nd^{3+} :YAG high-temperature thermometer, including non-contact thermometry on turbine engine blades and vanes and rare earth doped fibre luminescent temperature sensors.

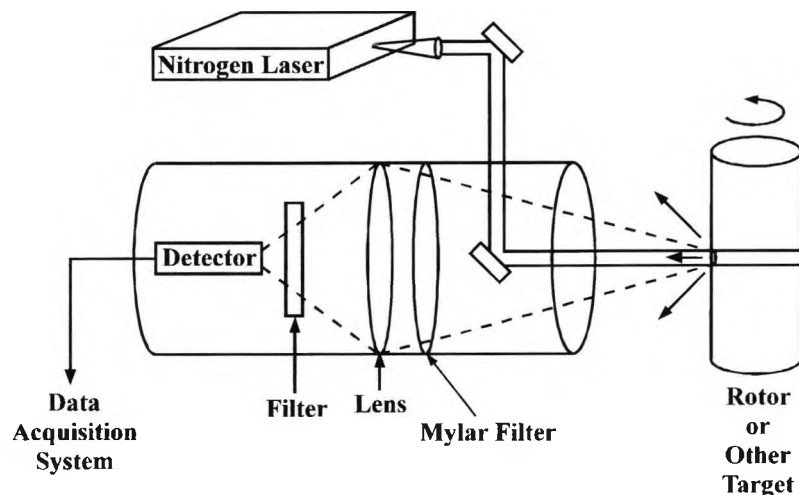


Fig.2.2 The fundamental elements of a remote fluorescence thermometry system

2.4.2 Fluorescence thermometer schemes

2.4.2.1 Fluorescence intensity-based schemes

The earliest and first commercial fibre optic thermometry system using the fluorescence technique was the Luxtron model 1000, shown in Fig.2.3, using europium-activated lanthanum and gadolinium oxysulfide as alternate sensor materials[10][28]. The fluorescence from these rare-earth phosphors consists of sharp lines originating from different excited states of the trivalent europium ion. Since the relative populations of these excited states after excitation are strong functions of temperature, the relative intensities of the emission lines are also quite temperature-dependent. By measuring the intensities of two lines originating on different excited states, and the ratio of the line intensities thus resulting, temperature may be determined from a knowledge of a prior calibration.

A further successful example of an early system is the ASEA model 1010 initially introduced by ASEA AG, a large Swedish automation and energy systems company. In this system, the sensor is a small crystal of gallium arsenide sandwiched between gallium aluminum arsenide layers[10][29]. By the use of two optical filters with adjacent pass bands, the intensity in each pass band is determined and measured and a ratio is constructed. A temperature calibration can thus be produced. The system is no longer commercially available, having been disposed of by ASEA several years ago[10].

Although a substantial number of intensity-based systems, such as the Luxtron model 1000, the ASEA model 1010 and several others, were built, the intensity-based technique was seen to have limitations in terms of performance and cost[30]. These limitations stem from the need of an additional 'reference channel', i.e. the transmitted intensity at another wavelength, for the separation of the effects of thermally induced changes in intensity from other non-thermal sources of signal change, such as fibre bending, light source fluctuations and detector degradation, and any electronic signal processing problems. As a result, a more successful technique based on the measurement of fluorescence lifetimes was developed[31]-[34] and has been much preferred in the development of fluorescence-based commercial systems to date.

2.4.2.2 Fluorescence lifetime-based schemes

The temperature-dependent lifetime of fluorescence in an appropriate material is the basis of the class of sensor discussed. There is a variety of fluorescent materials which are useful for temperature sensing, as have been considered above. Of those materials which have been selected, the most suitable tend to show a relatively long lifetime ($>10^{-6}$ s), so that no special high-speed electronic components are needed in the design of the lifetime detection circuitry, thus tending towards a low-cost system. In principle, any probe configuration can be used interchangeably, since the measurement of the fluorescence lifetime does not depend on the exact signal level or on the particular optical configuration used in the probe itself. A range of signal processing techniques for the detection of the fluorescence lifetime have been

reported in various fluorescence-based thermometric system and will be summarized below.

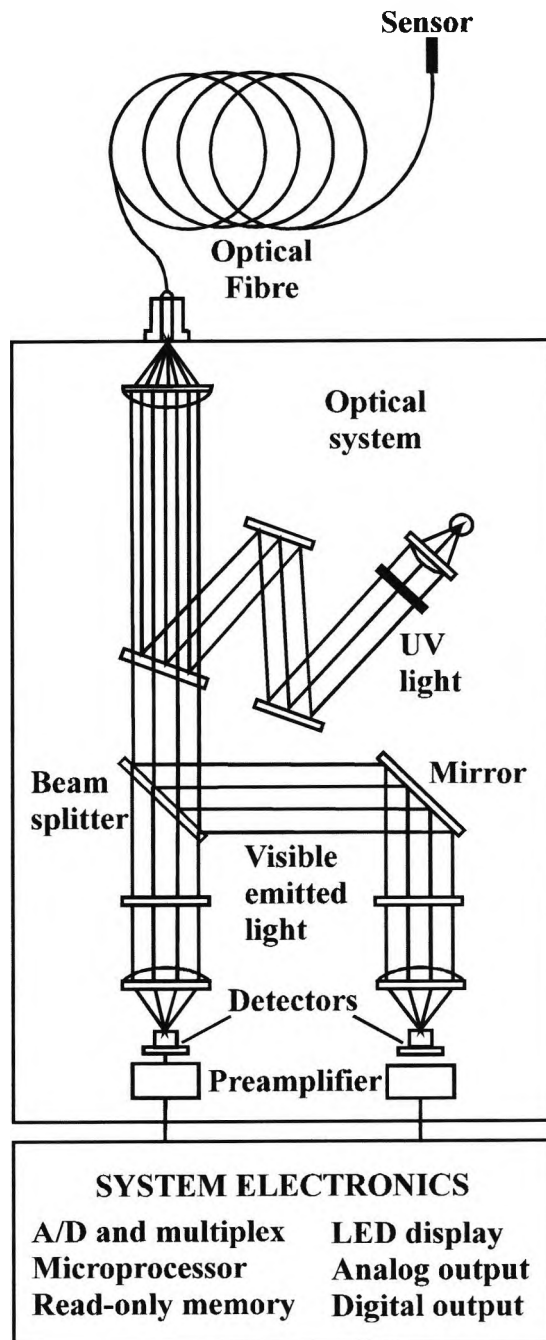


Fig.2.3 Schematic representation of Luxtron model 1000

Chapter 2 Fibre Optic Luminescence Thermometry: Background and Previous Work

Commercial products based on fluorescence lifetime technique are available now in Luxtron Corporation[35]. They are highly accurate, intrinsically safe, and immune to electromagnetic interference. These sensors operate within -200°C and 450°C range. Applications include biomedical, RF heating, microwave heating and processing, electronics and semiconductors.

The Luxtron model 790 has been designed for general purpose use including operation

- in high voltage or RF/Microwave fields
- inside microwave ovens and processing chambers
- on live electronic circuits and power supplies
- in plasma processing chambers

The temperature range of the model is -200°C to 450°C , the quoted calibrated accuracy is $\pm 0.1^{\circ}\text{C}$ RMS (root-mean-square) at point of calibration with a precision given as $\pm 0.1^{\circ}\text{C}$ RMS at 8 samples/measurement.

The Luxtron Model WTS-11 is designed as a fibreoptic transformer winding temperature monitor for direct measurement of transformer “hot spot” temperatures.

The manufactures data claims it

- provides accurate winding temperature during peak loading or emergency overloading of the transformer
- provides safe, cost-effective temperature monitoring in high voltage power transformers

- allows transformer loading based on true winding temperatures
- measures direct winding temperatures or oil temperatures
- enables the prediction of remaining insulation

It has been designed for field monitoring of high voltage power transformers. It is the world's first instrument capable of sensing temperature directly at the transformer windings. The claimed self-calibrating probes consist of a stable refractory photoluminescent material that is attached to the end of a length of optical fibre. A pulse of light from an LED in the instrument is sent down the fibre to the sensor which is in thermal contact with the winding, causing fluorescence of the sensor material. The decay time of the pulse fluorescence varies with the temperature, which is measured by the instrument. A lookup table provides the correlation and results are displayed locally on the front panel and transmitted to monitoring stations. The manufactures claim its measurement range is 0°C to 200°C, accuracy: $\pm 2^\circ\text{C}$ without calibration and resolution: 1°C for the display and 0.5°C for the analogue output.

There are several other models from Luxtron, such as Model 3100 for biomedical purposes and the model 500 series for OEM industrial or microwave applications.

2.4.2.3 Fluorescence line shift scheme

Each emission line is characterized by a wavelength for which the intensity is maximum. Its value may change slightly with temperature, and this is termed a line shift. Also, an emission line has a finite width, called the linewidth, which is often designated by the spectral width at half the maximum line intensity. Linewidth and line shift changes as a function of temperature are generally small, and are not

routinely used in fluorescence thermometry. However, Kusama et al[36] have utilized this approach for cathode-ray-tube thermometry. The cost of the spectrometer system needed for accurate measurement does not usually render this a strong competitor to other fluorescence-based methods.

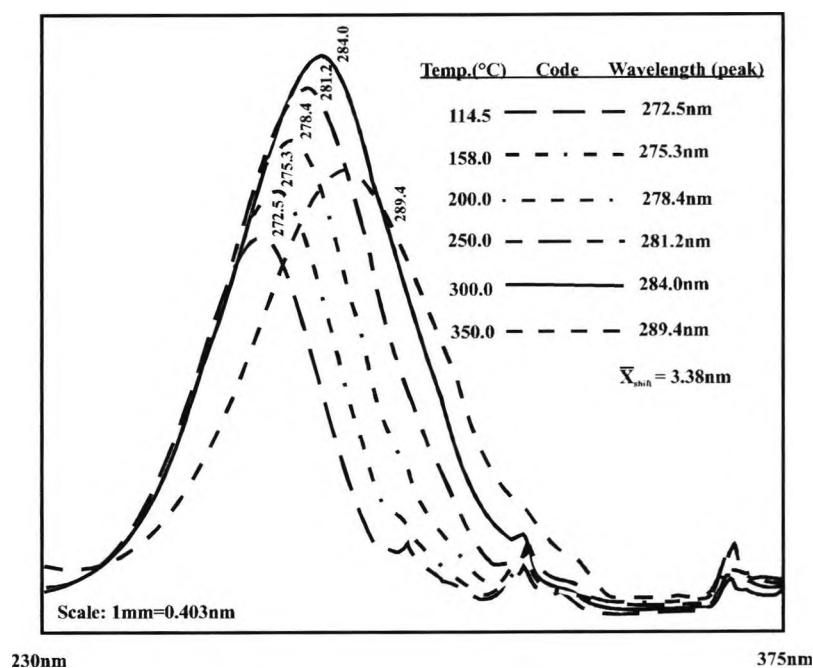


Fig.2.4 The temperature-dependent excitation spectra of $\text{Y}_2\text{O}_3:\text{Eu}$, as measured with a Perkin-Elmer model 650-10S spectrometer with a resolution of approximately 1 nm

2.4.2.4 Absorption band and excitation spectra temperature dependence

The absorption spectra of many phosphors consist of a relatively broad band in the blue or ultraviolet end of the spectrum, along with sharper absorption features in the visible and near-IR. The sharper features are often due to atomic transitions of the dopant atom and exhibit some temperature sensitivity. The broad absorption band, however, since it results from direct interaction with the host, may show a more marked temperature dependence.

Bugos[37] studied the temperature-dependent excitation spectra of a number of thermographic phosphors. An example is shown in Fig.2.4, which presents the temperature-dependent excitation spectra of $Y_2O_3:Eu$. The absorption band is seen to move toward the red end of the spectrum by about 30nm per 50°C (i.e., 0.6nm/°C).

2.4.3 Calibration methodology

To provide valid thermometric data, the response of a phosphor based temperature sensor must be calibrated against a known standard. At the very least, this requires that the quantity of interest (line intensity, lifetime, etc.) be measured as a function of temperature under known and repeatable conditions, with a stable and well-characterized thermometer serving as the reference. Ideally, the calibration measurements are carried out with a transfer standard. If so, and if the resulting data are taken under an appropriate protocol, traceability of the measurements to the International Temperature Scale[38], as maintained by the various national standards laboratories[39][40], can be established.

2.4.3.1 General approach and thermal considerations

The overall scheme of a relatively generic calibration system[41] is shown representatively in Fig.2.5. As might be expected, it constitutes a special case of the arrangement shown in Fig.2.2. The phosphor to be evaluated is either bonded onto a substrate with a high-temperature adhesive, or a small amount of it is spread into a ceramic boat. This sample is then centred inside an oven or furnace and silica-clad optical fibres are used to convey the luminous signals into and out of the high-

temperature cavity. A dye laser driven by a pulse nitrogen laser was used to tune the excitation signal to the wavelength of interest. The decaying-exponential fluorescence wave forms are gleaned from the optical background with a narrow band filter and converted to an electrical pulse train by a photomultiplier tube (PMT). A useful variation involves substitution of a monochromator for the optical filter, thus extending the flexibility of the arrangement. A digital sampling oscilloscope or some other waveform acquisition device is used to collect the fluorescence signals, which are then analyzed by computer to yield the fluorescence lifetime. The probe of the reference thermometer (e.g., a platinum resistance thermometer or a well-characterized thermocouple) is placed in direct contact with the phosphor sample inside the high-temperature cavity and its readings are stored in the memory of the computer, along with the decay time measurements, as the cavity is ramped up and down in temperature.

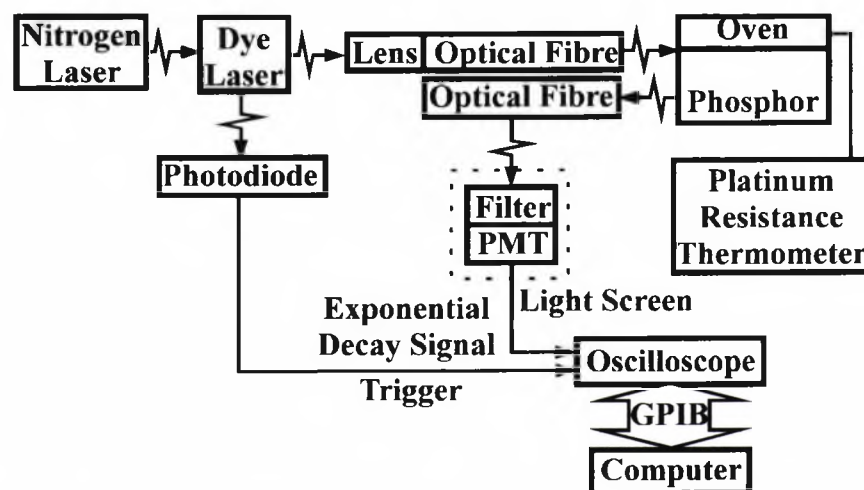


Fig.2.5 The characteristic experimental arrangement used to calibrate the temperature dependence of fluorescence

The overall accuracy and repeatability of the calibration depends critically on the quality and robustness of the reference standard and the stability and uniformity of the high temperature thermal field of the cavity[12]. As a practical matter, the reference thermometer must typically be encased in an armoured probe or it must have a surface passivation layer to minimize the effects of corrosion due to the oxidation that occurs during cycling to high temperatures. A more insidious problem is that created by thermal gradients in the high-temperature cavity. The lack of a totally uniform distribution of temperatures within the oven or furnace means that it is generally necessary to keep the phosphor target and the reference thermometer fixed in one place and in physical contact with each other during a calibration run. One remedy to the thermal gradient problem was devised by Crovini and Fericola[42] at the Colonnetti Institute in Italy. They custom-built an oven that was subsequently used in calibration studies of fluorescence decay thermometers. The temperature uniformity over the specimen of phosphor under study was $\pm 0.03^{\circ}\text{C}$. There are some other relevant studies by Cates et al[43], Alaruri et al[44], Dowell et al[41] and Gillies et al[45] in this field.

2.4.3.2 Signal processing considerations

When making fluorescence lifetime measurements, a decaying exponential waveform including noise and a d.c. offset is typically presented to the signal processing system. Composite signals consisting of multiexponential wave forms are encountered for some phosphors[46] and this can complicate the calibration process. The more routine problem, though, is that of measuring the parameters of a single-exponential wave form.

Two broad central issues that arise in synthesizing an appropriate signal processing system are (1) the choice of the data acquisition and signal averaging devices and (2) the choice of the algorithm used to analyze and reduce the data. The resulting measurement errors were found to decrease with continued averaging, but not without limit[47]. Several schemes[10] have been used to evaluate a fluorescence lifetime, for example, (1) the pulse measurement of fluorescence lifetime, which includes two-point time constant measurement[48], the integration method[49] and the digital curve fit method[50]. (2) phase and modulation measurement[51][52]. In this approach, the intensity of the excitation light is sinusoidally modulated so that the tangent value of the phase shift at the response is proportional to the fluorescence lifetime. A further approach includes (3) phase-locked detection of fluorescence lifetime[11][53], which includes the simple oscillator method[54], with phase-locked detection using a single reference signal[53] and phase-locked detection using two reference signals[55]. All the above methods have been reviewed in detail by Grattan and Zhang[10][11]. Very recently, a new scheme, involving the digital cross-correlation technique using a radionuclide-scintillation excitation source, has been described by Burden and Hieftje[56] to provide single-photon sensitivity and accurate lifetime analysis, even at low sample concentrations.

A series of studies examining the errors in a variety of algorithms running on the thermometry system host computer, shown in Fig.2.5, was undertaken. This series began with a preliminary and empirical investigation of the problems encountered in making a simple least-square fit of a two-parameter exponential curve to the observed

fluorescence data[57]. A more sophisticated subsequent study involved numerical Monte Carlo testing of both two-point and nonlinear least-squares algorithms, with Gaussian-distributed noise added to the simulated signals[58]. The use of Marquardt least-squared error algorithms and Kullback-Leibler stochastic distance analysis allowed for even more precise modelling and validation studies[59], including those incorporating the dc offset of the waveform into the model being tested. The final results were similar in nature to those found in the experimental evaluations of the various wave form-acquisition instruments: an optimum observation time that should be used in measuring the exponential decay may be established, in order to minimize the lifetime-estimation error caused by the noise[60]. Recently Zhang et al[61] implemented Prony's method for improving the computational speed, achieving a 98% decrease in run time and the author and the others[62] have extended this approach for use in a quasi-distributed temperature sensing system.

2.4.3.3 Low temperature arrangements

The discussion so far has focused on the calibration of phosphor thermometers over the range from room temperature through 1000°C and above. There have been several attempts at making fluorescence-based thermometers that work at cryogenic temperatures as well. The selection of the phosphor is an important issue, as many of these materials exhibit little or no temperature dependence in their lifetimes and intensities at low temperatures. As an example, Dowell and Gillies[63] found the fluorescence lifetime of $Y_2O_3:Eu$ (6.8%) changed by less than 3% between room temperature and 77.5K. The temperature dependence observed at low temperatures had already been published for several oxysulfide fluorescent materials[64]. In

Chapter 2 Fibre Optic Luminescence Thermometry: Background and Previous Work

particular, Wickersheim et al[65] have shown the fluorescence spectra of $\text{La}_2\text{O}_2\text{S:Tb}$ at both liquid nitrogen (77K) and liquid helium(4K) temperatures, illustrating there was a change in distribution of line strength as a function of temperature. Their data gave an indication that emission line intensity ratios could be used to determine temperature below 77K. They also discovered the temperature dependence of a number of other oxysulfide materials, including $\text{La}_2\text{O}_2\text{S:Eu}$. This has spurred Fonger and Struck[66] to conduct a detailed investigation and characterization of these materials, aimed at elucidating and modelling the emission. Krauss et al[67] have also studied $\text{La}_2\text{O}_2\text{S:Eu}$ at low temperatures (over the range from 193 to 293K) and achieved a resolution of 0.25K in their calibration activity. Sun[50] has shown the temperature dependence of fluorescence in $\text{Mg}_4\text{FGeO}_6\text{:Mn}$ down to 73K. Cates et al[64] extended the study of the temperature dependence of these materials down to liquid helium temperatures.

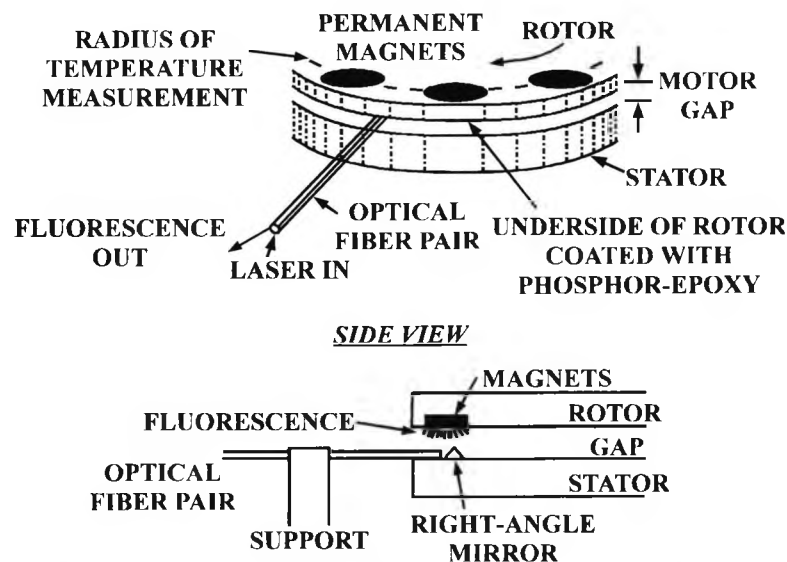


Fig.2.6 The experimental arrangement used to measure the armature temperature of an operating, high-speed, permanent-magnet motor

These studies have shown the validity of the technique for low temperature but probe construction in many cases is complex and it may lack robustness. These issues are addressed in this work.

2.4.4 Thermometry of moving surfaces

A phosphor target mounted on a surface moving at high speeds may translate or rotate by non-negligible amounts during the period required to make a decay time-based measurement of its temperature. Virtually any kind of light delivery and collection scheme used in the measurement system will have a limited field of view. As a result, the fluorescing region may move significantly within the field of view, perhaps even completely into then out of it, during the measurement period. This possibility is depicted in Fig.2.6, which illustrates how measurements were made on the armature of a high-speed motor, using only a single optical fibre to collect the emission[68]. The total amount of light reaching the detector will change with time as the fluorescing spot sweeps through the acceptance numerical aperture of the collection fibre. The efficiency of light collection will vary as a function of the rotation angle, being a maximum on the fibre axis and dropping to zero at points sufficiently far off the axis. The time dependence of the signal will be given by the product of the exponential time dependence and the (changing) optical collection efficiency factor, F . Allison et al[68] noted that the 538nm emission lifetime of the phosphor used in the study was temperature independent over the expected range of interest (room temperature to 100°C). The point-to-point intensity ratio of the moving signal, I_v , to the stationary signal, I_s , both at 538nm, yields the functional dependence of the efficiency factor at that particular speed. Thus,

$$F = I_v / I_s \quad (2.2)$$

Two such identical signals are depicted in Fig.2.7. When this function is used to normalize the acquired temperature-dependent signal, $I_v(t)$, which for Allison et al[68]

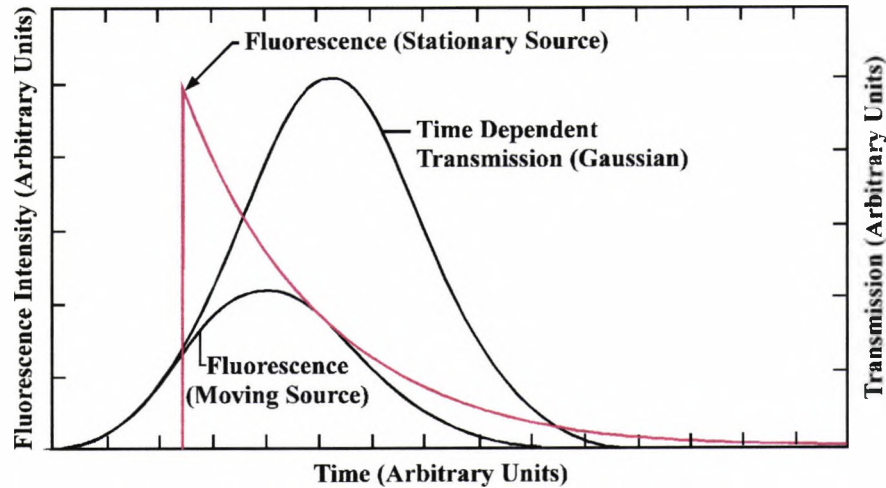


Fig.2.7 Illustration of the effect of motion on the fluorescence signal in the sensor system

was at a wavelength of 514nm, the intrinsic time dependence, $I_c(t)$, is revealed. The relationships should be

$$I_c(t) = I_v(t) / F \quad (2.3)$$

$$\log(I_c(t)) = -t / \tau + A \quad (2.4)$$

where τ is the characteristic decay time and A is a constant.

2.4.5 Surface and volumetric thermography

As conceived originally, phosphor thermography was intended foremost to be a means of depicting two-dimensional temperature patterns on surfaces and the predominant use of the technique was in imaging applications in aerodynamics. The method was termed “contact thermometry” since the phosphor was in contact with the surface to be monitored[12]. An alternative approach suggested by Urbach called

Chapter 2 Fibre Optic Luminescence Thermometry: Background and Previous Work

“projection thermography” involved the optical transfer and projection of a thermal image onto a phosphor screen for subsequent analysis[69]. The overall approach, however, has largely been overshadowed by the introduction of modern infrared thermal imaging techniques[12].

Buck developed a phosphor imaging system for transient aerodynamic measurements[70]. His approach used a three-colour video camera to view a fluorescing phosphor mixture. The ratio of the intensity of the blue part of the emission band to that of the green provided the signal of interest, as it was a function of temperature. Bizzak and Chyu[71] noted that the more conventional thermometry methods are not satisfactory for temperature and heat transfer measurements that must be made in the rapidly fluctuating conditions peculiar to the microscale environment. In their effort to develop a phosphor imaging system, the maximum error found for a surface the size of which was represented by a 1×1 pixel in their video system was 1.37°C , with an average error of only 0.09°C .

Taliaferro[72] used an image-intensified Cohu model 012A03 CCD camera to monitor the fluorescence intensity profiles of $\text{La}_2\text{O}_2\text{S:Eu}$ - and $\text{Y}_2\text{O}_2\text{S:Eu}$ - coated surfaces over the range from room temperature to 200°C . The precision of the imaging system was such that thermal gradients of $0.02^\circ\text{C}/\text{pixel}$ (at nominal temperatures of 35°C) could be resolved over the surface.

It has often been suggested that combustion flames could be diagnosed by seeding them volumetrically with phosphor particles. In fact, the flames themselves can in

some instances serve to excite the luminescence. By the 1980s, the performance of video cameras, segmented detectors, CCD array detectors, and laboratory computers provided greater data acquisition power and experimental design flexibility, leading to several new developments. A particularly clever conception by Goss et al[73] involved the visualization of the condensed-phase combustion of solid rocket propellant. They impregnated the fuel under test with YAG:Dy, and used the ratio of an F-level band at 496nm to a G-level band at 467nm as the signal of interest.

Very recently, Huang et al[74] described a CCD-based multi-functional flame monitoring system which measures simultaneously multiple parameters of a flame including size, temperature and colour.

2.5 Discussion

2.5.1 Performance characteristics

Phosphor thermometry systems can be divided roughly into two broad categories: those designed for laboratory investigations and those for field applications. The laboratory systems are typically used to explore the performance limits of the technique under highly controlled conditions, for instance, varying only one experimental or environmental parameter at any one time during the calibration studies. On the other hand, field-grade systems must be very robust in nature, with the phosphor target in particular being able to withstand extreme levels of thermal and mechanical shock, as could occur when measurements are actually being taken on machinery in use[12].

Table 2.1 presents a summary of the characteristics of several different but largely representative experimental arrangements, including laboratory-grade and field-deployed setups[12][75][76]. The fluorescence lifetime approach to determining the sample temperature would seem to be preferred to alternative methods in many types of field applications, especially those where large and broadband optical background signals (e.g., blackbody radiation) are present. Of course, ratios of temperature-dependent line intensities, or simply measurements of the individual line intensities as a function of temperature, also provide useful thermometric data.

2.5.2 Comparison with other techniques

One of the primary virtues of any type of noncontact thermometry is the elimination of electrical leads and/or other interconnections between the object under study, the sensor element(s) and associated read-out instrumentation. From a broader perspective, any measurement environment that has a high EMI/RFI background can lead to inductive coupling of electrical noise into the thermocouple and resistive temperature-device leads, whether the sensor is static or moving. In contrast to all of these limitations, phosphor thermometry could be a completely noncontact technique, and the photo-optical nature of the signal makes it immune to EMI/RFI pickup[12].

Competing non-contact techniques include radiometric IR thermography and optical pyrometry. Very sophisticated and highly developed versions of both classes of instrumentation are commercially available, and a substantial body of manufacturer literature describes the performance characteristics of the pertinent devices. The

Chapter 2 Fibre Optic Luminescence Thermometry: Background and Previous Work

Table 2.1 Summary of the characteristics of representative arrangements

Author(s)	Application	Phosphor /method	Design features	Range /uncertainty
Mannik et al (1987)	Noncontact thermometry of 540 MW electrical generator rotor surfaces	Gd ₂ O ₂ S:Eu, Y ₂ O ₂ S:Eu and La ₂ O ₂ S:Eu, <i>decay lifetime</i>	Ambient magnetic field of the generator was ≈ 1 T; measurement had spatial resolution of 4mm	41-73°C $\Delta T = \pm 2.0^\circ\text{C}$
Dowell (1989)	Design and evaluation of a thermal phosphor-based temperature standard	Y ₂ O ₃ :Eu (single crystals), <i>decay lifetime</i>	Fluorescence lifetimes were measured relative to a cesium-beam atomic clock	≈ 30 -800°C $\Delta T = \pm 6.4^\circ\text{C}$ (at $\approx 800^\circ\text{C}$)
Noel et al (1991)	Remote measurement of vane and blade temperatures in an operating turbine engine	YVO ₄ :Eu, Y ₂ O ₃ :Eu and YAG:Tb, <i>decay lifetime</i>	Phosphor layers from 4 to 35 μm thick applied by rf sputtering, e-beam deposition, chemical binder	450-1300°C relative error $\approx \pm 2\%$
Draina and Anderson (1992)	Temperature control of IC wafers during plasma etch and chemical vapor deposition processes	Luxtron MIH probes and custom-designed SEMATECH probe	Measurements made in vacuum and at low pressures relative to a type-K thermocouple or a PRT	25-400°C $\Delta T = \pm 10^\circ\text{C}$
Alaruri et al (1993)	Monitoring temperatures of turbine engine parts in a burner rig	Y ₂ O ₃ :Eu (4.52%) and YAG:Tb (5%), <i>decay lifetime</i>	Air-cooled fibreoptic probe with sapphire lens was developed ; its damage threshold was 3.5J/cm ²	27-1095°C accuracy quoted as $\pm 3\%$ for Y ₂ O ₃ :Eu
Chyu and Bizzak (1994)	2D surface temperature measurements/general heat transfer studies	La ₂ O ₂ S:Eu ³⁺ , <i>intensity ratio</i> of 512-620nm lines	80mJ excitation energy supplied by laser beam of 6.4mm- diam during 8ns pulses	18-60°C $\Delta T = \pm 0.5^\circ\text{C}$
Luxtron Corp. (1993)	Commercially available apparatus used in a wide variety of measurements	MFG2 phosphor-tipped fibreoptic probes, <i>decay lifetime</i>	Excitation and fluorescence return pulses transmitted over the same optical fibre (model 790 systems)	-200-450°C $\Delta T = \pm 0.1^\circ\text{C}$ rms, at calibration point
Anghel et al (1995)	Development of probes useful in low temperature industrial applications	Ruby crystal with fibreoptic couplings, <i>decay lifetime</i>	Green LED used to excite sensor, overall size of probe 4 \times 10mm, calibrated with type-K thermocouple	≈ 70 -30°C $\Delta T = \pm 0.3^\circ\text{C}$
Maurice et al (1995)	Development of probes for wide temperature sensing	Rare-earth doped fibre tipped fibre optic probes, <i>intensity ratio</i>	Laser diode or argon ion laser used to pump the doped fibre and filters or spectrometers were used to collect the signal	100-1000K $\Delta T = \pm 1.3\text{K}$
Grattan and Zhang (1994-1997)	Development of effective, compact, intrinsic probes for wide range temperature measurement	Rare-earth doped fibre fusion spliced to plain fibres, <i>decay time</i>	Laser diode was used to pump the doped fibre and the fluorescence signal collected by the photodetector	-190-1100°C $\Delta T = \pm 2$ -5°C

optimum thermometric resolution presently obtained via either technique is typically 0.1°C [12].

2.5.3 Opportunities for further research

As new applications for phosphor thermometry arise, there will be a concomitant need for target (thermometer probe) materials that have luminescence characteristics appropriate to the measurement being undertaken. More extensive studies will be needed to determine the optimum ratio of dopants for a possible sensing material, to characterize fully the temperature sensitivity of its fluorescence, and to evaluate its robustness. The fluorescence properties of other co-doped phosphors should be investigated as well.

At temperatures in the range of 1000°C and above, the fluorescence lifetimes of virtually all phosphors are very short. Once the lifetime drops below about $100\mu\text{s}$, the speed, resolution, and accuracy requirements placed on the data acquisition system typically call for the use of more sophisticated transient digitizers and fast pulse analyzers. If more were done to adapt the technique for use in phosphor thermometry systems, then the range over which temperature measurements could be made with this technique might be extended.

The potential of phosphors to sense still other physical quantities should continue to be explored. Interesting steps along this line have been taken by Egalon, Rogowski and colleagues[77][78], who investigated the possible use in chemical sensing applications of thin films of fluorescent material placed at the core/cladding interface

Chapter 2 Fibre Optic Luminescence Thermometry: Background and Previous Work

of fibreoptic probes. Recently the research group in the University of Strathclyde developed a lifetime sensor for Cu ion detection[79].

Further study is necessary to extend the application of phosphor thermometry from point temperature sensing to more distributed or average temperature sensing. A particular valuable advance would arise from the development of a technique which enables the signal processing to be fast as well as accurate.

Finally, it is necessary to clarify the characteristics and difference of each sensing scheme to optimize its appropriate application and cost benefit in use.

The following chapters in this work will focus on the above topics and investigate in a series of discrete chapters and sections the extension of the application of phosphor thermometry as widely as possible.

2.6 References

- [1] Application Note 290, *Practical Temperature Measurements*, HEWLETT PACKARD, 1997
- [2] E.H.McLaren and E.G.Murdock, The Pt/Au Thermocouple, National Research Council of Canada, Research Monograph NRCC 27703 (1987)
- [3] Y.G.Kim, K.S.Gam and K.H.Kang, Thermoelectric properties of the Au/Pt thermocouple, *Rev. Sci. Instrum.*, 69, 3577(1998)

Chapter 2 Fibre Optic Luminescence Thermometry: Background and Previous Work

- [4] M.N.Inci, J.S.Barton and J.D.C.Jones, A fibre-optic thermometric sensor based on the thermo-optic effect of titanium dioxide coatings, *Optics & Laser Technology*, 29, 121(1997)
- [5] X.Fang, R.G.May, A.Wang and R.O.Claus, A fiber-optic high-temperature sensor, *Sensors and Actuators A*, 44, 19(1994)
- [6] Sønnik Clausen, Local measurement of gas temperature with an infrared fibre-optic probe, *Meas. Sci. Technol.*, 7, 888(1996)
- [7] K.T.V.Grattan, The use of fibre optic techniques for temperature measurement, *Measurement and Control*, 20, 32(1987)
- [8] K.T.V.Grattan, Fiber optic techniques for temperature sensing, in *Fibre Optic Chemical Sensors and Biosensors*, Vol.II (ed. O.S.Wolfbeis), CRC Press, London, 151(1991)
- [9] K.A.Wickersheim, Fiberoptic thermometry: an overview, in *Temperature-Its Measurement and Control in Science and Industry*, Vol.6, Part 2 (ed. J.F.Schooley). American Institute of Physics, New York, 711(1992)
- [10] K.T.V.Grattan and Z.Y.Zhang, Fiber optic luminescent thermometry, in *Optical Fiber Sensor Technology 4. Environmental and Chemical Sensing* (eds. K.T.V.Grattan and B.T.Meggitt). Chapman & Hall, London, 133(1998)
- [11] K.T.V.Grattan and Z.Y.Zhang, *Fiber Optic Fluorescence Thermometry*, Chapman & Hall, London, 1995
- [12] S.W.Allison and G.T.Gillies, Remote thermometry with thermographic phosphors: Instrumentation and applications, *Rev. Sci. Instrum.*, 68, 2615(1997)
- [13] P.Pringsheim, *Fluorescence and Phosphorescence*, Interscience, New York, 1949

Chapter 2 Fibre Optic Luminescence Thermometry: Background and Previous Work

- [14] G.H.Dieke and H.M.Crosswhite, *Appl. Opt.*, 2, 675(1963)
- [15] W.H.Fonger and C.W.Struck, *J.Chem. Phys.*, 52, 6364(1970)
- [16] C.W.Struck and W.H.Fonger, *J. Appl. Phys.*, 42, 4515(1971)
- [17] Z.Y.Zhang, K.T.V.Grattan and A.W.Palmer, Thermal characteristics of alexandrite fluorescence decay at high temperatures, induced by a visible laser diode emission, *Journal of Applied Physics*, 73, 3493(1993)
- [18] G.Blasse, Luminescence of inorganic solids – from isolated centres to concentrated systems, *Prog. Solid State Chem.*, 18, 79(1988)
- [19] D.J.Robbins, B.Cockayne, B.Lent and J.L.Glasper, *J.Electrochem. Soc.*, 126, 1556(1979)
- [20] Z.H.Zhang, J.H.Herringer and N.Djeu, Monolithic crystalline fiber optic temperature sensor, *Rev. Sci. Instrum.*, 68, 2068(1997)
- [21] W.F.Vanderweg, T.J.A.Popma and A.T.Vink, Concentration-dependence of UV and electron-excited Tb³⁺ luminescence in Y₃Al₅O₁₂, *J. Appl. Phys.*, 57, 5450(1985)
- [22] L.J.Dowell, Los Alamos National Laboratory Technical Report No. LA 11873-MS, August 1990
- [23] L.J.Dowell, *J. Laser Appl.*, 3, 27(1991)
- [24] D.M.Deleeuw and G.W.Thooft, Method for the analysis of saturation effects of cathodoluminescence in phosphors - applied to Zn₂SiO₄-Mn and Y₃Al₅O₁₂-Tb, *J. Lumin.*, 28, 275(1983)
- [25] S.Imanaga, S.Yokono and T.Hoshima, *Jpn. J. Appl. Phys.*, 19, 41(1980)
- [26] M.J.Weber, in *The Handbook on the Physics and Chemistry of Rare Earths* (Eds. K.A.Gschneidner, Jr. and L.Eyring), North-Holland, Amsterdam, 1979, Chap35, 275(1979)

Chapter 2 Fibre Optic Luminescence Thermometry: Background and Previous Work

- [27] C.X.Guo, W.P.Zhang and C.S.Shi, Enhancement mechanism of luminescence of Re^{3+} (Eu^{3+} , Sm^{3+} , Dy^{3+}) in $\text{Y}_2\text{O}_2\text{S}$ phosphor by a trace of Tb^{3+} , *J. Lumin.*, 24-25, 297(1981)
- [28] K.A.Wickersheim and R.V.Alves, Fluoroptic thermometry: a new RF-immune technology, in *Biomedical Thermology*, Alan Liss, New York, 547(1982)
- [29] C.Ovren, M.Adoleson and B.Hök, Fibre optic systems for temperature and vibration measurements in industrial applications, in *Proceedings Int. Conf. Optical Techniques in Process Control*, The Hague, 1983
- [30] K.A.Wickersheim and M.H.Sun, Fiberoptic thermometry and its applications, *Journal of Microwave Power*, 22, 85(1987)
- [31] R.R.Sholes, J.G.Small, Fluorescent decay thermometer with biological applications, *Rev. Sci. Instrum.*, 51, 882(1980)
- [32] Th. Bosselmann, A.Reule and J.Schröder, Fiber-optic temperature sensor using fluorescence decay time, *Proc. 2nd Conf. Optical Fibre Sensors (OFS'84)*, SPIE Proceeding, 514, 151(1984)
- [33] K.T.V.Grattan and A.W.Palmer, A fibre optic temperature sensor using fluorescence decay, *SPIE Proceeding*, 492, 535(1984)
- [34] K.T.V.Grattan and A.W.Palmer, Infrared fluorescence 'decay-time' temperature sensor, *Rev. Sci. Instrum.*, 56, 1784(1985)
- [35] Temperature Measurement Products, LUXTRON Corporation, California, U.S.A., *Manufacture's data*, 1998
- [36] H.Kusama, O.J.Sovers and T.Yoshioka, *Jpn. J. Appl. Phys.*, 15, 2349(1976)

Chapter 2 Fibre Optic Luminescence Thermometry: Background and Previous Work

- [37] A.R.Bugos, S.W.Allison, D.L.Beshears and M.R.Cates, Emission properties of phosphors for high temperature sensor applications, in *Proceedings of the IEEE Southeastcon Conference* (IEEE, New York, 1988), 228(1988)
- [38] H.Preston-Thomas, *Metrologia*, 27, 3(1990)
- [39] Comité Consultatif de Thermométrie, *Techniques for Approximating the International Temperature Scale of 1990*(Bureau International des Poids et Mesures, Sèvres, France, 1990)
- [40] Comité Consultatif de Thermométrie, *Supplementary Information for the International Temperature Scale of 1990* (Bureau International des Poids et Mesures, Sèvres, France, 1990)
- [41] L.J.Dowell, W.N.Lutz, G.T.Gillies, R.C.Ritter, S.W.Allison and M.R.Cates, Calibration of a laser pumped, thermographic phosphor remote thermometry system, *Proc. Laser Inst. Am.*, 57, 135(1987)
- [42] L.Crovini and V.Fernicola, An oven to test fluorescent-decay temperature sensors, *Sens. Actuators B*, 7, 529(1992)
- [43] M.R.Cates, S.W.Allison, L.A.Franks, H.M.Borella, B.R.Marshall and B.W.Noel, *Proc. Laser Inst. Am.*, 49-51, 142(1985)
- [44] S.D.Alaruri, A.J.Brewington, M.A.Thomas and J.A.Miller, High-temperature remote thermometry using laser-induced fluorescence decay lifetime measurements of Y₂O₃-Eu and YAG-Tb thermographic phosphors, *IEEE Tran. Instrum. Meas.*, 42, 735(1993)
- [45] G.T.Gillies, L.J.Dowell, W.N.Lutz, S.W.Allison, M.R.Cates, B.W.Noel, L.A.Franks and H.M.Borella, *Proc. Laser Inst. Am.*, 63, 15(1988)

Chapter 2 Fibre Optic Luminescence Thermometry: Background and Previous Work

- [46] T.Sun, Z.Y.Zhang, K.T.V.Grattan and A.W.Palmer, Analysis of double exponential behaviour in alexandrite for optical temperature sensing applications, *Rev. Sci. Instrum.*, 68, 3442(1997)
- [47] L.J.Dowell, G.T.Gillies, M.R.Cates and S.W.Allison, Precision limits of waveform recovery and analysis in a signal-processing oscilloscope, *Rev. Sci. Instrum.*, 58, 1245(1987)
- [48] K.A.Wickersheim and M.H.Sun, Fiberoptic thermometry and its applications, *Journal of Microwave Power*, 22, 85(1987)
- [49] R.R.Sholes and J.G.Small, Fluorescent decay thermometer with biological applications, *Rev. Sci. Instrum.*, 51, 882(1980)
- [50] M.Sun, Fiberoptic thermometry based on photoluminescent decay times, in *Temperature – Its Measurement and Control in Science and Industry*, Vol.6, Part 2, American Institute of Physics, New York, 715(1992)
- [51] K.T.V.Grattan, R.K.Selli and A.W.Palmer, Ruby decay-time fluorescence thermometer in a fibre-optic configuration, *Rev. Sci. Instrum.*, 59, 1328(1988)
- [52] A.T.Augousti, K.T.V.Grattan and A.W.Palmer, Visible-LED pumped fiber-optic temperature sensor, *IEEE Transactions on Instrumentation & Measurement*, 37, 470(1988)
- [53] Z.Y.Zhang, K.T.V.Grattan and A.W.Palmer, Phase-locked detection of fluorescence lifetime and its thermometric applications, in *Proc. Int. Conf. Biomedical Optics '93*, Los Angeles, *SPIE Proceedings*, 1885, 228(1993)
- [54] Th. Bosselmann, *UK Patent Application GB2*, 113, 837A(1983)
- [55] Z.Y.Zhang, K.T.V.Grattan and A.W.Palmer, Fibre-optic high temperature sensor based on the fluorescence lifetime of alexandrite, *Rev. Sci. Instrum.*, 63, 3177(1992)

Chapter 2 Fibre Optic Luminescence Thermometry: Background and Previous Work

- [56] D.L.Burden and G.M.Hieftje, Digital cross-correlation technique for fluorescence-lifetime measurement using a radionuclide-scintillation excitation source, *Rev. Sci. Instrum.*, 69, 1595(1998)
- [57] W.N.Lutz, L.J.Dowell and G.T.Gillies, University of Virginia Technical Report No. UVA/532705/NEEP87/101, September 1986
- [58] L.J.Dowell and G.T.Gillies, Precision limits of lifetime estimation algorithms as determined by Monte-Carlo simulation - a comparison of theory and experiment, *Rev. Sci. Instrum.*, 59, 1310(1988)
- [59] L.J.Dowell and G.T.Gillies, Los Alamos National Laboratory Technical Report No. LA-UR-90-2621, August 1990
- [60] L.J.Dowell and G.T.Gillies, Errors caused by base-line offset and noise in the estimation of exponential lifetimes, *Rev. Sci. Instrum.*, 62, 242(1991)
- [61] Z.Y.Zhang, K.T.V.Grattan, Y.Hu, A.W.Palmer and B.T.Meggitt, Prony's method for exponential lifetime estimations in fluorescence-based thermometers, *Rev. Sci. Instrum.*, 67, 2590(1996)
- [62] T.Sun, Z.Y.Zhang, K.T.V.Grattan and A.W.Palmer, Quasi-distributed fluorescence-based optical fiber temperature sensor system, *Rev. Sci. Instrum.*, 69, 146(1998)
- [63] L.J.Dowell and G.T.Gillies, University of Virginia Technical Report No. UVA/532866/NEEP89/101, October 1988
- [64] M.R.Cates, D.L.Beshears, S.W.Allison and C.M.Simmons, Phosphor thermometry at cryogenic temperatures, *Rev. Sci. Instrum.*, 68, 2412(1997)
- [65] K.A.Wickersheim, R.A.Buchanan, L.E.Sobon, R.V.Alves and J.J.Pearson, Lockheed Missiles & Space Company, *Third Annual Report 4-17-69-1*, 41(1969)

Chapter 2 Fibre Optic Luminescence Thermometry: Background and Previous Work

- [66] C.W.Struck and W.H.Fonger, *J. Lumin.*, 1, 456(1970)
- [67] R.H.Krauss, R.G.Hellier and J.C.McDaniel, Surface-temperature imaging below 300K using $\text{La}_2\text{O}_2\text{S-Eu}$, *Appl. Opt.*, 33, 3901(1994)
- [68] S.W.Allison, M.R.Cates, B.W.Noel and G.T.Gillies, Monitoring permanent-magnet motor heating with phosphor thermometry, *IEEE Trans. Instrum. Meas.*, 37, 637(1988)
- [69] F.Urbach, N.R.Nail and D.Pearlman, *J. Opt. Soc. Am.*, 39, 1011(1949)
- [70] G.M.Buck, US Patent No. 4,885,633 (5 December 1989)
- [71] D.J.Bizzak and M.K.Chyu, Rare-earth phosphor laser-induced fluorescence thermal imaging-system, *Rev. Sci. Instrum.*, 65, 102(1994)
- [72] J.M.Taliaferro, S.W.Allison and K.W.Tobin, Martin Marietta Energy Systems, *Inc. Technical Report* No. ORNL/ATD-61, November 1991
- [73] L.P.Goss, A.A.Smith and M.E.Post, Surface thermometry by laser-induced fluorescence, *Rev. Sci. Instrum.*, 60, 3702(1989)
- [74] Y.Huang, Y.Yan, G.Lu and A.R.Reed, CCD-based multi-functional flame monitoring system, *Applied Optics and Optoelectronics, Proc. Applied Optics Divisional Conference of the Institute of Physics, 16-19 March Brighton, 1998* (Ed. K.T.V.Grattan), 151(1998)
- [75] E.Maurice, G.Monnom and D.B.Ostrowsky, High dynamic-range temperature point sensor using green fluorescence intensity ratio in erbium-doped silica fiber, *IEEE J. Lightwave Tech.*, 13, 1349(1995)
- [76] Z.Y.Zhang, K.T.V.Grattan, A.W.Palmer, T.Sun and B.T.Meggitt, Rare earth doped intrinsic fiber optic sensors for high temperature measurement up to 1100°C, in

Chapter 2 Fibre Optic Luminescence Thermometry: Background and Previous Work

12th International Conference on Optical Fiber Sensors, Vol.16, OSA Technical Digest Series (Optical Society of America, Washington DC, 1997), 556(1997)

[77] C.O.Egalon and R.S.Rogowski, Theoretical-model for a thin cylindrical film optical fiber fluorosensor, *Opt. Eng.*, 31, 237(1992)

[78] C.O.Egalon, R.S.Rogowski and A.C.Tal, Excitation efficiency of an optical fiber core source, *Opt. Eng.*, 30, 1328(1992)

[79] O.J.Rolinski and D.J.S.Birch, A fluorescence lifetime sensor for Cu(I) ions, *Meas. Sci. Technol.*, 10, 127(1999)

Chapter 3

Point Optical Temperature Sensors using Different Fluorescent Materials

3.1 Abstract

This work in this chapter reports on the thermographic characteristics and their potential, in this illustration, of point fibre optic temperature sensors using a range of active elements, e.g. crystalline materials, doped bulk glasses and rare-earth ion doped fibres. Their comparative value for low-cost, simple yet effective sensors is discussed. The models considered here are used to provide underpinning support for the experimental results obtained and are also applicable to the optimization of the selection of particular suitable fluorescent materials for thermometric use over a specific temperature region, or to be used as empirical calibration formulae in their operation. Thus the value of a sound understanding of the physical science processes underlying the nature of the variety of sensor materials can be seen and appreciated in the context of a good sensor system design, discussed in this Chapter.

3.2 Introduction

Crystalline materials and doped bulk glasses, using rare earth active ions, have been extensively studied by Grattan & Zhang[1] and other authors as the essential elements of fluorescence decay-time based fibre optical thermometers. In most cases, a single exponential decay is either seen, or more often assumed. Illustrations of this occur particularly in fibre optic temperature sensors where the doping level of the fluorescent active system is low, such as in Cr^{3+} doped chrysoberyl (alexandrite) which shows a single exponential when the doping level is less than $\sim 0.3\text{at.}\%$ [2]. However, with higher dopant levels, a deviation from a single exponential is observed in the same host crystal, and the effect of this is considered in detail in this work.

Another interesting group of materials for thermometric sensors, using optical techniques is that closely matched to the optimum wavelengths for telecommunications, amplifiers and fibre lasers which enables both the maximum cost benefits to be obtained and also offers some potential for compatibility with optical communication systems, in spite of their essentially different nature of operation. The development of, and subsequent research in, the erbium-doped silica fibre amplifier has been very successful, operating as it does at a wavelength of $1.55\mu\text{m}$, which is the optimum wavelength for low loss in optical communications. Prior to that, using Nd^{3+} ions as the active dopant seemed promising, matching the second telecommunications "window" close to a wavelength of $1.3\mu\text{m}$, but progress has been hampered by excited state absorption and in addition, gain limitations due to amplified spontaneous emission

effects in the material[3]. An alternative lies in using praseodymium, for which the ${}^1G_4 \rightarrow {}^3H_5$ transition in Pr^{3+} shows a broad emission band centered around $1.3\mu\text{m}$ and it should operate as a quasi-four-level system, making it one of the most promising routes for optical amplification on this $1.3\mu\text{m}$ wavelength band[4]. Fluoride glasses are preferred as the material host, because of the lower phonon energies and the consequent expected reduction in non-radiative decay[5]. Neodymium and ytterbium-doped silica fibre lasers operating near $1\mu\text{m}$, as well as erbium fibres at $1.5\mu\text{m}$, have been among the most successful fibre lasers[6].

All the above mentioned important ‘spin-offs’ from telecommunications, amplifiers and lasers are discussed in detail in this work for temperature sensing, employing the luminescent effects seen, especially the inherent fluorescence characteristics of the doped ‘laser’ fibres. Those are being particularly attractive as they are available at reasonable cost, due to the larger quantities now produced commercially. The underpinning science of the luminescent effects is also explored in this work to support the system design activity.

3.2.1 Sensor specification

Initially, in this section, results from the use of several bulk materials incorporated into sensors are reported, and results and performance compared. A general specification for such sensors is as given below:

- a) Wide temperature range: from liquid nitrogen temperature (77K) to beyond 1000K
- b) Error of the measurement: $\sim \pm 2^\circ\text{C}$ over the above temperature range

c) Sensitivity: $\geq 0.1\%/K$

and the fit of the results of the work to such a specification is discussed. The above specification would request a sensor useful for process control application, for example, with performance comparable to that of a typical thermocouple.

3.3 Bulk active material-based thermometry

3.3.1 Alexandrite-based thermometry

3.3.1.1 Previous work

Alexandrite is a chromium (Cr^{3+}) doped chrysoberyl and whose primary use is as a 'ruby-like' laser system, offering a wider wavelength range of operation. The work of Walling et al[2] has shown that if the Cr^{3+} site in the crystal possesses inversion symmetry, parity forbids electric dipole transitions between states of the d^3 configuration. As a consequence, a Cr^{3+} ion that resides on an inversion site shows a weak magnetic-dipole, non-phonon transition. Phonon-assisted vibronic transitions tend also to be weaker in this case than when the Cr^{3+} ion is in a non-inversion symmetry site. Alexandrite, on the other hand, has both inversion and non-inversion (mirror) sites present for the Cr^{3+} ion and with pulsed excitation, the fluorescence lifetime for the two sites was measured in that work to be 1.32 and $\sim 60ms$ respectively, for the mirror and inversion sites, at 4K. It was found that the fraction of the total Cr^{3+} ions that reside on the mirror site is 78 ± 3 percent for both the 0.1at.% and 0.3at.% samples[7], in which the inversion-site Cr^{3+} ions play only a minor role in the alexandrite emission. This is important in that the assumption of a single

exponential decay of the fluorescence can be justified. However, when the Cr^{3+} concentration is higher, the experimental results in this work reveal the fact that the contribution from the inversion-site Cr^{3+} can no longer be considered negligible, the consequences of which will be discussed in detail later.

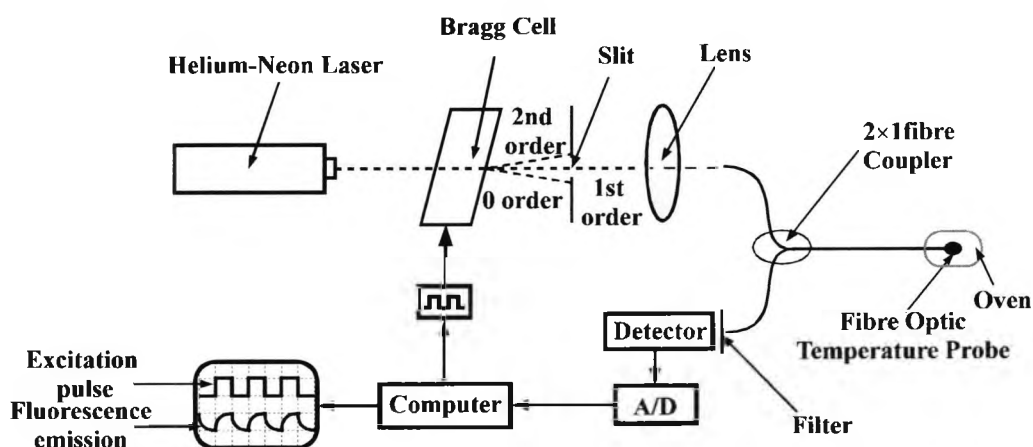


Fig.3.1 Experimental arrangement used in the temperature sensing tests

The single configurational coordinate model, based on the assumption of thermal equilibrium and including the effect of the non-radiative transitions, has been used by Grattan et al[1] and Zhang et al[8][9] to explain the case of these luminescent properties of alexandrite in the mirror-site very successfully. In the work herein, the same model can be found to fit the experimental results obtained very well, including not only the effects due to Cr^{3+} in the mirror site but also in the inversion site. A fuller knowledge of this behaviour is valuable for temperature sensing applications through the exploitation of the underlying processes, themselves having a sound theoretical foundation, to produce an effective sensor system.

3.3.1.2 Experimental configuration

Alexandrite, at a Cr^{3+} dopant level of up to 0.4at.%, was used as the material under investigation[10]. A schematic of such a fluorescence-based sensor system is shown in Fig.3.1, where the sensing head of the probe was designed to use alexandrite as the active species in a probe designed in a similar way to that described previously by Zhang et al[1]. A green Helium-Neon laser operating at a center wavelength of 543.5nm was employed as the excitation light source. Although alexandrite also absorbs in the red region of the spectrum, and thus in principle light from a laser diode operating between 635 and 670nm could be used[9], this higher power laser was chosen for convenience in this present study. This anticipates the rapid development of solid state blue/green lasers using novel technology discussed in the literature[11]. The laser beam was modulated through the use of an acousto-optic Bragg cell, the modulation frequency of which was adjusted by using a pulse signal generated by the digital output port of a computer. With a solid state source, direct electrical modulation of the light output could be obtained, thus reducing system costs.

In the configuration shown in Fig.3.1, the optical arrangement was such that the slit inserted along the optical path was used to block the stray light both from the zero and the second order to allow the modulated (first order) laser signal to excite the sample via the fibre optic probe. To do so, one end of a 2×1 optical fibre coupler, the core diameter of which was 200 μm , was located at the focal point of the lens through which the pumping light was transmitted to the alexandrite crystal sample, which was carefully bonded to the far end of the fibre. The probe was positioned in the center of

the test oven, the temperature of which could be varied and stabilized through use of a thermostatic control and was read using a *K*-type thermocouple in intimate contact with the fibre probe. A glass filter was used to prevent any reflected excitation light from saturating the photodetector and thus effectively transmitting only the fluorescence light coming from the active sensor material at the far end of the fibre. The detected response signal was then digitized by an analog-to-digital (A/D) converter connected to the computer and processed by the software written for the purpose.

3.3.1.3 Experimental results

The fluorescence signals from the alexandrite probe were detected and analyzed, following the termination of the excitation pulse at different temperatures, by using the experimental arrangement shown in Fig.3.1. At each stabilized temperature, it was found that the fluorescence decays exponentially with time after the termination of excitation light pulse, in a manner similar to that of the experimental signal shown in Fig.3.2, which was recorded when the temperature was 100°C. This clearly show that the signal can no longer be assumed to be represented by a single exponential decay, but can be fitted very well to a double exponential function, given by the following

$$f(t)=A_1\exp(-t/\tau_1) + A_2\exp(-t/\tau_2) + B \quad (0 \leq t \leq 160\text{ms}) \quad (3.1)$$

where A_1 and A_2 correspond to the initial separate fluorescence amplitudes; τ_1 and τ_2 are the corresponding fluorescence lifetimes; and B is the baseline offset. The fit of Eq.(3.1) to the experimental data shows that the associated error is within $\pm 1.5\%$,

which is accurate enough to serve as a calibration for a temperature sensing system based on it.

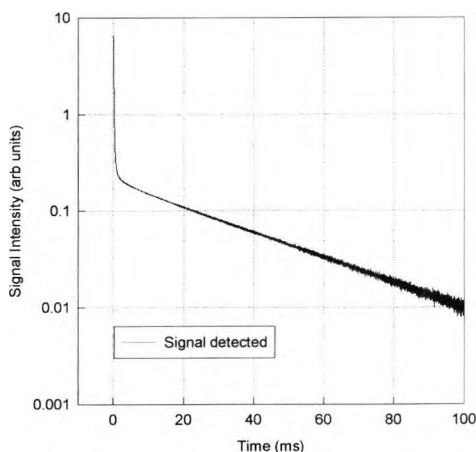


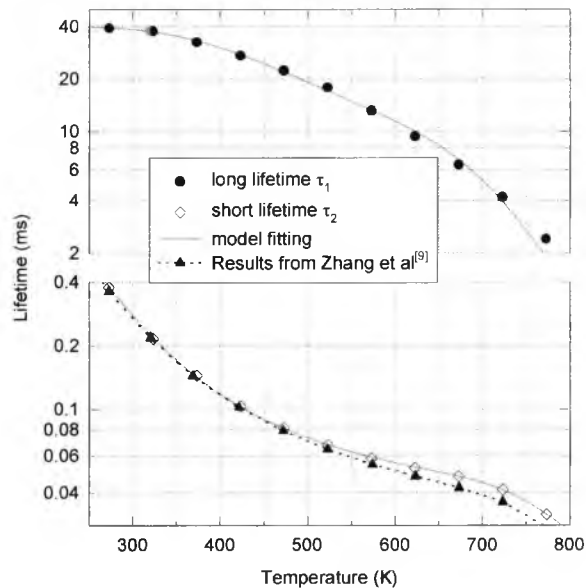
Fig.3.2 Fluorescence decay signal following the termination of pulse excitation at a temperature of 100°C

Over a range of temperatures from 273K to 773K, the fluorescence decay signal obtained has been analyzed and the two lifetimes expressed in Eq.(3.1) are obtained in this work by using the Marquardt non-linear least squares approximation algorithm[12]. As expected, both the lifetimes change as a function of temperature, as shown in Fig.3.3, in which the short and long lifetimes deduced from the analysis are represented separately by the open and the solid circles on the graphs.

In previous work on weakly doped samples, the single exponential decay of the fluorescence following optical excitation, over the region 200K-700K, could be successfully described by a two level model, such as has been used by Walling et al[2]. In this the assumption that the 4T_2 and 2E are in "quasi-thermodynamic equilibrium" was made and it was verified by Gayen et al[13] that the upper limit of the nonradiative

relaxation time was 27ps for the ${}^4T_2 \rightarrow {}^2E$ transition. However, in the temperature region beyond $\sim 700K$, the discrepancy between the fluorescence lifetime data and the results of the two-level model is quite significant[1] because the nonradiative transitions become stronger with increasing temperature beyond $\sim 700K$. Thus the configurational coordinate model, developed by Zhang et al[9] which considers the effect of nonradiative transitions, can be used to describe the fluorescence lifetime as a function of temperature, over a much wider range, in a very satisfactory way.

Fig.3.3 Experimental data on the two lifetimes observed, as a function of temperature, and the fitting curves obtained from the use of the configurational coordinate model



In this work, the two lifetime behaviour observed as a function of temperature is found also to be consistent with the configurational coordinate model, with some small differences seen in the corresponding parameters deduced from it.

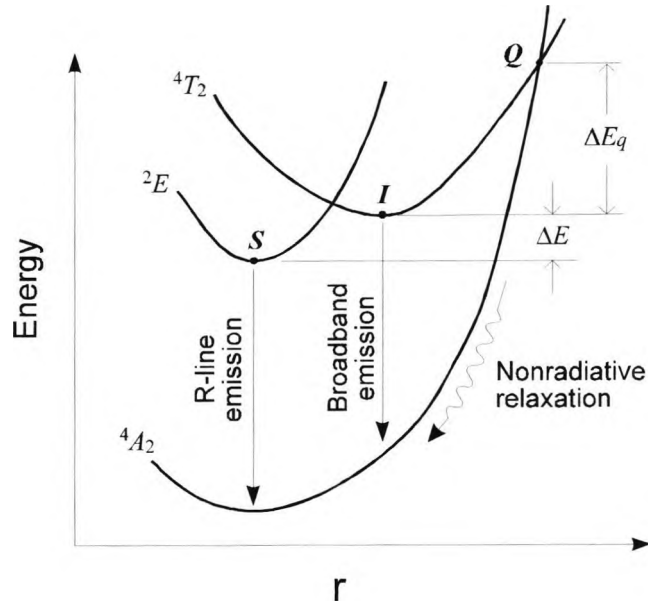


Fig.3.4 Schematic of the configurational coordinate model for Cr^{3+} fluorescence in alexandrite. r : the configurational coordinate (Zhang et al[9])

3.3.1.4 Theoretical explanation of the system performance

To include the effect of the nonradiative transitions, a single configurational coordinate model, shown in Fig.3.4, has been introduced by Zhang et al[1][9] (where further details may be seen). In the case of alexandrite, according to the model, the change of the total population of the 4T_2 and 2E states, n , is described by the rate equation

$$\frac{dn}{dt} = -(1/\tau_s)n_s - \left[1/\tau_i + (1/\tau_q)e^{-\Delta E_q/kT} \right]n_i \quad (3.2)$$

where n_s and n_i are the populations of 2E and 4T_2 respectively; τ_i and τ_s are the lifetimes of the 4T_2 and 2E states respectively; ΔE is the energy gap between the 4T_2 and 2E states; τ_q the thermal quenching lifetime; ΔE_q the thermal activation needed to elevate

ions at the bottom of the excited state to the level crossing Q; and k is the Boltzmann constant. On the assumption that the 4T_2 and 2E states are in "quasi-thermodynamic equilibrium", that is ,

$$\frac{n_i}{n_s} = C_d e^{-\Delta E/kT} \quad (3.3)$$

where C_d is the ratio of the degeneracy of the 4T_2 state to that of the 2E , with a value of 3 for alexandrite, the fluorescence lifetime, τ , can be therefore given by:

$$\tau = \tau_s \frac{1 + 3e^{-\Delta E/kT}}{1 + \alpha e^{-\Delta E/kT} + \beta e^{-(\Delta E_q + \Delta E)/kT}} \quad (3.4)$$

where $\alpha = 3\tau_s/\tau_i$; and $\beta = 3\tau_s/\tau_q$.

The solid line (fitting the open circles) in Fig.3.3 results from a least squares fitting of Eq.(3.4) to the short lifetime data from 273K to 773K for alexandrite. For this short lifetime as a function of temperature, the fitted values for ΔE , τ_s , τ_i , ΔE_q and $\ln\beta$ are listed in Table 3.1, with for comparison, those fitted using the configurational coordinate model by Zhang et al[9] to the emission from alexandrite at a low dopant concentration. The relative fitting error of the short lifetime in this work is ~0.9%. The small differences in the estimations of τ_s and ΔE_q between these two experimental results are derived from the different temperature regions considered. The similarity of the results shown in Table 3.1 implies that the contribution to the fluorescence lifetime of Cr^{3+} in the mirror site is approximately the same, regardless of the concentration. However, with the increase of the concentration, the existence of the inversion site in Cr^{3+} can no longer be neglected. Although this phenomenon has not been discussed in

detail in the previous work (as it was not relevant to the lower dopant level study), it is shown in this work that the longer lifetime associated with the Cr^{3+} in the inversion site can also be described by a model expressed in Eq.(3.4) and the solid line in Fig.3.3 (fitting the solid circles) results from a least squares fitting of Eq.(3.4) to the long lifetime data, over the range from 273K to 773K. The fitted values are also shown in Table 3.1 and the relative fitting error of the long lifetime is $\sim 4\%$. It is interesting to note that the Cr^{3+} ions in the mirror and inversion sites function in different energy levels but obey the same law and the resultant phenomenon is a superposition of contributions both from the mirror as well as the inversion sites.

3.3.1.5. Intensity-based measurements for temperature sensing

The fluorescence signal, the nature of which can be fitted by using the double exponential function as expressed in Eq.(3.1), provides not only details of the behaviour of the two important lifetimes which can be used for temperature sensing, discussed in detail above, but also information on the *intensities* associated with the two exponentials. The existence of *two* intensity signals, at closely related wavelengths, enables cross-referencing for any extraneous losses in the system and thereby a self-referenced sensor scheme using this can be envisaged.

The possibility of developing a temperature sensor using a fluorescence intensity ratio technique in rare-earth doped optical fibre was first investigated using erbium and ytterbium ions co-doped into a heavy-metal fluoride glass[14]. Later, Maurice et al[15][16] investigated a scheme involving the fluorescence intensity ratio technique as

Chapter 3 Point Optical Temperature Sensors using Different Fluorescent Materials

the basis for a commercially viable temperature sensor, involving the use of two wavelengths of the fluorescence emission from Er[15] at 530nm and 555nm, and the intensity ratio obtained was indicative of the associated temperature change. In the scheme discussed herein again using alexandrite as the sensor material, any drifts in the detector or source are automatically compensated as affecting equally each intensity associated with one of the lifetimes of the fluorescence. Therefore a powerful, alternative scheme for temperature sensing is possible. Fig.3.5 shows that the intensity ratio (R) of the short to the long lifetime decreases with the increase of temperature, thus providing an alternative means of temperature sensing, by making full use of the double exponential characteristics of the sensing sample.

Table 3.1 Values of parameters of the appropriate model fitted to the lifetime data and comparison with the previous work

	$\Delta E, \text{ cm}^{-1}$	$\tau_s, \text{ ms}$	$\tau_l, \mu\text{s}$	$\Delta E_q, \text{ cm}^{-1}$	$\ln\beta$
Zhang et al[9] (290-930K)	851.7	1.23	16.0	10807	24.8
short lifetime of this work(273-773K)	838.3	2.21	16.0	8275	20.0
long lifetime of this work(273-773K)	1718.4	39.92	784.0	7599	20.0

3.3.1.6 Comparison of the methods

It is useful here to draw some comparisons of the performance characteristics of the methods used. The sensitivities of the three possible measurement methods (long lifetime, short lifetime and intensity ratio), at selected temperatures over the region

Chapter 3 Point Optical Temperature Sensors using Different Fluorescent Materials

studied, are shown in Table 3.2. The sensitivities are defined as $\frac{1}{\tau} \frac{d\tau}{dT}$ for the lifetime measurements and $\frac{1}{R} \frac{dR}{dT}$ for the intensity ratio, and the temperature sensitivity associated with each is also given for a variety of temperatures over the range shown.

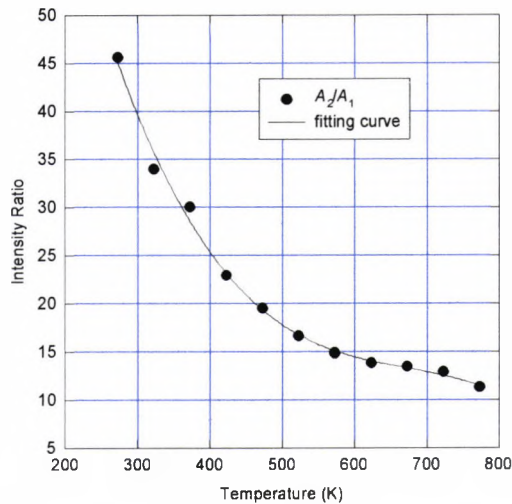


Fig.3.5 Intensity ratio (A_2/A_1) associated with the two intensities in alexandrite as a function of temperature

The double exponential characteristics of alexandrite offer an alternative method for temperature sensing by revealing the fact that with the increase of temperature, the intensity ratio of the short to long lifetime decreases and a comparison of the sensitivities of all the approaches considered is presented. This shows that the long lifetime is more sensitive in the high temperature region and the short lifetime in the lower temperature region. The intensity ratio method is less affected in sensitivity, but it improves as the temperature decreases. Although the sensitivity of the long lifetime is better than that of the short lifetime in high temperature region, the intensity of the

Chapter 3 Point Optical Temperature Sensors using Different Fluorescent Materials

long lifetime is usually less than one tenth of that of the shorter lifetime, thus the short lifetime is more applicable for most thermometer application.

Table 3.2 The comparative sensitivities of the three possible measurement methods (long lifetime, short lifetime and intensity ratio), at selected temperatures over a wide

temperature region

Sensitivity (%/K)	short lifetime $(1/\tau)(d\tau/dT)$	long lifetime $(1/\tau)(d\tau/dT)$	Intensity Ratio $(1/R)(dR/dT)$
273K	1.07%/K	0.08%/K	0.46%/K
373K	0.70%/K	0.29%/K	0.42%/K
473K	0.36%/K	0.46%/K	0.31%/K
573K	0.31%/K	0.60%/K	0.16%/K
673K	0.11%/K	0.75%/K	0.11%/K
773K	1.18%/K	1.43%/K	0.22%/K

3.3.1.7 Discussion

The work has exploited the double exponential behaviour of the fluorescence emission of alexandrite at higher dopant concentrations (>0.4at.%) and the results obtained are consistent with the phenomenon arising from the combination of emission from Cr^{3+} both in the mirror as well as in the inversion sites. The two lifetimes are found to fit the configurational coordinate model very well and the results obtained for the short lifetime are very close to those reported in previous work[2] which implies that the concentration difference has not changed the behaviour of Cr^{3+} in the mirror site, but enhanced the effect of Cr^{3+} in the inversion site. Although the energy level distribution in the inversion site is different from that in the mirror site, the behaviour of Cr^{3+} shows that it obeys the same law, which is important for wide range temperature sensing to which alexandrite is well suited.

The temperature range tested in this work is 273K–773K for convenience, and the previous work[1] has demonstrated that there is no problem for alexandrite to measure a much wider range of temperature, from 0K to 1000K. The errors estimated from this work are $\pm 1.5^\circ\text{C}$, $\pm 2.5^\circ\text{C}$ and $\pm 5.0^\circ\text{C}$ respectively for short-lifetime, long-lifetime and intensity ratio-based thermometries. Although the sensitivities listed in Table 3.2 vary with the temperature region, almost all of them meet the specification requirement that the sensitivity is better than 0.1%/K.

3.3.2 Praseodymium-based thermometry

Praseodymium-doped material has been very promising for lasers and amplifiers because of its broad emission band ($^1\text{G}_4\text{-}^3\text{H}_5$) centered around 1.3 μm , the second telecommunications ‘window’. The close proximity of the $^1\text{G}_4$ level to the lower ^3F levels necessitates the use of fluoride glasses rather than oxide glasses as the material host, because of the lower phonon energies and the consequent expected reduction in non-radiative decay. The purpose of this work is mainly to explore its fluorescence-based thermal behaviour, for application to sensor systems.

3.3.2.1 Previous work

The possibility of developing a temperature sensor with Pr^{3+} : ZBLAN glass was first investigated by Maurice et al[17] by using the fluorescence intensity ratio technique, where the experimental results published show that the ratio of the emission on the two major fluorescent bands changes with the variation of temperature, forming the basis of a useful sensor system. Further progress in the temperature sensing field with Pr^{3+} :

ZBLAN was reported by Baxter et al[17] where, in these experiments on fluorescent emission, blue light sources were adopted because they were seen to offer certain sensitivity advantages over the infra red (IR) laser diodes formerly used[16] with the added convenience of compatibility with lower cost optical detectors.

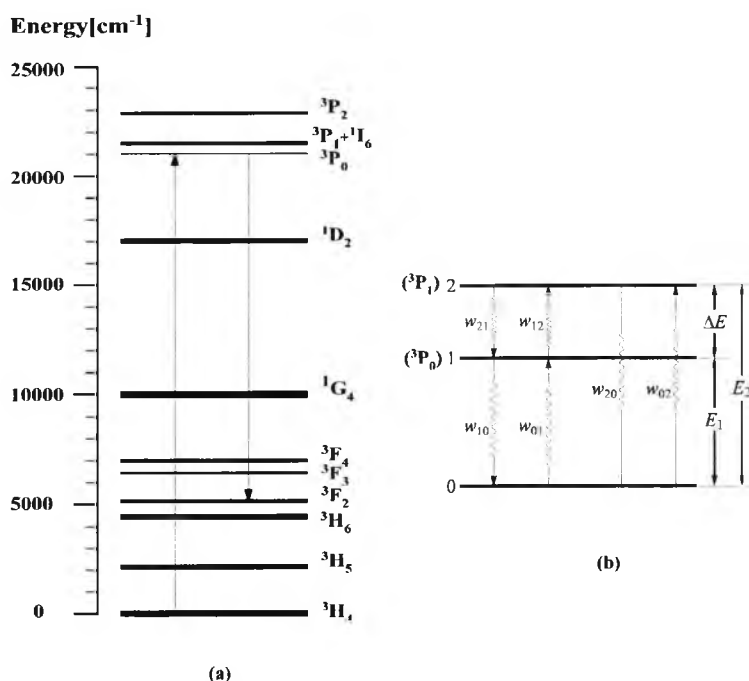


Fig.3.6 (a) Partial energy level diagram of praseodymium showing absorption to the ³P levels and emission ³P₀-³F₂[18]. (b) Three-level model configuration, showing the parameters involved in the model

An alternative to the intensity ratio technique, to exploit the fluorescence emission for thermometry, is the use of the change in the fluorescent decay time[1]. This non-intensity dependent approach (and with it the advantage of single wavelength monitoring) has been applied and the results may be compared with those from alexandrite and other materials reported in the literature. Using light in the blue region

of the spectrum, as shown in Fig.3.6(a), an excitation of the 3P_0 with respect to the 3F_2 state can be achieved. Transitions from the 3P_0 initial state to lower energy levels results in strong fluorescent peaks at many visible wavelengths, in particular around 635nm, due to the de-excitation to the 3F_2 final state[18]. This system is studied in this work[19], where emission from the 3P_0 level is accompanied by the corresponding blue-shifted emission from the 3P_1 level, owing to the small energy difference of $\sim 600\text{cm}^{-1}$ between these two levels (3P_0 and 3P_1).

3.3.2.2 Experimental configuration

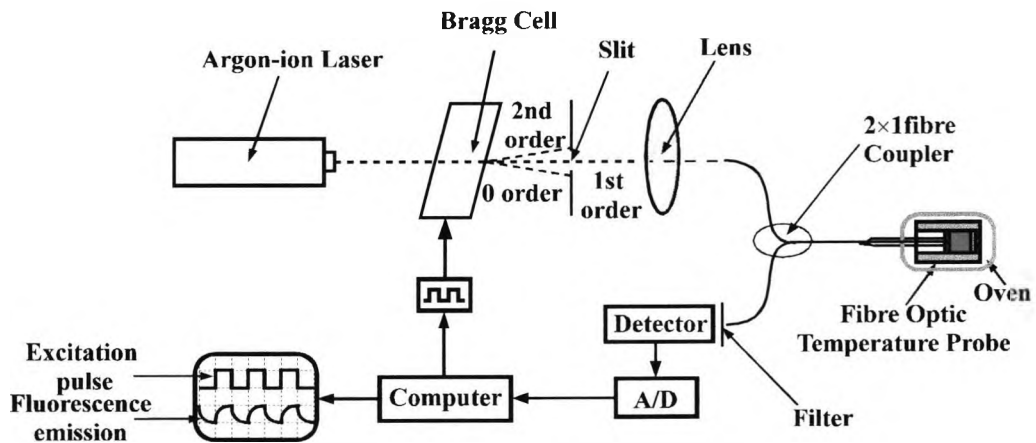


Fig.3.7 Experimental arrangement for the temperature sensor

The experimental arrangement used to determine the temperature-dependent lifetime performance of $\text{Pr}^{3+}:\text{ZBLAN}$ in a fibre optic thermometric probe is shown in Fig.3.7. In this case an argon ion laser, whose primary emission was centered at 488nm, was used to generate the pump radiation. This was a convenient source of collimated blue light to excite the material, and in a practical sensor it could be replaced by either a bright blue light emitting diode (LED) or a future blue laser diodes[11]. The laser

Chapter 3 Point Optical Temperature Sensors using Different Fluorescent Materials

beam was modulated through the use of an acousto-optic Bragg cell, the modulation frequency of which was adjusted by using a pulse signal generated by the digital output port of a computer. With a solid state source, direct electrical modulation of the laser/LED output could be used, thus reducing costs. In the configuration shown in Fig.3.7, the optical arrangement is such that the slit inserted along the optical path is used to block the stray light both from the zero and the second order to allow the modulated (first order) laser signal to excite the sample via the fibre optic probe. To do so, one end of a 2×1 optical fibre coupler, the core diameter of which is 200µm, is located at the focal point of the lens through which the pumping light was transmitted to the Pr³⁺: ZBLAN glass sample, which is situated at the far end of the fibre. The end face of the sample, which is connected to the fibre, served the function both of fixing the fibre in place and at the same time enlarging the contact area with the test glass. In previous work, glass or crystal-based probes have been constructed using metallized fibres[1] to withstand very high temperatures (up to ~600°C) and this pattern is well suited to Pr³⁺ optical systems. For calibration, the probe is positioned in the center of the oven, the temperature of which could be varied through a thermostatic control with the temperature read using a *K*-type thermocouple in close contact with the fibre probe. A glass filter is used to prevent the reflected excitation light from saturating the photodetector and thus effectively transmitting only the fluorescence light coming from the sensor material at the far end of the fibre. The detected response signal is then digitized by an analog-to-digital(A/D) converter connected to the computer and processed by the software written for the purpose.

3.3.2.3 Theoretical background and system model

Following the termination of the excitation light pulse, the fluorescence decay, assuming a single exponential behaviour with time, can be written as an exponential as a function of time, t , in this case by:

$$f(t) = A \exp(-t/\tau) + B \quad (3.5)$$

where A corresponds to the initial fluorescence amplitude; τ is the corresponding fluorescence lifetime; and B is the signal baseline offset.

On the basis of the above, the fluorescence decay signal of Pr^{3+} : ZBLAN with different dopant levels has been investigated over a range of temperatures and the experimental data, representing the lifetimes in Eq.(3.5), have been calculated by the use of the Marquardt non-linear least squares approximation algorithm[12].

In order to understand, and thus compare, the results obtained experimentally with those obtained from a suitable theory, a simple model has been developed, which is discussed below. As illustrated schematically in Fig.3.6(b), N_0 , N_1 and N_2 may be used to represent the numbers of atoms in the three states respectively which are illustrated in this model. The rate of change of N_0 , N_1 and N_2 may be described by:

$$\begin{aligned} \frac{dN_1}{dt} &= N_2 w_{21} - N_1 (w_{12} + w_{10}) + N_0 w_{01} \\ \frac{dN_2}{dt} &= N_1 w_{12} - N_2 (w_{21} + w_{20}) + N_0 w_{02} \\ \frac{dN_0}{dt} &= N_1 w_{10} + N_2 w_{20} - N_0 (w_{01} + w_{02}) \end{aligned} \quad (3.6)$$

where w_{ij} is the transition rate of the atoms from level i to level j (i, j are integers). In thermal equilibrium, the right hand side of each component in Eq.(3.6) should be equal to 0, that is

$$\begin{aligned} N_2^0 w_{21} - N_1^0 (w_{12} + w_{10}) + N_0^0 w_{01} &= 0 \\ N_1^0 w_{12} - N_2^0 (w_{21} + w_{20}) + N_0^0 w_{02} &= 0 \\ N_1^0 w_{10} + N_2^0 w_{20} - N_0^0 (w_{01} + w_{02}) &= 0 \end{aligned} \quad (3.7)$$

and

$$\begin{aligned} \frac{N_2^0}{N_1^0} &= \frac{g_2}{g_1} e^{-\Delta E/kT} = k_{21} \\ \frac{N_1^0}{N_0^0} &= \frac{g_1}{g_0} e^{-E_1/kT} = k_{10} \\ \frac{N_2^0}{N_0^0} &= \frac{g_2}{g_0} e^{-E_2/kT} = k_{20} \end{aligned} \quad (3.8)$$

where N_0^0 , N_1^0 and N_2^0 are the populations of the different energy levels at equilibrium and g_0 , g_1 and g_2 are the degeneracies of level 0, level 1 and 2 respectively; k is Boltzmann's constant; T is the temperature; and k_{ij} represents the ratio of the populations in levels i and j at equilibrium. Thus, based on the assumption that $E_1 \gg \Delta E$, $E_2 \gg \Delta E$, that is, $k_{10} \ll 1$, $k_{20} \ll 1$, the rate of change of N_1 and N_2 in such a system can be expressed by the following

$$\begin{aligned} \frac{dN_1}{dt} &= N_2 (w_{21} - k_{10} w_{10}) - N_1 (k_{21} w_{21} + w_{10} + k_{10} w_{10}) + N_0 k_{10} w_{10} \\ \frac{dN_2}{dt} &= N_1 (k_{21} w_{21} - k_{20} w_{20}) - N_2 (w_{21} + w_{20} + k_{20} w_{20}) + N_0 k_{20} w_{20} \end{aligned} \quad (3.9)$$

A Laplace transform may be applied to the above equation and the following expression can be obtained

$$N(t) = A_1 \exp(-t/\tau_1) + A_2 \exp(-t/\tau_2) + A_3 \quad (3.10)$$

where

$$\begin{aligned} 1/\tau_1 &= \frac{1}{2}[(1+k_{21})w_{21} + w_{20} + w_{10} + \sqrt{[(k_{21}-1)w_{21} + w_{10} - w_{20}]^2 + 4k_{21}w_{21}^2}] \\ 1/\tau_2 &= \frac{1}{2}[(1+k_{21})w_{21} + w_{20} + w_{10} - \sqrt{[(k_{21}-1)w_{21} + w_{10} - w_{20}]^2 + 4k_{21}w_{21}^2}] \end{aligned} \quad (3.11)$$

When the relaxation time is extremely short (w_{21} is quite large), the two resulting lifetimes can be expressed by the following relationships:

$$\tau_1 \approx 0 \text{ and } \tau_2 \approx (1+k_{21})/(w_{10}+w_{20}k_{21}) \quad (3.12)$$

which is the same result as that obtained from a two-level model based on the assumption of thermal equilibrium[20] showing that it is just one special condition of the generalized three-level model.

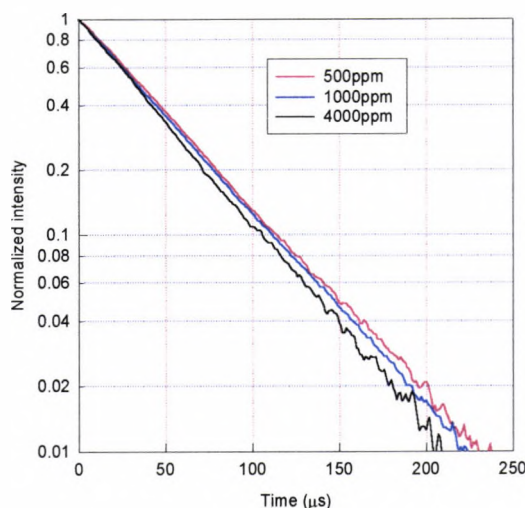


Fig.3.8 Fluorescence decay signal of Pr^{3+} : ZBLAN with different doping levels, at

a temperature of 320K, showing single exponential behaviour

The three-level model derived above has been shown to be a general model, taking account of the effect of thermal relaxation and this could be expressed by Eq.(3.11).

This model is found to support the results obtained from Pr^{3+} doped materials, which will be discussed in detail below.

3.3.2.4 Results of the experimental investigation

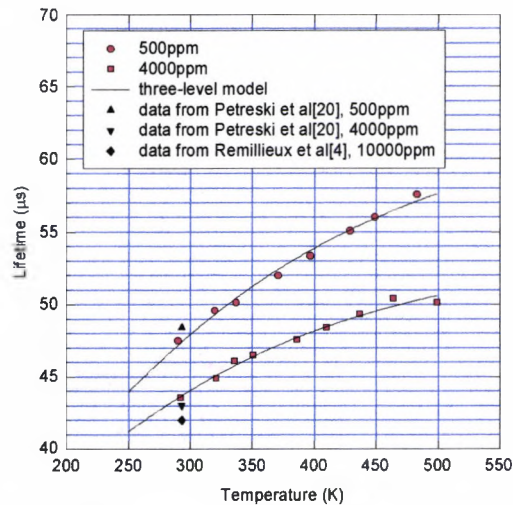


Fig.3.9 Fluorescence lifetime of Pr^{3+} : ZBLAN, as a function of temperature, with different concentrations of 500 and 4000ppm. Points represent measured data with the solid line the prediction of the three level model

The fluorescence decay characteristics of Pr^{3+} : ZBLAN in different concentrations, and at different temperatures, were obtained by converting the analog signal from the detector in Fig.3.8 to a digital form, and then passing it to the computer using the experimental setup shown schematically (Fig.3.7). In the theory, a single exponential decay behaviour has been assumed and an experiment was carried out to validate that this was indeed obtained in practice, by analyzing the temporal nature of the emission. The fluorescence decay curves thus obtained at a temperature of 320K, with different doping levels of Pr^{3+} in the glass, are shown in Fig.3.9. A comparison across these three different doping levels reveals that with an increase of the concentration, the rate of cross-relaxation also increases[20] which causes the decay of the 4000ppm sample to be much faster than those of the other two. The decay curves of the 1000ppm and

500ppm samples are very close to each other and only a small difference can be observed, because the rate of cross-relaxation is not so significant in these samples as

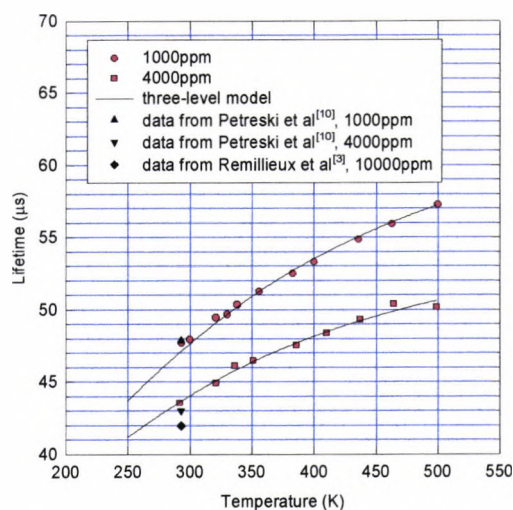


Fig.3.10 Fluorescence lifetime of Pr^{3+} : ZBLAN, as a function of temperature, with different concentrations of 1000 and 4000ppm. Points represent measured data with the solid line the prediction of the three level model

in that at 4000ppm. For each decay curve obtained at a different temperature and a different Pr^{3+} concentration, the Marquardt non-linear least squares approximation method is adopted to calculate the corresponding lifetime, the results of which are shown in Figs.3.9 and 3.10 respectively. The comparison of the results at different doping levels shows that the lifetime decreases with the increase of the concentration, which is consistent with the cross-relaxation explanation[20][21]. However, with increasing temperature, the tendency is for the lifetimes also to increase, a phenomenon which cannot be explained by the two-level model, shown in Eq.(3.12), and which is based on the assumption of thermal equilibrium[4]. The effect, however can be

described in a satisfactory way by using an alternative three-level model, as discussed below.

In the specific case of praseodymium, levels 2 and 3 in this model can be assumed to represent the 3P_0 and ${}^3P_1+{}^1I_6$ levels respectively, as shown in Fig.3.6(b). As a consequence of this, the experimental data shown in Fig.3.9 and Fig.3.10 can be seen to fit very closely the predictions of the three-level model for τ_2 in Eq.(3.11) when the following parameters are used: the energy difference (ΔE) equals 616 cm^{-1} ; the degeneracy ratio (g_2/g_1) is 16; the radiative lifetime for 3P_0 ($1/w_{10}$) is $34\ \mu\text{s}$; the relaxation time ($1/w_{21}$) is $34\ \mu\text{s}$ and for the 500ppm sample, the radiative lifetime of 3P_1 ($1/w_{20}$) is $73\ \mu\text{s}$; for 1000ppm, $72\ \mu\text{s}$; and for 4000ppm, $59\ \mu\text{s}$. The justification for the choice of these data to fit the model, giving as they do the excellent agreement seen between theory and experiment, is as follows. The radiative lifetime of the 3P_1 state ($1/w_{20}$) differs for the different dopants in Pr^{3+} in ZBLAN glass because of the existence of cross-relaxation[20]. The energy difference, ΔE , between 3P_1 and 3P_0 used is very close to the value of 630cm^{-1} which has been measured from the absorption spectrum in the same glass host and reported in the literature[5], the degeneracy ratio above is the same value as that from Baxter et al[17] and the radiative lifetimes of the 3P_1 and 3P_0 states measured above also show a close approximation to those from previous data[4][21] derived from the same material with the same concentration level, as shown in Fig.3.9 and Fig.3.10. The value of τ_1 in Eq.(3.11)

under the above conditions has been found to be very small, $\sim 8\mu\text{s}$, and its effect can be considered negligible. The relaxation time, $34\mu\text{s}$, in this experiment is of the same order of magnitude as the radiative lifetimes reported for the ${}^3\text{P}_0$ and ${}^3\text{P}_1$ [4][18] which implies that under these conditions, the assumption of thermal equilibrium is no longer reasonable, and shows why the simpler two level model cannot explain the observed phenomenon of the temperature dependence of Pr^{3+} : ZBLAN radiative emission very successfully. As a consequence, the results of the advanced three level theoretical model can be used as an effective calibration for temperature monitoring systems of this sort.

3.3.2.5 Discussion of praseodymium results

In this work, praseodymium has been investigated through the use of several samples of different doping levels for temperature sensor purposes based on the use of the fluorescence lifetime-based technique. The results obtained show that the lifetime increases with the decrease in dopant concentration and such performance is consistent with the effect of cross relaxation in the material. By contrast, many other fluorescent systems such as the Cr^{3+} -doped family all show a *decrease* in the lifetime of the fluorescence emission with increasing temperature [1] whereas in praseodymium, with the increase of the temperature, the lifetimes also increases. This phenomenon cannot be explained by the use of a two-level model based on the assumption of thermal equilibrium, but however, a three-level model which was developed in this work, taking into account the effect of thermalization, has been found satisfactory to explain

this observation. The parameters estimated from the three-level model are very close to those obtained from previous published work.

When making comparisons with the specification given, the results confirm the value of a praseodymium-doped fluorescence decay-time based sensor system for temperature measurement over the important region from room temperature to ~500K. Above that temperature, the ZBLAN host is subject to cracking and this sets an effective upper limit on the use of the material in optical thermometry. However, the lifetime can readily be measured using a relatively simple opto-electronic sensor system, and the theoretical fit provides an empirical calibration for the thermometer of satisfactory accuracy. Using such a sensor, a typical resolution of $\sim\pm 2\text{K}$ over the temperature range considered should be routinely achievable.

3.3.3 General discussion of alexandrite and praseodymium systems

The work discussed above has confirmed that these Cr^{3+} or rare-earth based crystalline materials can be used for temperature measurement over a wide range from liquid nitrogen temperatures(77K) to beyond 1000K[1] and the use of doped glasses, generally operating up to lower values of the maximum temperature (due to the detection of irreversible material changes) has complemented previous work on bulk-material based thermometry by Grattan et al[22]. However, in both cases, the life and integrity of the sensor is limited by the physical configuration of a probe constructed using a sample of crystalline material (usually a laser rod off-cut) or doped glass, and the nature of the glass and adhesive used. Even when working within the specified

operational envelope of the highest temperature glass, there is still the problem of the integrity of the probe if the maximum specified operational temperature is exceeded, either accidentally or in an unwise attempt to make measurements at higher temperatures, or severe temperature cycling tests are carried out. To try to overcome some of these problems, an investigation of fibre-based systems was carried out, and is reported in the next section.

3.4 Intrinsic doped fibre based thermometry

As fibre laser research continues to expand, an important ‘spin-off’ of this communications-based technology has been the potential to use such fibres for temperature sensing, employing the luminescent effects seen. The inherent fluorescence characteristics of the doped ‘laser’ fibres are particularly attractive and available at reasonable cost due to the larger quantities now produced commercially from a range of suppliers. Neodymium, erbium and later ytterbium doped fibres fall particularly into this category and are the subject of this novel study on the use of the highly successful decay time technique for intrinsic optical fibre point temperature sensor systems, operating up to even higher temperatures (~1200K)[23][24][25][26], as will be discussed in detail below

3.4.1 Previous work

The underpinning science of the luminescent effects in rare-earth doped fibres, for example the upper levels of Er-doped silica fibres, was explored by authors such as Mazzali et al[27] and Maurice et al[28] who developed a spectroscopic study of the fluorescence resulting from the pumping of Er-doped fibre, excited in the 800nm

region. The general physics background of rare-earth doped fibres, with a particular focus on laser operation, has been extensively reviewed by Digonnet et al[6]. A paper by Maurice et al[29] reported results on an intensity-based fluorescent sensor, dependent on the thermal behaviour of the relative emission of the Er species at 530nm and 555nm, obtaining a calibration curve in the temperature region from 100-1000K. Calibration errors were reported to be 1.3K in the worst case. Research by Imai et al[30] reported pumping at 1.48 μm , observing the more familiar broad 1.54 μm fluorescence spectrum, using the intensity ratio of the fluorescence emission at 1.530 μm and 1.552 μm as a means of temperature sensing. In addition, Ko et al[31] have discussed a distributed temperature sensor, again using pumping at 1.48 μm , and

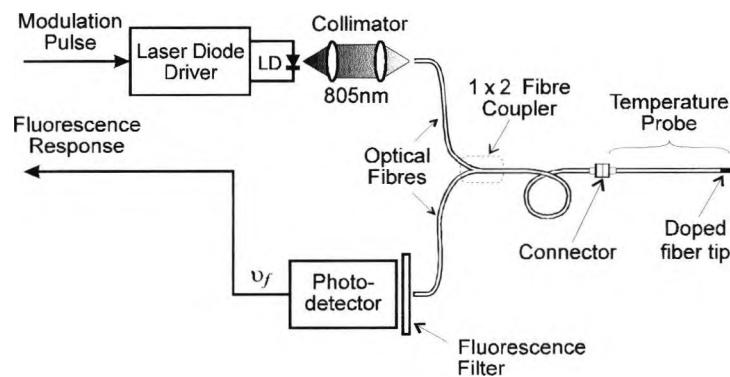


Fig.3.11 Experimental arrangement used for Er and Nd doped fibre intrinsic fluorescence-based sensors[23][24][32]

exploiting the amplification effects of the fibre on a signal at the laser wavelength of 1.53 μm . The characteristics reported for such a sensor were an operational range of 77K to 425K, a spatial resolution of 10m, and a measured length of 100m with a sensitivity of $-0.23\%K^{-1}$. The decay-time behaviour of both Nd and Er doped fibre intrinsic fluorescence-based sensors were investigated in some detail by Zhang et

Chapter 3 Point Optical Temperature Sensors using Different Fluorescent Materials

al[23][24][25][26], over a wide range covering the requirements of a number of potential applications in sensing, such as in the aerospace and the electricity industries, for example.

Table 3.3 Doped fibre samples test by Zhang et al[23][24][25][32]

Sensor	Dopant	Host	Diameter	Length	Upper limit
#1	Nd: 7.5%	Alumino-silicate	100/140 μ m	2mm	750 $^{\circ}$ C
#2	Er: 200ppm	SiO ₂ /Al ₂ O ₃ /GeO ₂ /P ₂ O ₅	3.8/125 μ m	50mm	1100 $^{\circ}$ C
#3	Er: 960ppm	SiO ₂ /Al ₂ O ₃ /GeO ₂ /P ₂ O ₅	3.8/125 μ m	50mm	1100 $^{\circ}$ C
#4	Er: 4370ppm	SiO ₂ /Al ₂ O ₃ /GeO ₂ /P ₂ O ₅	3.8/125 μ m	50mm	1100 $^{\circ}$ C

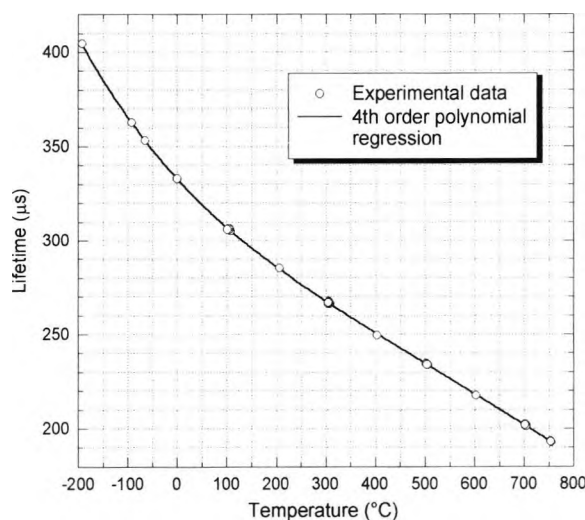


Fig.3.12 Experimental results of the thermal characteristics of Nd³⁺ doped fibre[23][24][25][32]

The experimental set-up, employed by Zhang et al[23][24][25][26] to test the performance of Nd and Er doped fibre sensors, is shown in Fig.3.11. The absorption band existing in both materials is over the region ~800nm, which was accessed by using power from a laser diode. The induced fluorescence emission from Nd-doped

Chapter 3 Point Optical Temperature Sensors using Different Fluorescent Materials

fibre at $\sim 1.06\mu\text{m}$ and $\sim 1.32\mu\text{m}$, or from Er-doped fibres at $\sim 1.54\mu\text{m}$ was received at the detection stage. Four different doped fibre samples tested by Zhang et al[23][24][25][26] are listed in Table 3.3. It was found by these authors[23][24][25][26][32] that the upper operating temperature limits for Nd and Er doped fibres are $\sim 750^\circ\text{C}$ and $\sim 1100^\circ\text{C}$, respectively, as prolonged exposure to temperatures above these limits will cause severe deterioration in the fluorescence properties of the fibres. After undergoing appropriate heat treatment to achieve stabilized and consistent thermal characteristics, the temperature probes, made from the four samples listed in Table 3.3, were calibrated by Zhang et al[23][24][25][26][32] and the results are depicted separately in Fig.3.12 and Fig.3.13.

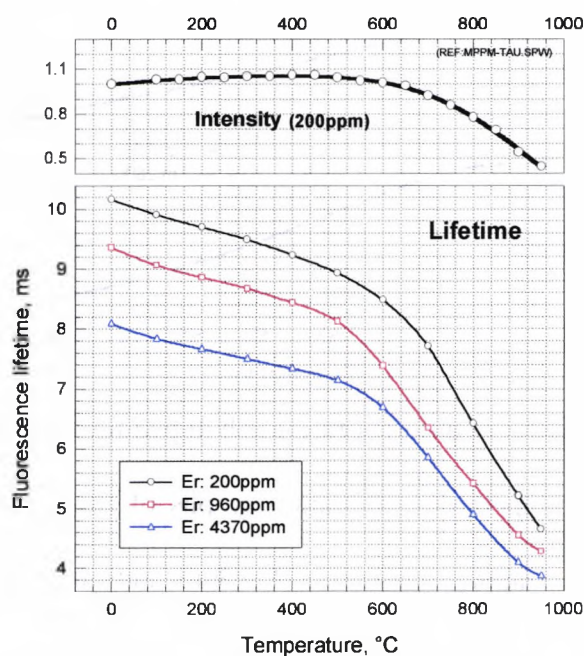


Fig.3.13 Fluorescence lifetimes of Er-doped fibres as a function of temperature[23][24][25][32]

The uncertainty of the measurement using the Nd-doped fibre probe evaluated and based on consecutive measurements was $\pm 2^\circ\text{C}$ over the entire region from -190°C to 750°C , with a measurement time of 1 second. Apart from differences in the values of the fluorescence lifetime among the three Er-doped fibre probes reported, their performance characteristics over the region $0\text{--}1100^\circ\text{C}$ are essentially similar, with a measurement uncertainty of 5°C and a response time of 5 seconds reported.

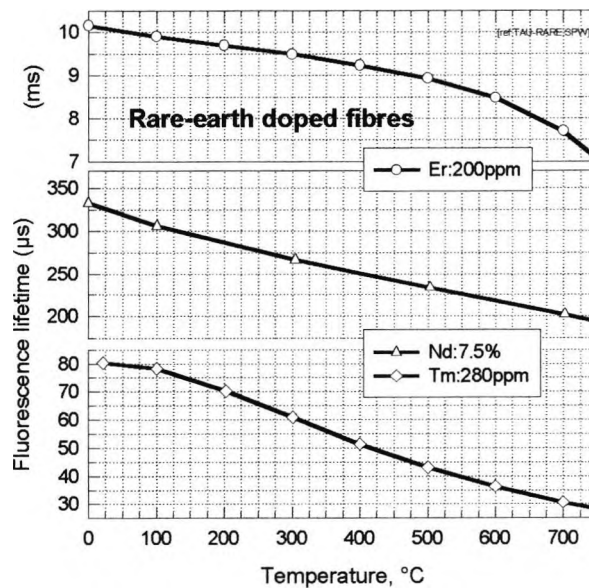


Fig.3.14 Comparison of different rare-earth doped fibre based thermometry

The similarity in the temperature calibration graphs of the fluorescence lifetimes of those three Er-doped samples shown in Fig.3.13 indicated that, apart from the reduction in lifetime caused by concentration quenching, the mechanisms of temperature dependence of the lifetimes of these three samples, of different Er concentrations, are essentially the same. The rapid reduction in the fluorescence intensity with increasing temperature over the region above 600°C , shown by the data

Chapter 3 Point Optical Temperature Sensors using Different Fluorescent Materials

from the fibre doped with a 200ppm Er concentration in Fig.3.13, revealed that the high temperature sensitivity of the lifetime over the corresponding region was mainly attributed to the thermal quenching of the Er fluorescence.

A further investigation to achieve higher temperature performance from fluorescence-based optical thermometers has been carried out by Zhang et al [33] by using thulium-doped fibre-based system. The thermal characteristics of the fluorescence of the Tm:280ppm doped fibre is shown in Fig.3.14, and compared with those of the other rare-earth doped fibres.

Overall, the results obtained from the Nd, Er and Tm samples look very promising for the development of effective, compact, intrinsic doped fibre temperature probes. They both show a clear relationship of decay time with temperature operation over a significant temperature range and they are robust with the doped material being fusion spliced to the connecting fibre, yielding high probe integrity. Simple sources and detectors, coupled with a convenient signal processing scheme, offer the prospect of fast response, both electronically and thermally.

It was considered necessary to try extend the measurement range and to investigate if Er doped fibre decay-time based optical thermometry could also be used in cryogenic temperature region ($77\text{K} \leq T \leq 273\text{K}$). This is discussed in detail in section 3.4.2, being complementary to work in the high temperature region ($273\text{K} \leq T \leq 1200\text{K}$). A range of such doped fibres exists and it was considered that other rare-earth doped fibre-based

thermometer schemes were worth pursuing, amongst which ytterbium doped fibre seems very promising as a material to use. This was investigated thoroughly in this work for potential temperature sensor applications, as discussed in section 3.4.3.

3.4.2 Erbium-doped fibre for cryogenic temperature measurement

3.4.2.1 Introduction

As considered above, Zhang et al have reported the use of sensors based on luminescence in Er-doped materials using both intensity[29] and decay-time-based techniques[23][24][25][32]. In that work, the prime application was for engine and assessment at elevated temperatures (up to 1000°C) but there is equally an interest in measurements at cryogenic temperatures for testing and analysis. Whilst the basic science underpinning the spectroscopy remains essentially that discussed in previous work, and thus is not reproduced here, both the thermal effects on the energy levels involved and the nature of the host medium play an important role. Interest in this region was stimulated through a recent paper by Kewell et al[34] in which was discussed an integrated temperature sensor in Er-doped silicon as an alternative means to exploit a temperature-dependent effect and create a simple sensing probe. However, whilst the results in that work were favorable in the capability of the probe to measure over a range from 150 - 10K, the optical arrangement was somewhat complex and expensive, requiring an Ar ion laser to excite the sample and an acousto-optic modulator for signal discrimination. At the output, a spectrometer was used, coupled with a fast rise time Ge detector and a commercial lock-in amplifier. All this

adds considerably to the instrumentation cost, even though potentially the probe itself is cheap and readily fabricated.

Of significance in the development of an effective cryogenic probe is not only a simple and inexpensive optical arrangement, but an optimized density of fluorescing species in the active volume of interest. In the previously reported work on Er-implantation of Si[34], a species surface density of $5 \times 10^{14} \text{ cm}^{-2}$ was achieved at the target using 190keV Er ions, giving a nearly Gaussian distribution at a peak range of $0.13\mu\text{m}$, into the target. This resulted in the familiar photoluminescence spectrum, peaking at a wavelength of $1.54\mu\text{m}$. As an alternative, commercial doped optical fibre is discussed for use in the work[35] in this paper, as it is now readily available from a range of manufacturers, and offers potentially a higher density of active species and thus a higher sensitivity through two important features: an increased fluorescence intensity and a stronger ion-ion interaction. The active volume of Er-doped material in the Si-implanted study was approximately $4 \times 10^{-15} \text{ m}^3$, whereas with the fibre approach, a much greater length could be used, even though the core diameter is relatively small. Thus, in this work, the active volume of the fibre used was approximately $6 \times 10^{-13} \text{ m}^3$, two orders of magnitude greater than the above. It is difficult to assess the percentage doping of the Er in the Si from the work of Kewell et al[34], but for the highly doped fibre samples used in the work herein, a high doping level of up to 4370 ppm Er was employed.

To address low temperature measurement in this research, a novel simplified cryogenic probe and instrumentation system, tested for measurements over the range from 77K (and potentially below) up to and beyond room temperature to a maximum temperature of 1200K is reported. The results obtained are shown to be compatible with those reported earlier[22][23][24][32] for the higher temperature range from 273K (0°C) upwards, and a better temperature resolution is obtained over that region using a fibre-based system than with the Er-implanted Si probe approach of Kewell et al[34].

3.4.2.2 Experimental arrangement

The system developed was modelled closely upon that reported earlier[25], and is illustrated in Figure 3.15. Three types of single mode Er-doped silica fibres of the same host composition ($\text{SiO}_2/\text{Al}_2\text{O}_3/\text{GeO}_2/\text{P}_2\text{O}_5$) with widely different Er concentrations (200, 960 and 4370 ppm) were tested, using fibres of core diameter approximately $3.8\mu\text{m}$ and overall diameter nominally $125\mu\text{m}$.

Excitation of the fluorescence in the $\sim 1.5\mu\text{m}$ wavelength region was achieved with the output from a laser diode operating at a wavelength of $\sim 980\text{nm}$ ($\sim 2\text{mW}$), which was pigtailed into the 980nm input arm of a wavelength division multiplexer (WDM) and launched, in turn, into each of the Er-doped fibre samples under test, as is shown schematically in Fig.3.15. The lengths of doped fibre samples tested were all of $\sim 50\text{mm}$, and they were placed in a temperature controlled environment during the experiments carried out. An infra-red sensitive InGaAs photodiode was used to detect

Chapter 3 Point Optical Temperature Sensors using Different Fluorescent Materials

the fluorescence emission at the 1550nm arm of the WDM in the experimental arrangement. The excitation light was pulse-modulated and the fluorescence decay was processed by using a phase-locked detection (PLD) scheme, proposed by Grattan & Zhang and described in detail elsewhere[1]

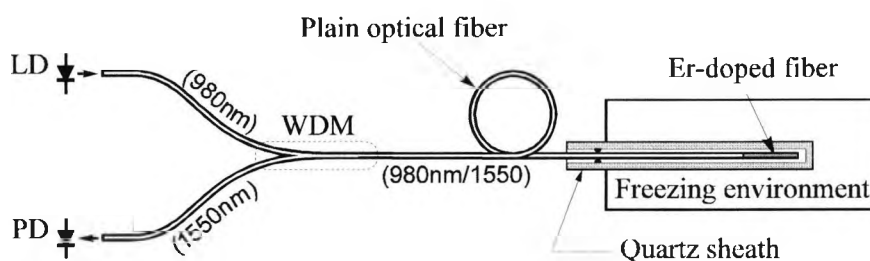


Fig.3.15 System arrangement used in the temperature sensing tests

The exponential nature of the fluorescence decays of the three Er-doped fibre samples at 0°C were discussed in previous work[23][24][25][32] and it was satisfying that they were found to be similar in this study. Only the fluorescence decay of the fibre containing the 4370ppm Er dopant showed something of a multi-exponential characteristic, in contrast to the clear single-exponential feature of the fluorescence decays of the other two lower Er doped counterparts. Thus, to achieve consistent measurements of fluorescence lifetimes of these samples, a single exponential approximation is assumed in estimating the fluorescence lifetimes, τ .

A series of low temperatures in the region of interest were obtained from the liquid nitrogen temperature (77K) upwards by creating freezing mixtures of several organic solvents. These mixtures have good temperature stability when made up when needed and used in a Dewar flask, and a reference temperature was obtained using a K-type

thermocouple. The high temperatures of interest were obtained by using a thermostatically controlled oven.

Each lifetime measurement was obtained from the superimposed temporal graph of 100 decay cycles at the corresponding temperatures. In contrast to the high temperature work, there was no need to remove the effect of background (black body) radiation for this low temperature analysis, as it lay well outside the wavelength sensitivity of the detector used.

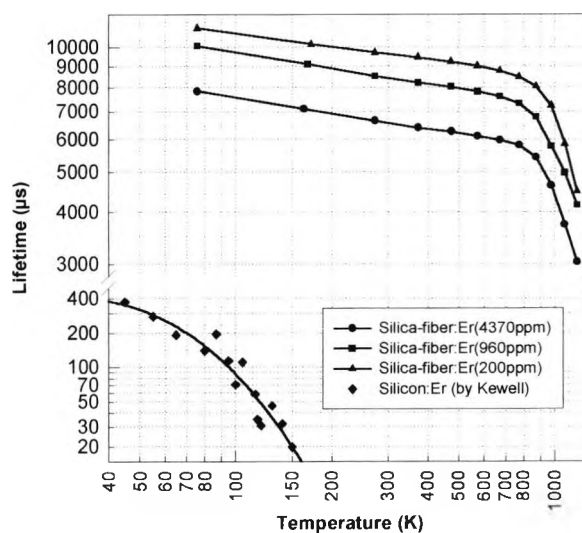


Fig.3.16 Results of the different Er-doped silica fibres over the wide temperature range ($77K \leq T \leq 1200K$)

3.4.2.3. Experimental results obtained

The probes used were tested over the temperature region from 77K to room temperature and then to high temperature, and results of these tests are shown in Figure 3.16. For the three samples of doped fibre, containing a wide range of Er

Chapter 3 Point Optical Temperature Sensors using Different Fluorescent Materials

dopants, a similar profile is seen with the calibration graphs in the newly explored cryogenic region up to approximately 273K, these lying approximately parallel to each other with a very similar slope to the linear component of the graph. The graphs can each be divided into two regions for each of the dopants used - showing two linear regions of temperature (T) $77 \leq T \leq 700\text{K}$ and $950 \leq T \leq 1200\text{K}$, with average slopes, m_1 and m_2 respectively, as shown in Table 3.4. Thus not only over the cryogenic region but over a wide temperature region ($77\text{K} \leq T \leq 1200\text{K}$), the lifetime measurements here show that good sensing performance is possible with doped fibre, achieving a precision of $\pm 5\text{K}$ in a system with a response time of 5s, meeting the general specification given, over the specific temperature range, in section 3.2.1.

Table 3.4 Slopes m_1 and m_2 for different temperature regions

temperature region	$77 \leq T \leq 700\text{K}$	$950 \leq T \leq 1200\text{K}$
slopes	$m_1 = 3.2\mu\text{s} / \text{K}$	$m_2 = 10\mu\text{s} / \text{K}$

3.4.2.4 Discussion of the Er-doped cryogenic fibre sensor

The results obtained for the sub-room temperature region show that an Er-doped fibre represents an effective sensor element, and this can also be achieved in a simple system. The results may be compared most closely with those of Kewell et al[34], also using Er as the active material. Such a comparison would suggest that the lifetime of the lanthanide dopant is profoundly affected by the host medium, even though the dopant level is lower than that of the fibre, as shown in Figure 3.16. Further, the profile is substantially different for Er-Si, as that calibration graph shape does not show the two linear regions (seen for the Er-fibre), and the lifetime of the species is at least an order of magnitude lower. This indicates that a higher accuracy in the measurement

Chapter 3 Point Optical Temperature Sensors using Different Fluorescent Materials

of the lifetime is needed for a comparable precision in the measurand, and the Er-silica fibre system is convenient in having quite a long lifetime (for example >10 ms for 200ppm Er at $T \leq 175\text{K}$). Thus the precision available in the temperature measurement herein ($77\text{K} \leq T \leq 1200\text{K}$) is better than that of the sensor from Kewell et al[34] at $\pm 5\text{K}$, by comparison to $\pm 11\text{K}$ which they reported ($40\text{K} \leq T \leq 150\text{K}$). Further, the optical system is much simpler as the source used is a solid state laser diode, detection is with a relatively inexpensive commercial photodiode and the sensor material is commercially available, and not custom-made as was the case for the Si-implanted sample.

The Er-fibre approach represents an improvement on previous work by some of the authors and as illustrated in earlier sections, where bulk material “laser” crystals and glasses were used[1]. In that work, the active material was fixed to the fibre through the use of cements or adhesives, many of which showed some difficulty with probe integrity when subjected to temperature cycling. By contrast, the fusion spliced fibre gives an excellent bond, and the fibre can be protected from the environment through the use of metal coatings, again an approach used successfully in the high temperature region[1].

Building upon results previously reported for Nd fibre[23], coupled with those in this section for Er, suggests that further work would be necessary to investigate the performance of other rare earth doped fibre species for temperature measurement to determine if an improvement in the temperature measurement precision is readily

achievable. The ytterbium doped fibre discussed in section 3.4.3 is one example of such a system, which is considered in some detail.

3.4.3 Yb doped fibre temperature sensors

3.4.3.1 Introduction

As discussed earlier, the field of fibre optic thermometry has seen considerable development in recent years, with an increasing variety of luminescent materials used[1][15][36], e.g. Cr^{3+} , for example in ruby and alexandrite[37][10], Pr^{3+} in ZBLAN[17][19], Nd^{3+} in glasses[23], garnets (YAG)[22] and fibres[24] and most recently Er^{3+} in fibres[25]. Two primary methods of fluorescent signal analysis have been found to be the most successful, i.e. the intensity and decay-time based approaches, and their comparative performance characteristics have been reported in a recent paper by Collins et al[38] and will be discussed in detail in Chapter 7. Previous work has been carried out on ytterbium using intensity-ratio methods – in this work the fluorescence decay-time approach is used to create a further point sensor.

3.4.3.2 Ytterbium doped fibre characteristics

Ytterbium doped fibres offer a wide range of applications as fibre lasers and amplifiers[6][39], and their ability to provide amplification over the very broad wavelength range from ~975nm to ~1200nm is expected to generate increasing interest in the near future[40]. Apart from their broad-gain bandwidth, Yb-doped fibre used in amplifiers can offer high output power and excellent power conversion efficiency[41]. There is also a wide range of possible pump wavelengths (~860nm to 1064nm),

Chapter 3 Point Optical Temperature Sensors using Different Fluorescent Materials

allowing for a variety of pumping schemes, including the use of diode lasers or even high-power Nd lasers. The simple energy level structure of ytterbium avoids problems like multiphonon decay, excited state absorption and concentration quenching.

Photoluminescence of Yb-doped fibres has been investigated by several researchers for sensing applications. The work by Paschotta et al[41] reported on the lifetime quenching in several Yb-doped fibres and the effect seemed to have been caused by an as yet unidentified impurity or structural defect, probably a color center, which may have degraded the performance of the Yb-doped fibre. Yb-related photoluminescence was also observed by Kimura et al[42] at room temperature from Yb-doped porous silicon layers prepared by an electrochemical method, developed for Er doping of porous silicon layers. After rapid thermal annealing in a pure argon atmosphere at high temperatures (above $\sim 900^{\circ}\text{C}$), samples show a sharp photoluminescence band at around $1.0\mu\text{m}$. Previous work by Maurice et al[43] discussed an intensity-based fibre optic sensor using specially developed and non-commercial Yb^{3+} doped fibre of $40\mu\text{m}$ diameter and 2000 ppm doping level. The device operated over a temperature range from room temperature to 600°C , with an accuracy of $\pm 1^{\circ}\text{C}$ being reported. A particular advantage of this species is the facility to use excitation sources which are cheap, high power and readily coupled into a range of fibres, associated with a fluorescence emission spectrum in the near infra red which again is well suited to use with sensitive detectors.

The work aims to extend the research reported previously by the authors and others, to conduct a fuller investigation of a series of commercial Yb^{3+} doped fibres, and to investigate the potential of fluorescence lifetime based sensor systems with this species, in order to consider an extended measurement range and to analyze the effects of dopant concentration on sensor performance. Results are fitted to a simple model, to provide a theoretical underpinning for the results obtained, and the effects of annealing[24] and an extended temperature range are considered. The response of the various fibre-based schemes and their sensitivities are compared, both with each other and with that of previous work.

3.4.3.3 Spectroscopic properties

The spectroscopy of the Yb^{3+} ion is relatively simple compared to that of other rare-earth ions. For all optical wavelengths, only two groups of levels are relevant: the $^2\text{F}_{7/2}$ ground state manifold and the $^2\text{F}_{5/2}$ excited state manifold. These consist of four and three sublevels respectively, and Fig.3.17(a) shows the cross sections for absorption and emission of Yb^{3+} in a germanosilicate glass. Previous work has shown that these absorption and emission cross sections are identical at the main peak of 976nm[40] and the rare-earth ion has a very broad absorption band across the infrared spectrum, resulting from the $^2\text{F}_{7/2}-^2\text{F}_{5/2}$ transition shown in Fig.3.17(b)[43]. De-excitation from the excited state $^2\text{F}_{5/2}$ metastable level is predominantly radiative because non-radiative transitions, due to phonon coupling or energy transfer with other energy levels, are inhibited except at very high temperatures, and thermal quenching occurs, which is discussed in detail in this work. The 976nm and 916nm absorption peaks are

essentially due to the transitions from the lowest energy sublevel of the ${}^2F_{7/2}$ manifold (${}^2F_{7/2}$ (a) in Fig.3.17(b)) to the two lowest energy sublevels of the ${}^2F_{5/2}$ manifold (${}^2F_{5/2}$ (a) and ${}^2F_{5/2}$ (b) in Fig.3.17(b), respectively). Since the third sublevel, ${}^2F_{5/2}$ (c), of the excited state manifold is well displaced from the other two sublevels, it may be assumed that its population is relatively small at the temperatures under investigation. Thermalization of the sublevel populations within each manifold is so fast that it can be assumed to be instantaneous, which implies that the underpinning science of the rare earth ion can be explained by the simple two-level model which is discussed in detail below.

Research by Paschotta et al[40] has revealed the fact that the details of the absorption and emission spectra depend, to some extent, on the host glass composition. The measured fluorescence decay times of typically around 0.8ms also vary by about 30% between different materials in fibre form: fibres with higher germanium content in the core (introduced to achieve a higher numerical aperture) tend to have shorter lifetimes (and correspondingly larger cross sections) while Yb^{3+} in a pure silicate glass (and also in some phosphosilicate glasses) has a lifetime around 1.5ms. Moreover, the emission spectra vary to some extent with pump wavelength, indicating some inhomogeneous broadening, although the broadening is dominantly homogeneous[44]. In this work, the ytterbium was doped into germanosilicate glass and drawn into a fibre, this principally being manufactured for telecommunications purposes.

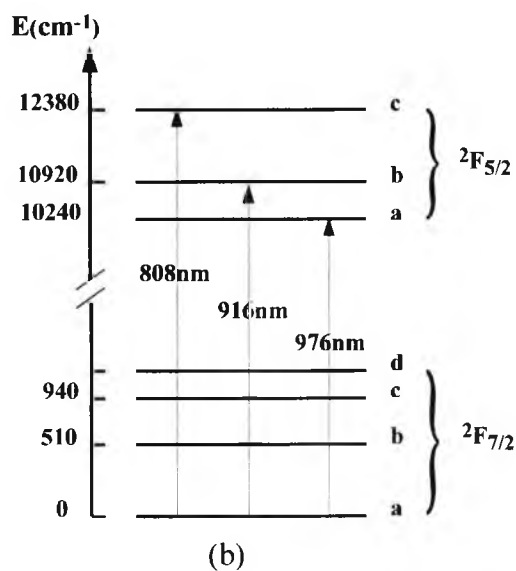
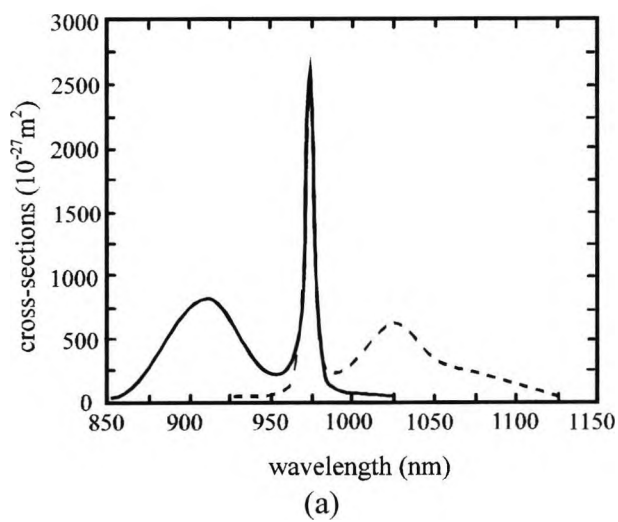


Fig.3.17 (a) Cross sections for absorption and emission of Yb^{3+} in a germanosilicate glass[40] (b) Schematic of energy levels of ytterbium ions

3.4.3.4 Experimental arrangement and initial tests

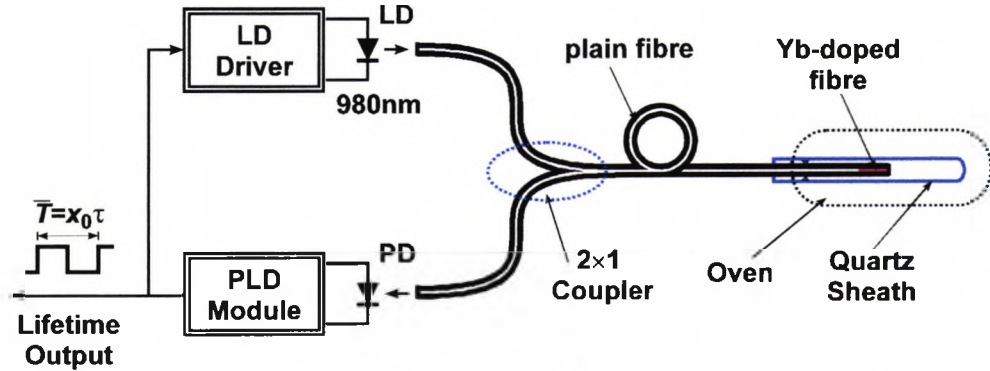


Fig.3.18 Experimental arrangement for the Yb³⁺ doped fibre thermometry LD-laser diode; PD-photodiode; PLD module-phase locked detection module

The thermal behaviour of Yb³⁺ doped fibres is demonstrated in this work by using the experimental arrangement which is shown in Fig.3.18. The laser diode, with a center wavelength of 980nm, is employed as the source, light from which couples well to a peak absorption band of the material[40]. This is conveniently the same source that may be used to excite Er³⁺ in a range of fibres. Three types of single mode Yb³⁺ doped silica fibres were put under test, termed here YbH, YbM and YbL (the final letter of the code refers to high, medium and low doping, as defined below, respectively). The fibres were manufactured by INO, Canada. The diameters of both the YbM and YbL samples were 3.4µm/125µm (core/cladding), while that of YbH was 2.8µm/124µm. The dopant concentration of YbH is Yb: 2.5wt%, Al: 8.3wt%, Ge: 0.5wt%; YbM is Yb: 1800ppm-wt, Al: 2100ppm-wt; and YbL is Yb: 550ppm-wt, Al: 2400ppm-wt. The effective numerical apertures of YbH, YbM and YbL are 0.26, 0.22 and 0.19 respectively. The deposited inner cladding for the three types are the same: P₂O₅ and F co-doped silica. A short length of doped fibre (5cm for all the three types) was used in

Chapter 3 Point Optical Temperature Sensors using Different Fluorescent Materials

these tests, this being an appropriate length to give adequate absorption of the pump light and sufficient fluorescence, as well as to be within the maximum length to achieve a stable temperature in the tube oven used (10cm for the CARBOLITE type: MTF 12.38/400, the central temperature of which is within at least $\pm 5^{\circ}\text{C}$ of that indicated) and considerably better, on average, over the period during which the results are taken. Where experiments were carried out taking samples over a period of several minutes, the short-term temperature fluctuations of the oven could be ignored. The doped fibre element was fusion-spliced to the sensor arm of a 2x1 optical fibre coupler and this bare-fibre sensor element was placed loosely in a quartz tube and centered in the stable oven. The 2x1 optical coupler was used to transmit the excitation light to the sensing probe, and to collect the resulting fluorescence response from the sensor element. An infra-red sensitive InGaAs photodiode was used to detect the fluorescence emission and the phase-locked detection (PLD) method was employed for processing the fluorescence signal[45][1], where the PLD module was used to transform the fluorescence signal into a TTL compatible frequency signal, whose period was then directly proportional to the measured fluorescence lifetime. This frequency signal was transmitted to a desktop computer which was equipped with a counter-and-timer card to monitor continuously the output and record the lifetime measurement.

After some initial tests, each sample was measured over a wide temperature range from room temperature to 700°C . It is clearly important in any practical application that a stable and reproducible response is seen. The previous work on Nd^{3+} doped fibre by Zhang et al[24] has shown that a significant change in the fluorescence characteristic

does occur if the doped fibre has been exposed to temperatures above a certain point. In order to enable the probe to possess a consistent and stable thermal characteristic, an “annealing” process was carried out, in a similar way to that of previous work with Nd-doped fibre. At each stabilized temperature, the corresponding lifetimes were recorded and compared to those before and after the heat treatment. The purpose of the heat treatment[24] was to “anneal” the doped fibre probe at a known elevated temperature to reduce the metastable conditions that appear to result during the fusion-splicing process in the doped fibre. A series of tests was carried out on the samples discussed and the results compared with those of a simple model, as discussed below.

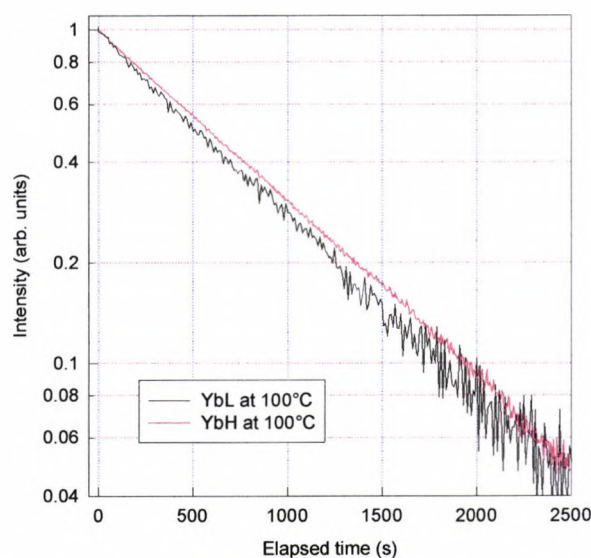


Fig.3.19 Fluorescence signals as a function of time from samples of YbH and YbL, shown separately at the same temperature of 100°C

3.4.3.5 Fluorescence decay characteristics

The fluorescence decay signal recorded for each sample, YbH, YbM and YbL, at a chosen stabilized temperature, is similar to that shown in Fig.3.19 for YbH and YbL

(for comparison at 100°C) normalized to their respective initial intensity levels. These graphs clearly show that the decay is single exponential regardless of the level of dopant concentration (the signal recorded for YbM is not shown on the graph because it is very close to that of YbL). However, the clear advantage of using a higher dopant level is seen here in the greater level of the fluorescence signal observed from the higher density of active species present and the consequent advantage that results in terms of signal-to-noise ratio of the detector. This choice thereby facilitates obtaining a higher resolution in the measurement and offering with that significant practical advantages in sensor use. The lifetime estimated from the signal shows that the lifetime of YbH is longer than that of YbL and that of YbM and YbL are very close, an unusual result in the light of previous studies on other luminescent ions[24][25]. This is attributed to the effect of host composition rather than to concentration quenching, because concentration quenching does not occur here due to the simple energy level structure of ytterbium involved in this fluorescent process.

3.4.3.6 Heat treatment and annealing

For the heat treatment and annealing process, each bare-fibre probe was gradually heated (to avoid thermal shock fracture) and the fluorescence lifetime data were recorded when the oven reached the designated maximum temperature, 700°C. This temperature was chosen on the basis of previous work on Nd[24] where a successful annealing temperature of 750°C was observed and initial studies on samples heated beyond 700°C, showing that this temperature was near the maximum where a stable lifetime could be achieved over a long period. As with neodymium-doped fibre, it was

Chapter 3 Point Optical Temperature Sensors using Different Fluorescent Materials

found that a stable plateau of the fluorescence lifetime with time, over several tens of hours, could not be achieved with temperatures considerably in excess of this. Thus 700°C was designated the optimum “annealing temperature” for Yb-doped fibre samples, and fibres used in this work were pre-heated in this way before calibration data were taken.

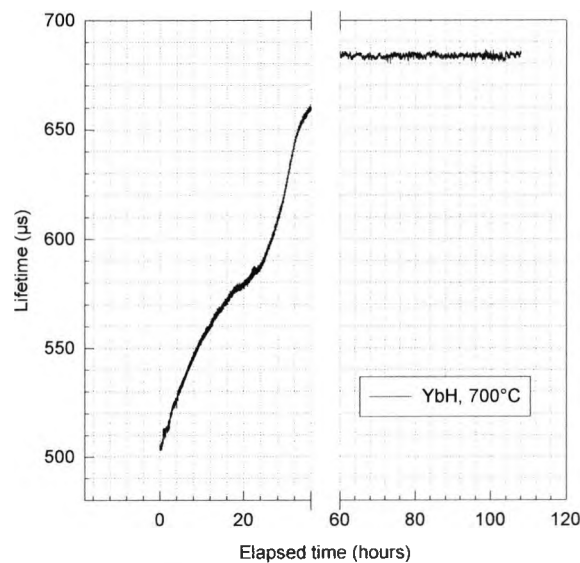


Fig.3.20 Temporal response of YbH at 700°C for more than 100 hours, showing the decay-time plateau

Each experiment to investigate this was carried out for about 100 hours and the temporal graphs obtained are similar to those depicted in Fig.3.20, for YbH. This shows that each fluorescence lifetime increases dramatically at the start of the process but finally reached a stable value at a temperature of 700°C. No sign of decomposition of the fluorescent species, which could have been indicated by a deterioration in the fluorescence intensity, was observed during each experiment, reinforcing the choice of this temperature of 700°C for the heat treatment of Yb³⁺-doped fibre probes for

thermometric use. After undergoing the prescribed annealing, using heat treatment at 700°C as is described above, the doped fibre probes were tested in several temperature cycling experiments. Fig.3.21 shows the temporal response of the fluorescence lifetime measurement for YbH at 700°C over a period of 15 hours, taken after the probe had experienced several temperature cycles from 60°C-700°C. The standard deviation of these experimental data is $\sim 2\mu\text{s}$, which gives rise to an equivalent temperature deviation of $\sim 1.1^\circ\text{C}$.

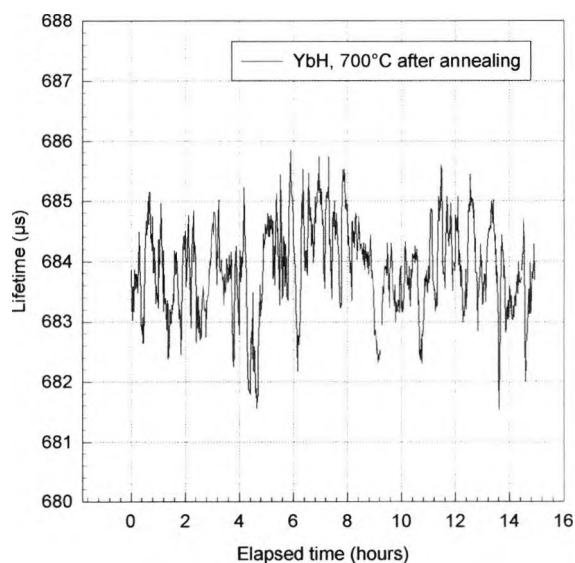


Fig.3.21 Temporal response of YbH at 700°C over a period of 15 hours taken after a temperature excursion, following initial annealing

Significant change can be seen in fluorescence lifetime as a function of temperature for each sample before and after annealing, for example the lifetime of YbH at 600°C changed by more than $170\mu\text{s}$ after the annealing process shown in Fig.3.22, corresponding to an equivalent temperature drift of $\sim 250^\circ\text{C}$ in an unannealed thermometer probe.

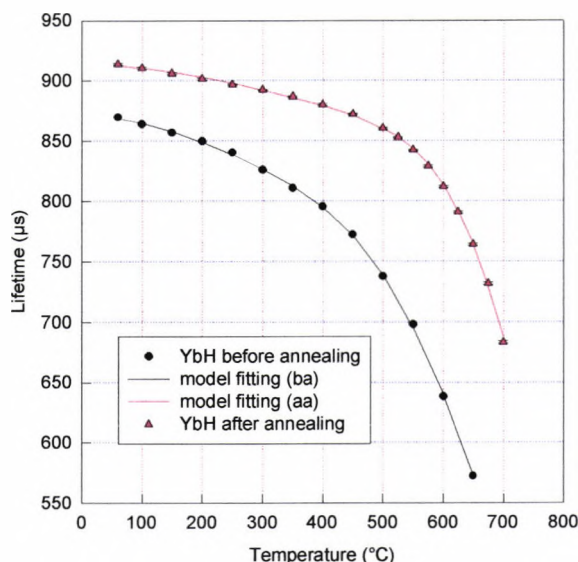


Fig.3.22 Fluorescence lifetime variation of YbH as a function of temperature before and after annealing recorded during several temperature cycles from 60°C to 700°C and back to 60°C

3.4.3.7 Probe calibration

In practical applications, it is essential that a calibration curve is derived from an annealed sample in order to achieve a stable and repeatable outcome. Although the three samples are all Yb doped, the calibration curves for each thermometer element are different, as are clearly shown in Figs. 3.22, 3.23 and 3.24 respectively, obtained from several temperature cycling experiments, with error bars representing the standard deviations obtained. The intensity of each probe observed decreases with increasing temperature, similar to that shown in Fig.3.24 for YbL. The deviation of the lifetime measurement in the roundtrip excursions from 60°C to 700°C are well within a $\pm 10^\circ\text{C}$ change for YbL, $\pm 7^\circ\text{C}$ for YbM and $\pm 5^\circ\text{C}$ for the YbH sample temperature error, corresponding to the maximum oven temperature instability. The

comparison of the fluorescence lifetime from each probe as a function of temperature is shown in Fig.3.25, in which the behaviour patterns of YbM and YbL are similar, while rather different from that of YbH. It should be remembered that the glass composition for each is different, as discussed earlier. This suggests that the host glass composition plays a key part in the thermal behaviour of the Yb doped fibres rather than simply the doping level of Yb ions, as it should be remembered that the glass composition for each sample is different, even though they were obtained from the same manufacturer.

3.4.3.8 Model of thermal behaviour of Yb-doped fibres

Each calibration curve can be explained very well by the use of a two-level model, taking into account the effect of thermal quenching, as was proposed by Zhang et al[9] to fit to the results of alexandrite-based thermometry. In this case, as shown in

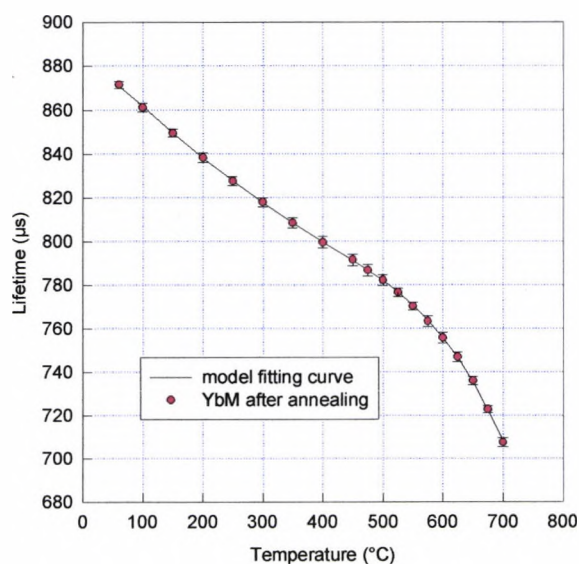


Fig.3.23 Fluorescence lifetime variation of YbM as a function of temperature after annealing, recorded during several similar temperature cycles to that of Fig.3.22

Fig.3.17(b), the energy levels involved are the ground level ${}^2F_{7/2}$ (a), level 1 ${}^2F_{5/2}$ (a) and level 2 ${}^2F_{5/2}$ (b). As mentioned earlier, the sublevel ${}^2F_{5/2}$ (c) is far removed from the other two sublevels and its contribution to the fluorescence can be ignored. The

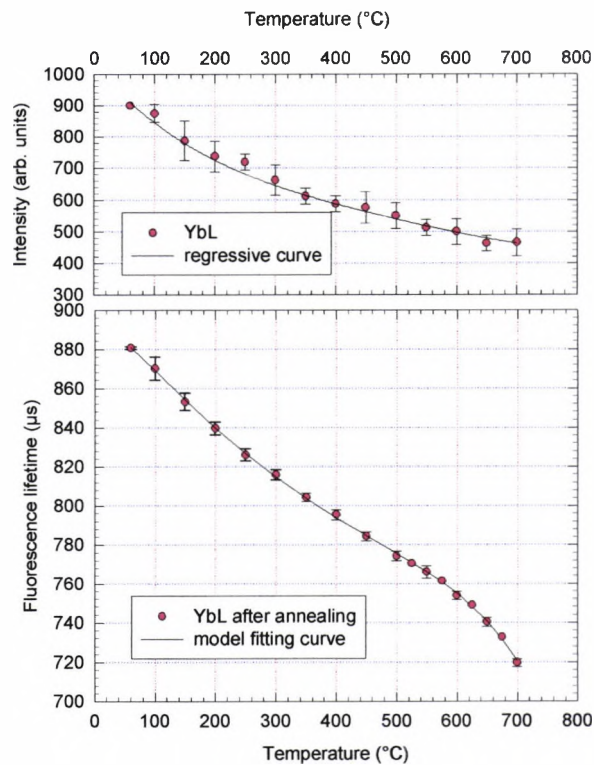


Fig.3.24 Fluorescence lifetime variation of YbL as a function of temperature after annealing, recorded during several similar temperature cycles to that of Fig.3.22

two level model proposed by Zhang et al[9] can be modified to give the following form for the lifetime, τ ,

$$\tau = \frac{1 + e^{-\Delta E/kT}}{\frac{1}{\tau_1} + \frac{1}{\tau_2} e^{-\Delta E/kT} + \frac{1}{\tau_q} e^{-(\Delta E + \Delta E_q)/kT}} \quad (3.13)$$

where τ_1 , τ_2 are the intrinsic lifetimes of levels 1 and 2, ΔE is the energy gap between levels 1 and 2, τ_q and ΔE_q are the lifetime and energy gap due to thermal quenching respectively and T is the Kelvin temperature.

The solid lines in Figs.3.22-3.24 result from a least squares fitting of Eq.(3.13) to the experimental data obtained from the roundtrip measurements for each sample from

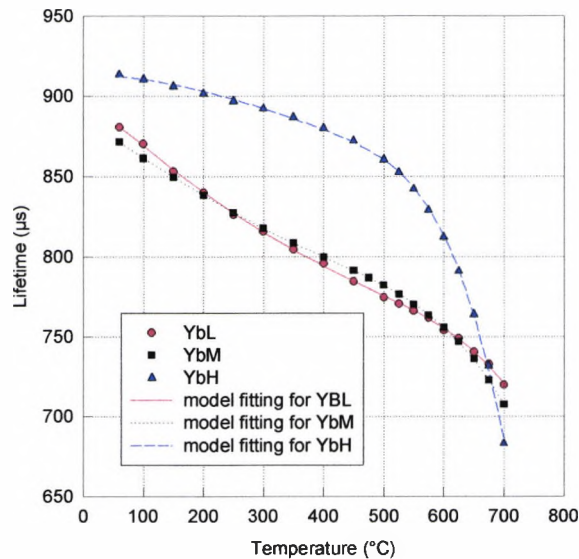


Fig.3.25 Comparison of fluorescence lifetimes from YbH, YbM and YbL as a function of temperature

60°C to 700°C. The fitted values for ΔE , τ_1 , τ_2 , ΔE_q and τ_q are listed in Table 3.5.

It is interesting to notice that the energy gap, ΔE , estimated from YbL and YbM is almost the same as that obtained from previous work of Maurice et al[43]. It may be

Chapter 3 Point Optical Temperature Sensors using Different Fluorescent Materials

assumed that the different calibration curves for YbH and YbL are mainly caused by the different energy gaps between levels 1 and 2 (ΔE) in each case, because the other parameters involved in the model shown in Table 3.5 are seen to be very close to each other, while for YbM and YbL they are caused by the different energy gap arising from thermal quenching (ΔE_q), because the other parameters are seen to be very similar. The parameter comparison for the YbH sample before and after annealing indicates that the heat treatment has considerably changed the physical characteristics of the material.

The fluorescence lifetime of each sample changes monotonically with temperature, and these characteristics are very well suited to wide temperature range thermometry.

However, the sensitivity, defined as $\frac{1}{T} \frac{\partial \tau}{\partial T}$, for each Yb-doped fibre based thermometer element is shown to be significantly different, in Fig.3.26. In general, the higher the sensitivity of a thermometer over a specific temperature region, the better suited it is to certain applications. A comparison of the sensitivities of YbH, YbM and YbL has indicated that from room temperature to $\sim 460^\circ\text{C}$, the YbL-based thermometer is preferable, while above 460°C , YbH based thermometry behaves very well and offers very high sensitivities when compared to the other two. The behaviour of YbM based thermometry is essentially in between that of the other two.

Table 3.5 List of parameters estimated from the two level model for the three samples, before and after annealing and compared with the work of Maurice et al[43]

SM–single mode; MM–multimode (*ba: before annealing; aa: after annealing)

	$\Delta E(cm^{-1})$	$\tau_1(\mu s)$	$\tau_2(\mu s)$	$\Delta E_q(cm^{-1})$	$\tau_q(\mu s)$
Maurice et al[43] 2000ppm (MM)	680				
YbH (ba*) 2500ppm (SM)	1285	873	357	4793	1.7×10^{-1}
YbH (aa*) 2500ppm (SM)	1301	914	548	7973	3.9×10^{-3}
YbM (aa) 1800ppm (SM)	685	899	543	6508	1.7×10^{-1}
YbL (aa) 550ppm (SM)	687	916	504	7558	6.9×10^{-2}

3.4.3.9. Discussion of Yb³⁺ thermometer schemes

A series of commercial Yb³⁺ doped fibres has been investigated for their potential for use as the key element of a fluorescence-lifetime based sensor system over a wide temperature range from 60°C to 700°C. Consistent results have been obtained for each sample after heat treatment and the temperature deviations obtained are $\pm 10^\circ\text{C}$, $\pm 7^\circ\text{C}$, $\pm 5^\circ\text{C}$ separately for the YbL, YbM and YbH samples with reference to the oven temperatures (limited by the $\pm 5^\circ\text{C}$ maximum temperature fluctuations in the oven). This response has somewhat outside the desired specification given earlier. Each calibration curve can be explained very well by a two level model, except that the parameters involved are somewhat different in each case. The comparison of sensitivities has offered a convenient mechanism for selecting the most suitable material for any specific applications.

Chapter 3 Point Optical Temperature Sensors using Different Fluorescent Materials

In previous work on Er and Nd doped fibres by Zhang et al[24][25] it was reported that the uncertainty of the measurement with a Nd-doped fibre probe was evaluated at 2°C over the entire region from -190°C to 750°C, with a measurement time of 1 second while that of Er-doped fibre probe is 5°C over the region from 0°C to 1100°C, with response time of 5 seconds. However, Yb-doped fibres, which have been discussed in detail above, revealed a slightly low precision over the region from 60°C to 700°C compared with the other two materials, but they offer a relative high sensitivity, especially above ~500°C for YbH, with an associated measurement time of ~2 seconds.

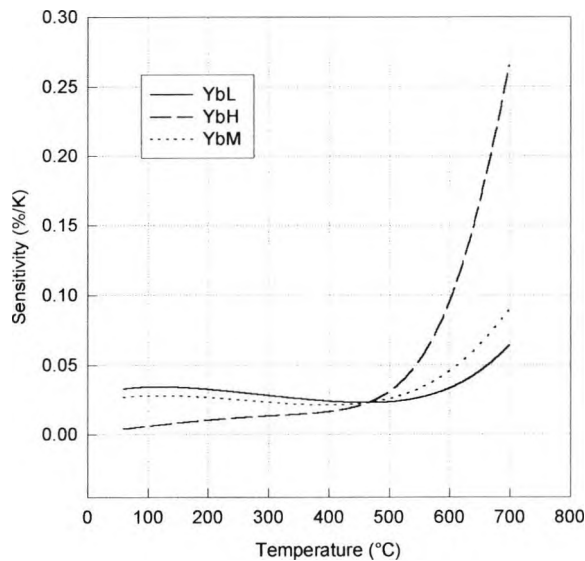


Fig.3.26 Sensitivity comparison of the three samples, YbH, YbM and YbL over the temperature region from 60°C to 700°C

Overall, the results obtained from these rare-earth doped fibres look promising for the development of effective, compact, intrinsic fibre temperature probes, although each

possesses its own individual characteristics. This is advantageous for use in quasi-distributed sensor systems, such as are discussed in Chapter 4[46], especially as Yb and Er doped fibres may be pumped by the same source wavelengths. On the positive side, they do show an unambiguous relationship of decay time with temperature, may operate over a significant temperature range and they are robust with the doped material being fusion spliced to the connecting fibre. Using simple and readily available light sources and detectors, coupled with a convenient signal processing system, they offer the prospect of a effective thermometer with the advantages of low cost, fast response and a wide measuring range.

3.5 Summary

A large variety of materials has been discussed in this Chapter for wide-range fluorescence-lifetime based temperature measurement. Generally, bulk active material-based thermometry is limited by its physical configuration and the nature of the glass: however, rare-earth doped fibres look very promising for the development of effective, compact, intrinsic doped fibre temperature probes. They do show a clear relationship of decay-time with temperature operation over a significant temperature range and they are robust with the doped material being fusion spliced to the connecting fibre, yielding high probe integrity. Most have met the specification given, or are close to it, and they can be excited and the fluorescence detected with convenient sources and detectors. Their potential for quasi-distributed, average and local temperature measurement will be discussed in Chapters 4 and 5, to expand upon the use of these materials in a wider range of optical fibre sensor systems.

3.6 References

- [1] K.T.V.Grattan, Z.Y.Zhang, *Fibre Optic Fluorescent Thermometry* (Chapman & Hall, London, 1995)
- [2] J.C.Walling, O.G.Peterson, H.P.Jensen, R.C.Morris and E.W.O'Dell, Tunable alexandrite lasers, *IEEE J. Quantum Electron.*, 12, 1302(1980)
- [3] S.F.Carter, D.Szebesta, S.T.Davey, R.Wyatt, M.C.Brierley and P.W.France, Amplification at 1.3 μm in a Pr³⁺-doped single-mode fluorozirconate fibre, *Electron. Lett.*, 27, 628(1991)
- [4] A.Remillieux, B.Jacquier, C.Linares, C.Lesergent, S.Artigaud, D.Bayard, L.Hamon and J.L.Beylat, Upconversion mechanisms of a praseodymium-doped fluoride fibre amplifier, *Physics D: Appl. Phys.*, 29, 963(1996)
- [5] J.Y.Allain, M.Monerie and H.Poignant, Tunable CW lasing around 610, 635, 695, 715, 885 and 910nm in praseodymium-doped fluorozirconate fibre, *Electron. Lett.*, 27, 189(1991)
- [6] M.J.F.Digonnet, ed., *Rare Earth Doped Fiber Lasers and Amplifiers* (Dekker, New York, 1993)
- [7] J.C.Walling, D.F.Heller, H.Samelson, D.J.Harter, J.A.Pete and R.C.Morris, Tunable alexandrite lasers: development and performance, *IEEE J. Quantum Electron.*, 10, 1568(1985)
- [8] Z.Y.Zhang, K.T.V.Grattan and A.W.Palmer, Temperature dependences of fluorescence lifetimes in Cr³⁺-doped insulating crystals, *Phys. Rev. B*, 11, 7772(1993)

Chapter 3 Point Optical Temperature Sensors using Different Fluorescent Materials

- [9] Z.Y.Zhang, K.T.V.Grattan and A.W.Palmer, Thermal characteristics of alexandrite fluorescence decay at high temperatures, induced by a visible laser diode emission, *J. Appl. Phys.*, 73, 3493(1993)
- [10] T.Sun, Z.Y.Zhang, K.T.V.Grattan and A.W.Palmer, Analysis of the double exponential behaviour in alexandrite for optical temperature sensing applications, *Rev. Sci. Instrum.*, 68, 3442(1997)
- [11] Shuji Nakamura, Light emission moves into the blue, *Physics World*, 11, 31(1998)
- [12] D.W.Marquardt, *J. Soc. Ind. Appl. Math.*, 431(1963)
- [13] S.K.Gayen, W.B.Wang, V.Petricevic, R.Dorsinville and R.R.Alfano, Nonradiative transition dynamics in alexandrite, *Appl. Phys. Lett.*, 49, 437(1986)
- [14] H.Berthou and C.K.Jørgensen, Optical-fiber temperature sensor based on upconversion-excited state fluorescence, *Opt. Lett.*, 15, 1100(1990)
- [15] E.Maurice, G.Monnom, B.Dussardier, A.Saissy, D.B.Ostrowsky and G.W.Baxter, Erbium-doped silica fibers for intrinsic fibre-optic temperature sensors, *Appl. Opt.*, 34, 8019(1995)
- [16] E. Maurice, G.Monnom, G.W.Baxter, S.A.Wade, B.P.Petreski and S.F.Collins, Blue LED-pumped point temperature sensor based on a fluorescence intensity ratio in Pr^{3+} :ZBLAN glass, *Proceedings of the 11th International Conference on Optical Fiber Sensors*, Sapporo, 188(1996)
- [17] G.Baxter, S.Wade, S.Collins, G.Monnom and E.Maurice, Rare-earth doped optical fibres for point temperature sensing, *Proc. SPIE*, 2841, 249(1996)

Chapter 3 Point Optical Temperature Sensors using Different Fluorescent Materials

- [18] B.P.Petreski, M.M.Murphy, S.F.Collins and D.J.Booth, Amplification in Pr^{3+} -doped fluorozirconate optical-fiber at 632.8nm, *Electron. Lett.*, 29, 1421(1993)
- [19] T.Sun, Z.Y.Zhang, K.T.V.Grattan and A.W.Palmer, Temperature dependence of the fluorescence lifetime in Pr^{3+} : ZBLAN glass for fiber optic thermometry, *Rev. Sci. Instrum.*, 68, 3447(1997)
- [20] A.A.Kaminskii, *Laser Crystals: Their Physics and Properties* (Springer, Berlin, 1981)
- [21] B.P.Petreski, P.M.Farrell and S.F.Collins, Cross-relaxation in praseodymium-doped fluorozirconate glass, *Opt. Commun.*, 132, 89(1996)
- [22] K.T.V.Grattan, J.D.Manwell, S.M.L.Sim and C.A.Willson, Lifetime investigation of fluorescence from neodymium-yttrium-aluminum garnet at elevated-temperature, *Optics Communications*, 62, 104(1987)
- [23] Z.Y.Zhang, K.T.V.Grattan, A.W.Palmer and B.T.Meggitt, Potential for temperature sensor applications of highly neodymium-doped crystals and fiber at up to approximately 1000°C, *Rev. Sci. Instrum.*, 68, 2759(1997)
- [24] Z.Y.Zhang, K.T.V.Grattan, A.W.Palmer and B.T.Meggitt, Spectral characteristics and effects of heat treatment on intrinsic Nd-doped fiber thermometer probes, *Rev. Sci. Instrum.*, 69, 139(1998)
- [25] Z.Y.Zhang, K.T.V.Grattan, A.W.Palmer, B.T.Meggitt and T.Sun, Fluorescence decay-time characteristics of erbium doped optical fiber at elevated temperatures, *Rev. Sci. Instrum.*, 68, 2764(1997)

Chapter 3 Point Optical Temperature Sensors using Different Fluorescent Materials

- [26] Z.Y.Zhang, K.T.V.Grattan, A.W.Palmer, B.T.Meggitt and T.Sun, Characterization of erbium-doped intrinsic optical fiber sensor probes at high temperatures, *Rev. Sci. Instrum.*, 69, (1998)
- [27] C. Mazzali, H.L.Fraguto, E.Palange and D.C.Dini, Fast method for obtaining erbium-doped fiber intrinsic parameters, *Electron. Lett.*, 32, 921(1996)
- [28] E.Maurice, G.Monnom, B.Dussardier, A.Saissy, D.B.Ostrowsky and G.Baxter, Thermalisation effects between upper levels of green fluorescence in Er-doped silica fibre, *Optics Lett.*, 19, 990(1994)
- [29] E.Maurice, G.Monnom and D.B.Ostrowsky, High-dynamic-range temperature-point sensor using green fluorescence intensity ratio in Er-doped silica fiber, *IEEE J. Lightwave Tech.*, 13, 1349(1995)
- [30] Y.Imai, T.Hokazono and T.Yoshida, Temperature sensing using 1.54 μ m fluorescence in Er-doped optical fibers, *Proc. 11th Conf. on Optical Fiber Sensors(OFS11)*, 268(1996)
- [31] P.K.Y.Ko, M.S.Demokan and H.Tam, Distributed temperature sensing with erbium doped fiber amplifiers, *IEEE J. lightwave Tech.*, 14, 2236(1996)
- [32] Z.Y.Zhang, K.T.V.Grattan, A.W.Palmer, T.Sun and B.T.Meggitt, Rare earth doped intrinsic fiber optic sensors for high temperature measurement up to 1100°C, *Proc. 12th International Conference on Optical Fiber Sensors (OFS'12)*, Williamsburg, Virginia, 556(1997)
- [33] Z.Y.Zhang, K.T.V.Grattan, A.W.Palmer and B.T.Meggitt, Thulium-doped intrinsic fibre optic sensor for high temperature measurements (>1100°C), *Rev. Sci. Instrum.*, 69, (1998)

Chapter 3 Point Optical Temperature Sensors using Different Fluorescent Materials

- [34] A.K.Kewell, G.T.Reed and F.Namavar, Integrated temperature sensor in Er-doped silicon, *Sensors & Actuators*, 65, 160(1998)
- [35] Z.Y.Zhang, T.Sun, K.T.V.Grattan and A.W.Palmer, Erbium-doped intrinsic fiber sensor for cryogenic temperature measurement, *Sensors and Actuators A*, 71, 183(1998)
- [36] V.C.Fernicola, Z.Y.Zhang and K.T.V.Grattan, Fiber optic thermometry based on Cr-fluorescence in olivine crystals, *Rev. Sci. Instrum.*, 68, 2418(1997)
- [37] Y.L.Hu, Z.Y.Zhang, K.T.V.Grattan, A.W.Palmer and B.T.Meggitt, Ruby-based decay-time thermometry: effect of probe size on extended measurement range (77-800K), *Sensors and Actuators A*, 63, 85(1997)
- [38] S.F. Collins, G.W. Baxter, S.A. Wade, T. Sun, K.T.V. Grattan, Z.Y. Zhang and A.W. Palmer, Comparison of fluorescence-based temperature sensor schemes: theoretical analysis and experimental validation, *J. Appl. Phys.*, 84, (1998)
- [39] S.V.Chernikov, Y.Zhu and J.R.Taylor, Supercontinuum self-Q-switched ytterbium fiber laser, *Optics Lett.*, 22, 298(1997)
- [40] R.Paschotta, J.Nilsson, A.C.Tropper and D.C.Hanna, Ytterbium-doped fiber amplifiers, *IEEE J.Quantum Electron.*, 33, 1049(1997)
- [41] R.Paschotta, J.Nilsson, P.R.Barber, J.E.Caplen, A.C.Tropper and D.C.Hanna, Lifetime quenching in Yb-doped fibres, *Optics Commun.*, 136, 375(1997)
- [42] T.Kimura, A.Yokoi, Y.Nishida, R.Saito and S.Yugo, Photoluminescence of ytterbium-doped porous silicon, *Appl. Phys. Lett.*, 67, 2687(1995)

Chapter 3 Point Optical Temperature Sensors using Different Fluorescent Materials

- [43] E.Maurice, S.A.Wade, S.F.Collins, G.Monnom, Self-referenced point temperature sensor based on a fluorescence intensity ratio in Yb³⁺-doped silica fiber, *Applied Optics*, 36, 8264(1997)
- [44] S.Magne, M.Druetta, J.P.Goure, J.C.Thevenin, P.Ferdinand and G.Monnom, An ytterbium-doped monomode fiber laser: amplified spontaneous emission, modeling of the gain and tunability in an external cavity, *J. Lumin.*, 60, 647(1994)
- [45] Z.Y.Zhang, K.T.V.Grattan and A.W.Palmer, Phase locked detection of fluorescence lifetime, *Rev. Sci. Instrum.*, 64, 2531(1993)
- [46] T.Sun, Z.Y.Zhang, K.T.V.Grattan and A.W.Palmer, Quasi-distributed fluorescence-based optical fiber sensor system, *Rev. Sci. Instrum.*, 69, 146(1998)

Chapter 4

Multiple Exponential Decay Analysis and Fluorescence-based Quasi-distributed Temperature Sensing System

4.1 Abstract

The use of multiple material, fluorescence-based sensors, where each is pumped by the same light source, and is emitting over the same spectral region, makes for a very simple, convenient and promising optical arrangement which can be applied in real-time, quasi-distributed temperature sensor systems. Quasi-distributed contrast with fully distributed sensor schemes in that measurements can only be made at specific, predefined positions along a fibre network. However, a major advantage is that they are potentially simpler and less expensive than fully distributed systems. The fluorescence lifetime approach is adopted in the system discussed, based upon the point sensor systems discussed in Chapter 3. An analysis scheme using Prony's method is reported, to enable exponential decays from either single material, two-material or even several element quasi-distributed sensors to be deconvolved and thus data and

Chapter 4 Multiple Exponential Decay Analysis and Fluorescence-based Quasi-distributed Temperature Sensing System

associated measurand information encoded in each individual signal to be recovered. In a similar way, multi-exponential decays arising from single sensor elements also can be deconvolved and analyzed, an additional advantage of the technique. In this work, in the development of an effective and rapid quasi-distributed temperature sensor algorithm, Prony's method is used for the estimation of the exponential time constants of a convoluted exponential fluorescence decay, with each individual decay corresponding to a different point and its associated temperature. Experimental results obtained are presented to justify the use of the approach in practical multi-exponential fluorescence decay analysis and to show a comparison of the Prony with an alternative, the Marquardt nonlinear least-squares approximation algorithm, to achieve the analysis most rapidly and effectively. The results show that the computational time for the Prony's approach is approximately one thousandth of that of the Marquardt's technique while the accuracy achieved using Prony's method is still high enough for practical use, as will be discussed.

4.2 Introduction

Fluorescent decay time techniques, coupled with optical fibres, have been widely used for the monitoring of temperatures over a wide range, using a variety of analysis techniques and sensor materials[1]. In most cases, a single exponential decay is either seen, or more often assumed, in order to obtain the non-intensity dependent measurement on which the method depends. Illustrations of this occur especially in fibre optic temperature sensors where the doping level of the fluorescent active system

Chapter 4 Multiple Exponential Decay Analysis and Fluorescence-based Quasi-distributed Temperature Sensing System

is small, such as Cr³⁺-doped chrysoberyl, which offers a single exponential with low doping levels (<0.1 wt%). However, with much higher dopant levels (e.g. >0.4 wt%), a deviation is observed from this idealized behavior in the same host crystal (see Section 3.3.1). The advantages of the higher dopant levels are readily seen in the greater level of the fluorescence signal observed from the higher density of active species present with consequent advantages that arise in terms of the signal-to-noise ratio of the detector, thereby facilitating obtaining a higher accuracy of the measurement or a faster response time of the system.

It is therefore essential that those significant number of systems which do show a double exponential behavior are properly analyzed in terms of extracting and separating the two decay time constants present, otherwise a considerable error can occur in the attribution of single exponential as a best fit to the data points. Further, the ability to extract two or more different exponential decay times from a single optical signal enables the possibility of using this method in the multiplexing of several sensors, each having its own distinctive decay time behavior. Quasi-distributed sensing had been demonstrated previously, for example by Theocharous[2] using an absorption-based system and several sensors of red Schott glass which were independently temperature sensitive. The time-of-pulse-propagation along the fibre was used with a higher bandwidth detection system to extract meaningful data on the convoluted multiple absorption which was observed. A problem that results from such a system is that the signal-to-noise ratio diminishes with each sensor "down-line" from

Chapter 4 Multiple Exponential Decay Analysis and Fluorescence-based Quasi-distributed Temperature Sensing System

the source and thus the accuracy obtainable with the more remote sensor elements is reduced.

As mentioned earlier in Chapter 1, work previously carried out on fully distributed temperature sensors has typically utilized either basic loss or scattering mechanisms in a single length of optical fibre which forms an extended sensor. Interrogation of this extended sensor element using optical time domain reflectometry (OTDR) permits the spatial variation of the measurand to be derived from the output information, thus allowing the measurand to be profiled within a certain specific spatial resolution along the fibre length[3]. A Rayleigh backscatter system based on holmium-doped fibre reported by Farries et al[4] showed a temperature resolution of $\sim 1^{\circ}\text{C}$ and a spatial resolution of $\sim 3.5\text{m}$ over the temperature range $\sim -200^{\circ}\text{C}$ to 100°C . Arguably the most successful distributed fibre optic sensor developed to date is the Raman-distributed temperature sensor scheme. Commercial systems based on this technology are available which are capable of operation over fibre lengths of up to 10km with $\sim 1^{\circ}\text{C}$ resolution and 1m spatial resolution[5]. A more recent and very significant development in the area of distributed sensing is the use of Brillouin scattering technique. Research work by the groups at NTT in Japan and the University of Kent at Canterbury have shown that the approach is capable of providing distributed temperature sensing over fibre lengths of up to 50km with temperature resolution of $\sim \pm 1^{\circ}\text{C}$ and spatial resolutions under 10m[5]. However, major advances in this area

Chapter 4 Multiple Exponential Decay Analysis and Fluorescence-based Quasi-distributed Temperature Sensing System

have been slow and the signal processing aspects are complex and expensive to implement.

In this work, an analysis scheme is reported which enables double and triple exponential decays to be deconvolved and thus data and measured information encoded in each individual exponential decay to be recovered. The prime application is seen in the use of a single optical signal recovered from several fluorescent sensors for temperature measurement, for example from these types of sensors in a quasi-distributed network, separated along an optical fibre or from a single sensor yielding a double exponential decay, where more accurate measurand encoded information is extracted from the variation of one or more of the exponential decays present. To achieve this, an analysis scheme based on Prony's method, which was first implemented by Zhang et al[6] to estimate the single exponential lifetime in fluorescence-based thermometers, is reported. This enables the combined double or triple exponential decays from such quasi-distributed sensors to be deconvolved, each having its own corresponding individual temperature characteristic. The performance of Prony's method can be greatly improved through the selection of both an optimized observation time and several algorithm-related parameters by using a Monte-Carlo simulation. Experimental results from previous work have shown the effectiveness of Prony's method in the single lifetime estimation by comparison to the use of a Marquardt nonlinear least-squares approximation algorithm[7][8], and this is the approach which is extended in this research.

4.3 Use of Prony's and Marquardt's algorithm

4.3.1 Signal processing consideration

Ideally, following the termination of the excitation light pulse, the fluorescence will decay exponentially with time and the observed decay signal f is given as a function of time t by

$$f(t) = A \exp(-t / \tau) + \varepsilon(t) \quad (0 \leq t \leq w) \quad (4.1)$$

where w is the length of observation period, termed the observation time; $\varepsilon(t)$ the non-periodic noise component attributed to various noise sources such as shot and excess noise in the photodetector and thermal noise in the electronic signal amplifiers. The two parameters A and τ are the initial fluorescence amplitude and the fluorescence lifetime, respectively. Either of them can be of sensing use, but the lifetime is a much preferred sensing parameter as its measurement is intrinsically independent of a precise measurement of the light intensity present at the sensor head.

As mentioned earlier, a number of numerical algorithms has been used for the estimation of fluorescence lifetime, with those based on a decay curve fit considered to be more effective[9]. One such example is the digital log-fit technique used in a fluorescence lifetime-based fibre-optical thermometer module utilizing a digital signal processor (DSP)[9].

Chapter 4 Multiple Exponential Decay Analysis and Fluorescence-based Quasi-distributed Temperature Sensing System

In practice, due to the dark current in the photodetector and the result of any background illumination or the presence of offset voltages in the electronic circuit, the actual observed decay signal $f(t)$ will inevitably contain a non-time varying component and thus a third parameter should be added into the two-parameter model of Eq.(4.1) giving[6]

$$f(t) = A \exp(-t / \tau) + \varepsilon(t) + B \quad (0 \leq t \leq w) \quad (4.2)$$

where the third parameter B is a constant reflecting this, over the measurement period, termed the base-line offset. This baseline offset can be numerically subtracted from the observed signal after digitization, where B in Eq.(4.2) can be considered as the residual of the base-line offset. The simulation work, carried out by Dowell et al[7] on the Marquardt nonlinear least squares approximation algorithms, has demonstrated that the residual of the base-line offset can severely impair the estimation accuracy of two-parameter based algorithms. Thus, a three-parameter Marquardt algorithm has been recommended as an improvement on this approach[7].

Noniterative algorithms using Prony's method[10] have been proposed by Zhang et al[6] for the estimation of the exponential lifetime in fluorescence-based thermometers and their performance has been evaluated using Monte Carlo simulations. Cross comparison has been made between a variety of Prony's algorithms and the results of other estimation methods[6]. It has been demonstrated that the performance of Prony's algorithms is quite close to that of Marquardt algorithms and with their

Chapter 4 Multiple Exponential Decay Analysis and Fluorescence-based Quasi-distributed Temperature Sensing System

simplicity and noniterative features, they are the better alternatives to the use of Marquardt counterparts, for real-time sensor application.

4.3.2 Prony's method

The approximation of an exponential process can be expressed in the following generalized form[10]:

$$f(x) = A_1 u_1^x + A_2 u_2^x + \dots + A_n u_n^x. \quad (4.3)$$

where A_i ($i = 1, 2, \dots, n$) are the amplitudes of each exponential component of u_i^x ($i = 1, 2, \dots, n$). To solve this kind of approximation using Prony's method, the values of $f(x)$ are specified as a set of N equally spaced points, f_j , where a linear change of variables has been introduced in advance in such a way that the data points are $x = 0, 1, 2, \dots, (N - 1)$. These points specify a set of linear equations:

$$f_{j+n\Delta N} + f_{j+(n-1)\Delta N}\alpha_1 + f_{j+(n-2)\Delta N}\alpha_2 + \dots + f_j\alpha_n = 0 \quad (4.4)$$

$$j = 0, 1, 2, \dots, (N - n\Delta N - 1)$$

where ΔN , the sample spacing index in each equation is an integer which satisfies $(N - n\Delta N) \geq n$ and α_i ($i = 1, 2, \dots, n$) are unknown coefficients. After the values of α_i ($i = 1, 2, \dots, n$) are determined, the $|\Delta N|$ th powers of u_i in Eq.(4.3), $u_i^{\Delta N}$ ($i = 1, 2, \dots, n$) may be found as the roots of the following algebraic equation:

$$y^n + \alpha_1 y^{n-1} + \alpha_2 y^{n-2} + \dots + \alpha_{n-1} y + \alpha_n = 0 \quad (4.5)$$

This is the basis of the method used.

4.3.3 Prony's estimation of fluorescence lifetimes

4.3.3.1 Two-parameter model

For the two parameter model, Eq.(4.1), $(N-\Delta N)$ linear equations can be directly formed from the N samples taken in the experiment, given as

$$f_{j+\Delta N} + f_j \alpha = 0, \quad j = 0, 1, 2, \dots, (N - \Delta N - 1) \quad (4.6)$$

The estimation of the lifetime will be given by

$$\tau = -(\Delta N)(\Delta t) / \ln(-1 / \alpha) \quad (4.7)$$

in which the approximation of α has been proposed by Zhang et al[6] by means of Prony's superposition and Prony's correlation methods, represented separately by

$$\alpha_{sup} = - \sum_{j=0}^{N-\Delta N-1} f_{j+\Delta N} \left(\sum_{j=0}^{N-\Delta N-1} f_j \right)^{-1} \quad (4.8)$$

$$\alpha_{cor} = - \sum_{j=0}^{N-\Delta N-1} f_{j+\Delta N} f_{j+k} \left(\sum_{j=0}^{N-\Delta N-1} f_j f_{j+k} \right)^{-1} \quad (4.9)$$

where k is the correlation distance index; and α_{sup} and α_{cor} are the superposition and correlation approximations of α respectively.

Monte Carlo simulations have been applied to these two varieties of Prony's method, under the assumption that the noise component $\varepsilon(t)$ is independent of the fluorescence decay and identically distributed with a Gaussian probability density having a standard deviation, σ_ε . The measure of the performance was given by a noise-to-error transfer factor m_ε as

Chapter 4 Multiple Exponential Decay Analysis and Fluorescence-based Quasi-distributed Temperature Sensing System

$$\sigma_{\tau} / \tau = m_{\epsilon} (\sigma_{\epsilon} / A) \tag{4.10}$$

where σ_{τ} / τ is the normalized error in estimating the lifetime.

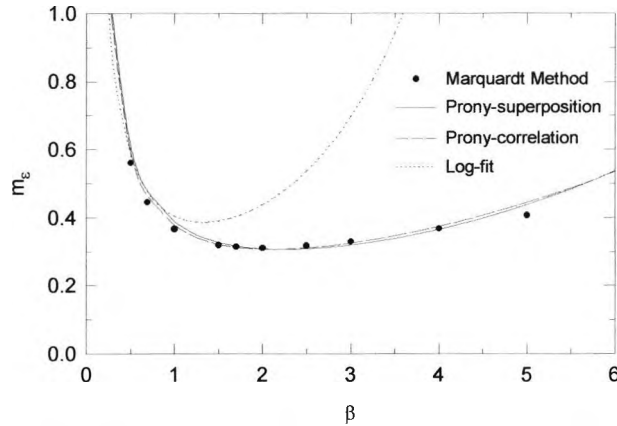


Fig.4.1 Cross comparison between various two-parameter, model based, lifetime-estimation algorithms[6][7]

A cross comparison between various two-parameter algorithms is presented in Fig.4.1 to illustrate their noise-suppression abilities[6]. The general performance of the two-parameter model was shown to be quite similar to that of the two-parameter Marquardt least-squares algorithm[7], with the superposition approach slightly better than that of its correlation counterpart. Both algorithms give their optimum performance in the vicinity of $\beta = 2-2.25$ and $\Delta N = N/4$, where $\beta = w / \tau$ was termed the normalized observation time. The noise-to-error transfer factor m_{ϵ} of the log-fit algorithm[9] was substantially higher than those of the other three methods and its optimum observation time β is about 1.3. In addition, m_{ϵ} is much more sensitive to the departure of β from the optimum value (to either side) and its tolerance to the operational observation time was quite narrow.

Chapter 4 Multiple Exponential Decay Analysis and Fluorescence-based Quasi-distributed Temperature Sensing System

The performance of any two-parameter, model-based estimation algorithm inherently deteriorates due to the presence of a base-line residue in the observed signal. Thus, where an excessive base-line residual was unavoidable, the three-parameter model, expressed by Eq.(4.2), and discussed below was used.

4.3.3.2 Three-parameter model

The three-parameter model in Eq.(4.2) may be transformed into the following form[6],

$$\Delta f(t) = A' \exp(-t / \tau) \quad (4.11)$$

where A' was constant related simply to the unknown parameter A . Thus, the two varieties of Prony's method discussed above were modified to solve the three-parameter approximation problem by substituting f_j ($j = 0, 1, 2, \dots, N-1$) by the differentials

$$\Delta f_j = f_j - f_{j+\Delta j}, \quad j = 0, 1, 2, \dots, (N'-1) \quad (4.12)$$

where $N' = N - \Delta j$ and Δj was the differential space index. Monte Carlo simulations of the two varieties of Prony's method were modified for the three parameter model and it was found that the optimum performance was located in the region of $\beta = 4.5-5$ and $\Delta j = N/2$. Cross comparison between the three-parameter Marquardt algorithm and its Prony counterpart was shown in Fig.4.2. Some similarities could be seen with the Prony correlation being slightly better than its superposition counterpart and the noise-to-error transfer factor in the three-parameter Prony model was a little higher than Marquardt algorithm, but a run-time comparison showed that the use of Prony's

Chapter 4 Multiple Exponential Decay Analysis and Fluorescence-based Quasi-distributed Temperature Sensing System

model produce a reduction in the running time, when compared to Marquardt algorithm, by 98%.

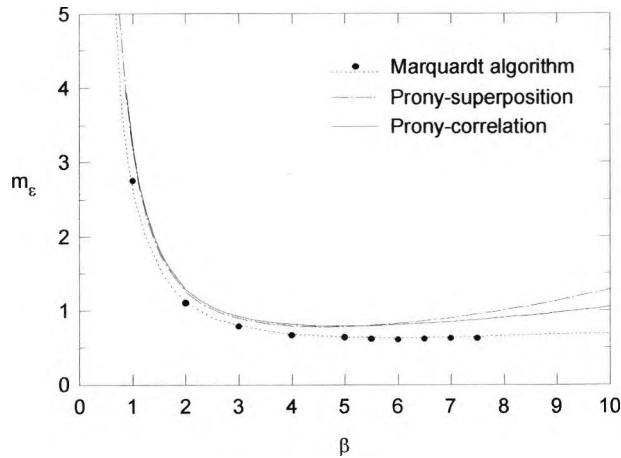


Fig.4.2 Cross comparison between the three-parameter Marquardt algorithm and its Prony's counterparts

The performance of Prony's method has been demonstrated in a real sensor situation by Zhang et al[6] which it showed no substantial differences in the performance compared with that using the Marquardt algorithm while the execution time of Prony's method was much shorter than that of the Marquardt algorithm. Prony's method did represent a better choice for microcomputer and DSP-based fluorescence thermometer systems aiming for real-time measurement and high accuracy. This work is designed to extend the use of Prony's method to a quasi-distributed temperature sensing system, via an analysis of double exponential decays.

4.4 Double exponential temperature sensing system

When double exponential decay signals, arising from two single point temperatures or produced by the output of a single sensor, are received by the same photodetector at the same time, an analysis of the double exponential model is necessary in order to obtain data on the two point temperatures simultaneously or recover the real temperature behavior[11]. In such a case, the fluorescence decay signal, $f(t)$ will contain two exponential components, and is given by:

$$f(t) = A_1 \exp(-t / \tau_1) + A_2 \exp(-t / \tau_2) + \varepsilon(t) + B \quad (0 \leq t \leq w) \quad (4.13)$$

where A_1 and A_2 are the initial separate fluorescence amplitudes; τ_1 and τ_2 the corresponding fluorescence lifetimes; and $\varepsilon(t)$, B and w are as defined in Eq.(4.2). The above double exponential model has not been discussed in detail, and the use of Prony's method, considered below, has opened up a new and rapid solution which offers sufficient precision for this purpose.

4.4.1 Prony's estimation of double exponential decay lifetimes

4.4.1.1 Four-parameter model

Under certain favorable circumstances, the observed fluorescence decay signal can be free of any baseline offset. Thus Prony's method, discussed above, can be directly applied to the approximation in the form of a four-parameter model, given by

$$f(t) = A_1 \exp(-t / \tau_1) + A_2 \exp(-t / \tau_2) + \varepsilon(t) \quad (4.14)$$

and according to Eq.(4.4), $(N - 2\Delta N)$ linear equations can be directly formed from the N samples, f_j ($j = 0, 1, \dots, N - 1$), given as

Chapter 4 Multiple Exponential Decay Analysis and Fluorescence-based Quasi-distributed Temperature Sensing System

$$f_{j+2\Delta N} + f_{j+\Delta N}\alpha_1 + f_j\alpha_2 = 0, \quad j = 0, 1, 2, \dots, (N - 2\Delta N - 1) \quad (4.15)$$

or represented by the following matrix form:

$$\mathbf{Y} = \mathbf{X}\mathbf{A} \quad (4.16)$$

$$\text{where } \mathbf{Y} = \begin{bmatrix} f_{2\Delta N} \\ f_{2\Delta N+1} \\ \vdots \\ f_{N-1} \end{bmatrix}, \quad \mathbf{X} = \begin{bmatrix} f_{\Delta N} & f_0 \\ f_{\Delta N+1} & f_1 \\ \vdots & \vdots \\ f_{N-\Delta N-1} & f_{N-2\Delta N-1} \end{bmatrix} \quad \text{and } \mathbf{A} = \begin{bmatrix} -\alpha_1 \\ -\alpha_2 \end{bmatrix}$$

By means of the least squares method, matrix \mathbf{A} in Eq.(4.16) can be calculated by the use of the following matrix algorithm:

$$\mathbf{A} = \left[\mathbf{X}^T \mathbf{X} \right]^{-1} \mathbf{X}^T \mathbf{Y} \quad (4.17)$$

$$\text{and } \left[\mathbf{X}^T \mathbf{X} \right] = \begin{bmatrix} \sum_{j=0}^{N-2\Delta N-1} f_{j+\Delta N}^2 & \sum_{j=0}^{N-2\Delta N-1} f_j f_{j+\Delta N} \\ \sum_{j=0}^{N-2\Delta N-1} f_j f_{j+\Delta N} & \sum_{j=0}^{N-2\Delta N-1} f_j^2 \end{bmatrix}$$

It is found in the simulations discussed later, that the least squares method does not offer the optimum solutions for matrix \mathbf{A} . Thus an auxiliary matrix \mathbf{Z} is introduced to solve the problem by use of the correlation method. Multiplied by \mathbf{Z}^T , Eq.(4.16) becomes

$$\mathbf{Z}^T \mathbf{Y} = \mathbf{Z}^T \mathbf{X} \mathbf{A}$$

$$\mathbf{A} = \left[\mathbf{Z}^T \mathbf{X} \right]^{-1} \mathbf{Z}^T \mathbf{Y} \quad (4.18)$$

$$\text{where } \mathbf{Z} = \begin{bmatrix} f_{\Delta N+k} & f_k \\ f_{\Delta N+k+1} & f_{k+1} \\ \vdots & \vdots \\ f_{N+k-\Delta N-1} & f_{N+k-2\Delta N-1} \end{bmatrix}, \quad 0 \leq k \leq \Delta N$$

Chapter 4 Multiple Exponential Decay Analysis and Fluorescence-based Quasi-distributed Temperature Sensing System

$$\text{and } |\mathbf{Z}^T \mathbf{X}| = \begin{bmatrix} \sum_{j=0}^{N-2\Delta N-1} f_{j+\Delta N} f_{j+\Delta N+k} & \sum_{j=0}^{N-2\Delta N-1} f_{j+\Delta N+k} f_j \\ \sum_{j=0}^{N-2\Delta N-1} f_{j+k} f_{j+\Delta N} & \sum_{j=0}^{N-2\Delta N-1} f_{j+k} f_j \end{bmatrix}, \quad |\mathbf{Z}^T \mathbf{Y}| = \begin{bmatrix} \sum_{j=0}^{N-2\Delta N-1} f_{j+2\Delta N} f_{j+\Delta N+k} \\ \sum_{j=0}^{N-2\Delta N-1} f_{j+2\Delta N} f_{j+k} \end{bmatrix}$$

with $k = 0$, the solution offered by Eq.(4.18) being in the least squares form, where after α_1, α_2 are determined by Eq.(4.18), $u_1^{\Delta N}$ and $u_2^{\Delta N}$ are the roots of the algebraic equation:

$$y^2 + \alpha_1 y + \alpha_2 = 0 \tag{4.19}$$

$$\text{where } \begin{cases} u_1^{\Delta N} = \frac{-\alpha_1 + \sqrt{\alpha_1^2 - 4\alpha_2}}{2} \\ u_2^{\Delta N} = \frac{-\alpha_1 - \sqrt{\alpha_1^2 - 4\alpha_2}}{2} \end{cases}$$

Then the two estimations of lifetime will be given by

$$\begin{cases} \tau_1 = -\Delta / \ln(u_1) \\ \tau_2 = -\Delta / \ln(u_2) \end{cases} \tag{4.20}$$

where Δ is the sampling time interval used.

4.4.1.2 Five-parameter model

In most cases, some element of baseline offset in the received fluorescence signal is actually present due to the background light or dark current in the photodetector. It has to be taken into account, giving the general model for a double fluorescence decay signal expressed in Eq. (4.13). In fact, such an approximation can be directly converted to the form of a four-parameter model, of the type of Eq. (4.14), by taking the differential of the exponential signal,

Chapter 4 Multiple Exponential Decay Analysis and Fluorescence-based Quasi-distributed Temperature Sensing System

$$\Delta f(t) = A'_1 \exp(-t / \tau_1) + A'_2 \exp(-t / \tau_2) + \varepsilon'(t) \quad (4.21)$$

where A'_1 , A'_2 and $\varepsilon'(t)$ are defined in a similar way to that Eq.(4.13). Thus Prony's method, as discussed above for the four-parameter model, can be applied to the approximation problem for the five-parameter model, by substituting f_j ($j = 0, 1, \dots, N-1$) by the differentials,

$$\Delta f_j = f_j - f_{j+\Delta j}, j = 0, 1, \dots, (N'-1) \quad (4.22)$$

where $N' = N - \Delta j$; Δj is the differential space index.

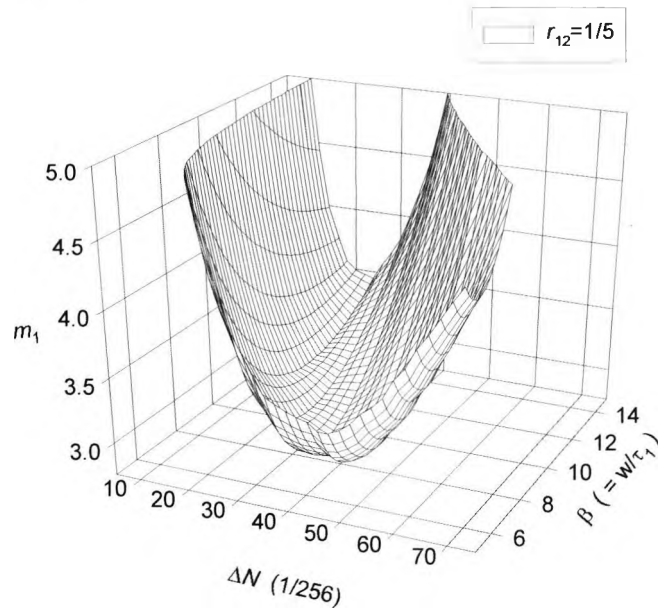


Fig.4.3 Noise-to-error transfer factor, m_1 , as a function of ΔN and β

4.4.2 Simulation results

Monte-Carlo simulations are applied to the approximation using the four-parameter model, Eq.(4.14), the results of which can be extended to the other model, illustrated by Eq.(4.13), as mentioned above. In these simulations, the number of samples taken from each generated double exponential decay signal is fixed at 256, and the noise

Chapter 4 Multiple Exponential Decay Analysis and Fluorescence-based Quasi-distributed Temperature Sensing System

component $\varepsilon(t)$ is added under the assumption that it is independent of the double fluorescence decay process and identically distributed with a Gaussian probability density, having a standard deviation, σ_ε . The presence of such a noise component will result in errors in the estimation of the experimental lifetimes. Two parameters, m_1 and m_2 , termed the noise-to-error transfer factors are defined as measures of the impact of the noise on the lifetime estimation, which are given by

$$\begin{aligned}\sigma_{\tau_1} / \tau_1 &= m_1(\sigma_\varepsilon / A_1) \\ \sigma_{\tau_2} / \tau_2 &= m_2(\sigma_\varepsilon / A_2)\end{aligned}\tag{4.23}$$

where σ_{τ_1} / τ_1 and σ_{τ_2} / τ_2 are the normalized errors in estimating the lifetimes; and σ_ε / A_1 and σ_ε / A_2 are the normalized noise deviations that are set to reasonable levels (at 0.1%) during the simulations. It is found that under simulation conditions that m_1 and m_2 are essentially constants with regard to the noise level σ_ε and independent of the amplitude ratio, A_1 / A_2 .

The performance of Prony's algorithm can be greatly optimized by careful selection of the observation window width, w and the numerical sample space index ΔN , as well as the correlation space k . An example is shown in Fig.4.3, with simulation results obtained when $\tau_1 / \tau_2 = 1/5$, where $\beta = w / \tau_1$ is the normalized observation window width.

The effectiveness of the algorithm is also found by observing how well differentiated are the two exponential time constants, as is illustrated in Fig.4.4 by the data on noise-

Chapter 4 Multiple Exponential Decay Analysis and Fluorescence-based Quasi-distributed Temperature Sensing System

to-error transfer factors, m_1 and m_2 , with respect to different ratios of the two time constants. The data shown in Fig.4.4 were obtained from simulations with β , ΔN and k optimized for the estimation of τ_1 . On the one hand, as is shown in Fig.4.4, the values of m_1 and m_2 , and hence the estimation errors, rise dramatically when the two time constants are approaching each other, then soar towards infinity with their ratio reaching one. On the other hand, with the two time constants diverging in magnitude from each other, e.g., $r_{12}(=\tau_1/\tau_2) \leq 0.04$ when $\tau_1 < \tau_2$, the reduction in m_1 is insignificant, while m_2 starts to rise. Similar curve tendencies are seen when $\tau_1 > \tau_2$,

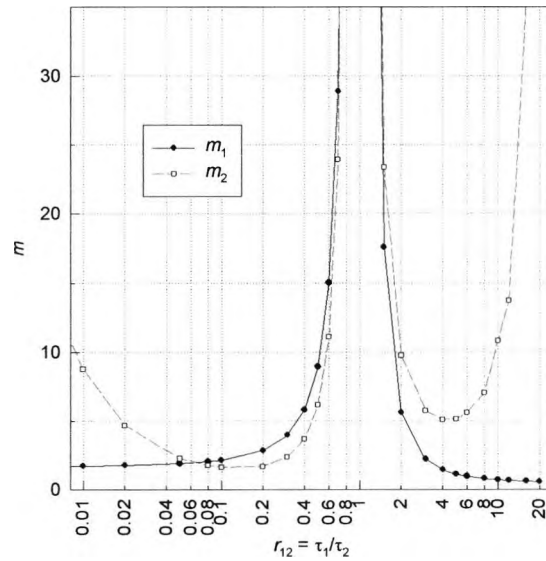


Fig.4.4 Noise-to-error transfer factor, m_1 , as a function of the ratio of the two time

constants, $r_{12}(=\tau_1/\tau_2)$

but m_2 is much greater than m_1 . The latter reveals that when β , ΔN and k are optimized in favor of the estimation of the longer time constant, a much higher error will result in the estimation of its shorter counterpart. Therefore, to make the

Chapter 4 Multiple Exponential Decay Analysis and Fluorescence-based Quasi-distributed Temperature Sensing System

estimation accuracy as consistent as possible for both the exponential time constants, two compromises have to be made. First, the observation and numerical calculation gives the conclusion that β , ΔN and k should be optimized in favor of the estimation of the shorter time constant. Second, an acceptable region for the difference between the two time constants should be considered, e.g., taking $\tau_1 / \tau_2 \approx 0.02 \sim 0.5$, for example.

The optimized observation window width, β_{opt} is closely related to the time-constant ratio r_{12} , as is shown in Fig.4.5 by the simulation results. When $r_{12} < 1$, it can be approximated by the following expression:

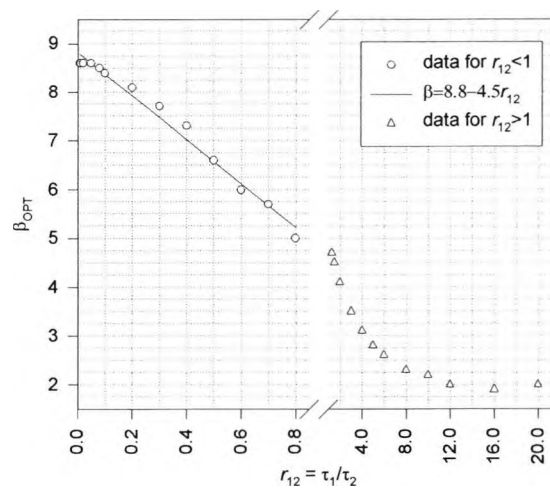


Fig.4.5 Relationship between the optimized observation window, β_{opt} and the time-

constant ratio, $r_{12} (= \tau_1 / \tau_2)$

$$\beta_{opt} \approx 8.8 - 4.5r_{12} \tag{4.24}$$

as is illustrated in Fig.4.5. However, the optimized numerical sample spacing index, ΔN defined in the algorithm is more or less a constant over a wide range of the time-

Chapter 4 Multiple Exponential Decay Analysis and Fluorescence-based Quasi-distributed Temperature Sensing System

constant ratio as shown in Fig.4.6, e.g., the optimized ΔN is 36/256 for $r_{12} < 0.6$. It is also found that the optimum value for k is $\Delta N/2$.

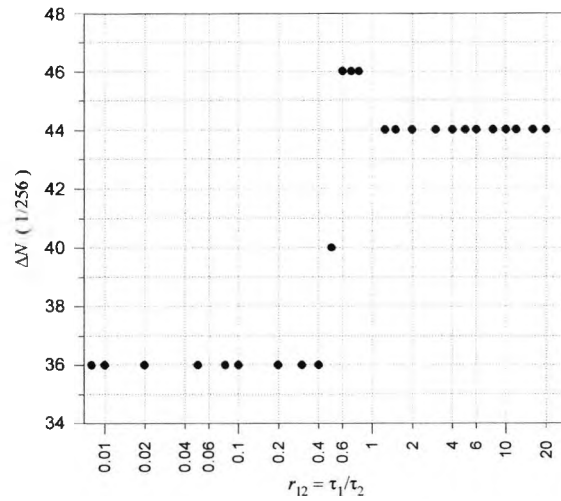


Fig.4.6 The optimum values of ΔN as a function of $r_{12} (= \tau_1 / \tau_2)$

4.4.3 Comparison with the Marquardt method

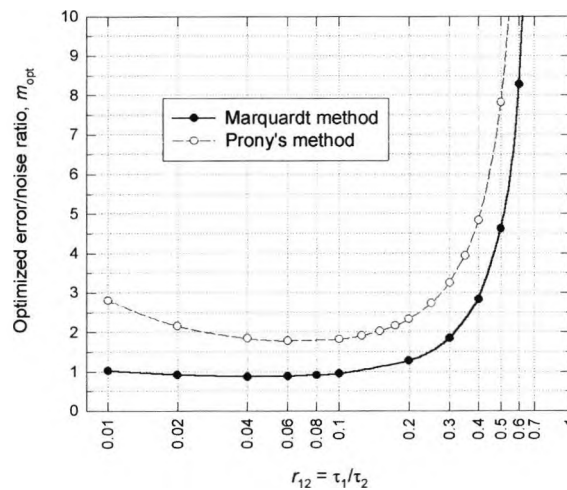


Fig.4.7 Comparison of accuracies of Marquardt and Prony's methods

A comparison of the estimation accuracies of the Marquardt and Prony's algorithms is presented in Fig.4.7[12]. Obviously the former performs better, and thus the resource issue involved must be considered for optimum use of their techniques. Running time

Chapter 4 Multiple Exponential Decay Analysis and Fluorescence-based Quasi-distributed Temperature Sensing System

tests of the two algorithms were carried on a personal computer based on an Intel-486 CPU. The running time of Prony's algorithm is $\sim 1.0\%$ of that of Marquardt algorithm, an important advantage favoring its use, all other aspects being equal.

4.4.4 Application of the technique in multi-exponential decay time sensor system

4.4.4.1 Sensor systems

In this work, the application of Prony's algorithm discussed above is demonstrated for application in a quasi-distributed or multi-material sensor system. The specification for such a sensor system (discussed in Chapter 3) is that the measurement error should be within $\pm 5^\circ\text{C}$ over the region from -100°C to 100°C . A schematic of such a system is shown in Fig.4.8, where the sensing head of the probe comprises a combination of two different sensing materials, sensor 1 and sensor 2 in a sandwich structure. Two different sensor combinations are evaluated in experiments, these being system A: alexandrite-ruby; and system B: alexandrite-YAG:Cr³⁺. Our previous work has shown, for example that alexandrite has good performance at high temperatures (750°C) where the fluorescence intensity from a ruby sample falls off, and with it the resolution obtainable from a ruby-only sensor [13]. Equally other materials such as Cr: LiSAF have very high sensitivities over a narrow region (0°C – 100°C)[14] but very poor performance at temperatures less than 0°C . In combination with ruby, for example, the freezing range as well as the region above 0°C could be covered, taking advantage of the narrow, specific sensitivity of the Cr: LiSAF. A blue LED operating at a center wavelength of 442 nm is used as an excitation light source and is modulated

Chapter 4 Multiple Exponential Decay Analysis and Fluorescence-based Quasi-distributed Temperature Sensing System

by a pulse signal, v_m , generated by the digital output port of a desktop computer. The response signal, which contains the fluorescence information from both sensors, is conveyed to the photodetecting stage by a 300 μ m core diameter, 1 \times 2 fibre coupler. A fluorescence filter, F_1 , is used to prevent the reflected excitation light from saturating the photodetector, showing the simplicity of the practical optical arrangement. The detected response signal is digitized by an analog-to-digital (A/D) converter inside the computer and processed using the proposed Prony's algorithm.

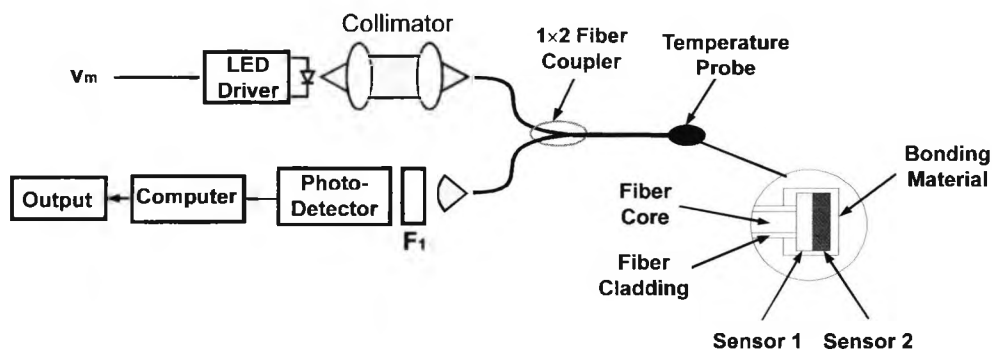


Fig.4.8 Schematic of the dual sensor arrangement, where two different sensor combinations for the probe are tested, system A: alexandrite-ruby; system B:

alexandrite-YAG:Cr³⁺

At room temperature, the ratio of the lifetimes in both sensor combinations is about 1:10. As is illustrated in Fig.4.8, at such a ratio the two temperature-dependent exponential components can readily be deconvolved by using Prony's method. Such an arrangement can deal with both the conditions of a single material with a double exponential decay behavior or a quasi-distributed system where the minimum number of two temperature probes are joined in series along a single optical cable. This is

Chapter 4 Multiple Exponential Decay Analysis and Fluorescence-based Quasi-distributed Temperature Sensing System

clearly a simple simulation with two decay-time profiles being involved, but it is essential if the validity of the method is to be proved and the system evaluated for being capable of dealing with a greater number of elements and decay time profiles, and giving a successful outcome.

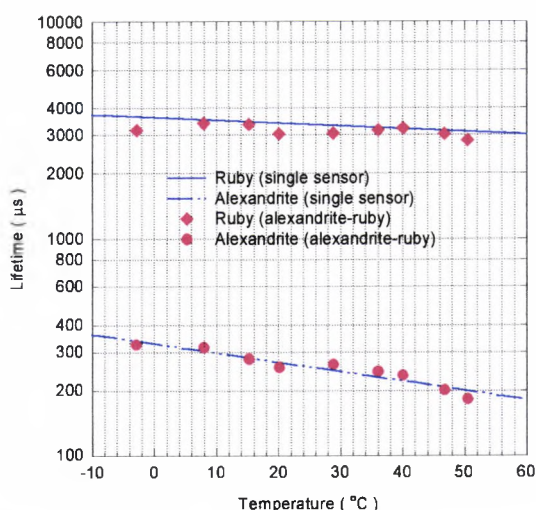


Fig.4.9 Experimental comparison of lifetimes of ruby and alexandrite with the use of the double and single Prony's method (-10–60°C)

4.4.4.2 Experimental results from these systems

The experimental results from sensor combination A (alexandrite - ruby) over the region 0°C-50°C, processed by the double exponential Prony's method, are shown in Fig.4.9, in which the results obtained with the use of the single Prony's method for separate ruby and alexandrite samples are also shown to enable a cross-comparison to be made. It is very satisfactory to see that the lifetimes of alexandrite and ruby as a function of temperature obtained by the use of the double Prony's method are similar to those obtained using the single Prony's method from the separate corresponding

Chapter 4 Multiple Exponential Decay Analysis and Fluorescence-based Quasi-distributed Temperature Sensing System

sensors, but there are slight fluctuations compared with their single sensor counterparts. This results from the fact that in combination A, ruby (~1.5mm thick), the signal of which is weaker than alexandrite (~0.5mm thick), is arranged to be behind (i.e. further away from the source) the alexandrite sample and the ratio of the signal from the ruby, compared to that from alexandrite, is quite small in the combined system. By comparison, the combination, B, in Fig.4.8 involves a sandwich of

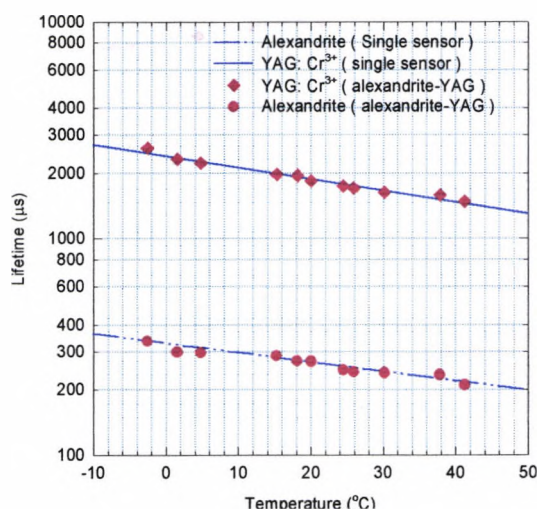


Fig.4.10 Experimental comparison of lifetimes of YAG:Cr³⁺ and alexandrite with the use of the double and single Prony's methods (-10–50°C)

YAG:Cr³⁺ and alexandrite with the thicknesses of each being ~0.5mm, and it is shown that this can give much better system results, which are shown in Fig.4.10. The data revealing the lifetime of alexandrite and YAG:Cr³⁺ as a function of temperature in Fig.4.10 are in close agreement with those obtained from single sensor experiments. The results clearly show that extracting two separate decay time constants with the use of the double Prony's method is not only efficient but also accurate enough to make it possible to multiplex these two sensors effectively. This is a major step forward, and

Chapter 4 Multiple Exponential Decay Analysis and Fluorescence-based Quasi-distributed Temperature Sensing System

opens up the possibilities for several more sensors being multiplexed on a single fibre optic cable.

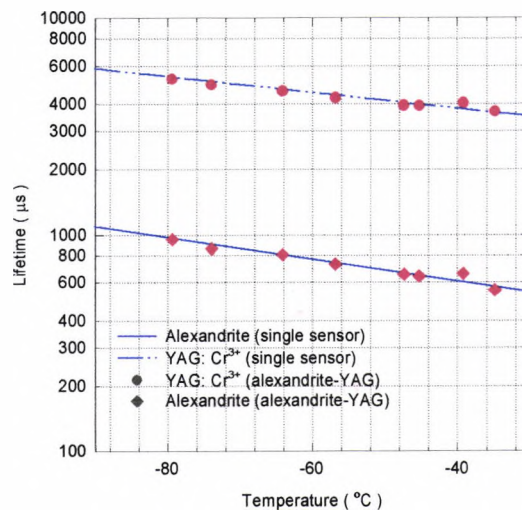


Fig.4.11 Experimental comparison of lifetimes of YAG:Cr³⁺ and alexandrite with double and single Prony's analysis in the subroom temperature region

Fig.4.11 shows a lifetime analysis of YAG:Cr³⁺ and alexandrite over the low temperature region from -90°C to -30°C. The extracted lifetimes of YAG:Cr³⁺ and alexandrite with the double Prony's method fit the comparison graphs of the single sensor performance well and give confidence to the proposal that the distributed sensor scheme can be used effectively with these materials over the sub-room temperature regime, as well as in the higher temperature regions.

The results presented have shown that double exponential characteristics can be extracted from sandwiches of two materials, excited by the same optical source, modulated in the same way, along a fibre optic cable. The extracted decay time

Chapter 4 Multiple Exponential Decay Analysis and Fluorescence-based Quasi-distributed Temperature Sensing System

behavior using Prony's method shows a close comparison with that seen for the materials individually, and the signal processing to achieve this is simple and easy to perform with a PC. Results have been obtained over experiments below room temperature (to -90°C) and above in limited tests to show the veracity of the mathematical approach, meeting the requirement of the system with a precision of $\pm 5^{\circ}\text{C}$ within the region of -100°C - 100°C . Although the results given in themselves do not, as yet, represent a major development in temperature probes *per se*, they do show the real possibilities of a single source, detector and fibre, simple modulation, decay-time based quasi-distributed sensor using several such elements formed together. Taking this a step further led to an investigation of a triple element sensing system, discussed below.

4.5 Triple exponential temperature sensing system

4.5.1 Theoretical background

When several exponential decay signals, derived from, for example, three individual temperature measurement points or yielded by three separate sensors, are received by the same photodetector at the same time, an analysis of the convoluted exponential signals is necessary in order to extract, both individually and simultaneously, the temperatures at these several points. In an analysis of this system, following the termination of the excitation light pulse, the combined signal $f(t)$, emitted by in this example, the three sensors, is given as a function of time t by:

$$f(t) = A_1 \exp(-t / \tau_1) + A_2 \exp(-t / \tau_2) + A_3 \exp(-t / \tau_3) + \varepsilon(t) + B \quad (0 \leq t \leq w) \quad (4.25)$$

Chapter 4 Multiple Exponential Decay Analysis and Fluorescence-based Quasi-distributed Temperature Sensing System

where A_1 , A_2 and A_3 are the initial separate fluorescence amplitudes; τ_1 , τ_2 and τ_3 are the corresponding fluorescence lifetimes; $\varepsilon(t)$ the noise component and B the baseline offset. The above model has not been discussed in detail before and the use of Prony's method considered below, has opened up a new solution for the model.

The baseline in the approximation model shown in Eq.(4.25) for a triple exponential decay can be detected by the use of appropriate data processing. Thus, according to Eq.(4.4), $(N-3\Delta N)$ linear equations can be formed directly from the N samples, taken as $f_j (j = 0, 1, \dots, N-1)$, given as

$$f_{j+3\Delta N} + f_{j+2\Delta N}\alpha_1 + f_{j+\Delta N}\alpha_2 + f_j\alpha_3 = 0 \quad (4.26)$$

$$j = 0, 1, 2, \dots, (N - 3\Delta N - 1)$$

which can also be expressed clearly by the following matrix form:

$$\mathbf{Y} = \mathbf{X}\mathbf{A} \quad (4.27)$$

$$\text{where } \mathbf{Y} = \begin{bmatrix} f_{3\Delta N} \\ f_{3\Delta N+1} \\ \vdots \\ f_{N-1} \end{bmatrix} \quad \mathbf{X} = \begin{bmatrix} f_{2\Delta N} & f_{\Delta N} & f_0 \\ f_{2\Delta N+1} & f_{\Delta N+1} & f_1 \\ \vdots & \vdots & \vdots \\ f_{N-\Delta N-1} & f_{N-2\Delta N-1} & f_{N-3\Delta N-1} \end{bmatrix} \quad \mathbf{A} = \begin{bmatrix} -\alpha_1 \\ -\alpha_2 \\ -\alpha_3 \end{bmatrix}$$

By means of the least squares method, matrix \mathbf{A} in Eq.(4.27) can be calculated by the use of the following matrix algorithm:

$$\mathbf{A} = [\mathbf{X}^T \mathbf{X}]^{-1} \mathbf{X}^T \mathbf{Y} \quad (4.28)$$

It is found, in simulation experiments discussed later, that the least squares method does not offer the optimum solution for matrix \mathbf{A} . Thus, an auxiliary matrix \mathbf{Z} has

Chapter 4 Multiple Exponential Decay Analysis and Fluorescence-based Quasi-distributed Temperature Sensing System

been introduced to solve the problem by the use of the correlation method. Multiplied by \mathbf{Z}^T , Eq.(4.27) then becomes

$$\mathbf{A} = [\mathbf{Z}^T \mathbf{X}]^{-1} [\mathbf{Z}^T \mathbf{Y}] \quad (4.29)$$

where

$$\mathbf{Z} = \begin{bmatrix} f_{2\Delta N+k} & f_{\Delta N+k} & f_k \\ f_{2\Delta N+k+1} & f_{\Delta N+k+1} & f_{k+1} \\ \vdots & \vdots & \vdots \\ f_{N-\Delta N-1+k} & f_{N-2\Delta N-1+k} & f_{N-3\Delta N-1+k} \end{bmatrix}$$

After α_1, α_2 and α_3 are determined by Eq.(4.29), $u_1^{\Delta N}, u_2^{\Delta N}$ and $u_3^{\Delta N}$ can be seen as the roots of the algebraic equation:

$$y^3 + \alpha_1 y^2 + \alpha_2 y + \alpha_3 = 0 \quad (4.30)$$

4.5.2 Simulation results

Monte Carlo simulations may be applied to the approximation obtained using the model, shown in Eq.(4.25). In these simulations, the noise component $\varepsilon(t)$, is added under the assumption that it is independent of the convoluted exponential decay process and identically distributed with a Gaussian probability density having a standard deviation, σ_ε . The presence of such a noise component will result in errors in the estimation of the experimental lifetimes, if not properly considered in the analysis. Three parameters, termed the noise-to-error transfer factors, m_1, m_2 and m_3 , may be defined to be the measures of the noise effect on the lifetime estimation, and these are given by

$$\sigma_{\tau_1} / \tau_1 = m_1(\sigma_\varepsilon / A_1); \quad \sigma_{\tau_2} / \tau_2 = m_2(\sigma_\varepsilon / A_2); \quad \sigma_{\tau_3} / \tau_3 = m_3(\sigma_\varepsilon / A_3) \quad (4.31)$$

Chapter 4 Multiple Exponential Decay Analysis and Fluorescence-based Quasi-distributed Temperature Sensing System

where σ_{τ_1}/τ_1 , σ_{τ_2}/τ_2 and σ_{τ_3}/τ_3 are the normalized errors in estimating the lifetimes; σ_ϵ/A_1 , σ_ϵ/A_2 and σ_ϵ/A_3 are the normalized noise deviations which are set to the same reasonable levels as before (of 0.1%) during the simulations. The

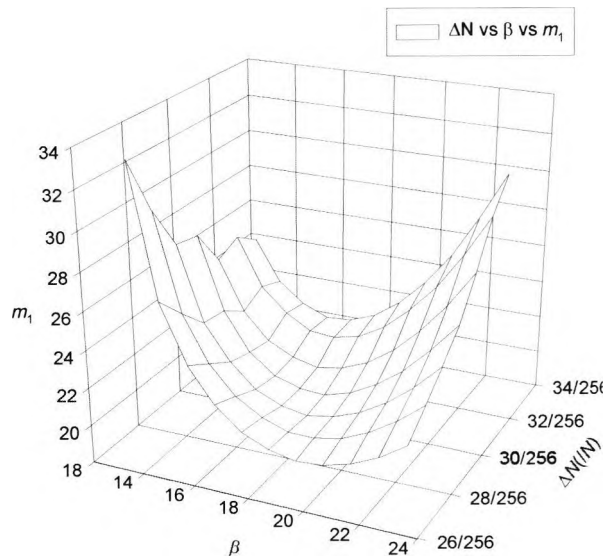


Fig.4.12 Noise-to-error transfer factor, m_1 , as a function of ΔN and β

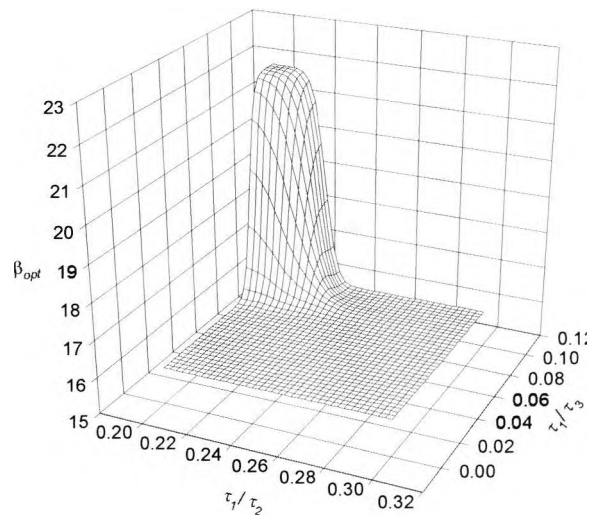


Fig.4.13 The optimized observation window, β_{opt} , and the time-constant ratios performance of the Prony's algorithm can be greatly optimized by the careful selection of the observation window w , and the numerical sample space index, ΔN , as well as the

Chapter 4 Multiple Exponential Decay Analysis and Fluorescence-based Quasi-distributed Temperature Sensing System

correlation space, k . An example of this is shown in Fig.4.12, with simulation results obtained when $r_{12}(\tau_1/\tau_2)=1/5$, $r_{13}(\tau_1/\tau_3)=1/10$, where $\beta = w/\tau_1$ is the normalized observation window width. However, as indicated by Fig.4.13 and Fig.4.14, over the wide range of the time constant ratio of $r_{12}(\tau_1/\tau_2)$ and $r_{13}(\tau_1/\tau_3)$, the optimized normalized observation window width (β_{opt}), which is associated with the estimation of the shortest lifetime, τ_1 , is more or less a constant e.g. $\beta_{opt} = w/\tau_1 = 16$ in a similar way to the optimized numerical sample spacing index, $\Delta N/(N)$, defined in the algorithm, i.e. $30/(256)$. It was also found that the optimum value for k is approximately $\Delta N/30$.

4.5.3 Experimental arrangement for quasi-distributed fibre optic sensor scheme

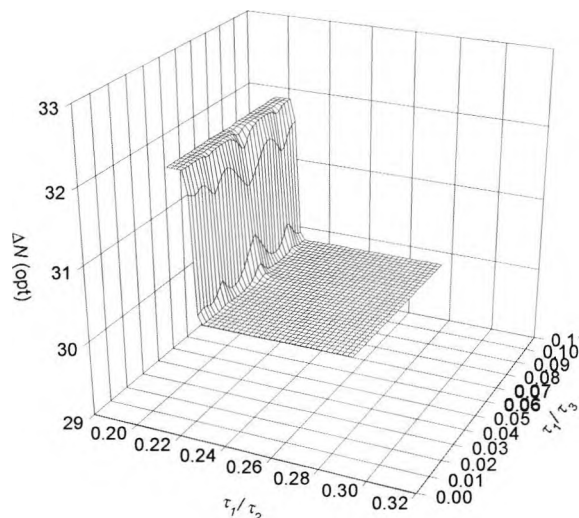


Fig.4.14 The optimal values of ΔN as a function of time-constant ratio

In this work, the application of Prony's algorithm discussed above is demonstrated in its application to a quasi-distributed (or alternatively a multi-material) sensor system. In this case, the bulk material sensor discussed before is replaced with a more practical

Chapter 4 Multiple Exponential Decay Analysis and Fluorescence-based Quasi-distributed Temperature Sensing System

and convenient fibre optic version and using this arrangement, three sensor elements are considered representing a simple, basic multi-element fibre optic sensor scheme. A schematic of such a system is shown in Fig.4.15, where three different rare-earth doped fibres here are used as the sensors, each having its own individual temperature dependence characteristics. This built upon the success of previous work on single doped fibre point sensors using the fluorescence decay in rare-earth fibre doped with Nd^{3+} , Er^{3+} and Tm^{3+} as the essential sensing element[15][16][17], discussed in Chapter 3.

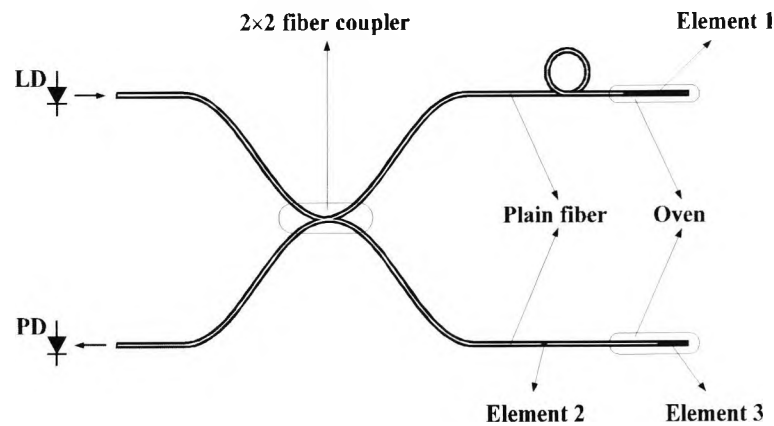


Fig.4.15 Schematic of the experimental arrangement used in this work. LD–laser diode; PD–photodiode

4.5.3.1 System characteristics

An infrared (IR) laser diode operating at a centre wavelength of 813nm was used as the excitation light source and its output was modulated by a pulse signal generated by the digital output port of a desktop computer. A 50 μm core diameter, 2x2 fibre coupler was employed to transfer the excitation light to the two ends of the coupler which are connected to the rare-earth doped fibres and to convey the combined

Chapter 4 Multiple Exponential Decay Analysis and Fluorescence-based Quasi-distributed Temperature Sensing System

fluorescence signal to the IR sensitive InGaAs photodiode. One of the ends of the fibre was connected to such a single mode fibre (element 1, thulium doped fibre), the length of which is 9cm, of core diameter of 15 μm , and overall diameter of 125 μm , having a rare earth dopant concentration level of 280ppm. The other end was joined to two different rare-earth doped fibres, connected in series, one a 0.5mm long multimode Nd³⁺ doped fibre (element 2), the core diameter of which is 100 μm , the overall diameter 140 μm , and of concentration 7.5%; the other was a 3cm long single mode Er³⁺ doped fibre (element 3), the core diameter of which is 4 μm , of the overall diameter 125 μm and having a doping level of 4370ppm, each of these representing successful sensor elements when used individually[15][16][17]. The materials chosen were also convenient in that the individual decay times of the fluorescence signal from each differed significantly over a range from several milliseconds to several microseconds. This facilitated the analysis process and enabled greater accuracy to be obtained from the method for each decay separately. Their lengths were chosen on the basis of achieving an approximately similar level of fluorescence signal from each, bearing in mind the concentration of dopant in the fibre, which varied considerably from sample to sample.

The absorption and fluorescence spectra[18] of these rare earth ions in silica-based fibre show a common absorption peak at approximately 810nm, with a fluorescence peak in the vicinity of 1.5 μm , which suggests the possibility of using a simple arrangement of a single light source and a single photodetector. The response signal

Chapter 4 Multiple Exponential Decay Analysis and Fluorescence-based Quasi-distributed Temperature Sensing System

detected at the photodetector may be digitized by using an analog-to-digital (A/D) converter attached to the computer and processed using the Prony's algorithm that has been discussed earlier.

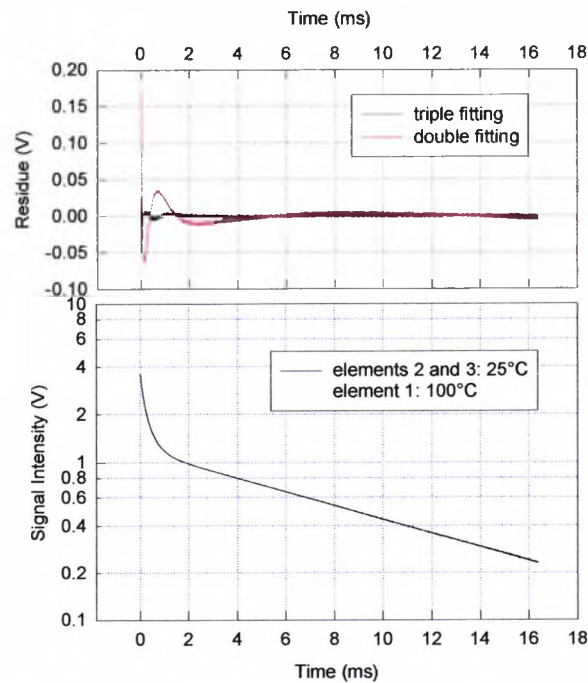


Fig.4.16 The superposed fluorescence decay signal when the temperature of elements 2 and 3 is 25°C and that of element 1 is 100°C (with the residue results coming from the double and triple exponential fitting separately)

4.5.3.2 System calibration

At each stabilized temperature, during the calibration process, it was found that the fluorescence decayed exponentially with time after the termination of excitation light pulse, in a manner similar to that of the experimental signal recorded, shown in Fig.4.16, when the temperature of elements 2 and 3 was 25°C and that of element 1 was 100°C. This clearly shows that the signal is the superposition of several

Chapter 4 Multiple Exponential Decay Analysis and Fluorescence-based Quasi-distributed Temperature Sensing System

exponential signals, and in an analysis, it was found that it could be fitted very well to the model described by Eq.(4.25). Here both the triple Prony method as well as the Marquardt approximation algorithm are used to deconvolve the combined signals obtained over the various calibration points which are similar to those shown in Fig.4.16. This clearly shows a response which is not single exponential, and the analysis that was carried out indicates that it is, in fact, not bi-exponential but tri-exponential.

4.5.3.3 System test and evaluation

A system test was carried out to evaluate the performance of the sensor. The first experimental arrangement used was developed to keep the temperature of elements 2 and 3 stabilized at 25°C in a water bath while changing the temperature of element 1 from 100°C to 900°C, and the experimental results analyzed, which were obtained by both Prony's and Marquardt's methods, are shown in Fig.4.17. Because the lifetimes of elements 3 and 1 differ greatly, in order accurately to obtain the lifetime values, different optimum observation window widths, w , have been selected for use with Prony's method. In this work, the sample rate of the signal is 1MHz, the observation window for the estimation of the performance of element 1 was in the vicinity of 1792 μ s, while for elements 2 and 3 it was 4096 μ s. Over the wide range of temperatures, both analysis results show that the lifetime of element 1 changes, as expected, with temperature while those elements 2 and 3 remain the same because of their stabilized thermal environment at 25°C. The comparison of the use of these two methods shows that the values of lifetimes deconvolved for the three elements are

Chapter 4 Multiple Exponential Decay Analysis and Fluorescence-based Quasi-distributed Temperature Sensing System

similar for each approach. The relative error of the estimation using Marquardt's method is within 1.0% for all the three lifetime constants, which shows that it is reasonable in this work to use this method as a standard comparison with the favored Prony approach. The tendency of the variation of lifetimes of element 1, derived from both methods, is seen to be similar as a function of temperature, which means that the sensitivity of both methods is essentially the same, implying that the accuracy of

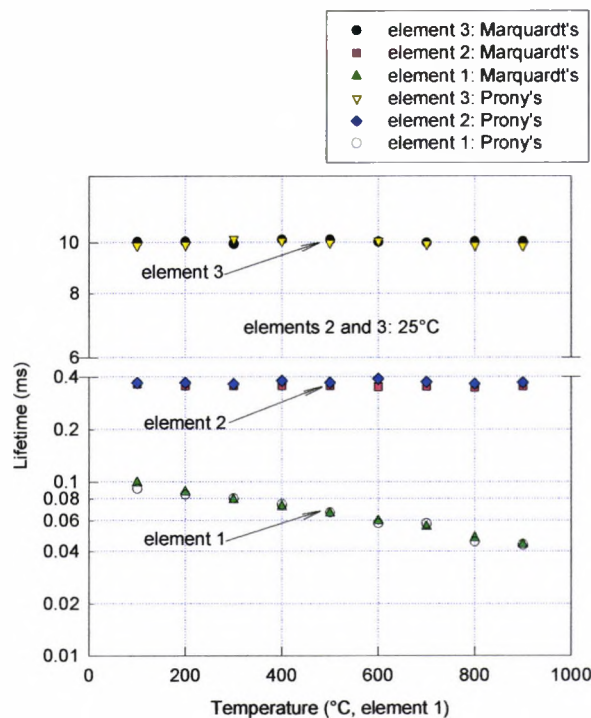


Fig.4.17 Deconvolved constants for the three elements using Marquardt's as well as Prony's approach when the temperature for elements 2 and 3 is 25°C and that of element 1 varies from 100 to 900°C

Prony's method is high enough for practical use and estimated at $\pm 6^\circ\text{C}$. Of greater importance is the fact that the computational time for Prony's method is actually approximately one thousandth that of Marquardt's, which makes real-time

Chapter 4 Multiple Exponential Decay Analysis and Fluorescence-based Quasi-distributed Temperature Sensing System

measurement and determination of the temperature data possible using a PC-based system.

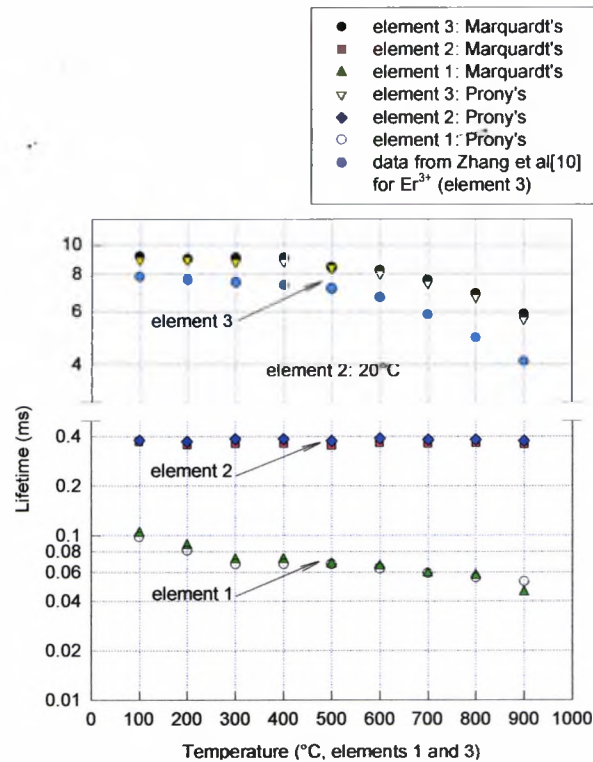


Fig.4.18 Deconvolved lifetime constants for the three elements using Marquardt's as well as Prony's approach when the temperature for element 2 is 20°C and that of elements 1 and 3 varies from 100 to 900°C

The second experimental arrangement used to investigate the system performance was to put elements 3 and 1 in the stabilized oven and raise the temperature from 100°C to 900°C while element 2 was maintained at room temperature. The lifetime variations with temperature for elements 3 and 1 are shown clearly in Fig.4.18 and, because of the stability of the room temperature environment in which it was kept, the lifetime of

Chapter 4 Multiple Exponential Decay Analysis and Fluorescence-based Quasi-distributed Temperature Sensing System

element 2 shows no change. The decay curves for 800°C and 900°C are shown in Fig.4.19, from which the three corresponding lifetimes may be deconvolved. The same observation window, as explained above, is used in Prony's method and the estimated results obtained by using both methods for elements 3 and 1 are similar. Again the lifetime variation tendency shown by elements 3 and 1 and obtained by both methods is the same.

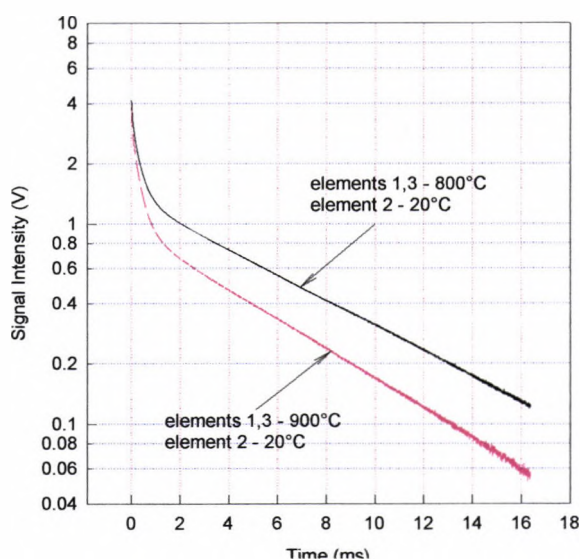


Fig.4.19 The superposed fluorescence decay signals when the temperature of elements 2 is 20°C and that of elements 1 and 3 is 800 and 900°C, respectively, for the upper and lower graphs

By using Prony's method, each individual exponential signal from the different rare earth doped fibres can be deconvolved from the superposed signal and the variation of the time constant associated with each as a function of temperature obtained is similar to that directly derived from the single sensor. This is shown in Fig.4.18, in which the

Chapter 4 Multiple Exponential Decay Analysis and Fluorescence-based Quasi-distributed Temperature Sensing System

experimental results from the work of Zhang et al[16] are derived by using a single sensor of Er^{3+} (element 3) doped fibre, the concentration of which is 4370ppm, and pumped by the laser diode operating at $\sim 980\text{nm}$ with the emission detected at 1550nm , where a close comparison is seen. The results are not identical due to the differences in the pump source and the length of the doped fibre used, but the fact that the trend is the same is very satisfactory evidence of the veracity of the approach.

4.6 Summary

Prony's method has been applied in the above work to estimate the lifetimes of the convoluted double and triple exponential combined signal for the sensor network, each component of which contains its corresponding temperature information, arising from a novel intrinsic quasi-distributed thermometer. Theoretical analysis and supporting experimental results both show that the method is accurate enough through the careful selection of the observation window width and the other algorithm based parameters, for many practical purposes. This is of the order of $\pm 6^\circ\text{C}$ in this work. The use of Prony's method, associated with the quasi-distributed temperature sensing arrangement, shows its potential for practical use in a real-time temperature measurement and control system of the simple and inexpensive sensor approach discussed. The most promising advantage of Prony's method is that it was shown to save computational time by a factor of 10^2 - 10^3 when compared to the Marquardt's nonlinear least squares method, yet there remains adequate sensitivity in the temperature measurement over a range almost as wide as that when using the

Chapter 4 Multiple Exponential Decay Analysis and Fluorescence-based Quasi-distributed Temperature Sensing System

Marquardt approach. The variation of the lifetimes as a function of temperature, deconvolved by Prony's method, is essentially similar to that obtained directly by use of the single temperature sensor.

Multi-point or quasi-distributed temperature sensing and monitoring are very important in laboratory, biomedical as well as other industrial applications. This work has shown the potential of a simple sensor network, for such applications, for example, to temperature sensing in transformers, where several separated measurements are needed, but the cost of a fully distributed system is hardly justified.

4.7 References

- [1]. K.T.V.Grattan, Z.Y.Zhang, *Fibre Optic Fluorescent Thermometry* (Chapman & Hall, London, 1995)
- [2] E.Theocharous, *Proceedings of the 1st Optical Fiber Sensors Conference* (OFS 83) (IEE, London, 1983)
- [3] K.T.V.Grattan and B.T.Meggitt, *Optical Fiber Sensor Technology*, Vol.1 (Chapman & Hall, London, 1995)
- [4] M.C.Farries et al, Distributed temperature sensor using holmium(+3)-doped fiber, in *Proc. OFC'87*, Reno, NV, 170(1987)
- [5] A.D.Kersey, A review of recent developments in fiber optic sensor technology, *Optical Fiber Technology*, 2, 291(1996)

Chapter 4 Multiple Exponential Decay Analysis and Fluorescence-based Quasi-distributed Temperature Sensing System

- [6] Z.Y.Zhang, K.T.V.Grattan and A.W.Palmer, Prony's method for exponential lifetime estimations in fluorescence-based thermometers, *Rev. Sci. Instrum.*, 67, 2590(1996)
- [7]. L.J.Dowell and G.T.Gillies, Errors caused by baseline offset and noise in the estimation of exponential lifetimes, *Rev. Sci. Instrum.*, 62, 242(1991)
- [8] D.W.Marquardt, *J.Soc.Ind. Appl. Math.*, 11, 431(1963)
- [9] M.Sun, Fiberoptic thermometry based on photoluminescent decay times, in *Temperature – Its Measurement and Control in Science and Industry*, Vol.6, Part 2, American Institute of Physics, New York, 715(1992)
- [10] F.B.Hildebrand, *Introduction to Numerical Analysis*, 2nd edition (McGraw-Hill, New York, 1974)
- [11] T.Sun, Z.Y.Zhang, K.T.V.Grattan and A.W.Palmer, Analysis of double exponential fluorescence decay behavior for optical temperature sensing, *Rev. Sci. Instrum.*, 68, 58(1997)
- [12] Z.Y.Zhang, T.Sun, K.T.V.Grattan and A.W.Palmer, Deconvolution of fluorescence decays and estimation errors, *Proc. SPIE*, Vol.2980, 90(1997)
- [13] Y.L.Hu, Z.Y.Zhang, K.T.V.Grattan, A.W.Palmer and B.T.Meggitt, Design aspects of a Ruby-based fiber optic thermometer probe for use in the cryogenic region (>77K), *Rev. Sci. Instrum.*, 67, 2394(1996)
- [14] Z.Y.Zhang, K.T.V.Grattan and A.W.Palmer, Cr:LiSaF fluorescence lifetime based fiber optic thermometer and its applications in clinical RF heat treatment, *Proc. SPIE*, 1885, 300(1993)

Chapter 4 Multiple Exponential Decay Analysis and Fluorescence-based Quasi-distributed Temperature Sensing System

- [15] Z.Y.Zhang, K.T.V.Grattan, A.W.Palmer and B.T.Meggitt, Potential for temperature sensing applications of highly neodymium-doped crystals and fiber at up to approximately 1000°C, *Rev. Sci. Instrum.*, 68, 2759(1997)
- [16] Z.Y.Zhang, K.T.V.Grattan, A.W.Palmer, B.T.Meggitt and T.Sun, Fluorescence decay-time characteristics of erbium-doped optical fiber at elevated temperatures, *Rev. Sci. Instrum.*, 68, 2764(1997)
- [17] Z.Y.Zhang, K.T.V.Grattan, A.W.Palmer and B.T.Meggitt, Thulium-doped intrinsic fiber optic sensor for high temperature measurements (>1100°C), *Rev. Sci. Instrum.*, 69, 1998
- [18] B.J.Ainslie, S.P.Craig and S.T.Davey, The absorption and fluorescence spectra of rare earth ions in silica-based monomode fiber, *J.Lightwave Technol.*, 6, 287(1988)

Chapter 5

Average and Local Temperature Rare Earth Fibre-based Sensing Systems

5.1 Abstract

Average, rather than point specific temperature measurement is important in a number of industrial situations. In the work discussed in Section 5.2, a method to improve this type of measurement using the fluorescence lifetime-related mathematical parameter, the singular value (SV), is discussed in detail. The analysis reported shows that with rare-earth doped fibres used as temperature sensor probe elements for average temperature measurement, such a system works well especially when the lifetimes obtained from different sensing probes are very close to each other. The SV scheme, based on matrix theory, is important because the average temperature-dependent singular value possesses the characteristics of both high speed and high precision. An average temperature sensing scheme has been demonstrated in experiments carried out over the region from 20°C to 100°C, in which Nd³⁺ doped fibres are employed as the intrinsic temperature sensor elements. When two temperature sensing probes are used in the measuring region, the precision determined for the average temperature

estimation was found to be $\pm 3.6^\circ\text{C}$. When three sensors are employed instead of two, the precision is similar at $\pm 3.4^\circ\text{C}$. Results obtained indicate that with more sensor elements used in the sensing region, the accuracy achieved was not diminished due to the averaging effect in the measurement.

Another important temperature sensing issue is to determine local extremes of high temperatures with reference to a relatively stable background. Data on this temperature rise from optical sensor probes are analyzed in detail in Section 5.3, by using a mathematical relationship, based on a correlation coefficient ratio scheme using fluorescence decay time information associated with the hot part of the fibre. In schemes incorporating this mathematical approach, two separate sensor configurations have been demonstrated, one of which is to use short, single lengths of fibre spliced into a network and the other a long single length of doped fibre, using both Nd and Er doped fibre materials. The results show that the correlation coefficient ratio, R , used will deviate from and be smaller than unity with the increase of the temperature of the localized region where the heat is applied, thereby providing the mechanism for a simple high temperature excursion detection system.

5.2 Average temperature sensing system

5.2.1 Introduction

The most familiar fibre optic temperature sensors discussed in the literature and available commercially are the point sensors discussed in previous chapters, to measure the temperature at a specific position[1], contrasting them with fully distributed

sensors[2] or quasi-distributed temperature sensors[3] which are used for multi-point measurements. However, there is often the need to know the average temperature over some spatial distribution, such as in the automatic management of heating installations in buildings[4], and the evaluation of the average temperature in applications as wide as those in agriculture[5], for example. Considerable effort has been devoted to research into simple and inexpensive average temperature sensors, such as the non-optical method which employs an amorphous magnetic tape as a delay line, where the propagation time of the magnetostrictive wave in the tape is dependent on the average temperature [6]; while in the fibre optic sensor area, the work reported by Looney et al[7] has been based on determining the optical length of the fibre. In that work, with a suitable system of characterization and calibration, the change in the index of refraction of the fibre core could provide a means of temperature determination with a precision of about 0.1°C: however, to the author's knowledge, no experimental results have yet been published to confirm the theoretical estimation.

There are a number of ways of determining average lifetime, such as

$$\tau = \frac{\int_0^{t_\infty} t \cdot f(t) dt}{\int_0^{t_\infty} f(t) dt} \quad (t_\infty \rightarrow \infty), \text{ where } f(t) \text{ is the fluorescence decay signal starting from}$$

time, $t = 0$; t_∞ is the observation time of the decay. In this work, the average lifetime

is defined as $1/\tau = \sum_i 1/\tau_i$ ($i=1, 2, \dots$), where τ_i ($i=1, 2, \dots$) is the lifetime of

different probes.

5.2.2 Fluorescence-based measurement approach

Several recent reports of average temperature measurements, complementing those above, include the use of popular Bragg grating sensors[8]. These provide an attractive quasi-distributed temperature sensing capability, as many gratings can be written into a fibre. However, such sensors suffer from limited temperature-induced spectral displacements ($\sim 0.01\text{nm/K}$ in the near IR) and simultaneously are highly sensitive to fibre strain. More recently, long-period fibre gratings have been proposed for temperature sensing offering higher resolution (0.1nm/K) but the high bend sensitivity of these long-period gratings may also cause undesirable changes of the spectral response. Previous work by Grattan and Zhang[1] has suggested that the fluorescence measurement approach is well suited to average temperature measurement, because of its relatively simple configuration and robust characteristics. It is the essential approach chosen in this work, where a novel method using the so-called singular value (SV) scheme is introduced, and its potential practical applications are considered and discussed.

The fluorescence-based point sensor approach has been investigated for a wide variety of materials by a number of researchers[1][9]. In this method, the excitation pulse from a light emitting diode (LED) or laser diode (LD) source is chosen to be well matched to the absorption in the material to cause a number of levels in the ions to be populated, and the subsequent fluorescence decay from these levels may conveniently be monitored with the use of a single simple detector. The determination of the temperature-related fluorescence lifetime is independent of possible variations in the

source intensity and a number of different numerical algorithms have been used for the estimation of the actual fluorescence lifetime itself, as discussed in Chapter 4. The work of Dowell et al[10] and Zhang et al[11] provide further details of these methods. Prony's method has considerable value for practical applications in point and quasi-distributed temperature sensing[11], but the disadvantage in its use is that its performance is closely related to the selection of relevant parameters in the method and for a large temperature measurement range, the observation window width has to be changed correspondingly in order to achieve optimum precision[11].

The aim of this work has been to show that an alternative mathematical scheme, easier to use and well suited to average measurement, can be employed. An objective has been to retain the advantages of Prony's method, but eliminate some of its sensitivities, to produce a useful sensor method for this application. As a result, the SV scheme, which is not very sensitive to parameter selection, but retains the merits of high precision and Prony's high speed, is introduced and discussed in detail for application to average temperature measurement using fluorescence-based data.

5.2.3 Theoretical background and simulation

As discussed earlier, in Section 4.3.1, following the termination of the excitation light pulse, the fluorescence decay signal $f(t)$, obtained from a typical sensing probe, can be given as a function of time, t , by

$$f(t) = A\exp(-t/\tau) + B + \varepsilon(t) \quad (0 \leq t \leq w) \quad (5.1)$$

Chapter 5 Average and Local Temperature Rare Earth Fiber-based Sensing System

where w is the observation window width, $\varepsilon(t)$ is the noise component attributed to various sources; A and τ are the initial fluorescence amplitude and the fluorescence lifetime respectively; and B is the baseline offset. The fluorescence lifetime, τ , is the temperature dependent parameter.

The procedure for carrying out the average temperature measurement is relatively straightforward where more than one probe (the number depending on the average process) is positioned within the active space of the environment to be monitored. The fluorescence lifetime detected from each probe may be related to the corresponding temperature and further an average temperature measurement can be made which is independent of the use of several discrete probes where simple mathematical manipulation of the data obtained is then applied to give the average temperature. The experimental arrangement discussed in this work is simple and low cost and employs only a single light source, and one detector with several probes arranged within the sensing environment, where each is made of the same sensor material (Nd^{3+} doped fibre is the active material in this experiment, due to its very satisfactory performance in previous work[1] on point sensors).

The singular value SV is the characteristic parameter related to the average temperature and used in this work. Its origin and meaning are discussed in detail in the following sections, in terms of its relationship between fluorescence lifetime and the average temperature, which may thus be obtained.

Several different number of probe elements are now considered, beginning with the use of the method with a single probe.

5.2.3.1 One lifetime, one probe system

As discussed earlier in Section 4.3.1, the function, representing the relationship between the lifetime (and thus the temperature) and the signal obtained, shown in Eq.(5.1) can be simplified if the baseline of the resultant signal from the detector can be removed mathematically from the original signal, $f(t)$.

$$f'(t) = A \exp(-t / \tau) + \varepsilon(t) \quad (0 \leq t \leq w) \quad (5.2)$$

In Prony's method[11], as discussed in Section 4.3.3, there is an important non-intensity dependent parameter, α , which links the lifetime and the digitized signal, and where the relationship between them is shown in Eq.(5.3) and Eq.(5.4), i.e.,

$$f'_{j+\Delta N} + f'_j \alpha = 0, \quad j = 0, 1, 2, \dots, (N - \Delta N - 1) \quad (5.3)$$

$$\tau = -(\Delta N)(\Delta t) / \ln(-1 / \alpha) \quad (5.4)$$

where f'_j , ($j = 0, 1, \dots, N - 1$) are the digitized signals. ΔN is the sample space index and Δt the time interval used in the digitization process. The precision of Prony's method is directly determined through the estimation of the parameter, α . It has been shown in that work carried out and discussed, that the optimum estimation of α is closely related to the selection of the observation window width and the sample space index but there is a considerable saving in computing time in its use, thus making it suitable for real time estimation. It was reported that the noise-to-error transfer factor of the lifetime estimation is smaller than 0.31[11].

Alternative methods for the accurate determination of the lifetime, and thus the temperature are particularly valuable if the resulting computation is simpler or the time involved in it is shorter. One such approach introduced in this work is the singular value (SV) scheme, and an analysis showing the background to this method is given in this section. The function $f_r(t)$, is introduced where this is defined as $f'(t)/A$, which, as can be seen, is a function of the fluorescence lifetime. It is thus reasonable to expect that the characteristic parameters relating to this function $f_r(t)$ are related only to the lifetime, τ , and further, its variation with temperature. In order to obtain the temperature-dependent parameter required to characterize the output of the sensor, the values of $f_r(t)$ may be specified first as a set of N equally spaced points, f_{r_i} , where a linear change of variables has been introduced in such a way that the set of data points, i , is given by 0, 1, 2, ..., $N-1$. Thus one $N \times 1$ matrix, \mathbf{F} , can be formed from the numerical data f_{r_i} and this is given by

$$\mathbf{F} = \left[f_{r_0}, f_{r_1}, \dots, f_{r_{(N-1)}} \right]^{-1} \quad (5.5)$$

By singular value decomposition[12], the expression in matrix \mathbf{F} can be given by

$$\mathbf{F} = \mathbf{Y}\mathbf{M}\mathbf{X}^T \quad (5.6)$$

where \mathbf{X} is the orthogonal $n \times n$, $n=1$, matrix containing the standardized eigenvectors of $\mathbf{A}^T \mathbf{A}$; \mathbf{Y} is a $m \times m$, $m=N$, orthogonal matrix such that $\mathbf{Y}^T \mathbf{A}\mathbf{X} = \mathbf{M}$, where \mathbf{M} can be written in partitioned form as $\left[\mu^d, \mathbf{0} \right]^T$, an $n \times n$ diagonal, submatrix μ^d with one column for each axis alongside an $N \times 1$ submatrix of zeros where the elements of μ are termed its singular values. This is the key to the approach proposed in this work to

use a simple, temperature-dependent parameter for characterization and calibration. The SV is a characteristic parameter of the matrix F and in this work it will be shown to be related to the average temperature.

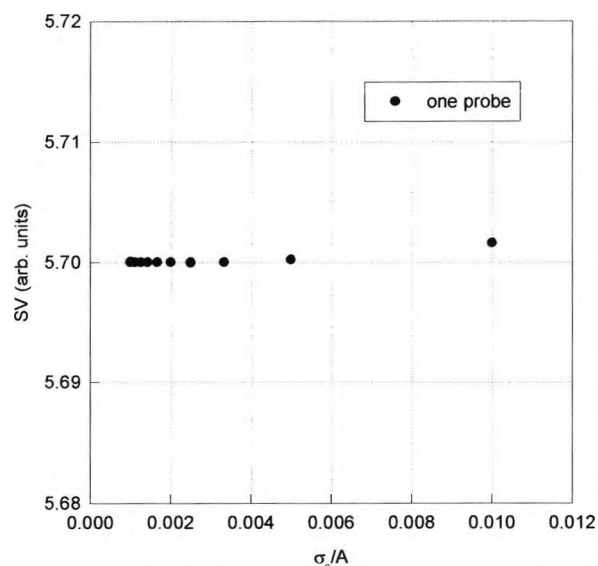


Fig.5.1 Behaviour of the singular value, SV, as a function of normalized noise deviation in a one-probe sensing system

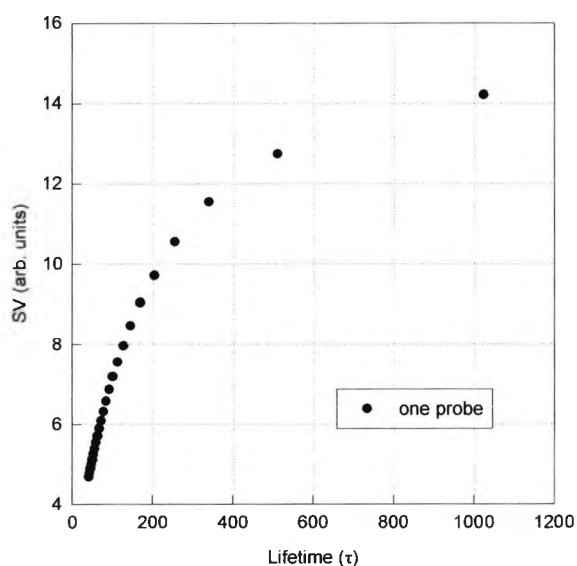


Fig.5.2 Behaviour of the singular value, SV, as a function of fluorescence lifetime in a one-probe sensing system, showing sensitivity to fluorescent lifetime

To investigate its use, a similar Monte Carlo simulation method to that applied in the previous work[11] was employed here, using the reasonable assumption that the noise component $\varepsilon(t)$ is independent of the fluorescence decay and distributed with a Gaussian probability density having a certain standard deviation. The presence of such a noise component will result in errors in the estimation of the lifetime and the SV and the parameter, m_ε , termed the *noise-to-error transfer*, is defined as a measure of the impact of the noise on the estimation, and given by

$$\sigma_{SV} / SV = m_\varepsilon (\sigma_\varepsilon / A) \quad (5.7)$$

where σ_{SV} / SV is the normalized error in estimating the singular value, SV, and σ_ε / A is the normalized noise deviation, which is set to a reasonable value (of 0.1%) during the simulations. It can be seen from Fig.5.1, showing a plot of SV as a function of σ_ε / A , that the performance of SV in the matrix \mathbf{F} is not sensitive to the variations of amplitude, A . Looking at the variation of σ_ε / A over the range of from 0.1% to 1%, the fluctuation of SV is below 0.05%. However, Fig.5.2 shows that SV changes dramatically and monotonically, as a function of the lifetime, τ . A comparison of the influence of both lifetime and the amplitude of the signal on the SV shows that the amplitude effect is negligible (Fig.5.1) and it implies that the SV method is useful for sensors where the lifetime is seen to vary with SV, but not the signal amplitude. The algebraic function, the characteristic root, SV, is now closely linked with the physical parameter, τ , the lifetime, and thus the temperature, as Fig.5.2 shows.

Previous work on lifetime-based temperature sensing by Zhang et al[11] has shown that by using Prony's method, through a careful selection of the normalized window width β , (w/τ), and the sample space index ΔN , the value of m_ϵ can be reduced to be as small as 0.31. However, the simulation results shown in Fig.5.3 for m_ϵ as a function of β reveal that no matter which normalized window width (β) is selected, the value of m_ϵ , for the estimation of SV is always larger than 0.9, which shows that the repeatability of the SV scheme is not as good as that of Prony's method for a system generating one single lifetime with a temperature dependence, i.e., using one sensor probe element alone. However, with a system generating several lifetimes from several discrete probes, there are a number of advantages, which are discussed below, initially for a two probe, two lifetime system.

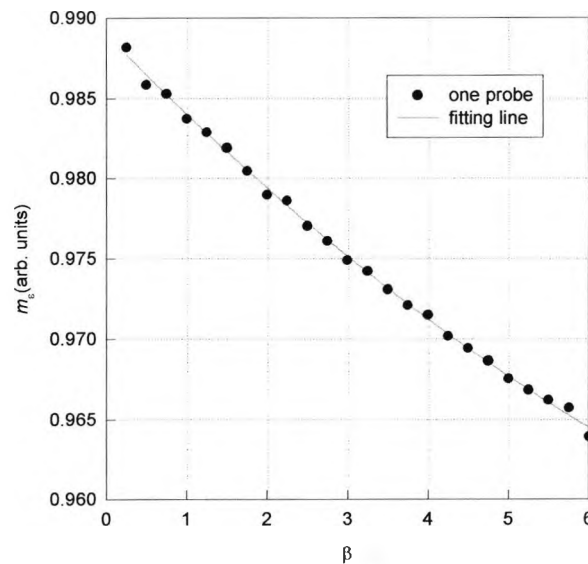


Fig.5.3 Noise-to-error transfer factor, m_ϵ , as a function of the normalized observation window width β in a one-probe system

5.2.3.2 Two lifetimes, two probe system

In the case of a sensing system yielding two lifetimes, from two probes, the resultant fluorescence decay signal, $f''(t)$, will contain two exponential components and this may be given by

$$f''(t) = A_1 \exp(-t / \tau_1) + A_2 \exp(-t / \tau_2) + \varepsilon(t) \quad (0 \leq t \leq w) \quad (5.8)$$

where A_1 and A_2 are the initial separate fluorescence amplitudes; τ_1 and τ_2 are the corresponding fluorescence lifetimes; and $\varepsilon(t)$ and w are as defined in Eq.(5.1). The total sensing system is envisaged as comprising a single fibre loop from the source to the detector, with two short pieces of doped fibre representing the probe elements themselves inserted into the plain silica fibre at the points where the temperature is to be measured and the doped fibre fusion spliced to create a single loop. Previous work[13] has been done on the deconvolution of the two signals representing two lifetimes combined which has shown that when the ratio of the two time constants $\tau_1/\tau_2 \approx 0.02\sim 0.5$, the noise-to-error transfer factor m_1 will be about 2.0 under the condition of optimum selection of the relevant parameters. When the two time constants of the two lifetimes from the two probes approach each other closely, m_1 will rise dramatically and approach infinity with their ratio reaching one, indicating that deconvolution becomes impossible. However, when the same material is employed for each of the two probes used for an average temperature measurement, the lifetimes detected from each probe are usually very close to each other (except within the very high temperature region where rapid thermal quenching occurs) and deconvolution by Prony's method is impossible. In this case, the SV method comes into its own as an

Chapter 5 Average and Local Temperature Rare Earth Fiber-based Sensing System

approach which can solve the problem of average temperature estimation, with good measurement precision.

The same procedure, as discussed previously has been employed here for the detailed analysis of the observed signal where the function $f'(t)$ is replaced by $f''(t)$. Figs.5.4 and 5.5 are the results of a simulation obtained when the ratio of the two time constants is set to 1.1. An example of where this may occur is with two Nd-based probes at temperatures of 20 and 150°C. As is shown in Fig.5.4, the SV changes

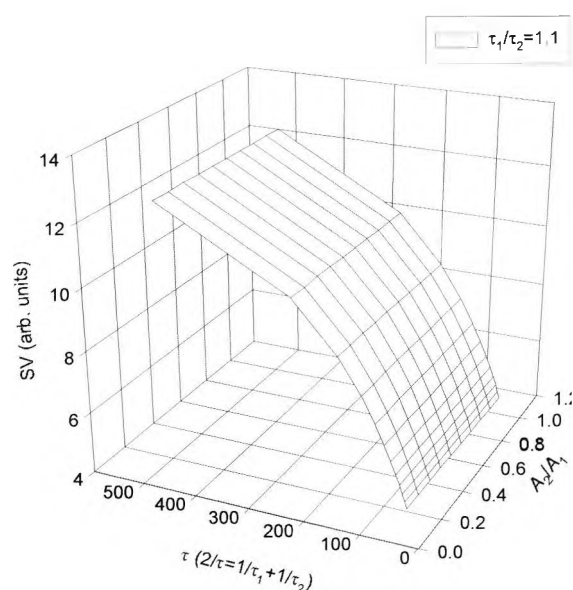


Fig.5.4 Variation of SV as a function of average lifetime τ , $2/\tau = 1/\tau_1 + 1/\tau_2$, and the amplitude ratio in a two-probe sensing system ($\tau_1/\tau_2 = 1.1$)

rapidly with the variation of the observed lifetime τ , where $2/\tau = 1/\tau_1 + 1/\tau_2$, while remaining insensitive to the variation of the ratio of the two initial amplitudes, indicating that the SV method can be considered as essentially amplitude independent. The lifetime τ , defined as the mean of the lifetimes of the two probes is adopted here as

Chapter 5 Average and Local Temperature Rare Earth Fiber-based Sensing System

this average lifetime and is found to be closely linked to the mathematical parameter, SV, showing its value in average temperature determination. Fig.5.5 shows the variation of m_e , as a function of the normalized observation window width β , where $\beta=N\Delta t/\tau$, and the amplitude ratio, given by A_2/A_1 . It is again seen be relatively insensitive to this ratio, changing only slightly from 0.99 to 0.96 with the increase of the normalized observation window width over a very wide range from 0 to 7. Compared with the use of Prony's method[13], the selection of the observation window width is relatively unimportant here and makes the SV method quite simple to use, enabling it to be applied to a wider temperature range of measurement. By

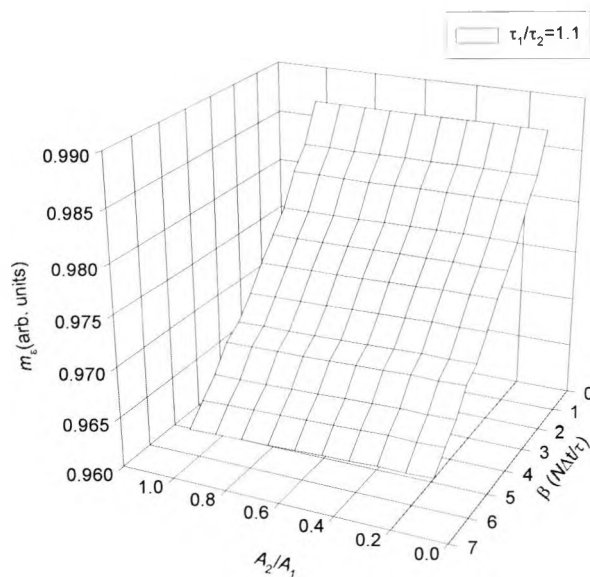


Fig.5.5 Noise-to-error transfer factor, m_e , as a function of the amplitude ratio and the normalized observation window width β in a two-probe sensing system

$$(\tau_1/\tau_2=1.1)$$

contrast, with the use of Prony's method, the observation window width has to be varied when used over a wider temperature range. The smaller value of the *noise-to-error-transfer factor*, compared to that of Prony's method and its value and distinctive

Chapter 5 Average and Local Temperature Rare Earth Fiber-based Sensing System

characteristic for the case where the lifetimes are close show the value of the SV method for average temperature sensing using multiple probes.

5.2.3.3 Three lifetimes, three probe system

The sensor scheme is further expanded in the next illustration. For a system generating three lifetimes, corresponding to a three-probe sensing system, the fluorescence decay signal, $f'''(t)$, will now contain three exponential components and is given by

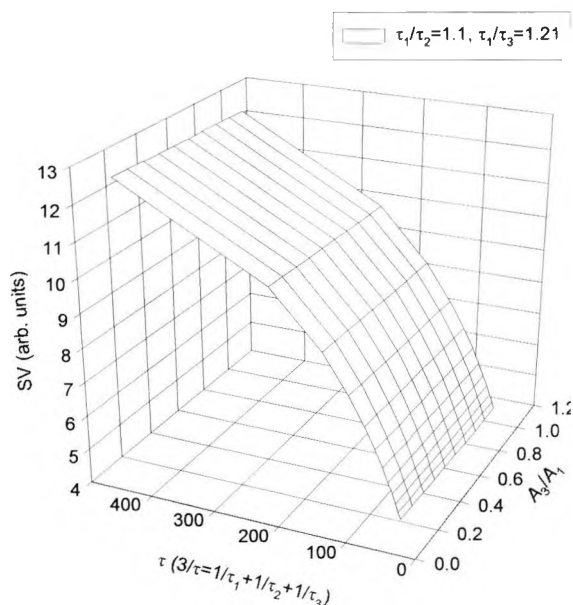


Fig.5.6 Variation of SV as a function of average lifetime τ , $3/\tau=1/\tau_1+1/\tau_2+1/\tau_3$, and the amplitude ratio in a three-probe sensing system ($\tau_1/\tau_2=1.1$, $\tau_1/\tau_3=1.21$)

$$f'''(t) = A_1 \exp(-t/\tau_1) + A_2 \exp(-t/\tau_2) + A_3 \exp(-t/\tau_3) + \varepsilon(t) \quad (0 \leq t \leq w) \quad (5.9)$$

where A_1 , A_2 and A_3 are the initial separate fluorescence amplitudes; τ_1 , τ_2 and τ_3 are the corresponding fluorescence lifetimes; and $\varepsilon(t)$ and w are as defined in Eq.(5.1). A similar sensing system configuration to that discussed for two probes is envisaged, this time with three sensor elements fused into the fibre loop. The SV scheme may again be usefully employed for average temperature sensing purposes. The results of the

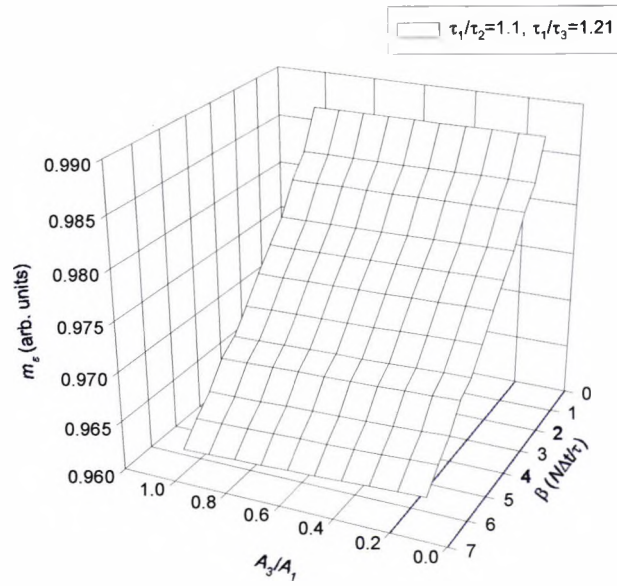


Fig.5.7 Noise-to-error transfer factor, m_ε , as a function of the amplitude ratio and the normalized observation window width β in a three-probe sensing system

$$(\tau_1/\tau_2=1.1, \tau_1/\tau_3=1.21)$$

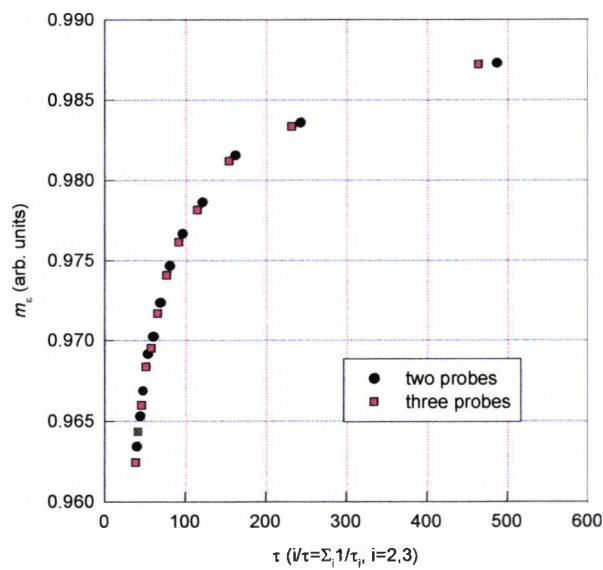


Fig.5.8 Variation of noise-to-error transfer factor m_ε , as a function of average lifetime showing consistent behaviour under different sensing systems of two and three probes

simulation shown in Figs.5.6 and 5.7 confirm the negligible effect of the amplitude

ratio variation on the SV value and m_ϵ . The dominant changes in the SV are as a function of the observed lifetime, τ , now given by $3/\tau=1/\tau_1+1/\tau_2+1/\tau_3$, which represents the average temperature. The value of m_ϵ , decreases slightly with the increase of the normalized observation window width and again the simulation suggests the system can usefully be employed over a much wider temperature range when compared with Prony's method[3]. Unlike Prony's method, with the number of probes increased to three, m_ϵ remains almost the same, as is shown clearly in Fig.5.8. The results of this simulation mean that there are no restrictions (at least in signal analysis terms) on the number of the probes that may be used. The variations of SV as a function of the

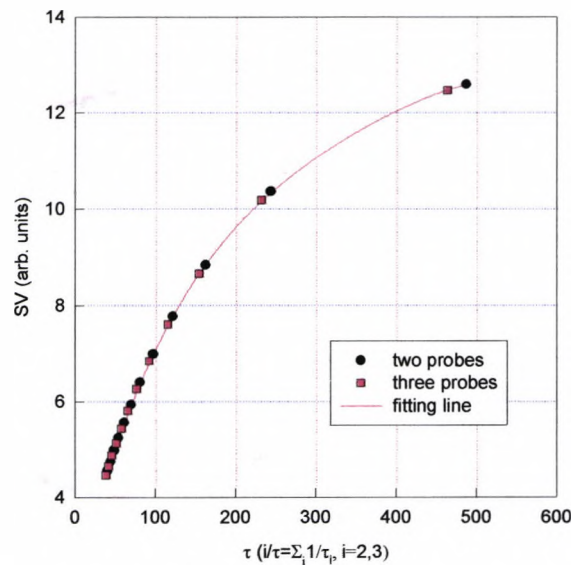


Fig.5.9 Behaviour of SV as a function of average lifetime, showing consistent performance under different sensing systems of two and three probes

average lifetime, defined above, τ ($i/\tau=\sum_{i=2,3}1/\tau_i$), for the two and three probe situations are consistent with a single function for both cases, shown in Fig.5.9, for which the correlation coefficient of the two curves is as high as 99.99%.

5.2.4 Experimental verification and results

5.2.4.1 Experimental setup

In order to verify the results of the simulation described, an experimental investigation of various systems using several probes has been carried out. One such system is illustrated schematically in Fig.5.10 where the doped fibre sensor elements are fused into a fibre loop. The length of plain fibre in the loop is essentially unimportant as the attenuation of the optical signal is trivial in this part of the sensor system. Thus the whole fibre loop could be hundreds of meters in length, if necessary, to distribute the sensitive elements to the various locations over which an average temperature is to be measured. Equally the loop can be short, and a few meters in length, if required. The

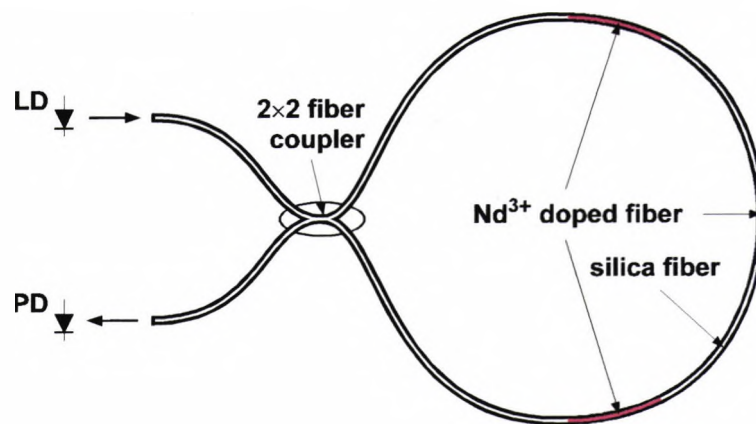


Fig.5.10 Schematic of the experiment setup used illustrated with three doped fibre sensor elements. The separation of the Nd^{3+} fibre elements can vary widely in practical situations. LD—laser diode source; PD—photodetector

distribution of the active sensor elements along the loop has no relevance in the comparison with the simulation and on the practical sensing mechanism of the probe system.

Chapter 5 Average and Local Temperature Rare Earth Fiber-based Sensing System

The aim of the experimental setup has been to create an average temperature measurement system, based upon the use of a series of intrinsic doped fibre elements, each of which measures the temperature along its short length, where all the elements are distributed and fused into a single silica fibre loop. The excitation light source was an infrared (IR) laser diode operating at a center wavelength of 788nm, modulated by a pulse signal generated by the digital output of a computer. The light was conveyed through a 50/125 μ m diameter, 2 \times 2 fibre coupler to the sensing loop formed by the two branches of the coupler containing, in this demonstration, either two or three pieces of Nd³⁺ doped silica fibre, the (core/cladding) diameter of which is 3.5 μ m/125 μ m, respectively, each piece being of 50mm length. The doped fibre can be wrapped into a relatively small loop and each sensor element is assumed to represent a point measurement over its length. Compared to most fully distributed sensor systems for temperature measurement using nonlinear optical effects, for example, the spatial resolution is good at being ≤ 1 m. Fully distributed commercial optical sensors using nonlinear effects and “time-of-flight” techniques have typical spatial resolutions of a few meters, although work is being done on techniques to reduce this. The design of the loop and the choice of element length was such as to make good use of the pump light for a closely matching degree of absorption in each element, aiming to ensure the emission intensity due to each piece was broadly similar. Before reaching the single InGaAs photodetector, the light passed through a filter, which was used to prevent the reflected excitation light from saturating the photodetector. The signal produced was digitized by an analog-to-digital converter attached to the computer and then

processed by corresponding software to reveal the temperature-dependent parameter. Temperature data were calibrated with respect to a K-type thermocouple.

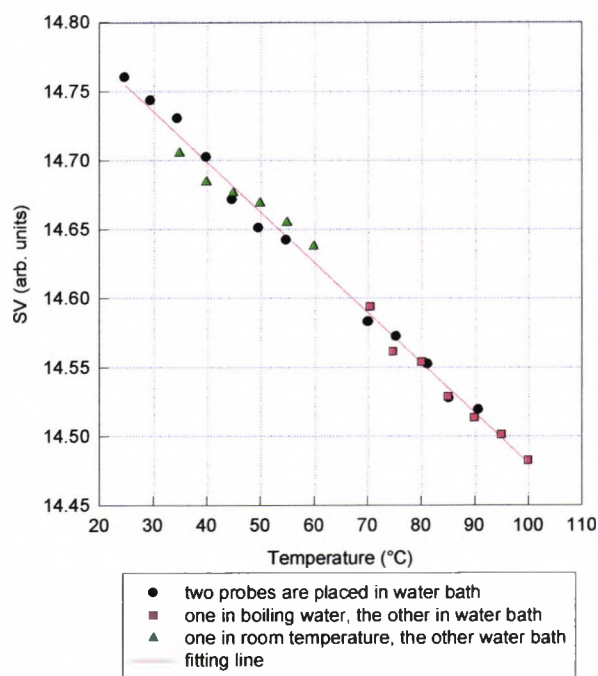


Fig.5.11 Experimental data showing the SV variation with the average temperature from 20-100°C with two sensing elements located in the measuring area, under different temperature conditions

5.2.4.2 Use of two probes

The first experimental setup to test the sensor system was designed to use two pieces of Nd³⁺ doped fibre (two sensor elements) spliced to the two branches of a 2×2 coupler. This is shown schematically (in that case with three sensor elements, but otherwise it is similar) in Fig.5.10. Three groups of experimental data, obtained for a series of average temperature measurements, are included in Fig.5.11 and analyzed using the SV scheme. The first group was obtained when the two sensors experienced

the same variation of temperature by being placed together in a water bath, the temperature of which was varied from room temperature (25°C) to boiling temperature (100°C) and the second group was taken where one element was stabilized in boiling water (100°C) while the other was in the same water bath, the temperature of which was varied. The third data set was taken where the situation was similar to that of the above, the difference being that one probe was held at room temperature (20°C) instead of being placed in the boiling water. For convenience for practical applications, a linear fit was employed to produce a calibration graph and the correlation coefficient obtained was as high as 0.991. The precision of the average temperature measurement obtained was within $\pm 3.6^\circ\text{C}$ when the SV scheme was used in the analysis. With an increase in the number of the sensing probes, the error caused by the noise in the system is expected to be broadly similar, when using the SV approach to data analysis. In order to investigate this, a second experimental setup was used in this work where another element was added to the sensing loop, to create the system shown in Fig.5.10. Again it should be remembered that the length of plain fibre used to join the sensor elements is essentially irrelevant to the functioning of the scheme.

5.2.4.3 Use of three probes

The experimental results shown in Fig.5.12 were all obtained from a three sensor loop, of the type schematically illustrated in Fig.5.10. Three groups of data are included: the first was obtained by leaving three elements in the same water bath and varying the temperature in the same way, the second was obtained with one sensor in boiling water and the other two in the variable temperature water bath; and the third by exposing one

probe to room temperature and changing the temperatures of the other two. Fig 5.12 shows the results obtained when using the SV scheme, where the correlation

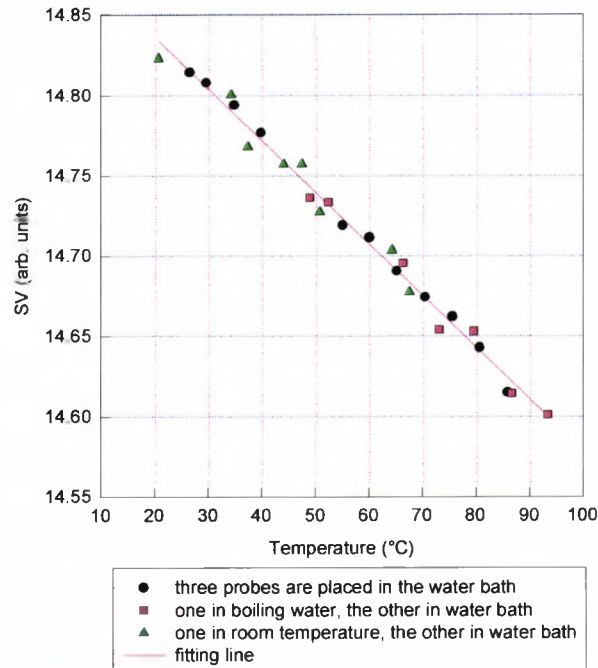


Fig.5.12 Experimental data showing the SV variation with the average temperature from 20-100°C with three sensing elements located in the measuring area, under different temperature conditions

coefficient of the line was 0.987. The precision of the SV scheme for the three probe experiment obtained was $\pm 3.4^\circ\text{C}$, this being quite similar to that obtained above with two probe elements but slightly improved because of the averaging effect with the use of an additional probe. As a comparison, with a single-probe system using a similar optical arrangement, a precision of $\pm 3.9^\circ\text{C}$ and correlation coefficient of 0.990 were obtained when using the SV scheme. The same experimental data for a one probe system, and processed by Prony's method shows a largely comparable precision of

$\pm 3.2^{\circ}\text{C}$, but confirms the advantage of using Prony's method in single point temperature measurement.

The SV scheme possesses very useful practical characteristics of high speed and high precision for average temperature measurement. The close relationship of the SV to the average fluorescence lifetime τ , ($1/\tau = \sum_{i=2,3} 1/\tau_i$) has been readily established.

5.2.5. Discussion of the SV scheme in average temperature measurement

The work has shown the value of the use of the SV scheme, in simulation with a series of experimental measurements to confirm the results of the calculation. For single point temperature sensing, work reported in earlier Chapters has shown that Prony's method shows an advantage of higher accuracy over the SV scheme, while for average temperature sensing, the results of this investigation have shown that the SV scheme is promising to use due to its high speed, high accuracy, and consistency. The Monte Carlo simulation carried out shows that for this type of temperature sensing, the SV approach has greater potential for average temperature measurement with multiple sensors than Prony's. This arises because of the comparative insensitivity of the SV approach to a range of factors which are likely to arise experimentally. Thus no matter what observation window is selected, the effect of its selection is not as important as that for Prony's method[13]. Additionally, unlike Prony's method, the error caused by the additional noise with the increase of the number of sensing probes is similar and because of the averaging effect, the precision of the result is in fact slightly improved, as has been demonstrated. Experimental results obtained on the use of the SV

Chapter 5 Average and Local Temperature Rare Earth Fiber-based Sensing System

approach illustrate that the precision of the average temperature measurement obtained by using the SV scheme is $\pm 3.6^{\circ}\text{C}$ for the two probe system and $\pm 3.4^{\circ}\text{C}$ for the three probe system with Nd as the active element. The scheme can readily be extended to other sensor materials, such as have been reported in quasi-distributed temperature measurements[3] by the author and others.

The use of a single long doped fibre sensor probe element as a possible alternative to the sensor element sections is not a practical proposition, due to the high degree of absorption by the dopants in a fibre of such length. For most practical purposes, the sensor element should have sufficient absorption to generate a measurable level of fluorescence in the next element. Thus highly doped probe elements are preferred with a short, 50mm length for each, and it is unlikely that more than ten elements ultimately could be used with a total length of 500mm, as this would severely limit the potential for wide spatial distribution of the sensor probe elements if they were not split into many short probe lengths along the multimeter length of the fibre loop.

Thus a useful alternative technique for the analysis of data from multiple quasi-distributed sensor elements distributed to generate an average temperature measurement, without monitoring the temperatures of each element individually has been developed, and satisfactory results obtained using a simple data analysis approach.

In some cases, it is also important to detect the higher excursions, such as in those alarm or emergency situations. The following section discusses both the sensor system and the corresponding signal processing issues for such a system.

5.3 Local temperature excursion detection

5.3.1 Introduction

Previous work has shown that[14][15][16] fusion spliced fibre-to-fibre links have superior mechanical properties to adhesives and mechanical couplings in fluorescence-based sensors when exposed to extremes of temperatures, for which a range of doped fibre materials is available[1]. An important temperature sensing issue is the measurement of localized extremes of temperature or excursions to much higher temperatures, with reference to a relatively stable background. This is typical of alarm or emergency signalling situations, where the *indication* that the rise in temperature has taken place is more important than a precise measurement of either the temperature itself or its position along the fibre network. Thus a much lower level of accuracy than the typical 2-5°C of previous measurements using single point probes incorporating such doped fibre[16] could be tolerated for this type of specialized application, where the speed of response to the change is of greater importance, and a time constant typically of a few seconds may be considered acceptable here. Fortunately, in the measurement systems previously discussed[14][15], there is often a “trade-off” between precision and speed of response, reflecting the degree of signal averaging carried out on the raw data. Typical applications of such a sensor system include fire alarm devices, via either average or localized “spot” temperature monitoring.

In this aspect of the work, a doped-fibre based intrinsic sensor system is discussed and two approaches to creating such a system using different configurations are considered. In one the use of short, single lengths of fibre spliced into a network is discussed, and in the second a long single length of doped fibre is used, both for monitoring and thus potential alarm purposes. The signal processing aspects of these systems are examined theoretically and results reported on their comparative performance characteristics.

5.3.2 Theoretical background

Fluorescence may be excited in a doped fibre, in both situations, through the use of a pulse of light from an appropriate laser diode source in a similar way to the situation discussed earlier[15]. As before, it is found that following the termination of the excitation light pulse, the fluorescence decay signal can be written as an exponential as a function of time, t , by:

$$f(t) = A \exp(-t / \tau_1) + B + \varepsilon(t) \quad (5.10)$$

where A corresponds to the initial fluorescence amplitude; τ_1 is the corresponding fluorescence lifetime, which is temperature-dependent; B is the signal baseline offset and $\varepsilon(t)$ is the noise component attributed to various sources. The component B in Eq.(5.10) can be removed easily in the signal processing and $\varepsilon(t)$ can be reduced to minimum by averaging, then the simplified form resulting is as shown in the following:

$$f'(t) = A \exp(-t / \tau_1) \quad (5.11)$$

If one section of the fluorescence material (in either the long doped fibre loop or at one of the discrete sections) is exposed to a higher temperature, for example, due to contact with a flame or a hot body, the fluorescence signal obtained will be seen to deviate from the above exponential form and can be given by:

$$f''(t) = B_1 \exp(-t / \tau_1) + B_2 \exp(-t / \tau_2) \quad (5.12)$$

in which τ_1 and τ_2 are the fluorescence lifetimes derived from the hot and cold sections separately, where τ_1 corresponds to the decay time associated with the original temperature, τ_2 to that for the high temperature; and B_1 and B_2 are the amplitudes of each fluorescence component.

In order to detect the presence of the 'hot spot', i.e., the fluorescence component corresponding to the high temperature, which is superimposed on the stable signal corresponding to the background temperature, an appropriate mathematical treatment is necessary. Previous work has shown that Marquardt's[10], as well as Prony's method[13], may be used to solve the problem, and considerations on processing time have been discussed earlier. Although Prony's algorithm saves a considerable amount of computing time, its precision is particularly affected by the selection of the relevant algorithm parameters, including the ratio of τ_1 and τ_2 . When the τ_1 and τ_2 are very close to each other, it is impossible to discriminate them by using Prony's method[13]. In order to solve this problem, an alternative correlation coefficient ratio scheme which is the basis of the approach used in this work, is discussed in detail here.

5.3.2.1 Correlation ratio scheme

The signals in Eq.(5.11) and Eq.(5.12) can be normalized by using the following approach:

$$f_1(t) = \exp(-t / \tau_1) \quad (5.13)$$

$$f_2(t) = B_1 \exp(-t / \tau_1) + (1 - B_1) \exp(-t / \tau_2) \quad (5.14)$$

The cross correlation coefficient, $R_{12}(0)$, can be calculated by using the following procedure:

$$\begin{aligned} R_{12}(0) &= \int_0^{\infty} f_1(t) f_2(t) dt \\ &= \frac{\tau_1}{2} B_1 + \frac{\tau_1 \tau_2}{\tau_1 + \tau_2} (1 - B_1) \end{aligned} \quad (5.15)$$

As a result, the autocorrelation coefficient of $f_1(t)$, $R_{11}(0)$, may be given by:

$$\begin{aligned} R_{11}(0) &= \int_0^{\infty} f_1^2(t) dt \\ &= \frac{\tau_1}{2} \end{aligned} \quad (5.16)$$

A correlation coefficient ratio, R , then can be given by

$$\begin{aligned} R &= R_{12}(0) / R_{11}(0) \\ &= B_1 + \frac{2\tau_2}{\tau_1 + \tau_2} (1 - B_1) \end{aligned} \quad (5.17)$$

When one portion of the fluorescent material is exposed to a higher temperature, normally the lifetime τ_2 will become smaller than the lifetime τ_1 [18], that is, the correlation coefficient ratio R in Eq.(5.17) will become smaller than unity and with the increase of the temperature excursion, the ratio R will continue to become even smaller, signalling the presence of the localized temperature rise. On the other hand, the correlation coefficient ratio R shown in Eq.(5.17) also contains the term B_1 , which is related to the intensity of the fluorescence component from the fibre at the stable

background temperature. As a result, when a further piece of fibre is spliced into the network shown in Fig.5.13(a) and second region of high temperature is also used, the correlation coefficient decreases, indicating that overall, the higher temperature region is larger than when one region only is used. Normally, the effect of B_1 on the output function can be neglected because the length of fibre held at the stable background temperature is usually much longer than that in the high temperature region, and this is especially the case in the configuration shown in Fig.5.13(b).

5.3.3. Experimental arrangement

In this work, the use of the correlation coefficient ratio scheme for the measurement of localized extremes of temperature or an excursion to higher temperatures, with reference to a relatively stable background temperature has been demonstrated for application in two variations of a practical sensor system, a schematic of which is shown in Fig.5.13. In Fig.5.13(a), a sensing system, based upon the use of short, single lengths of fibre, fused into a single silica fibre loop is illustrated. This type of scheme minimizes the length of doped fibre used but limits the overall active length over which the measurement may be made. An alternative scheme is shown in Fig.1(b), in which a longer single length of doped fibre, one short length of which is exposed to the elevated temperature, is employed, thereby enabling the local temperature excursion to be monitored at any point along the fibre, as will be shown later.

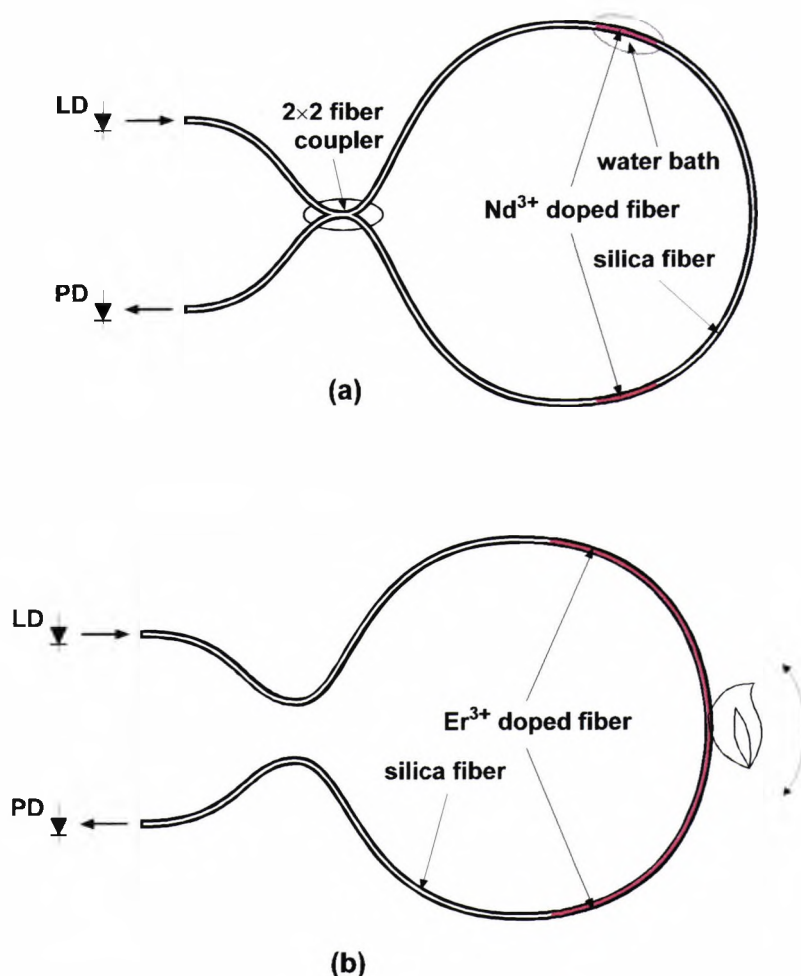


Fig.5.13 Schematic of the two configurations demonstrated

(a) sensing system based on short, single lengths of Nd doped fibres, fused into a network (b) sensing area formed by using a long length of Er doped fibre, one short piece of which is exposed to the temperature excursion

For the system in Fig.5.13(a), neodymium doped fibre was used, for which the excitation light source was an infrared (IR) laser diode (LD) operating at a center wavelength of 788nm and modulated by a pulse signal generated by the digital output of a computer. The light was conveyed through a 50/125 μ m diameter, 2x2 fibre coupler to the sensing loop formed by the two branches of the coupler containing, in

Chapter 5 Average and Local Temperature Rare Earth Fiber-based Sensing System

this demonstration, two pieces of Nd^{3+} doped silica fibre (York Ltd., type No. ND95020/E), the diameter of which is $3.5\mu\text{m}/125\mu\text{m}$, each being of 5cm length. Before reaching the InGaAs photodetector, the outgoing light passed through a filter, which was used to prevent the reflected excitation light from saturating the photodetector. The signal produced was digitized by an analogue-to-digital converter attached to the computer and then processed by the corresponding software to reveal the temperature-dependent parameter. Temperature data were calibrated with respect to a K-type thermocouple.

For the system illustrated by Fig.5.13(b), erbium doped fibre at 200ppm was used for the sensor loop. Tests were then carried out on the performance of this second

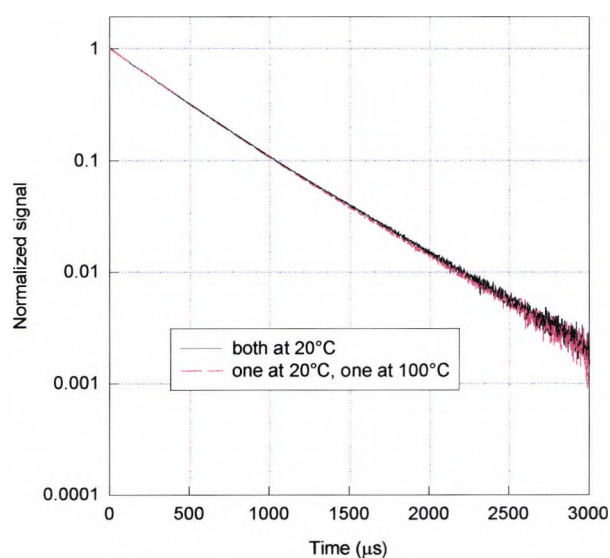


Fig.5.14 The fluorescence decay time signals detected using the configuration shown in Fig.5.13(a), for sensors (1)both at 20°C and (2)one at 20°C and the other at 100°C

configuration using the single long length of fibre. In this case the excitation light source was a laser diode operating at a wavelength of $\sim 980\text{nm}$, with a pigtailed output of $\sim 1.5\text{mW}$. The relatively lightly doped fibre ($\sim 200\text{ppm Er}$), of 1 metre length, was used to avoid saturation of the absorption over a short distance, to ensure that a fluorescence signal is generated at all points along the doped fibre. The fact that the intensity of the fluorescence signal varies with distance is unimportant in this, an analysis of the decay time of the fluorescence, provided that there is sufficient signal received at the detector, as was the case in this work with fibre of the particular length.

5.3.4 Results obtained from the sensor systems

5.3.4.1 Temperature excursion effect

The first set of measurements was taken with the system described in Fig.5.13(a), where two discrete lengths of doped fibre are used and the temperature of one was raised above ambient. The experimental data were taken when one piece of the doped fibre was held at room temperature (20°C), while the other piece was placed in a water bath, the temperature of which was varied from room temperature (20°C) to the water bath boiling temperature (100°C). The effect of small variations in room temperature ($\sim \pm 2^\circ\text{C}$) can be ignored as having minimal effect on the lifetime, τ_1 . The signals detected from one piece of doped fibre at room temperature, as well as from that at 100°C are shown in Fig.5.14, from which it can be seen that these two graphs are very close to each other, indicating that the increase of temperature from 20°C to 100°C does not cause a dramatic change of the lifetime with the use of the Nd doped fibre. The double exponential nature of the convoluted signal corresponding to 100°C cannot

be detected visually, because the values of τ_1 and τ_2 are very close to each other, although in fact the latter is smaller. To identify the local extreme of temperature, the correlation coefficient ratio scheme discussed earlier is employed to analyze the signal received, the result of which is shown in Fig.5.15. It can be seen that with one piece of fibre stabilized at 20°C and the temperature of the other increasing from 20°C to

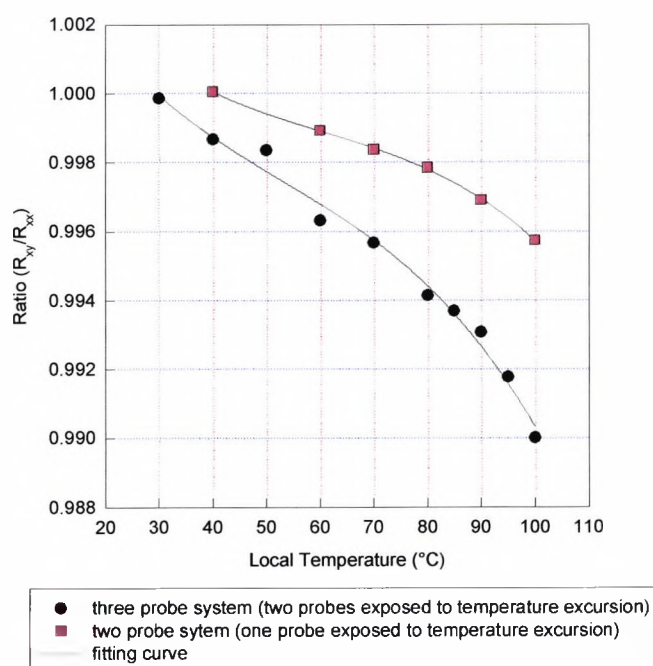


Fig.5.15 The results of the correlation ratio scheme employed using the system shown in Fig.5.13(a), showing the variation of the ratio with temperature, with a two and a three probe system

100°C, the correlation coefficient ratio decreases, with the values all being smaller than unity, as predicted from the theoretical analysis, thus producing an effective means of identifying the presence of the local temperature rise.

The second set of measurements was taken with the same system described in Fig.5.13(a) but this time with three doped fibre elements. One piece of the doped fibre was held at room temperature (20°C), while the other two were placed in a water bath, the temperature of which was varied from room temperature (20°C) to 100°C. The signal was detected and processed in a similar way to that shown above and its correlation coefficient ratio as a function of the local temperature is also shown in Fig.5.15. When comparing the two curves in Fig.5.15, obtained separately with a two and a three probe system respectively, the results indicate that with a larger local high temperature region, the correlation coefficient ratio drops more rapidly with temperature and thus becomes more sensitive to its variation.

The system described in Fig.5.13(b) is now evaluated and signals obtained as a function of local temperature at a variety of discrete temperatures over the range from room temperature to ~300°C are shown for comparison in Fig.5.16. Again, it is difficult to visualize the double exponential nature of the signal even with the localized temperature as high as ~300°C, the maximum used in this study, due to the fact that only a short length was exposed to the higher temperature. This is due to the relatively small magnitude of the change of the lifetime of the small sample of the fluorescent material at the higher temperature and the relatively short length of the very hot fibre.

Fig.5.16 also shows a plot of the *apparent* lifetime, obtained by using Marquardt's method (section 3.3.1), using an oversimplified analysis which assumes a single exponential nature for the signal received, to show how this would appear if the true double exponential nature of the signal were not known. A small decrease in this

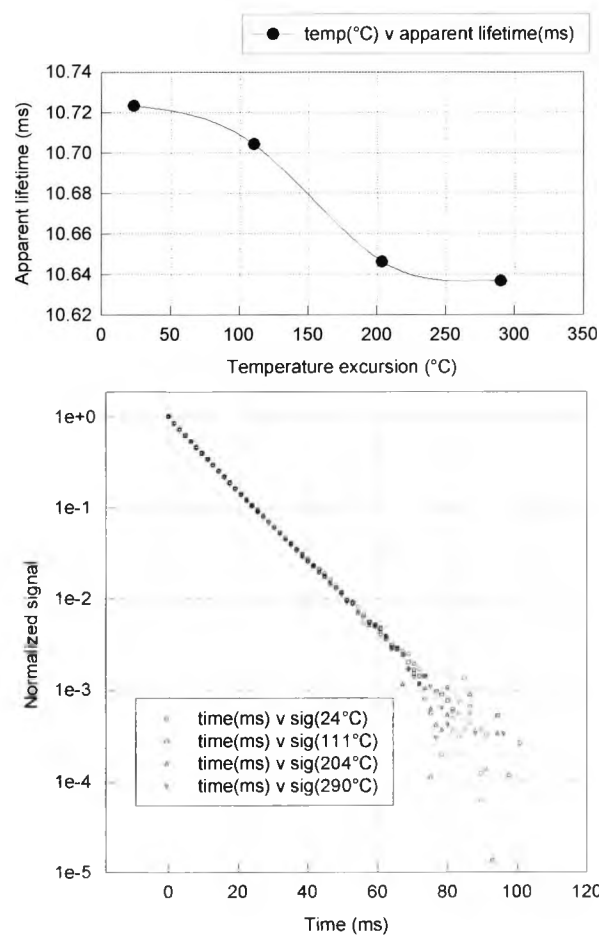


Fig.5.16 The fluorescence decay time signals detected from the configuration shown in Fig.5.13(b) for a range of temperatures (24°C, 111°C, 204°C and 290°C) and the apparent lifetime variation with temperature due to a simple analysis assuming a single exponential decay

Chapter 5 Average and Local Temperature Rare Earth Fiber-based Sensing System

apparent lifetime value is seen with temperature over the range shown. However, this approach is ineffective to make meaningful measurements in a quantitative sensor system by contrast with the use of the correlation coefficient ratio scheme which can detect the variation of the localized temperature very well, the result of which is shown in Fig.5.17. With the increase of the temperature over a range from 24°C to ~300°C, the correlation coefficient ratio decreases and the corresponding ratios, R , observed are all smaller than unity, showing similar results to those obtained above with discrete lengths of fibre. Because the sensing materials employed in Fig.5.13(a) and Fig.5.13(b) are different, the calibration curves shown in Fig.5.15 and Fig.5.17 are themselves different, but the trends are the same, as would be expected from the theory outlined. It would also be appropriate to use either material or even others not illustrated, such as Ho or Tm in each of these configurations (Fig.5.13(a) or (b)), to create this type of intrinsic temperature sensor, for example to cover a different range.

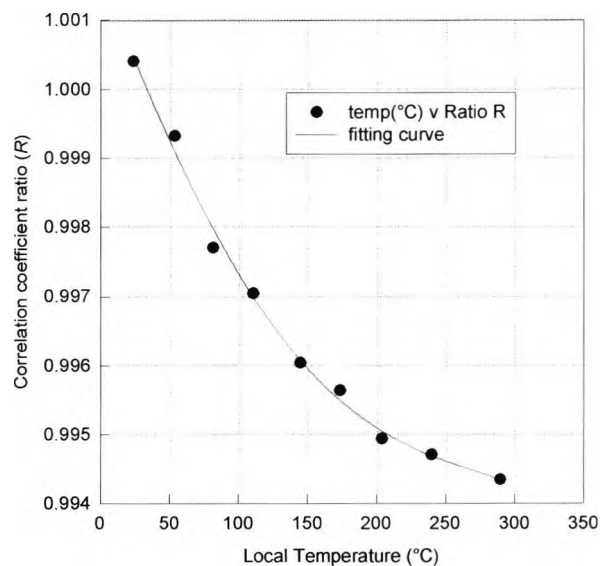


Fig.5.17 The results of the correlation coefficient ratio scheme employed in the system shown in Fig.5.13(b), for a range of temperatures up to 300°C

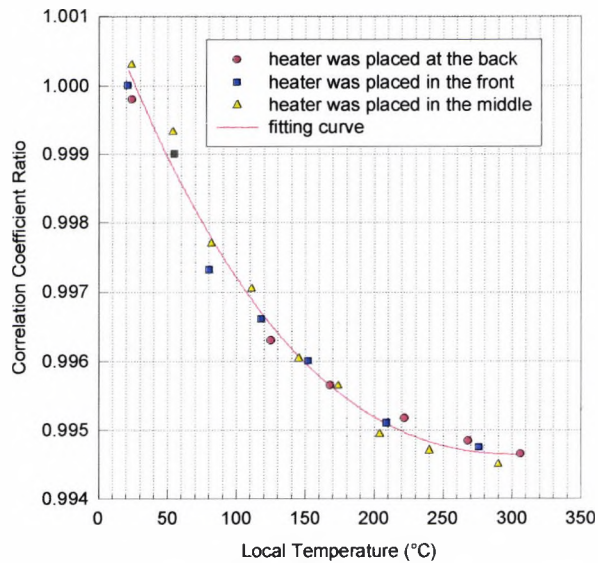


Fig.5.18 The correlation coefficient as a function of temperature, showing no effect of the location of the temperature excursion applied to the sensing fibre, with three different positions of the heater with respect to the fibre listed as shown

5.3.4.2 Location effect

It is an important issue for this type of system to be able to detect the temperature excursion regardless of its location along the fibre. The correlation coefficient-based system described in Fig.5.13(b) has been tested to see whether the above requirement can be satisfied. To do so, regions (of about 15cm, the length of the oven used) in the first third of the 1m fibre length, in the middle of the length, and over the last third of the length were exposed to a range of temperatures up to $\sim 300^{\circ}\text{C}$. The experimental data illustrated in Fig.5.18 show that the calibration graph produced is independent of position as all the curves lie together, and a common correlation coefficient of the fitted curve to all the data points is 98.66%. This confirms that each calibration curve, as a function of temperature excursion, is essentially similar. For the situation where the length of the fibre at the local higher temperature is short compared with the whole

sensitive length, the above requirement can always be satisfied, and this is especially true for the configuration described in Fig.5.13(b).

Using the data of Figs.5.15 and 5.18, the precision of the temperature excursion may be estimated approximately at $\pm 5^{\circ}\text{C}$ for the configuration of Fig.5.13(a) and $\pm 15^{\circ}\text{C}$ for Fig.5.13(b). The time constant for a measurement is a few seconds, and acceptable for alarm purposes, using a Pentium PC for signal and data processing. Higher precision could be obtained at the expense of a longer data analysis time. For alarm purposes, the relatively large value of temperature precision is acceptable in most situations, where local excursions of several hundred degrees may occur, for example in a fibre exposed to fire or hot gases.

In this work, in the setup shown in Fig.5.13(b), the sensing length is relatively short at 1m, but this could be increased by using fibre with a lower doping level or increased optical pumped power. In either case the aim is to avoid saturation which ultimately limits the effective length which may be used. It is envisaged that systems of $\sim 5\text{-}10\text{m}$ of active length could be configured with appropriate fibres and pump sources.

5.3.5 Discussion of local temperature measurement

Fluorescence-based doped fibre intrinsic temperature sensing systems for determining local extremes of high temperatures have been demonstrated in this section, the basis of which is the use of the correlation coefficient ratio scheme outlined. Two separate schemes were illustrated with both short and a single long length of fibre, using both

Nd and Er doped materials, in both cases at relatively low doping levels to avoid saturation. The analysis shows that when there is an excursion to higher temperatures with reference to the stable background, the correlation coefficient ratio R will deviate from and be smaller than unity, indicating a temperature rise. The increase of the deviation, where the ratio R becomes smaller as would be expected from theory, enables the magnitude of the local temperature change to be determined, and thus an effective sensor system to be configured.

5.4 Summary

Two signal processing schemes have been proposed separately in this chapter to measure both the average and local temperatures. Both schemes possess the characteristic of high speed and consistency and are appropriate for specific applications, where the speed of response to the temperature change is of greater importance, with a little lower level than the typical 2°C precision reported.

5.5 References

- [1] K.T.V.Grattan and Z.Y.Zhang, *Fiber Optic Fluorescence Thermometry* (Chapman and Hall, London, 1995)
- [2] A.H.Hartog, "Distributed fiber-optic sensors", in *Optical Fiber Sensor Technology*, Edited by K.T.V.Grattan and B.T.Meggitt, (Chapman & Hall, London, 1995)

Chapter 5 Average and Local Temperature Rare Earth Fiber-based Sensing System

- [3] T.Sun, Z.Y.Zhang, K.T.V.Grattan and A.W.Palmer, Quasi-distributed fluorescence-based optical fiber temperature sensor system, *Rev. Sci. Instrum.*, 69, 146(1997)
- [4] E.A.Kayafas, G.Campourakis and S.Porizias, An average temperature daily model to be applied in automatic management of heating installations of buildings, *Measurement and Control*, ch48, 17(1985)
- [5] B.Goyette, C.Vigneault, B.Panneton and G.S.V.Raghavan, Method to evaluate the average temperature at the surface of a horticultural crop, *Canadian Agricultural Engineering*, 38, 291(1996)
- [6] K.Shirae and A.Honda, Average temperature transducer using amorphous magnetic tape, *IEEE Transactions on Magnetics*, 17, 3151(1981)
- [7] L.Looney and P.Forman, Fiber-optic large area average temperature sensor, Proceedings of the tenth International Conference on Optical Fibre Sensors, Glasgow, *Proc.SPIE*, Vol. 2360, ch.141, 215(1994)
- [8] Y. J. Rao, In-fibre Bragg grating sensors, in *Optical Fiber Sensor Technology, Vol. II* (Eds K T V Grattan and B T Meggitt) ch11, Chapman & Hall, London
- [9] M.Sun, Fiberoptic thermometry based on photoluminescent decay times, *Temperature: Its Measurement and Control in Science and Industry*, 6, 715(1992)
- [10] L.J.Dowell and G.T.Gillies, Errors caused by base-line offset and noise in the estimation of exponential lifetimes, *Rev. Sci. Instrum.*, 62, 242(1991)
- [11] Z.Y.Zhang, K.T.V.Grattan, Y.L.Hu, A.W.Palmer and B.T.Meggitt, Prony's method for exponential lifetime estimations in fluorescence-based thermometers, *Rev. Sci. Instrum.*, 67, 2590(1996)

Chapter 5 Average and Local Temperature Rare Earth Fiber-based Sensing System

- [12] M.J.R. Healy, *Matrices for Statistics* (Clarendon Press, Oxford, 1986)
- [13] T.Sun, Z.Y.Zhang, K.T.V.Grattan and A.W.Palmer, Analysis of double exponential fluorescence decay behaviour for optical temperature sensing, *Rev. Sci. Instrum.*, 68, 58(1997)
- [14] Grattan K T V and Meggitt B T, *Optical Fiber Sensor Technology*, Vol.3 (Chapman and Hall: London, 1998)
- [15] Z Y Zhang, K T V Grattan, A W Palmer and B T Meggitt, *Rev. Sci. Instrum.*, 68, 2759(1997)
- [16] Z Y Zhang, K T V Grattan, A W Palmer, B T Meggitt and T Sun, *Rev. Sci. Instrum.*, 68, 2764(1997)
- [17] M J F Digonnet, *Rare Earth Doped Fiber Lasers and Amplifiers* (Marcel Dekker, Inc.: New York, 1993)
- [18] Collins S F, Baxter G W, Wade S A., Sun T, Grattan K T V, Zhang Z Y and Palmer A W, *J. Applied Physics*, 1998

Chapter 6

Temperature and Strain Sensitivities of Rare-Earth Doped Fibres

6.1 Abstract

With current research in structure monitoring driving interest in the development of intrinsic (in-fibre) sensors for simultaneous strain and temperature monitoring, a new sensor approach to this issue is presented. In this, the fluorescence decay-time technique, which has been discussed in previous Chapters as a method of temperature monitoring with a range of materials is extended to investigate the strain sensitivity of probes using Nd as well as Yb doped fibre, in both single and multimode form. For each of these fibres, strain and its comparison with temperature sensitivity is presented, 'stress annealing' effects are investigated and the potential for compact, multi-parameter intrinsic sensors using Nd doped or Yb doped fibre is discussed.

6.2 Introduction

6.2.1 Simultaneous strain and temperature monitoring

A major priority of monitoring systems for so-called 'smart' structures is the need to make multiple and often simultaneous measurements of strain and temperature within the structure. Temperature compensation is a common problem in the design of many instrumental systems, and the cross-sensitivity of many strain monitoring sensors to temperature is a particular limitation in making effective use of such devices. A number of schemes have been proposed for temperature-strain discrimination using single sensor systems and these have been reviewed, for example by Jones[1], indicating a range of possibilities for such sensors. Illustrations of these include using interferometers and polarimeters, incorporating air cavities[2], using birefringent Fabry Perot devices, two mode fibres, a Brillouin scattering scheme[3] and Fourier Transform spectroscopy. In general such systems are complex and relatively expensive to implement, and methods which are intrinsic to the fibre (based upon in-fibre devices), including Bragg gratings are to be preferred, to avoid for example, the phase ambiguities of interferometry and offering compatibility with wavelength division multiplexing. Several fibre Bragg grating (FBG) based techniques have been demonstrated for temperature-strain discrimination, for example using a reference FBG[4], dual wavelength FBGs[5], non-sinusoidal FBG[6], FBGs written in different diameter fibre[7], FBG in combination with a rocking filter[8], FBGs used with a long period grating[9], FBG in combination with a Fabry-Perot[10], FBGs and an in-line fibre etalon[11], FBGs written in PANDA fibre[12] and FBGs written in bow-tie

Chapter 6 Temperature and strain sensitivities of rare-earth doped fibres

fibre[13]. However, these specified FBG systems are generally expensive compared to 'stand-alone' gratings at common wavelengths, for example those written for communications applications, thus adding considerably to the cost and complexity of the system.

Very recently, alternative advanced thin-film sensor techniques using palladium –13% chromium based strain gauges and platinum – 13% rhodium versus platinum based thermocouples, that can provide accurate surface strain and temperature measurements, have been the subject of development work at NASA Lewis Research Center[14]. The fabrication was relatively complicated and mainly designed to meet the urgent needs in aeronautic and aerospace research where stress and temperature gradients are high and aerodynamic effects need to be minimized. However, the advantages of the use of optical methods are well known, and particularly applicable to strain and temperature monitoring in aerospace and other specialized environments.

Techniques for the simultaneous measurement of strain and temperature with intrinsic and closely located sensor elements which are in-fibre are thus still very important aspects of instrumentation research. Previous work reported on doped fibre fluorescent materials, both bulk and fibre[15-19] had not considered if there was a strain sensitivity of the fluorescence lifetime of rare-earth doped silica fibre. In reporting this phenomenon for the first time, a study to investigate it is discussed in this work, where the strain characteristics of two of the most important and popular of the

temperature sensor elements, neodymium and ytterbium doped silica fibre, in single-mode as well as multimode form, is investigated over a range of temperatures.

6.2.2 Cr³⁺ and rare earth doped fluorescence-based sensor systems

Cr³⁺ doped crystals and garnets, as well as bulk glass have been used as essential elements of several fluorescence decay-time based temperature probes[15][19]. There has also been previous work on the pressure (and implicitly the stress or strain) sensitivity of such Cr³⁺ crystals and garnets has been discussed as the basis of pressure (as well as temperature) sensors. Pressure will generally affect the luminescence and spectral absorption properties of a material, but this has only been significant at very high (kilobar) pressures. However, the nature of this effect has not been as well studied or understood as are the effects of temperature on luminescence. The application of pressure may be viewed as the imposition of a compressive strain from all directions and hence a knowledge of the material pressure dependence also lends insight into its strain dependence[20]. To be specific, the work reported by Shen et al[21] indicated that both pressure (and thus strain) and temperature have a significant effect on the lifetime of chromium doped into yttrium aluminum garnet (Cr³⁺:YAG). The room temperature lifetime of Cr³⁺:YAG was observed to change from 1.7ms at ambient pressure to 42ms at 220kbar and the 20K lifetime from 8.8ms at ambient pressure to 67ms at 240kbar. The main effect of high pressure is to increase the ⁴T₂₋₂E state energy separation, where the application of pressure results in a reduction of the ⁴T₂₋₂E admixture and as a consequence, an increase in the lifetime. An interesting phenomenon which was also reported in that work was that as the pressure was raised

from 100 to 240 kbar, the room temperature and 20K lifetimes were seen to increase keeping a constant lifetime ratio, that is, the lifetime ratio is pressure independent. The pressure effect on the lifetimes of other Cr^{3+} doped crystals, such as ruby[22], $\text{Cr}^{3+}:\text{Gd}_3\text{Sc}_2\text{Ga}_3\text{O}_{12}$ and $\text{Cr}^{3+}:\text{Gd}_3\text{Ga}_5\text{O}_{12}$ [23] have also been reported and similar results have been published.

Measurements of the pressure dependence of the lifetime of rare-earth ion doped crystals, such as $\text{Gd}_2\text{O}_2\text{S}:\text{Tb}$ and $\text{La}_2\text{O}_2\text{S}:\text{Eu}$ have also been made[20]. These two phosphors exhibit the strongest pressure dependence of all the materials surveyed, which makes the investigation of the effect of stress (or strain) on rare-earth doped fibres, which are relatively more convenient to configure as sensing materials than bulk crystals, particularly valuable. Strains of up to 2000 microstrain ($\mu\epsilon$) can routinely be tolerated with standard fibres of diameters in the 100-200 μm diameter region. It is thus important to investigate the explicit strain dependence of these materials in fibres, in particular if they are to form elements of simultaneous temperature and strain measuring probes, configured with one or more doped fibre element for intrinsic fibre optic sensing. The theoretical background to a generalized two element sensor is discussed below, into which doped fibre elements may be configured. The performance of such fibres under various strain and/or temperature excursions is considered, results reported, and a discussion of their characteristics for potential use with an in-fibre sensor system follows.

6.3. Theoretical background

Optical fibre sensors offer significant advantages over conventional gauges if thermal effects and physical strain can be separated. An ideal sensor system from which two measurand-dependent observables, τ_1 and τ_2 , e.g. the fluorescence lifetimes produced by two, possibly different, rare-earth doped fibres, at a certain temperature T and a specific strain ε may be considered. In practice, both observables each show some sensitivity to both ε and T , so that [1]

$$\begin{bmatrix} \tau_1 \\ \tau_2 \end{bmatrix} = \begin{bmatrix} K_{1T} & K_{1\varepsilon} \\ K_{2T} & K_{2\varepsilon} \end{bmatrix} \begin{bmatrix} T \\ \varepsilon \end{bmatrix} \quad (6.1)$$

and if $K_{1T}K_{2\varepsilon} - K_{2T}K_{1\varepsilon} \neq 0$, the temperature and strain can be calculated by using the following equation:

$$\begin{bmatrix} T \\ \varepsilon \end{bmatrix} = \frac{1}{K_{1T}K_{2\varepsilon} - K_{2T}K_{1\varepsilon}} \begin{bmatrix} K_{2\varepsilon} & -K_{1\varepsilon} \\ -K_{2T} & K_{1T} \end{bmatrix} \begin{bmatrix} \tau_1 \\ \tau_2 \end{bmatrix} \quad (6.2)$$

that is, the simultaneous measurement of strain and temperature by using two sensing elements is possible with a knowledge of the calibration parameters of the system. The temperature and strain errors arising from the above system may be estimated respectively below as:

$$|\delta T| = \frac{|K_{2\varepsilon}||\Delta\tau_1| + |K_{1\varepsilon}||\Delta\tau_2|}{|K_{1T}K_{2\varepsilon} - K_{2T}K_{1\varepsilon}|} \quad (6.3)$$

$$|\delta\varepsilon| = \frac{|K_{2T}||\Delta\tau_1| + |K_{1T}||\Delta\tau_2|}{|K_{1T}K_{2\varepsilon} - K_{2T}K_{1\varepsilon}|} \quad (6.4)$$

A particular description of the simultaneous discrimination of temperature and strain based on the use of dual elements, for example, two different doped fibres or one

Chapter 6 Temperature and strain sensitivities of rare-earth doped fibres

doped fibre combined with grating or interferometer, is possible in terms of Eqs. (6.1) and (6.2) with the error tolerance being estimated from Eqs.(6.3) and (6.4).

For some cases, the sensor constructed may possess relatively large cross-sensitivity and elements of the sensor characteristic matrix change with applied strain and temperature, i.e., K_{1T} , K_{2T} , $K_{1\epsilon}$ and $K_{2\epsilon}$ become nonlinear functions of the variations of temperature and strain. This will introduce large errors in the calculation of the variations of temperature and strain when the matrix inversion technique is used, because the latter technique assumes constant values for K_{1T} , K_{2T} , $K_{1\epsilon}$ and $K_{2\epsilon}$. The error analysis under this situation has been explored in detail by Jin et al[24] and a new approach ANN (an Artificial Neural Network), has been proposed to solve the problem by Chan et al[25] and it was reported that for a sensor with large cross-sensitivity/nonlinearity, the improvement in accuracy using ANN is significant.

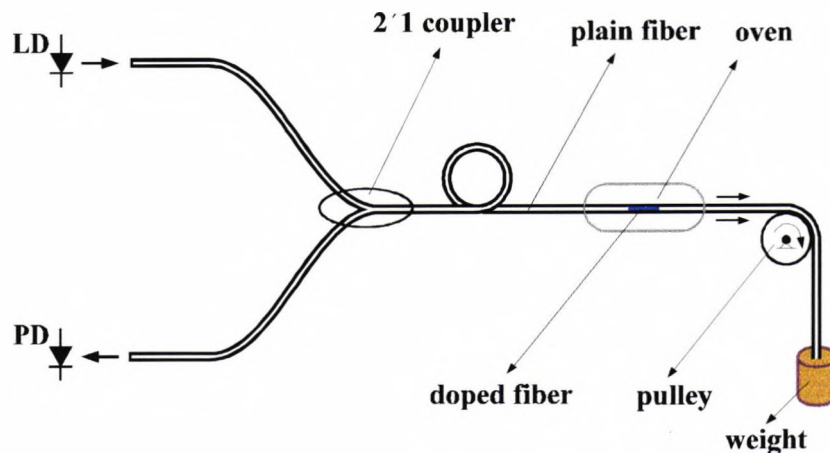


Fig.6.1 Simplified schematic of the experimental arrangement for the strain test of Nd doped fibre

6.4. Temperature and strain effects on Nd-doped fibres

6.4.1 Experimental arrangement

The experimental arrangement used for the measurement of the strain-induced fluorescence characteristics of several Nd-doped fibres over a range of temperatures up to 150°C is illustrated in Fig.6.1. A laser diode with a center wavelength of 830nm is employed as the source, light from which couples well to a major absorption band of the material[18][19]. Two types of Nd doped fibres were put under test, one of which was multimode, of diameter (core/cladding) 100µm/140µm and having a dopant level of 7.5wt% (Pirelli Ltd.); the other is single-mode 'laser' fibre, the diameter of which was 3µm/125µm (York Ltd.) with a dopant level ~300ppm. A short length of doped fibre (1cm for the multimode, 26cm for the single-mode) of appropriate length to give an adequate absorption of the pump light and sufficient fluorescence signal was fusion-spliced to the sensor arm of a 2×1 optical fibre coupler and this sensor element was placed loosely in a stainless tube and centered in a stable oven (CARBOLITE type: MTF 12/38/400). The other end of the doped fibre was fusion spliced to a piece of plain fibre, on which a weight was applied by means of a pulley. Thus, the magnitude of the weight can be related easily to the value of the strain exerted on the doped fibre through a knowledge of both its dimensions and mechanical properties. The 2×1 optical fibre coupler was used to transmit the excitation light to the sensing probe, and to collect the resulting fluorescence response from the sensor element. The photodetector used was a silicon based, highly sensitive, high-speed avalanche photodiode (APD) module and the phase-locked detection (PLD) method was

employed for processing the fluorescence signal [26], where the PLD module was used to transform directly the fluorescence signal into a TTL compatible frequency signal, whose period is then directly proportional to the measured fluorescence lifetime. This frequency signal was transmitted to a desktop computer which was equipped with a counter-and-timer card to monitor continuously the output and record the lifetime measurement.

When the doped fibre was stretched by using a calibrated constant weight and kept at a stabilized temperature, the PLD scheme is accurate enough to keep the fluctuation of the sampled lifetime data within $\pm 0.05\mu\text{s}$, which excludes other possibilities for a lifetime variation than that due to the strain imposed (within the quoted oven sensitivity), to produce the phenomenon observed in the strain sensitivity test. For the multimode Nd doped fibre, a strain level of up to $1400\mu\epsilon$ has been applied and tests carried out over a range of temperatures, whilst for the single-mode fibre, a limit of $600\mu\epsilon$ has been set, due to its different physical properties. These values are chosen to be below the experimentally observed strain which causes fibre fracture, and represent an extension of $>1\%$ and just less than 1% respectively. Fibre fracture was observed at $\sim 2.4\%$ extension ($\sim 2400\mu\epsilon$ in the multimode fibre test at room temperature)

6.4.2 Experimental results

6.4.2.1 Multi-mode fibre

At each of stabilized temperatures used, these being room temperature ($\sim 20^\circ\text{C}$), 60°C , 100°C and 150°C , the magnitude of the weight applied to the multimode Nd doped

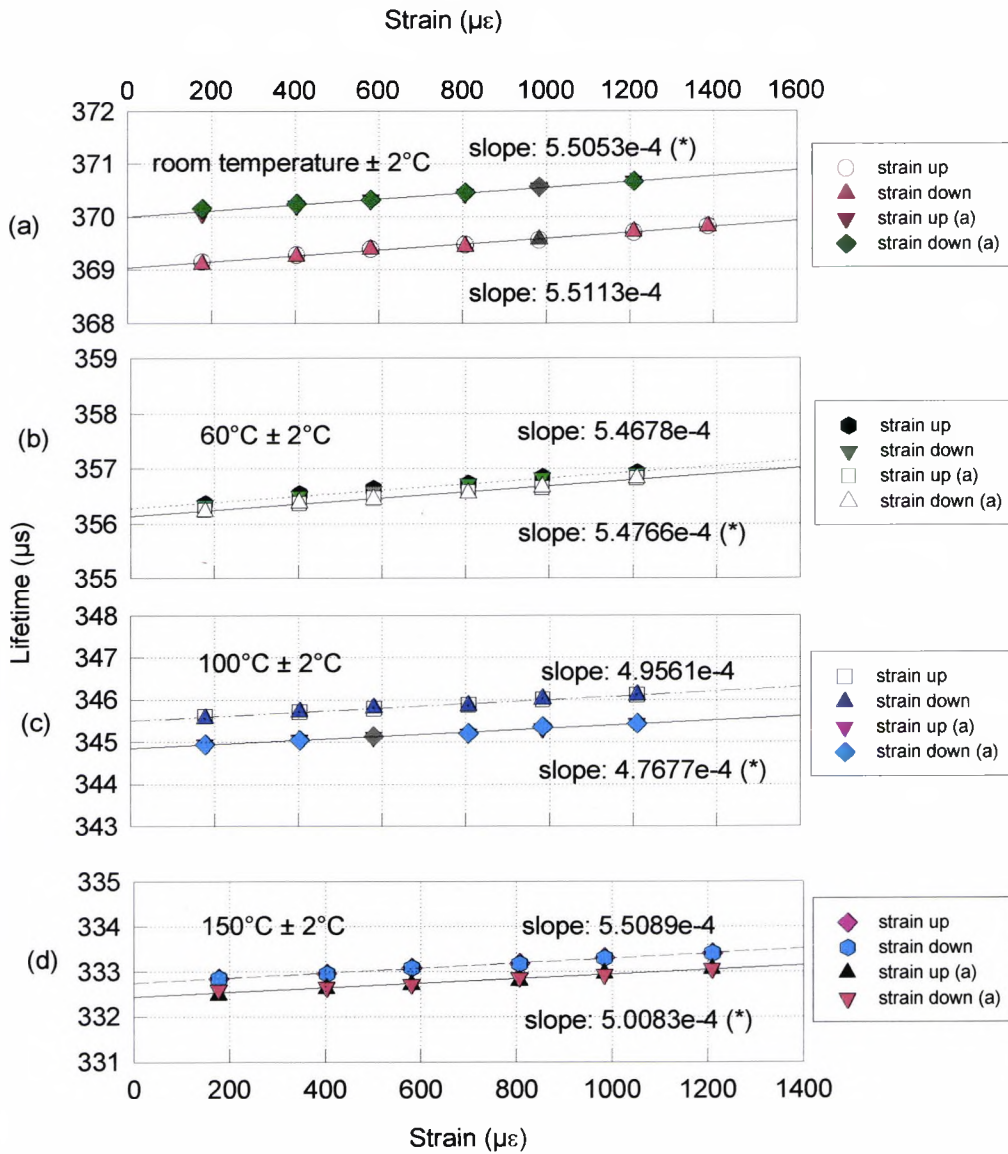


Fig.6.2 The lifetime variation of multimode Nd doped fibre as a function of strain over a range of temperatures before and after "stress annealing", (graphs marked (*)) showing the strain sensitivity of the fluorescence lifetime keeps almost constant regardless of the variation of temperature and strain. (a)-(d) Temperatures are room temperature, 60°C , 100°C , 150°C respectively ($\pm 2^\circ\text{C}$ in each case)

fibre was increased, step by step, giving increments of $\sim 200\mu\epsilon$, to ensure that the strain

on the doped fibre increased gradually and progressively from 0 to 1400 $\mu\epsilon$. The corresponding fluorescence lifetimes which were monitored, as a function of converted strain, are presented in Fig.6.2. Results are shown for each temperature and for strain applied ('strain up') and strain removed ('strain down') (i.e. one 'roundtrip') to investigate if any hysteresis occurred and could be observed.

The results show that with increase of temperature, the lifetime of the fluorescence generated by the doped fibre at the same level of strain decreases dramatically compared with the strain-induced lifetime variations, at constant temperature (the temperature characteristics have been discussed in detail elsewhere[8][9]). At each stabilized temperature also shown in Fig.6.2, the lifetime of the fluorescence signal observed from the multimode Nd doped fibre increases quite linearly with increasing strain, where the rate of the variation is approximately $5(\pm 0.5) \times 10^{-4} \mu\text{s}/\mu\epsilon$ and the lifetime variation induced by the maximum applied strain (1400 $\mu\epsilon$) is equivalent to the lifetime change caused by a temperature variation of about 2.5°C. The 'roundtrip' strain test undertaken, with weights applied and then removed progressively showed that the sensing system is free from hysteresis and the system is fully reversible, both of which are characteristics essential for effective sensor application. It is interesting to notice that the normalized slope of each linear plot of fluorescence lifetime versus strain is almost the same regardless of the increase of temperature, as shown in Fig.6.3, which indicates that the strain-induced lifetime variation rate is strain and temperature independent. Similar results have been reported by Shen et al in experiments on the application of pressure to bulk Cr³⁺:YAG[11] samples. This stable behaviour of the

multimode Nd doped fibre under applied stress makes it highly suitable for accurate and reproducible sensor calibration and signal compensation.

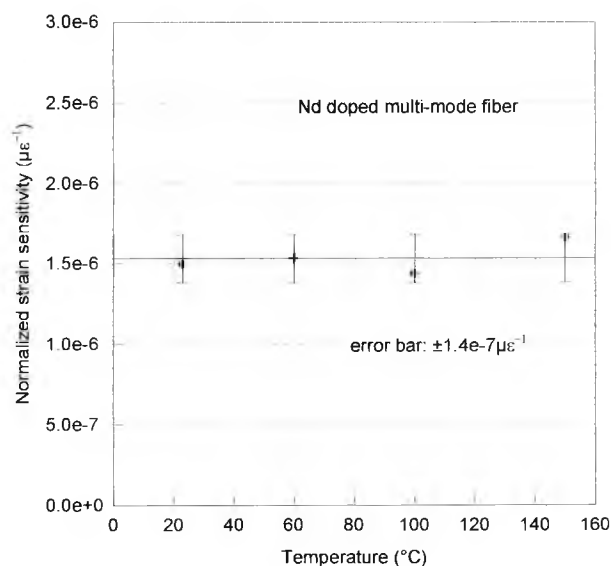


Fig.6.3 The normalized strain sensitivity of the fluorescence lifetime for multimode Nd doped fibre, as a function of temperature

Fig.6.4 clearly shows that fluorescent lifetime changes dramatically with the variation of temperature, with the effect of strain superimposed over the temperature region studied. The lifetime is seen to change by approximately $0.6\mu\text{s}$ when the strain changes from $180\mu\epsilon$ to $1210\mu\epsilon$, as indicated in Fig.6.4, which lifetime change is equivalent to that caused by a temperature variation of approximately 2°C . Thus, although the magnitude of the temperature effect is greater, the two effects are independent and repeatable, facilitating strain and temperature separation in sensor systems using these materials.

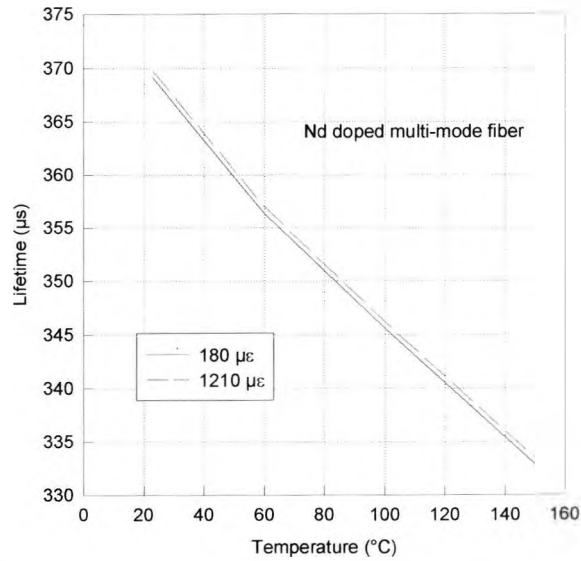


Fig.6.4 Lifetime variation of multimode Nd doped fibre as a function of temperature as well as strain: solid line 180µε applied, dashed line 1210µε applied

In a parallel way to the thermal annealing discussed for temperature sensing using doped fibre, a study of the ‘stress annealing’ process, in which a weight was applied to a single doped fibre for a long period to see whether there is a change in its fluorescence lifetime characteristics, has also been undertaken. In this work, a multimode Nd fibre was ‘stress annealed’ for 100 hours under a constant 800µε strain and the results obtained before and afterwards are shown in Fig.6.2 ((a) to (d) for several temperatures; the asterisk(*) represents the results obtained after ‘stress annealing’), which shows that this has no effect on the lifetime behaviour of the multimode Nd doped fibre under such stress. The $\leq 1\mu\text{s}$ shift of lifetime before and after the ‘stress annealing’ at room temperature shown in Fig.6.2 (a) is due to the fact that the room temperature had drifted over the course of the work. The slight drift of lifetime at the other temperatures recorded in Fig.6.2 (b) to (d) was caused by the

calibration error of the oven (typically $\pm 2^\circ\text{C}$) and the reproducibility of the temperature of the study, reinforcing the observation that the fibres are particularly sensitive to temperature changes. In general, the multimode Nd doped fibre under test was shown to have a lifetime sensitivity of $0.28(\pm 0.03)\mu\text{s}/^\circ\text{C}$ to temperature and $5(\pm 0.5)\times 10^{-4}\mu\text{s}/\mu\epsilon$ to strain. As mentioned earlier, tests showed a value of $2400\mu\epsilon$ was the strain 'in the limit' for the multimode Nd doped fibre sensor at room temperature in this study (at which the probe broke), although the doped fibre may be able to endure higher strain because the breaking point each time in the experiment was not located in the doped fibre or at the fusion splice, but within the multimode plain fibre used for coupling. With the increase of temperature, it was shown that the maximum value of strain the doped fibre can sustain decreases by $\sim 8\mu\epsilon/^\circ\text{C}$.

6.4.2.2 Single-mode fibre

Several tests were carried out on a sample of single-mode Nd fibre, originally purchased for use in a simple fibre laser. The fibre used had the following characteristics: $3.5\mu\text{m}$ core diameter and $125\mu\text{m}$ outer diameter, NA of 0.21 and core composition of $\text{SiO}_2\text{-GeO}_2$ glass with ~ 300 parts in 10^6 of Nd^{3+} . An investigation was made to see if the results obtained from it were consistent with those from the multimode fibre.

Tests were carried out over the same temperature range as was used for the multimode fibre and the results of a fluorescence lifetime versus strain plot for single-mode fibre at 150°C are shown in Fig.6.5, in which the lifetime variation rate measured was

approximately $4(\pm 1) \times 10^{-4} \mu\text{s}/\mu\epsilon$ with no hysteresis seen in the “roundtrip”. Errors are larger than was observed with the multimode fibre, due to the poorer coupling of light from the same source into the single-mode fibre and the much lower level of fluorescence signal observed. However, the calibration graph produced is quite consistent with the results obtained from the multimode Nd doped fibre, although the dopant level and fibre length used were not the same, and the population of the modes of the fibre different in the two cases.

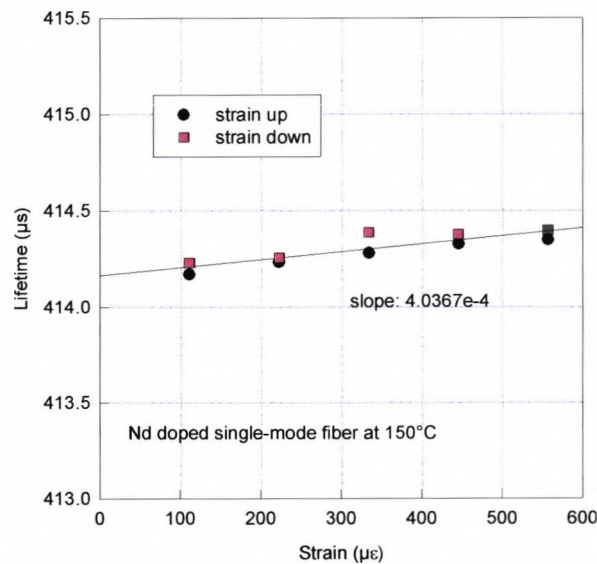


Fig.6.5 Lifetime variation of single-mode Nd doped fibre as a function of strain, at 150°C, for both strain applied (strain up) and removed (strain down)

6.4.3 Discussion of the results for Nd-doped fibre

The above investigation of the characteristics of Nd doped fibres, multimode as well as single-mode, in terms of their strain characteristics, has revealed a number of interesting conclusions both on the nature of the fibre itself and its utility as a practical sensor. This effect is complementary to their well-known thermal behaviour, where

this type of fibre has shown itself satisfactory for thermometry due to its high temperature sensitivity. In sensor use, any stress effect present in the fibre can be compensated in the signal processing, allowing its influence to be removed easily by the software, responding to the calibration. Furthermore, there is no hysteresis of the lifetime observed in the strain 'roundtrip' and this feature is very important in sensor applications. Also 'stress annealing' results show that the doped fibre sensor is not sensitive to environmental stress treatment with long term stress application.

6.5 Temperature and strain effect on Yb-doped fibres

6.5.1 Experimental arrangement

The experimental arrangement used for the measurement of the strain-induced fluorescence characteristics of the Yb-doped fibre over a range of temperatures up to 150°C is essentially illustrated in Fig.6.1, which is similar to the setup for the Nd-doped fibre strain test described above[27]. In this case, however a laser diode with a center wavelength of 980nm is employed as the source, light from which couples well to a major absorption band of the material[28], and conveniently this is the same source that may be used to excite Er in a range of fibres, facilitating their use together in a network. The Yb doped fibre under test was single mode, of diameter (core/cladding) 2.8µm/124µm and having a dopant level of 2.5wt% (INO, Canada). Preliminary tests showed that a 4cm length of doped fibre was an appropriate length to give an adequate absorption of the pump light and yield sufficient fluorescence signal, and this was fusion-spliced to the sensor arm of a 2×1 optical fibre coupler. This sensor element was placed loosely and centered in a stable test oven (CARBOLITE

Chapter 6 Temperature and strain sensitivities of rare-earth doped fibres

type: MTF 12/38/400). The other end of the doped fibre was fusion spliced to a piece of plain fibre, on which a weight was applied by means of a pulley to create a known stress along its axis. A 2×1 optical fibre coupler was used to transmit the excitation light to the sensing probe, and to collect the resulting fluorescence response from the sensor element. An InGaAs photodetector was employed with the phase-locked detection (PLD) method for processing the fluorescence signal[26] and the signal was transmitted to a desktop computer which was equipped with a counter-and-timer card to monitor continuously the output and record the lifetime measurement mode.

When the doped fibre was stretched by using a calibrated constant weight and kept at a stabilized temperature, the fluctuation of the sampled lifetime data was within $\pm 1.5\mu\text{s}$, which makes the long time averaging (~ 1.5 hours) used necessary to show the strain effect clearly. This is clearly longer than would routinely be applied in any practical sensor situation, but is used here to minimize the errors for any single strain measurement to calibrate the system. For the moment, the system is configured to examine static rather than dynamic strain. For the single mode Yb doped fibre used, a strain level of up to $800\mu\epsilon$ has been applied and tests were carried out over a range of temperatures up to the normal specified temperature of the fibre itself. These values are chosen to be below the experimentally observed strain which causes fibre fracture, and represent an extension of up to 0.8%.

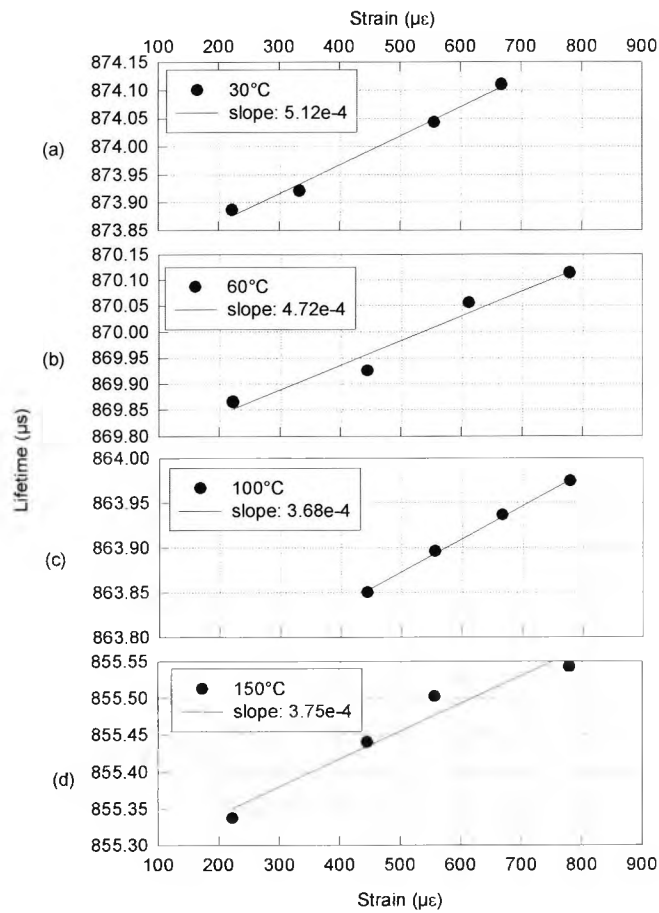


Fig.6.6 The lifetime variation of the single mode Yb doped fibre as a function of strain over a range of temperatures showing the strain sensitivity of the fluorescence lifetime.

(a)-(d) Temperatures are 30°C, 60°C, 100°C, 150°C respectively ($\pm 5^\circ C$ in each case)

6.5.2 Experimental results

At each of stabilized temperatures used, these being 30°C, 60°C, 100°C and 150°C, the magnitude of the weight applied to the Yb doped fibre was increased, step by step, in increments of $\sim 200\mu\epsilon$, to ensure that the strain on the doped fibre rose gradually and progressively from 0 to $800\mu\epsilon$. The corresponding fluorescence lifetimes monitored and averaged over hundreds of cycles, as a function of converted strain, are presented

in Fig.6.6. Results are shown for each temperature and for strain applied to investigate more fully the tendency shown by this change.

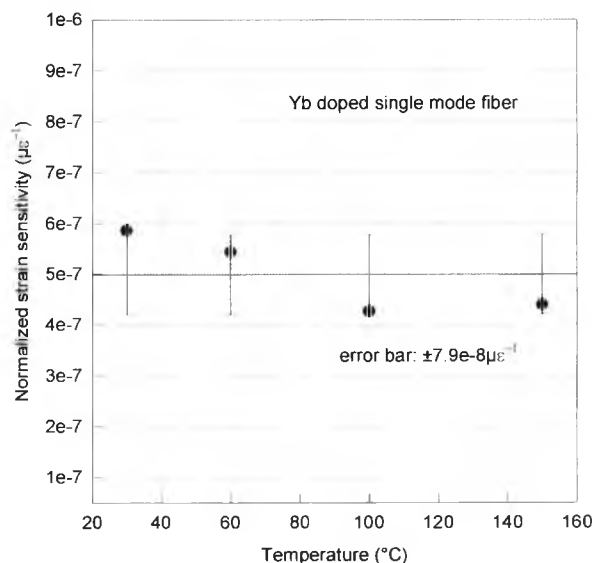


Fig.6.7 The normalized strain sensitivity of the fluorescence lifetime for single mode Yb doped fibre, as a function of temperature over the region 30-150°C

The results show that with the increase of temperature, the lifetime of the fluorescence generated by the doped fibre decreases dramatically compared with the strain-induced lifetime variations, the temperature characteristic of which has been discussed in detail elsewhere by the authors[29]. At each stabilized temperature also shown in Fig.6.6, the lifetime of the fluorescence signal observed from the Yb-doped fibre increases quite linearly with increasing strain, where the rate of the variation is approximately $4.3(\pm 0.8) \times 10^{-4} \mu\text{s}/\mu\epsilon$ and the lifetime variation induced by the maximum applied strain ($800\mu\epsilon$) is equivalent to the lifetime change caused by a temperature variation of about 5°C. The above section has shown that the lifetime variation rate of Nd doped fibre with increasing strain is approximately $5(\pm 0.5) \times 10^{-4} \mu\text{s}/\mu\epsilon$, which is within experimental

error the same as that of Yb in this work, although the fibre modes, concentration level and the rare earth ion are different in each case. This would appear to suggest that the silica host makes the main contribution to the strain effect although the actual mechanism has not been examined in detail. It is interesting to notice that the normalized slope of each linear plot of fluorescence lifetime versus strain is almost the same regardless of the increase of temperature, as shown in Fig.6.7. This is similar to the results discussed above on Nd-doped fibre, which also indicated that the strain-induced lifetime variation rate is temperature independent. Similar results have been reported by Shen et al in experiments on the application of pressure to bulk Cr^{3+} :YAG[21] samples. This configuration of the stable behaviour of the single mode Yb doped fibre under applied stress makes it highly suitable for accurate and reproducible sensor calibration and signal compensation.

Fig.6.8 clearly shows that fluorescent lifetime changes dramatically with the variation of temperature, with the effect of strain superimposed over the temperature region studied. The lifetime is seen to change by approximately $0.3\mu\text{s}$ when the strain changes from $200\mu\epsilon$ to $800\mu\epsilon$, as indicated in Fig.6.8, which lifetime change is equivalent to that caused by a temperature variation of approximately 4°C . Thus, although the magnitude of the temperature effect is greater, the two effects are independent and repeatable, facilitating strain and temperature separation in sensor systems using these materials. In general, the single mode Yb doped fibre under test was shown to have a lifetime sensitivity of $0.07(\pm 0.01)\mu\text{s}/^\circ\text{C}$ [28] to temperature which yields a $6.1 \times 10^{-3}^\circ\text{C}/\mu\epsilon$ ratio of the strain to temperature sensitivity.

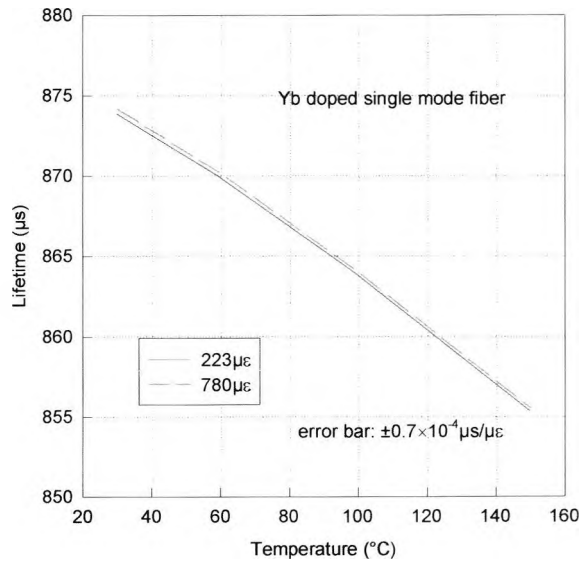


Fig.6.8 Lifetime variation of single mode Yb doped fibre as a function of temperature as well as strain: solid line 200µε applied, dashed line 800µε applied

6.5.3 Discussion of Yb-doped fibre results

The above investigation of the strain characteristics of single mode Yb doped fibres, has revealed a number of interesting conclusions both on the nature of the fibre itself and its potential utility as a practical sensor. This effect is complementary to its thermal behaviour, investigated previously, where this type of fibre has shown itself satisfactory for thermometry due to its high temperature sensitivity. In sensor use, any stress effect present in the fibre can be compensated in the signal processing, based on the lifetime variation rate being independent of the temperature, and the strain applied, showing no significant change with the type of doped rare earth ion, concentration level and mode form, allowing its influence to be removed easily by the software used, and responding to the calibration of the system.

6.6 Summary

The investigation of strain and temperature sensitivities of Nd and Yb doped fibres has been carried out in this work. Results obtained are compared with each other, showing that the lifetime variation rate of the doped fibres with increasing strain is temperature independent, and the rates are within experimental error the same, although in each case, the fibre modes, the dopant concentration level and the rare earth ion itself are different. Their stable behaviour may form the basis of a dual element sensor with which to obtain stress and temperature information independently in so-called “smart structure”. This may use two doped fibre elements, possibly for ease of signal processing each having different dopants (different thermal characteristics), or it may comprise a doped fibre with another stress sensitive element, such as an in-fibre Fabry-Perot filter or Bragg grating. Work has begun by the authors and others in this field[30] and a number of possibilities are being explored.

Through the comparison of the stress effect of Nd and Yb obtained, it seems that the lifetime variation when the strain applied is selected closely to the nature of the host material rather than the dopant primarily. To aid the sensor designer, further work needs to be done on the stress behavior of various doped fibres, in particular to investigate their performance as a function of several additional factors, such as the length of fibre used, the effect of heat treatment and especially the host material for sensor optimization.

6.7 References

- [1]. J.D.C.Jones, Review of fibre sensor techniques for temperature-strain discrimination, *Proc. 12th International Optical Fibre Sensors Conference*, Williamsburg, VA, USA, October, 1997, OSA Tech. Digest Series, 16, 36(1997)
- [2] E.J.Friebele, M.A.Putnam, H.J.Patrick, A.D.Kersey and A.S.Greenblatt, Ultrahigh-sensitivity fibre-optic strain and temperature sensor, *Optics Letters*, 23, 222(1998)
- [3] T.R.Parker, M.Farhadiroushan, R.Feced, V.A.Handerek and A.J.Rogers, Simultaneous distributed measurement of strain and temperature from noise-initiated Brillouin Scattering in optical fibres, *IEEE Journal of Quantum Electronics*, 34, 645(1998)
- [4] W.W.Morey, G.Meltz and J.M.Welss, *Proc. OFS'8*, paper PD-4, 1992
- [5] M.G.Xu, J.L.Archambault, L.Reekie and J.P.Dakin, Discrimination between strain and temperature effects using dual-wavelength fiber grating sensors, *Electron. Lett.*, 30, 1085(1994)
- [6] G.P.Brady, K Kally, D.J.Webb, D.A.Jackson, L.Zhang and I.Bennion, Recent developments in optical-fiber sensing using fiber Bragg gratings, *SPIE 2839*, 8(1996)
- [7] S.W.James, M.L.Dockney and R.P.Tatam, Simultaneous independent temperature and strain measurement using in-fibre Bragg grating sensors, *Electron. Lett.*, 32, 1133(1996)
- [8] S.E.Kanellopoulos, V.A.Handerek and A.J.Rogers, Simultaneous strain and temperature sensing with photogenerated in-fiber gratings, *Opt. Lett.*, 20, 333(1995)

- [9] H.J.Patrick and S.T.Vohra, Fibre Bragg grating with long period fibre grating superstructure for simultaneous strain and temperature measurement. *European Workshop on Optical Fibre Sensors*, 8-10 July 1998, Peebles, Scotland, 264(1998)
- [10] L.A.Ferreira, R.A.B.Lobo, J.L.Santos and F.Farahi, Simultaneous measurement of displacement and temperature using a low finesse cavity and a fiber Bragg grating, *Photon. Technol. Lett.*, 8, 1519(1996)
- [11] H.Singh and J.Sirkis, *OFS'11*, 108(1996)
- [12] M.Sudo, M.Nakai, K.Himeno, S.Suzaki, A.Wada and R.Yamauchi, Simultaneous measurement of temperature and strain using PANDA fibre grating, *OFS'12*, 170(1997)
- [13] L.A.Ferreira, F.M.Araujo, J.L.Santos and F.Farahi, Simultaneous strain and temperature sensing using an interferometrically interrogated fibre Bragg grating written in bow-tie fibre, *European Workshop on Optical Fibre Sensors*, 8-10 July 1998, Peebles, Scotland, 49(1998)
- [14]. J.F.Lei and H.A.Will, Thin-film thermocouples and strain-gauge technologies for engine applications, *Sensors and Actuators A*, 65, 187(1998)
- [15]. K.T.V.Grattan, Z.Y.Zhang, *Fibre Optic Fluorescent Thermometry* (Chapman & Hall, London, 1995).
- [16]. V. Fericola and R.Galleano, Optical fibre thermometry by laser-induced fluorescence, *Proceedings of TEMPMEKO'96*, 6th International Symposium on Temperature and Thermal Measurements in Industry and Science, Levrotto&Bella – Torino, Italy, 427(1996)

- [17]. Z.Y.Zhang, K.T.V.Grattan, A.W.Palmer, B.T.Meggitt and T.Sun, Fluorescence decay-time characteristics of erbium-doped optical fibre at elevated temperatures, *Rev. Sci. Instrum.*, 68, 2764(1997)
- [18]. Z.Y.Zhang, K.T.V.Grattan, A.W.Palmer and B.T.Meggitt, Spectral characteristics and effects of heat treatment on intrinsic Nd-doped fibre thermometer probes, *Rev. Sci. Instrum.*, 69, 139(1998)
- [19] Z.Y.Zhang, K.T.V.Grattan, A.W.Palmer and B.T.Meggitt, Potential for temperature sensor applications of highly neodymium-doped crystals and fibre at up to approximately 1000°C, *Rev. Sci. Instrum.*, 68, 2759(1997)
- [20] S.W.Allison and G.T.Gillies, Remote thermometry with thermographic phosphors: Instrumentation and applications, *Rev. Sci. Instrum.*, 68, 2615(1997)
- [21]. Y.R.Shen and K.L.Bray, Effect of pressure and temperature on the lifetime of Cr^{3+} in yttrium aluminum garnet, *Physical Review B*, 56, 10882(1997)
- [22]. J.H.Eggert, K.A.Goettel and I.F.Silvera, Ruby at high pressure. II. Fluorescence lifetime of the *R* line to 130gpa, *Physical Review B*, 40, 5733(1989)
- [23]. U.Hommerich and K.L.Bray, High-pressure laser spectroscopy of $\text{Cr}^{3+}:\text{Gd}_3\text{Sc}_2\text{Ga}_3\text{O}_{12}$ and $\text{Cr}^{3+}:\text{Gd}_3\text{Ga}_5\text{O}_{12}$, *Physical Review B*, 51, 12133(1995)
- [24] W.Jin, W.C.Michie, G.Thursby, M.Konstantaki and B.Culshaw, Simultaneous measurement of strain and temperature: error analysis, *Opt. Eng.*, 36, 598(1997)
- [25] C.C.Chan, W.Jin, A.B.Rad and M.S.Demokan, Simultaneous measurement of temperature and strain: an artificial neural network approach, *IEEE Photonics Technology Letters*, 10, 854(1998)

- [26] Z.Y.Zhang, K.T.V.Grattan and A.W.Palmer, Phase-locked detection of fluorescence lifetime, *Rev. Sci. Instrum.*, 64, pp2531, 1993
- [27] T.Sun, Z.Y.Zhang, K.T.V.Grattan and A.W.Palmer, Intrinsic doped fluorescence decay-time based measurements – strain and temperature characteristics for sensor purposes, *Rev. Sci. Instrum.*, 69, 4186(1998)
- [28] R.Paschotta, J.Nilsson, A.C.Tropper and D.C.Hanna, Ytterbium-doped fibre amplifiers, *IEEE J.Quantum Electron.*, 33, 1049(1997)
- [29] T.Sun, Z.Y.Zhang, K.T.V.Grattan and A.W.Palmer, Ytterbium-based fluorescence decay time fibre optic temperature sensor systems, *Rev. Sci. Instrum.*, 69, 4179(1998)
- [30]] T.Liu, G.F.Fernando, Z.Y.Zhang and K.T.V.Grattan, Strain and temperature measurements using interferometric and rare-earth doped fibre sensor techniques for composite materials, *Eurosensors XII, Proceedings of the 12th European Conference on Solid-State Transducers and the 9th UK Conference on Sensors and their Applications*, Southampton, UK, 13-16 September 1998 (Ed. N.M.White), 323(1998)

Chapter 7

Comparison of Two Fluorescence-based Schemes using Intensity and Decay Time Approaches

7.1 Abstract

The performance of the two most promising fluorescence-based temperature sensing techniques, namely the fluorescence intensity ratio (FIR) and fluorescence lifetime (FL) schemes, have been compared. Theoretical calibration graphs for the two methods produced in this work illustrate the useful monotonic change of the response with temperature variation. Comparison of the responses and the sensitivities of the two schemes show that at very low temperatures the FIR method exhibits a significant variation with temperature, while the response of FL method becomes constant with its sensitivity approaching zero. With increasing temperature, the FIR and the FL methods (with short relaxation times and shorter intrinsic lifetimes of the upper energy levels) share a similar sensitivity over a wide temperature range. The presence of a long relaxation time or a longer intrinsic lifetime of the upper level in the use of the FL method is seen to give a less satisfactory response.

Experimental data obtained for a range of dopant ions in various host materials are found to be consistent with the results of the theoretical analysis, with each material considered having a specific energy gap difference. The sensitivities of each material are compared graphically, which would allow the most appropriate sensor for an intended application to be selected. Comparison is made with the results of systems described earlier, and of literature reports on similar materials using the FIR approach.

7.2 Introduction

The underlying physical principle exploited in the temperature sensors described earlier using ions doped into appropriate hosts is the thermalization which occurs between closely-spaced excited ionic energy levels when the levels are populated using an appropriate excitation source, usually an LED or LD. The two schemes compared in this Chapter exploit very different aspects of the resultant fluorescence emission from these levels in several promising materials. Both schemes have the major advantage of being independent of possible fluctuations of the excitation source, which is very important for robust temperature sensing.

Fluorescence lifetime (FL) based temperature sensing techniques have been investigated over a number of years[1][2]. Pulsed excitation is required and the subsequent temperature-dependent fluorescence decay from the excited levels may be monitored with a single detector and appropriate electronics. Analysis of the

Chapter 7 Comparison of two fluorescence-based schemes

exponential decay enables the fluorescence lifetime to be determined, as has been discussed in detail in previous Chapters

At the same time various investigations into devices based on a fluorescence intensity ratio (FIR) in rare-earth-doped optical materials (including fibres) have been undertaken and reported in the literature[3][4]. In this technique, the fluorescence from two closely-spaced levels to a common final state is monitored, at the appropriate wavelengths, and the ratio of the two emission intensities is calculated, resulting in a temperature-dependent quantity which is also independent of the source intensity. Generally a periodic excitation is used in conjunction with phase-sensitive detection to improve the signal-to-noise ratio because the intensity from the upper level will be small at low temperatures.

Both these sensor techniques show considerable promise and have been studied in detail for a range of materials, some of which have been discussed in earlier Chapters, so a comparison of the merits of each scheme is of particular interest. Given the wide-range of possible applications for temperature sensors, it is clear that as industry requires specialized sensors for specific processes, no one sensor of either type using a given material or active ion will be suitable for all situations of high or low temperature monitoring, range, sensitivity and stability. However a comparison of the underlying physical basis of the two techniques is of particular value in the development and selection of the most appropriate method to be used in any specific application.

7.3 Background theory

7.3.1 FL scheme

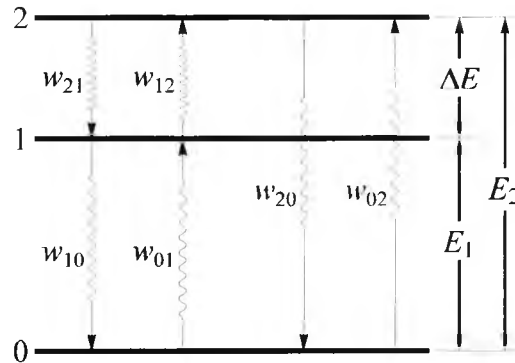


Fig.7.1 Schematic energy level diagram of the three level model of a typical fluorescent ion

The simplified energy level diagram of a typical fluorescent material depicted in Fig. 7.1 shows two closely-spaced upper states, levels 1 and 2 (energy separation ΔE), which may decay radiatively to level 0. When levels 1 and 2 are excited through some pumping scheme (the details of which are not important here) the relevant populations, N_0 , N_1 and N_2 respectively, are given by the following rate equations[5]

$$\begin{aligned} \frac{dN_1}{dt} &= N_2 A_{21} - N_1 (w_{12} + A_{10}) + N_0 w_{01} \\ \frac{dN_2}{dt} &= N_1 w_{12} - N_2 (A_{21} + A_{20}) + N_0 w_{02} \\ \frac{dN_0}{dt} &= N_1 A_{10} + N_2 A_{20} - N_0 (w_{01} + w_{02}) \end{aligned} \quad (7.1)$$

where A_{ij} and w_{ij} are the spontaneous transition rate and the absorption rate, respectively, of the ions from level i to level j (where i, j are integers). Thermalization

occurs between the excited levels and so $b_{21} = \frac{g_2}{g_1} e^{-\Delta E_{21}/kT}$ represents the ratio of the

populations in levels 1 and 2 at equilibrium, with g_1 and g_2 being the respective degeneracies, k Boltzmann's constant and T the kelvin temperature. Applying a Laplace transform to Eq. (7.1), and if the relaxation time of the upper levels is not very short, the resulting reciprocal lifetime is

$$\frac{1}{\tau} = \frac{1}{2} \left[(1 + b_{21})A_{21} + A_{20} + A_{10} - \sqrt{[(b_{21} - 1)A_{21} + A_{10} - A_{20}]^2 + 4b_{21}A_{21}^2} \right] \quad (7.2)$$

When the relaxation time between levels 1 and 2 is extremely short (due to rapid thermalization), the resultant fluorescence lifetime will be given by

$$\tau = (1 + b_{21}) / (A_{10} + A_{20}b_{21}) \quad (7.3)$$

the same result as that obtained from the use of a two-level model based on the assumption of thermal equilibrium[6][7]. Measurements to obtain the lifetime can be performed at either just one of the fluorescence wavelengths or over a larger bandwidth covering all decays from the thermalizing levels. The equations can be readily modified if more than two excited levels are involved.

7.3.2 FIR scheme

For radiation at a particular wavelength corresponding to the transition from levels $i \rightarrow f$ the intensity exhibits the proportionality[7]

$$I_{if} \propto N_i \omega_{if} A_{if} \quad (7.4)$$

where ω_{if} is the angular frequency of the radiation. If the separate fluorescence lines from two closely-spaced levels (1 and 2 in Fig. 7.1) are monitored, the intensity ratio for the transitions from levels 1 and 2 to level 0 will therefore be given by

$$R = \frac{I_{20}}{I_{10}} = \frac{N_2 \omega_{20} A_{20}}{N_1 \omega_{10} A_{10}} = \frac{\omega_{20} A_{20}}{\omega_{10} A_{10}} \frac{g_2}{g_1} \exp\left(\frac{-\Delta E_{21}}{kT}\right) = B \exp\left(\frac{-\Delta E_{21}}{kT}\right) \quad (7.5)$$

with $B = \frac{\omega_{20} A_{20}}{\omega_{10} A_{10}} \frac{g_2}{g_1}$.

The underlying physical basis of the two fluorescence temperature sensors of interest is given in Eqs. (7.2) and (7.3) for the FL method and Eq. (7.5) for the FIR method. It is clear that both techniques result in a quantity which is independent of the source intensity, as required of an effective temperature monitoring scheme, and which is also a non-linear function of temperature. The actual variation of this quantity with temperature, although very different for the two methods, provides the calibration for the system.

7.4 Theoretical temperature dependence and sensitivity

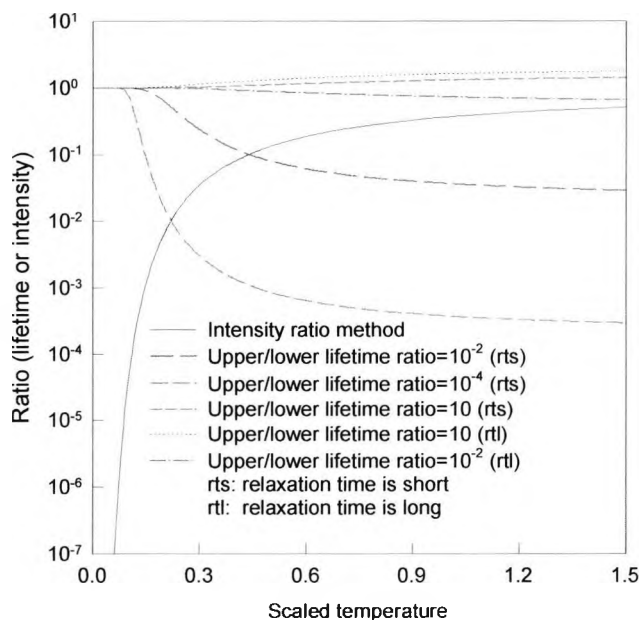


Fig.7.2 Comparison of the performance of the FIR and FL methods with scaled temperature variation, for various parameter values

In order to compare the two methods, the response characteristics given by Eqs. (7.2), (7.3) and (7.5) have been plotted in Fig. 7.2, using a degeneracy ratio g_2/g_1 of 1, as a

Chapter 7 Comparison of two fluorescence-based schemes

function of a scaled dimensionless temperature parameter t , with $t = kT/\Delta E_{21}$ (where typical values of $T = 1000$ K, $\Delta E_{21} = 1000$ cm⁻¹ give $t = 0.69$). The function represented by Eq. (7.5) for the FIR method may be plotted directly, but for the FL method it is more convenient to display τ/τ_1 , being the ratio of the thermalized lifetime, τ , from Eqs. (7.2) or (7.3) to the lower level lifetime, $\tau_1 (= 1/A_{10})$. The upper and the lower levels have different lifetimes and so curves for the lifetime method are plotted for three different values of $\tau_2/\tau_1 (= A_{10}/A_{20})$, where τ_2 is the upper level lifetime, namely 10, 10⁻² and 10⁻⁴ and $A_{21} \gg A_{10}$ has been assumed in the plot of Eq. (7.2). In order to plot Eq. (7.5) it has been assumed that the transition rate and angular frequency ratios are both 1 (the second assumption is true provided levels 1 and 2 are closely spaced), i.e. $B = 1$. Therefore both sets of graphs are shown as ratios on the same vertical axis in which a logarithmic scale has been used in order that the trends may be seen more clearly.

The responses of the two methods to temperature change are very different, even though all the curves exhibit a useful monotonic change in response with temperature variation. At very low temperatures, the fluorescence lifetime is approximately equal to the lifetime of the lower level, and at higher temperatures it either decreases or increases, depending on the intrinsic lifetime ratio of the upper and lower levels. When the intrinsic upper level lifetime is shorter than the lower ($\tau_2/\tau_1 < 1$), the lifetime decreases with temperature increase, but the rate of decrease depends upon the lifetime ratio of the upper and lower levels, as well as the relaxation time. The smaller lifetime

ratio of the two levels with the shorter relaxation time (i.e. Eq. (7.3)) gives a greater variation in the lifetime with temperature. When the upper level intrinsic lifetime is longer than the lower ($\tau_2/\tau_1 > 1$), the lifetime increases as the temperature increases and when the intrinsic lifetime of the upper level is greater, the variation with temperature is larger. The intensity ratio, on the other hand, increases rapidly with increasing temperature at low temperatures, and the rate of increase itself decreases with increasing temperature until it asymptotes to 1 at very high temperatures. It is clear that both methods will not work particularly well at very high temperatures (approximately $T > 1000$ K, where fortunately black body techniques become relatively easy to use), and that the fluorescence lifetime method also will not perform so satisfactorily at very low temperatures ($T < 200$ K). However, even though the intensity ratio varies significantly at low temperatures, such a large difference in intensities may be difficult to detect in a practical system in the presence of system noise. At room temperature either method could be used, as in each case the quantity of interest shows significant variation with temperature.

In comparing these two types of sensors it is also worthwhile comparing the sensitivity, S , defined as the fractional rate of change of the response, r , with temperature, i.e.

$\frac{1}{r} \frac{\partial r}{\partial T}$. The sensitivity for the FIR method may be obtained from Eq. (7.5) to be

$$S = \frac{1}{R} \frac{\partial R}{\partial T} = \frac{\Delta E_{21}}{kT^2} = \frac{k}{\Delta E_{21}} \frac{1}{t^2} \quad (7.6)$$

whilst for the FL method (where S_l is defined as the sensitivity for long relaxation time situation and S_s for short relaxation time) the expression may be written as

$$S_l = \frac{1}{\tau} \frac{\partial \tau}{\partial T} = \frac{-\frac{A_{21}}{A_{10}} b_{21} + \frac{\left(\frac{A_{21}}{A_{10}} b_{21} + \frac{A_{21}}{A_{10}} + 1 - \frac{A_{20}}{A_{10}}\right) \frac{A_{21}}{A_{10}} b_{21}}{\sqrt{\left[(b_{21}-1) \frac{A_{21}}{A_{10}} + 1 - \frac{A_{20}}{A_{10}}\right]^2 + 4 \left(\frac{A_{21}}{A_{10}}\right)^2 b_{21}}}}{(1+b_{21}) \frac{A_{21}}{A_{10}} + \frac{A_{20}}{A_{10}} + 1 - \sqrt{\left[(b_{21}-1) \frac{A_{21}}{A_{10}} + 1 - \frac{A_{20}}{A_{10}}\right]^2 + 4 b_{21} \left(\frac{A_{21}}{A_{10}}\right)^2}} \frac{k}{\Delta E_{21} t^2} \quad (7.7)$$

$$S_s = \frac{1}{\tau} \frac{\partial \tau}{\partial T} = \left(1 - \frac{1}{1+b_{21}}\right) \left(\frac{1 - \frac{A_{20}}{A_{10}}}{1 + \frac{A_{20}}{A_{10}} b_{21}}\right) \frac{k}{\Delta E_{21} t^2} \quad (7.8)$$

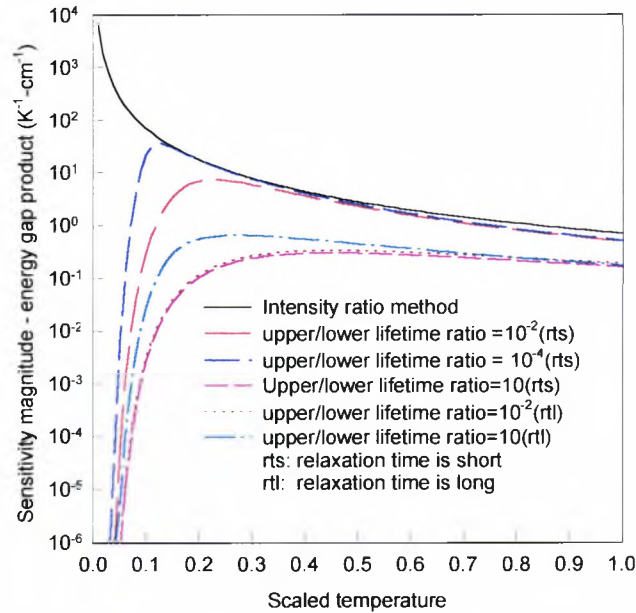


Fig.7.3 Sensitivity-energy gap products of the FIR and FL methods as a function of the scaled temperature, for various parameter values

In Fig. 7.3 the magnitude of the sensitivity-energy gap product, $S \cdot \Delta E$, obtainable directly from Eqs. (7.6) to (7.8), has been plotted as a function of the scaled

temperature, as this gives an expression which is independent of the energy gap. Three different values of the ratio of the upper to lower level lifetimes have been used and the degeneracy ratios have been set to 1, as before. It is interesting to observe the very similar sensitivities for the FIR and FL curves over much of the temperature range when the intrinsic lifetime ratio of the upper to lower level is smaller than 1 and the relaxation time is very short (such as occurs with alexandrite and verified by Gayen *et al*[8], where the nonradiative relaxation time was 27 ps for the ${}^4T_2 \rightarrow {}^2E$ transition). However, when the relaxation time is long or the upper lifetime is larger than the lower, the sensitivity reduces considerably over the same temperature region for the FL scheme. Among materials for FL data having long relaxation time, the use of an upper/lower ratio larger than 1 gives better sensitivity than its counterparts having the ratio smaller than 1. At very low temperatures, the sensitivity of the FL method diminishes significantly, which is to be expected given the flattening of the corresponding response curves in Fig. 7.2. In contrast, the FIR sensitivity is enhanced at very low temperatures although, as noted above, this corresponds to a very large intensity ratio and it may be affected significantly by system noise.

7.5 Comparison of theory with data

In order to verify the above theoretical analysis a number of experimental data sets for the two methods are displayed in Figs. 7.4 and 7.5 and compared with theory. Fig. 7.4 shows FL data, displayed as τ_2/τ_1 (as in Fig. 7.2), plotted as a function of scaled temperature. The FL data were obtained from materials discussed earlier and in the literature: crystals of ruby[1], alexandrite[9], Cr^{3+} :YAG[1] and bulk Pr^{3+} :ZBLAN[5] and have been fitted to Eq.(7.3) for the first three materials, as shown in the diagram. In the case of praseodymium the author and the others[5] found that the relaxation

Chapter 7 Comparison of two fluorescence-based schemes

time is of the same order of magnitude as the intrinsic lifetimes of the upper and lower levels and the upper/lower lifetime ratio is approximately 2, which implies that Eq. (7.2). should be used to fit the data. For ruby, alexandrite and Cr^{3+} :YAG, some data in the high temperature region were not used in the fitting procedure, as the lifetime decreases rapidly as a function of temperature at higher temperatures where thermal quenching occurs, an effect which cannot be described with the simplified model implicit in Eq. (7.3). Elsewhere[1] it has been shown that these data can be fitted very well when more energy levels than are shown in Fig. 7.1 are included. Nevertheless the fit to data for these four materials is very good and supports the approach implied in Eqs. (7.2) and (7.3).

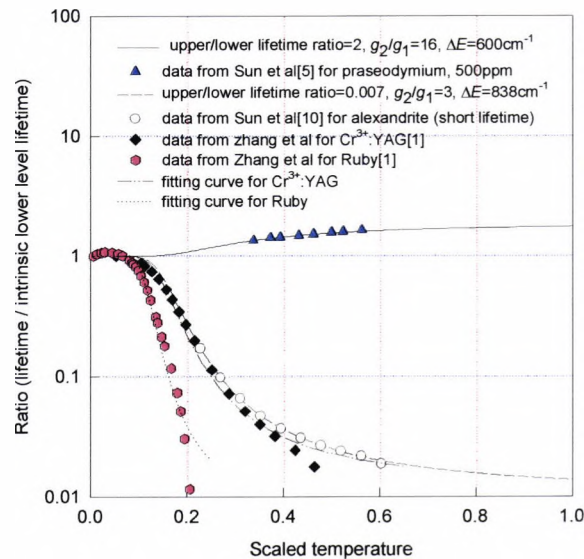


Fig.7.4 The lifetime ratio data as a function of the scaled temperature for crystals of ruby, alexandrite, Cr^{3+} :YAG and bulk Pr^{3+} :ZBLAN, where fitting curves are plotted based on Eqs.(7.3) and (7.2)

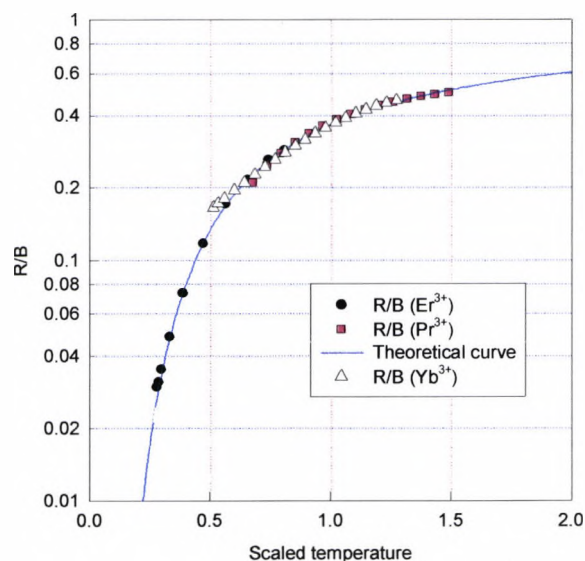


Fig.7.5 Normalized FIR data as a function of the scaled temperature for Er^{3+} -doped fibre, Yb^{3+} -doped fibre and bulk Pr^{3+} :ZBLAN, where fitting curves are plotted based on Eq.(7.5)

In Fig. 7.5 normalized FIR data are shown as a function of the scaled temperature for Er^{3+} -doped fibre[4], Yb^{3+} -doped fibre[10] and bulk Pr^{3+} :ZBLAN[11]. Each data set was fitted using Eq. (7.5) in which the normalizing factor B and ΔE_{21} were the free parameters. All data were divided by the appropriate value of B , and so the three data sets in Fig. 7.5 follow the same curve, as anticipated from Fig. 7.2. The agreement between the experimental results and theory is again very good and the simple theory of operation of FIR sensors implied by Eq. (7.5) is confirmed.

7.6 Temperature responses and sensitivities

On the basis of the theory behind the FL and FIR responses, it is now appropriate to compare the non-normalized data, with fitted curves, as functions of temperature so

that actual measurement requirements may be appreciated. The system responses in Figs. 7.6 and 7.7 (data from Figs. 7.4 and 7.5) show the lifetime and intensity ratio for the FL and FIR methods respectively, with Eqs. (7.6), (7.7) and (7.8) used to fit the data.

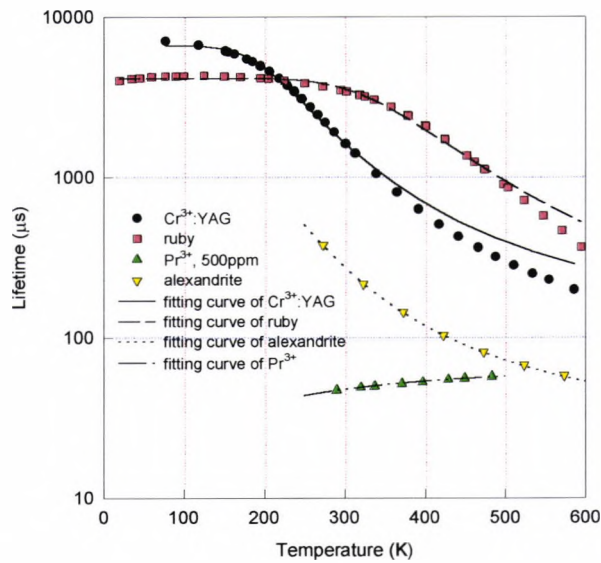


Fig.7.6 The temperature responses for the FL scheme for crystals of ruby, alexandrite, Cr^{3+} :YAG and bulk Pr^{3+} :ZBLAN, where fitting curves are plotted based on Eq.(7.2) and Eq.(7.3)

Praseodymium is one of the few cases where data are available for both methods using similar samples over comparable temperature ranges. It can be seen that the variation of the FIR method is more rapid than that of the FL method over the temperature region from 250 K to 550 K. The signal-to-noise ratio is assumed to be high so that system noise is not an important consideration.

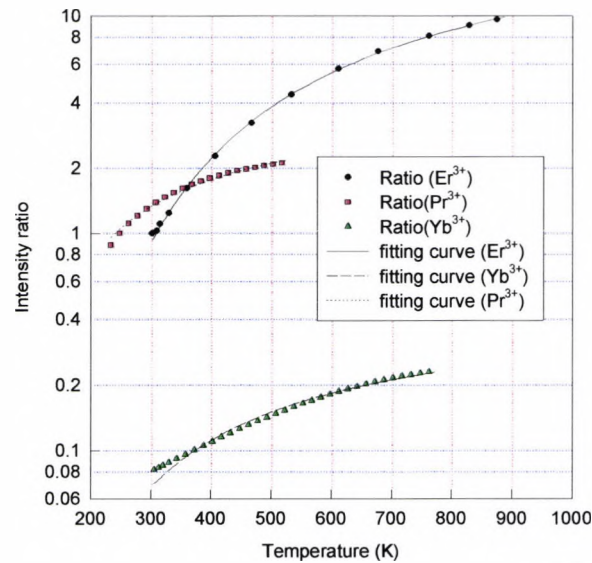


Fig.7.7 The temperature responses for the FIR scheme using Er³⁺-doped fibre, Yb³⁺-doped fibre and bulk Pr³⁺:ZBLAN, where fitting curves are plotted based on Eq.(7.5)

For the other FL data the relaxation time between the upper and lower levels is extremely short and the resultant lifetime, described by Eq. (7.3), is greater. Alexandrite[1][9] is a typical example and the lifetime ratio (for the short lifetime) matches the theoretical curve very well using the following parameters: τ_2/τ_1 is approximately 0.007, a degeneracy ratio of 3 and energy gap between 4T_2 and 2E is assumed[9] to be 838 cm^{-1} . As seen in Fig. 7.4, a larger difference between the two intrinsic lifetimes and the shorter lifetime of the upper level gives a greater variation of lifetime with temperature.

The duration of the fluorescence lifetime as well as its sensitivity with temperature should be considered when designing a FL sensor. If the lifetime is too short, the frequency response of the detector arrangement should be chosen to match the signal,

Chapter 7 Comparison of two fluorescence-based schemes

while the existence of a long lifetime makes the measuring procedure longer in a practical instrument based on this approach, which is not ideal for real-time monitoring.

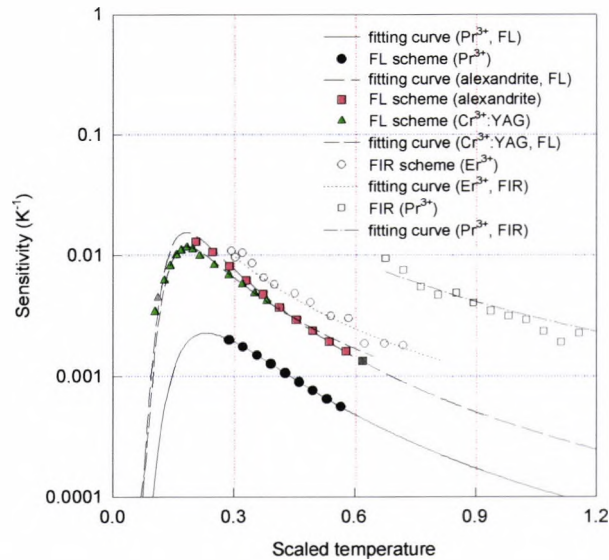


Fig. 7.8 A global comparison of the sensitivities of both methods, comparing experimental and theoretical data

The data in Fig. 7.7 for the FIR method in three dopant materials have intensity ratios not too far removed from 1, which should enable any of them to be used in practical devices over the indicated temperature ranges with a good signal-to-noise ratio.

Fig. 7.8 shows a comparison of the sensitivities of both methods by using all the data previously presented and the theoretical curves fitted to the data. The best sensitivity is that of FIR with Pr^{3+} , over the temperature region of 250 K to 500 K, supporting the theory described above. For the FL scheme, the sensitivity of alexandrite is better than that of praseodymium and $\text{Cr}^{3+}:\text{YAG}$, and for the FIR scheme, the sensitivity of Pr^{3+} is

better than that of Er^{3+} . The wide variety of sensitivities reported show that this important parameter is not only closely related to the upper/lower lifetime ratio and the relaxation time, as shown clearly in Fig. 7.3, but also the energy gap difference. For the same material, Pr^{3+} :ZBLAN glass, the sensitivity of the FIR scheme is greater than that of the FL scheme over the temperature range considered, which supports the theory that the sensitivity of a material with a longer relaxation time is less than when using the intensity ratio method (FIR), for the same material.

7.7 Discussion

The above comparison shows that at very low temperatures the FIR method has a higher sensitivity and thus is to be preferred for temperature monitoring as the response for the FL method tends to a constant value with its sensitivity approaching zero. However, over a wider range the difference between the responses is less evident, especially for the case when the intrinsic lifetime of the upper level is shorter than the lower and the relaxation time is short. Many other factors need to be taken into account in any practical comparison of these responses, including the spectroscopic details of the dopant ion and the technical issues associated with constructing a sensor based on these results. The behaviour of such an instrument based on either method will also depend on which levels of the particular dopant ion are involved. In particular the signal-to-noise ratio actually achieved will be strongly related to factors such as the source used, its wavelength and its relationship to the absorption spectrum, the ease of coupling to the optical fibre, the detection sensitivity and the geometry of the probe. Thus very large intensity ratios may cause problems of

Chapter 7 Comparison of two fluorescence-based schemes

accuracy, as do very short lifetime measurements ($\tau \leq 1 \mu\text{s}$) in low cost instrumentation. However, the analysis presented here is helpful in the selection, and a process of cross-referencing and cross-calibration of one method to the other may be used to widen and optimize the range of the sensor, in the same way that the use of blackbody radiation has been demonstrated as a cross-referencing approach to measurement of both higher ($T > 500\text{K}$) and lower ($T < 500\text{K}$) temperatures with the same probe[12].

The presence of the blackbody radiation can present a problem with the intensity ratio method at higher temperatures ($T > 500\text{K}$) unless it is effectively filtered out, or the wavelength of measurement is short ($\lambda < 700\text{nm}$) where the effect is less obvious. However, at $T > 1000\text{K}$ it is almost impossible to remove unless a pulsed approach to the fluorescence excitation is used, to enable discrimination against the direct current blackbody radiation background which is inevitably present. Usually for the FL method, when the relaxation time is relatively short, a shorter intrinsic lifetime of the upper level occurs and a higher sensitivity can be obtained for measurement purposes. However, when the relaxation time is long, a material with a longer upper level lifetime gives a better sensing characteristic. Both the FIR and FL method with a short relaxation time and shorter upper level lifetime, share a similar sensitivity over a wide range of temperatures, despite having a different response to temperature variations.

7.8 References

1. K.T.V. Grattan and Z.Y. Zhang, *Fiber Optic Fluorescence Thermometry* (Chapman and Hall, London, 1995)
2. M. Sun, Fiberoptic thermometry based on photoluminescent decay times, *Temperature: Its Measurement and Control in Science and Industry*, 6, 715 (1992).
3. W.M. Morey, W.H. Glenn and E. Snitzer, *Proc. ISA*, 261 (1983)
4. G.W. Baxter, S.A. Wade, S.F. Collins, G. Monnom and E. Maurice, *SPIE Proc.* 2841, 249 (1996)
5. T. Sun, Z.Y. Zhang, K.T.V. Grattan, A.W. Palmer and S.F. Collins, *Rev. Sci. Instrum.*, 68, 3447(1997)
6. A.A. Kaminskii, *Laser crystals: Their physics and properties* (Springer-Verlag, Berlin, 1981)
7. O. Svelto, *Principles of Lasers*, 3rd edn (Plenum, New York, 1989), 70(1989)
8. S.K. Gayen, W.B. Wang, V. Petricevic and R.R. Alfano, *Applied Phys. Letts.* 49, 437 (1986)
9. T. Sun, Z.Y. Zhang, K.T.V. Grattan, A.W. Palmer and S.F. Collins, *Rev. Sci. Instrum.*, 68, 3442(1997)
10. E. Maurice, G. Monnom, G. W. Baxter, S. A. Wade and S. F. Collins, A self-referenced point temperature sensor based on a fluorescence intensity ratio in Yb^{3+} doped silica fibers, *Appl. Opt.* 36, 8264 (1997)
11. S.A. Wade, B.P. Petreski, S.F. Collins, G.W. Baxter and E. Maurice, *Proc. 20th Australian Conference on Optical Fiber Technology*, (IREE, Sydney, 1995), 331 (1995)

Chapter 7 Comparison of two fluorescence-based schemes

12. Z.Y. Zhang, K.T.V. Grattan and A.W. Palmer, *Rev. Sci. Instrum.*, 63, 3177 (1992)

Chapter 8

Conclusions and Future Work

8.1 Summary of achievements

The main purpose of the work as a whole has been to extend the research on luminescence thermometry based on the foundation of the work on fibre optic sensor technology summarized in Chapter 1, and especially the review of previous work in the phosphor thermometry area in Chapter 2.

Several specific achievements have been made in this work and are summarized below:

- A large variety of luminescent materials, e.g., crystalline materials, doped bulk glasses and rare-earth ion doped fibers, have been discussed in Chapter 3 for their potential for wide range temperature measurement. Their comparative value for low-cost, simple yet effective sensors is discussed. The models considered are used to provide underpinning support for the experimental results obtained and are also applicable to the optimization of the selection of particular suitable fluorescent materials for thermometric use over a specific temperature region, or to be used as empirical calibration formulae in their operation.

Chapter 8 Conclusions and Future Work

- Multi-point or quasi-distributed intrinsic temperature sensing system arrangements have been discussed in Chapter 4 for potential sensor applications. An analysis scheme using Prony's method is reported, to enable exponential decays from either single material, two-material or even several element quasi-distributed sensors to be deconvolved and thus data and associated measurand information encoded in each individual signal to be recovered. In a similar way, multi-exponential decays arising from single sensor elements also can be deconvolved and analyzed, an additional advantage of the technique. In this work, in the development of an effective and rapid quasi-distributed temperature sensor algorithm, Prony's method is used for the estimation of the exponential time constants of a convoluted exponential fluorescence decay, with each individual decay corresponding to a different point and its associated temperature. Experimental results obtained are presented to justify the use of the approach in practical multi-exponential fluorescence decay analysis and to show a comparison of the Prony with an alternative, the Marquardt nonlinear least-squares approximation algorithm, to achieve the analysis most rapidly and effectively
- Average and local temperature measurement, rather than point specific temperature sensing, are important in a number of industrial situations. Chapter 5 in this thesis has proposed two different fluorescence-based configurations coupled with corresponding mathematical signal processing schemes to meet the requirement of high speed and consistency. The analysis reported shows that with rare-earth doped fibers used as temperature sensor probe elements for average temperature measurement, such a system works well especially when the lifetimes obtained

from different sensing probes are very close to each other. The SV scheme, based on matrix theory, is important because the average temperature-dependent singular value possesses the characteristics of both high speed and high precision. Data on local temperature detection from optical sensor probes are analyzed in detail by using a mathematical relationship, based on a correlation coefficient ratio scheme using fluorescence decay time information associated with the hot part of the fiber. The results show that the correlation coefficient ratio, R , used will deviate from and be smaller than unity with the increase of the temperature of the localized region where the heat is applied, thereby providing the mechanism for a simple high temperature excursion detection system.

- Whilst recognizing their strong dependence on temperature variation, the fluorescence lifetimes of rare earth doped fibres are found for the first time in Chapter 6 to be sensitive to another physical quantity, strain, in addition. Results obtained are compared with each other, showing that the lifetime variation rate of the doped fibers with increasing strain is temperature independent, and the rates are within experimental error the same, although in each case, the fiber modes, the dopant concentration level and the rare earth ion itself are different. Their stable behaviour may form the basis of a dual element sensor with which to obtain stress and temperature information independently in multiple element devices.
- The performance of the two most promising fluorescence-based temperature sensing techniques, namely the fluorescence intensity ratio (FIR) and fluorescence lifetime (FL) schemes, have been compared in Chapter 7. Comparison of the responses and the sensitivities of the two schemes show that at very low

temperatures the FIR method exhibits a significant variation with temperature, while the response of FL method becomes constant with its sensitivity approaching zero. However, at low temperatures, the FLR method may suffer from a SNR problem in the detected output and limit accuracy. With increasing temperature, the FIR and the FL methods (with short relaxation times and shorter intrinsic lifetimes of the upper energy levels) share a similar sensitivity over a wide temperature range. The presence of a long relaxation time or a longer intrinsic lifetime of the upper level in the use of the FL method is seen to give a less satisfactory response.

8.2 Future work

As discussed in this work, several of the fluorescence materials can be used to sense other physical quantities, such as strain, as well as temperature making it necessary to discriminate temperature and the other quantities simultaneously. Work has begun by Liu et al[1] in this field and a number of possibilities should continue to be explored, e.g. the use of neural network approaches on optical fibre temperature sensor systems[2].

Fibre laser sensors, which are different from the conventional sensors, offer several potential advantages[3], such as

- broad gain bandwidth: (1) tunable source (50nm); (2) short pulses (<50fs); (3) broadband source (20nm)
- high power into single mode fibre (5W)

- fibre cavity – easy device integration (modulators and filters)

New possibilities for their application to temperature sensing are worthy of exploration and it may lead to better performance with simpler sensor configurations compared to more conventional passive fibre sensors.

Improvements in the methods of active material bonding, especially for phosphor powders, are necessary. A particular valuable advance would arise from the development of a technique that would produce thin, durable, spray-on coatings like those created by flame and plasma deposition, but without the need for high-temperature combusting gases and expensive apparatus.

More extensive studies will be needed to evaluate the thermal characteristics of new appropriate luminescent materials and their optimum performance. Theoretical exploration is also necessary to help explain the behaviour of the active material and possibly render a probe-by-probe calibration unnecessary.

Finally the potential of luminescence lifetime-based techniques may help to solve residual problems in other sensing areas, such as in chemical sensing, gas detection, more widespread strain sensing, etc. The necessary modifications and developments for each specific application need to be further explored.

8.3 References

- [1] T.Liu, G.F.Fernando, Z.Y.Zhang and K.T.V.Grattan, Strain and temperature measurements using interferometric and rare-earth doped fibre sensor techniques for composite materials, *Eurosensors XII, Proceedings of the 12th European Conference on Solid-State Transducers and the 9th UK Conference on Sensors and their Applications*, Southampton, UK, 13-16 September 1998 (Ed. N.M.White), 323(1998)
- [2] A.S.Zhang, *Final Report*, School of Engineering, University of Greenwich, 1998.11.12
- [3] B.Y.Kim, Fiber Lasers for Sensing, in *European Workshop on Optical Fibre Sensors* (Eds. Brian Culshaw and Julian D.C.Jones), 12(1998)

List of Publications

Journal papers

1. T.Sun, Z.Y.Zhang, K.T.V.Grattan and A.W.Palmer, Intrinsic doped fiber fluorescence-lifetime based high temperature alarm sensor, *Sensors & Actuators A*, 71, 183(1998)
2. T.Sun, Z Y Zhang, K T V Grattan and A W Palmer, Intrinsic strain and temperature characteristics of Yb-doped silica-based optical fibers, *Rev. Sci. Instrum.*, 70, 1447(1999)
3. S F Collins, G W Baxter, S A Wade, T Sun, K T V Grattan, Z Y Zhang and A W Palmer, Comparison of fluorescence-based temperature sensor schemes: theoretical and experimental validation, *Journal of Applied Physics*, 84, 4649(1998)
4. T Sun, Z Y Zhang, K T V Grattan and A W Palmer, Intrinsic doped fluorescence decay-time based measurements-strain and temperature characteristics for sensor purposes, *Rev. Sci. Instrum.*, 69, 4186(1998)
5. T Sun, Z Y Zhang, K T V Grattan and A W Palmer, Ytterbium-based fluorescence decay time fiber optic temperature sensor systems, *Rev. Sci. Instrum.*, 69, 4179(1998)
6. T Sun, Z Y Zhang, K T V Grattan and A W Palmer, Determination of local high temperature excursion in an intrinsic doped fiber fluorescence-based sensor, *Rev. Sci. Instrum*, 69, 2930(1998)
7. Z Y Zhang, K T V Grattan, A W Palmer, B T Meggitt and T Sun, Characterization of erbium-doped intrinsic optical fiber sensor probes at high temperatures, *Rev. Sci. Instrum.*, 69, 2924(1998)

List of Publications

8. T Sun, Z Y Zhang, K T V Grattan and A W Palmer, Application of singular value decomposition in average temperature measurement using fluorescence decay techniques, *Rev. Sci. Instrum.* 69, 1716(1998)
9. Z Y Zhang, T Sun, K T V Grattan and A W Palmer, Er-doped intrinsic fiber sensor for cryogenic temperature measurement, *Sensors and Actuators A*, 71, 183(1998)
10. T Sun, Z Y Zhang, K T V Grattan and A W Palmer, Quasi-distributed fluorescence-based optical fiber temperature sensor system, *Rev. Sci. Instrum.*, 69, 146(1998)
11. Z Y Zhang, K T V Grattan, A W Palmer, B T Meggitt and T Sun, Fluorescence decay-time characteristics of erbium-doped optical fiber at elevated temperatures, *Rev. Sci. Instrum.*, 68, 2764(1997)
12. T Sun, Z Y Zhang, K T V Grattan and A W Palmer, Temperature dependence of the fluorescence lifetime in Pr^{3+} : ZBLAN glass for fiber optic thermometry, *Rev. Sci. Instrum.*, 68, 3447(1997)
13. T Sun, Z Y Zhang, K T V Grattan and A W Palmer, Analysis of the double exponential behaviour in alexandrite for optical temperature sensing applications, *Rev. Sci. Instrum.*, 68, 3442(1997)
14. T Sun, Z Y Zhang, K T V Grattan and A W Palmer, Analysis of double exponential fluorescence decay behavior for optical temperature sensing, *Rev. Sci. Instrum.*, 68, 58(1997)

Conference papers

1. K T V Grattan, Z Y Zhang and T Sun, Progress in Rare-earth Doped Fluorescence Decay Time Fiber Optic Sensor Systems, *IMEKO'15*, 1999

List of Publications

2. S A Wade, S F Collins, G W Baxter, T Sun, Z Y Zhang, K T V Grattan, A W Palmer and G Monnom, Fluorescence characteristics of several Yb-doped optical fibers for temperature sensing applications, *13th International conference on optical fiber sensors, Kyongju Korea, Apr. 12-16, 1999, Korea*
3. T Sun, Z Y Zhang, K T V Grattan and A W Palmer, Intrinsic doped fiber fluorescence-lifetime based high temperature alarm sensor, Eurosenors XII, Southampton, 13-16 Septemeber, 1998, Pub: IOP Publishing, Bristol, UK, 299(1998)
4. T Sun, Z Y Zhang, K T V Grattan and A W Palmer, Quasi-distributed and average temperature measurement using fluorescent sensor technology, *Applied Optics and Optoelectronics*, 16-19 March 1998, The Brighton center, Pub: IOP Publishing, Bristol, 117(1998)
5. Z Y Zhang, K T V Grattan, A W Palmer, BT Meggitt and T Sun, Characteristics of doped fibre intrinsic optical fibre sensor probes for wide range and high temperature operation, *European Workshop on Optical Fibre Sensors*, 8-10 July, 1998, Peebles, Scotland, 26(1998)
6. T Sun, Z Y Zhang, K T V Grattan and A W Palmer, Alexandrite-based optical temperature sensing: comparison of different fluorescence-based approaches, *12th International conference on optical fiber sensors, Williamsburg Marriott, Oct. 28-31, 1997, Williamsburg, Virginia*, Pub: OSA/IEEE Proceedings, Vol.16, 198(1997)
7. Z Y Zhang, K T V Grattan, A W Palmer, T Sun and B T Meggitt, Rare earth doped intrinsic fiber optic sensors for high temperature measurement up to 1100°C, *12th International conference on optical fiber sensors, Williamsburg Marriott, Oct. 28-31, 1997, Williamsburg, Virginia*, 556(1997)

List of Publications

8. S F Collins, K T V Grattan, Z Y Zhang, T Sun and A W Palmer, Comparison of fluorescence-based temperature sensor schemes using intensity ratioing and exponential decay in rare earth materials, *12th International conference on optical fiber sensors, Williamsburg Marriott, Oct. 28-31, 1997, Williamsburg, Virginia*, 194(1997)
9. Z Y Zhang, K T V Grattan, A W Palmer, T Sun and B T Meggitt, Intrinsic doped fibre decay-time based optical thermometry at elevated temperatures. *Sensors and their applications VIII*, edited by A T Augousti and N M White, *Proceedings of the eighth conference on sensors and their applications*, held in Glasgow, Scotland 7-10 September 1997, 251(1997)
10. Z Y Zhang, T Sun, K T V Grattan and A W.Palmer, The deconvolution of fluorescence decays and estimation errors, 8-14 Feb. 1997, *SPIE Proceedings*, Vol. 2980, 90(1997)
11. T Sun, Z Y Zhang, K T V Grattan and A W Palmer, Interpretation of Multi-exponential decay analysis for fluorescence based optical temperature sensor scheme, paper presented at *IMEKO'97 World Congress*, Tampere, Finland: Proc. published by IMEKO
12. T Sun, Z Y Zhang, K T V Grattan and A W Palmer, fluorescence -based decay-time sensing: multiexponential signal processing approach, Institute of *Physics Optical Group, Optical Sensing And Its Applications*, Dublin Institute of Technology, Ireland, 13 November 1996, Pub: IOP, London
13. T Sun, Z Y Zhang , K T V Grattan and A W Palmer, Evaluation of Prony's method in double exponential fluorescence decay analysis for temperature sensing, *Applied Optics and Opto-Electronics*, Reading, U.K., 16-19 Sep. 1996, 459(1996)